ABSTRACT

Title of Dissertation: MODELING APPROACHES FOR TREATMENT WETLANDS

James Nagle Carleton, Doctor of Philosophy, 2009

Directed By: Professor Hubert J. Montas, Fischell Department of Bioengineering

Although treatment wetlands can reduce pollutant loads, reliably predicting their performance remains a challenge because removal processes are often complex, spatially heterogeneous, and incompletely understood. Although initially popular for characterizing wetland performance, plug flow reactor models are problematic because their parameters exhibit correlation with hydraulic loading. One-dimensional advective-dispersive-reactive (ADE) models are also inadequate because longitudinal

dispersion in wetlands is often non-Fickian as a result of steep velocity gradients. Models that make use of residence time distributions have shown promise in improving performance characterization, particularly when interdependencies of stream-tube scale velocities and reaction rate coefficients are considered (the "DND" approach). However this approach is limited to steady-state conditions, and to an assumption that transverse mixing is nil.

This dissertation investigates three aspects of wetland modeling and is organized in a journal paper format. The first paper describes development of a DND model which accommodates non-steady-state conditions. The model processes flow and inlet concentration time series, and calculates as output effluent concentration time series. A version of the code allows optimization of model parameters by minimization of summed squared deviations between predicted and measured effluent concentrations. In example comparisons, model results compare favorably with measured data.

The second paper develops an analytical solution to a two-dimensional advective-dispersive-reactive equation, in which all flux terms are expressed as power functions of the transverse dimension. For uniform inlet concentration this idealized heterogeneity model is similar to a DND model, but with the inclusion of transverse diffusion. An example is used to illustrate the beneficial impact that transverse mixing has on reactor performance.

The third paper describes development of a model based upon a stochastic interpretation of the ADE. The solution technique that is employed results in a bicontinuum model that for steady-state conditions becomes a weighted sum of two

exponential decline functions. For low and intermediate degrees of mixing, model results nicely match those of the corresponding idealized heterogeneity model, and for high mixing they match results of the corresponding one-dimensional ADE. Comparisons against data suggest the bicontinuum model may represent wetland performance better than the DND model in some but not all cases.

MODELING APPROACHES FOR TREATMENT WETLANDS

By

James Nagle Carleton

Dissertation submitted to the Faculty of the Graduate School of the
University of Maryland, College Park, in partial fulfillment
of the requirements for the degree of
Doctor of Philosophy
2009

Advisory Committee:
Dr. Hubert J. Montas, Chair/Advisor
Dr. Kaye L. Brubaker
Dr. Adel Shirmohammadi
Dr. J. Court Stevenson
Dr. David R. Tilley

Dedication

For Ethan and Audrey, each equally my pride and joy.

Acknowledgements

I would like to express my deep appreciation and gratitude to my advisor, Dr. Hubert Montas, for the patient guidance and mentorship he provided to me, all the way from when I was first considering applying to the PhD program in the Biological Resources Engineering Department, through to completion of this degree. Dr. Montas' intellectual heft is matched only by his genuinely good nature and down-to-earth humility, and I am truly fortunate to have had the opportunity to work with him.

I would also like to thank my committee members, Drs. Kaye Brubaker, Court Stevenson, Dave Tilley, and Adel Shirmohammadi for the friendly guidance, thought-provoking suggestions, and the general collegiality that each of them offered to me over the years. In a similar vein, I'd like to recognize Drs. Andy Baldwin, Jennifer Becker, and Pat Kangas for the contributions that each of them made to my intellectual growth during my years of study at the University of Maryland.

Finally, I'd be remiss if I didn't acknowledge the innumerable sacrifices made by my wife, Luci, in shouldering far more than her fair share of the parenting and household burdens while I pursued this final degree.

Table of Contents

List of Figures

List of Acronyms and Abbreviations

ADE	Advection dispersion equation
BOD	Biochemical oxygen demand
COD	Chemical oxygen demand
DND	Damköhler number distribution
FWS	Free water surface
HLR	Hydraulic loading rate
kVD	Reaction rate coefficient distribution
OEW	Orlando easterly wetlands
PDF	Probability density function
PFR	Plug flow reactor
REV	Representative elementary volume
RTD	Residence time distribution
SSF	Subsurface flow
TIS	Tanks in series
TOC	Total organic carbon
TN	Total nitrogen
TP	Total phosphorus

Chapter 1: Introduction

1.1 Justification

Throughout our history human beings have relied upon aquatic resources for survival. When settled agriculture first emerged, and alongside it the civilizations that agriculture enabled to flourish, it is no coincidence that it took root in major river valleys such as those of the Tigris and Euphrates, the Nile, the Yellow, and the Indus, where plentiful water was available to support both direct consumptive needs and the irrigation of crops (De Blij, 1981). As civilizations grew in sophistication and organization, city dwellers built systems for both delivering drinking water from clean, upstream sources, and disposing of sewage and runoff downstream. As long as human population densities were small enough, this approach served the public interest adequately: waste loads were small enough that ecosystems were able to accommodate them without incurring excessive damage. Processes such as nutrient cycling, plant uptake and microorganism predation that are now understood to occur naturally in rivers, streams, and wetlands as well as in terrestrial ecosystems, were unknowingly being exploited to absorb nutrients and neutralize pathogens originating from human and domestic animal wastes. Eventually though, human populations grew to the point that urban waste loads became too large to be assimilated by the environment without overwhelming these natural processes and resulting in objectionable impacts (e.g. loss of fisheries, offensive odors, disease transmission) to receiving waters.

Even away from established urban centers the increasing scale of human activities took a growing toll on aquatic resources. In North America, population growth and westward expansion in the 19th century brought about nearly wholesale conversion of what had been hundreds of millions of acres of native prairie grasslands into agricultural land used almost entirely for growing a handful of grain crops. Where abundant wetlands had once adorned the land, ditches and tile drains were used to alter hydrologic pathways so that surface water would not linger and cropped acreage could be maximized (Prince, 1997). In other areas, marshes were obliterated by in-filling to create new land, for example adjacent to bays and navigable rivers, thus allowing new cities to be built along shipping routes. From the 1780s to the 1980s about 53 percent of all the wetland acreage in the conterminous United States is estimated to have been lost to such practices (Mitsch and Gosselink, 2000).

During recent decades development of modern agricultural methods and the "green revolution" has meant that more pounds of food can be grown on a given acre of land, but at the expense of much greater applications of fertilizer as well as toxic chemicals (pesticides), and consequently greater losses of these materials to waterways. Similarly, development of cities has brought increased commerce and an increased standard of living for many people, but at the expense of increased loads of urban pollutants (both point and nonpoint source) to waterways. As one consequence, estuarine and coastal waters around the world, including the Chesapeake Bay and the Gulf of Mexico, are now impaired by summertime anoxic "dead zones" fueled by excessive riverborne nutrient loads. The widespread conversion of pollution-absorbing wetlands to pollution-generating urban and

agricultural lands can thus be seen as having caused inevitable damage to water quality in the United States and elsewhere.

Unfortunately while recognition of the need to limit discharges of pollutants into waterways has been a driver of national environmental policy for decades now, widespread public recognition of the environmental benefits conferred by wetlands has been slower in coming. By the late 1960s the impacts of unregulated sewage and industrial effluents on rivers and lakes in the U.S. helped feed a growing sense of public outrage over the declining state of the environment that led to creation of the Environmental Protection Agency in 1970 and passage of the Clean Water Act in 1972, the objective of which was and is to "restore and maintain the chemical, physical, and biological integrity of the Nation's waters". Paradoxically, until as recently as the late 1980s, when then-President George H.W. Bush issued his "no-net-loss" policy, drainage and destruction of wetlands was an accepted practice in the U.S. that was at times actively encouraged by government policies (Mitsch and Gosselink, 2000). Over most of American history the general public attitude toward wetlands seems to have been that they were wastes of otherwise-useful acreage at best, and sinister refuges or breeding grounds for dangerous creatures and malaria-spreading mosquitoes at worst. Although public attitudes toward wetlands have been slow to change, since the latter half of the 20th century a growing body of research has demonstrated that wetlands provide a variety of environmental benefits, including fish and wildlife habitat, flood control and water quality improvement.

One application of the knowledge emerging from this work has been the construction of wetlands (new or restored) for the express purpose of water treatment,

i.e. pollutant removal. Although the study of treatment wetlands has become almost a discipline in itself, many crucial processes governing pollutant removal in wetlands remain imperfectly understood, and models used for characterizing performance suffer from limitations that reflect this lack of knowledge. In light of this issue, the goal of this study is to identify modeling methodologies suitable for assessing treatment wetland performance.

This dissertation is organized as follows. Chapter 1 provides an introduction that includes a literature review and a description of research objectives. Chapters 2 through 4 consist of manuscripts written for publication in peer reviewed journals. The first of these, presented in Chapter 2 and published as Carleton and Montas, 2007, describes development and analysis of a non-steady-state treatment wetland model. The second manuscript, presented in Chapter 3 and published as Carleton and Montas, 2009, describes development of a two-dimensional steady-state model for a domain representing a wetland possessing idealized representations of heterogeneity in governing attributes. The third manuscript, which details development of a bicontinuum model for a domain with stochastic heterogeneity, is presented in Chapter 4 and is in review as of this writing. Chapter 5 presents a comparison of various wetland models against performance monitoring data. Chapter 6 provides a summary and conclusions, with suggestions for future research. It should be noted that because of the paper structure of this dissertation, the most specific literature presentation on investigated topics is given in Chapters 2 to 4, while Chapter 1 serves mainly to frame the overall analysis.

1.2 Literature Review

1.2.1 Wetland Treatment History

The use of wetlands for treating water pollution has enjoyed an explosion of interest in recent decades, following experiments first conducted at the Max Planck Institute in Germany in the 1950's that demonstrated a capacity for macrophytes to enhance the degradation of high-strength phenolic wastes (Seidel, 1976), and spurred later by a number of studies conducted in various locales which demonstrated that a wide variety of natural wetland types can trap or transform pollutants, and thereby help to preserve downstream water quality (e.g. Bartlett et al., 1979; Davis et al., 1981; Fetter et al., 1978; Grant and Patrick, 1970; Lee et al., 1975; Novitzky, 1978; Olsen, 1993; Simpson et al., 1983). As a consequence of this body of work, since around the mid-1980's manufactured or "constructed" wetlands have become popular around the world as low-cost systems for treating a wide variety of wastewaters, including urban stormwater and agricultural runoff (Kadlec and Wallace, 2009). Although treatment wetlands can reduce loads and/or concentrations of various pollutants, predicting their performance reliably, or designing them in order to meet effluent limits, remains a challenge in part because removal processes are complex and multifaceted, and because biological and physical features underlying these processes are heterogeneous spatially, and in some cases temporally as well.

The nutrients nitrogen and phosphorus in excess quantities are probably the most pervasive water pollutants worldwide. In part because of the role that wetlands play in naturally processing these substances, treatment wetlands have often been built specifically to attenuate water borne nutrients. Mechanisms involved in wetland

processing of nutrients have been relatively thoroughly studied, and are therefore better understood than mechanisms at work for most other pollutants. For these reasons, this chapter includes a special focus on processes involved in wetland nutrient attenuation and removal.

1.2.2 Treatment Wetland Types

Constructed treatment wetlands can be divided into the broad general categories of free-water surface (FWS), and subsurface-flow (SSF) systems. FWS wetlands contain macrophytes rooted in soil and partially submerged in standing water typically less than 0.4 m deep. The surface of the water column in a FWS wetland is open to the atmosphere, and flow occurs through and around stands of emergent plant stems (Figure 1.1). SSF systems are similar, except plants may be rooted in a more permeable substrate (e.g. gravel) through which flow primarily occurs, bringing wastewater into contact with the substrate and plant roots. SSF systems may be further divided into the categories of vertical and horizontal flow systems (Kadlec and Wallace, 2009), depending upon the predominant direction of water movement.

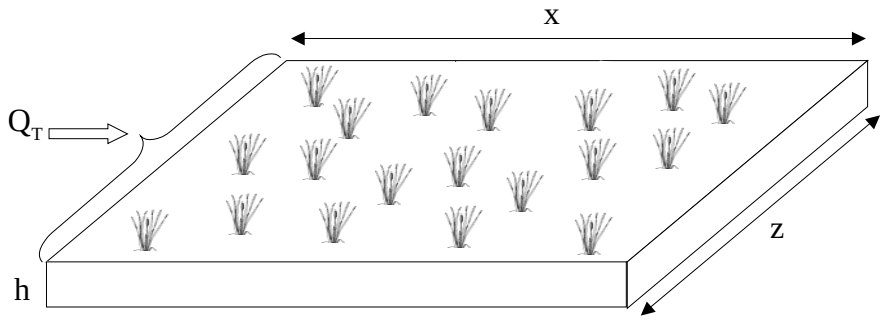

Figure 1.1 Definition sketch for a FWS wetland.

1.2.3 Pollutant Processing in Wetlands

Compared with other kinds of ecosystems, wetlands have "higher rates of biological activity" (Kadlec and Knight, 1996), which allows them to transform or sequester many kinds of pollutants that occur in wastewater and runoff. Macrophytes have adaptations (e.g. aerenchyma: porous tissue spaces that permit diffusion of air from the atmosphere to the roots) that allow them to grow in anaerobic sediments, and shallow water depths tend to limit the exhaustion of oxygen in the water column. Thus eutrophication of wetlands via increased nutrient inputs does not typically result in the kinds of hypoxic dead zones that have become common in lakes, reservoirs and estuaries, although dissolved oxygen and redox potential may nevertheless decrease with depth through the water column (Tao et al., 2006). Within the otherwise anaerobic sediments, local aerobic zones (the oxidized rhizosphere) surround the roots of emergent macrophytes as a result of radial leakage of oxygen (Brix, 1997). Unlike purely terrestrial or aquatic environments, wetlands therefore possess both aerobic and anaerobic zones in close proximity and intimate contact with each other – a circumstance which, uniquely among natural environments, allows the close

coupling of sequential oxidative and reductive processes that are necessary for the complete removal of some constituents, notably nitrogen.

Also unlike terrestrial or aquatic environments, in wetlands the presence of detrital litter and dense emergent plant stems brings water borne constituents into close contact with epiphytic biofilms, increasing the efficiency of processing of labile constituents like BOD (Tchobanoglous and Schroeder, 1987), dissolved phosphorus (Pietro et al., 2006; Scinto and Reddy, 2003), and various forms of nitrogen (Bastkiven et al., 2003; Eriksson, 2001; Eriksson and Weissner, 1997; Eriksson and Weissner, 1999; Toet et al., 2003; Thoren, 2007). Macrophytes further appear to increase the retention of suspended solids and associated pollutants (e.g. phosphorus, metals) by impeding flow and enhancing sedimentation (Leonard and Luther, 1995; Leonard and Croft, 2006; Thornton et al., 1997; Saiers et al., 2003), and perhaps by inhibiting sediment resuspension (Braskerud, 2001), resulting in higher rates of removal of such entities from the water column than tend to occur in open water systems such as ponds.

1.2.4 Nutrient Removal

The mechanisms of nitrogen and phosphorus removal in wetlands are quite different from each other. Nitrogen is removed primarily via a multiple-reaction pathway that proceeds from organic nitrogen through ammonia/ammonium (NH_3/NH_4^+), to nitrite (NO_2^-), nitrate (NO_3^-), and finally molecular nitrogen (N_2), which is lost to the atmosphere. This complex series of reactions requires, among other things, the presence of zones that are at different redox potentials, in close contact with each other. Because the final step (denitrification) represents a one-way

loss of nitrogen from the system, the ability of wetlands to remove nitrogen is theoretically inexhaustible: wetlands should be able to continue removing nitrogen indefinitely. By contrast, the primary loss mechanisms for phosphorus are all saturable, meaning that in the absence of active management, wetlands should eventually reach a state of rough equilibrium between input and output phosphorus loadings. Of course wetlands are open systems in constant contact with other parts of the biosphere, so the distributions of phosphorus and other elements within various wetland compartments may also be affected by the activities of biological entities (e.g. insects, muskrats, birds) capable of transporting these materials into or out of a wetland through processes such as predation and excretion.

1.2.5 Processing of Nitrogen

Total Kjeldahl nitrogen refers to the sum of reduced forms of nitrogen, that is organic nitrogen-containing compounds (proteins, urea, etc.) plus NH_3/NH_4^+. Within wetlands, microbially-mediated transformation processes inter-convert various forms of nitrogen. A process called "ammonification" (or mineralization) refers to the decomposition of organic nitrogen, with consequent release of NH_3/NH_4^+. This can occur under either aerobic or anaerobic conditions. Within most wetlands, the ionized (NH_4^+) form of ammonia tends to predominate (Kadlec and Knight, 1996). This is a function of the ammonium ion's acid dissociation constant (pKa), which has a value of around 9.3 at typical ambient temperatures and of the fact that pH's within wetlands usually fall below this level. Photosynthesis by phytoplankton and macrophytes can in some cases however drive pH high enough during the day time that substantial losses of NH_3 may occur by volatilization (Vymazal, 2007). The

NH_4^+ form may be lost from the water column by cation exchange onto negatively charged binding sites on soil (especially clay) particles in the sediments (Mitsch and Gosselink, 2000). Ammonia/ammonium is the preferred form of nitrogen as a nutrient for most wetland plant species, and some loss from the water column occurs via direct plant uptake and incorporation into organic matter.

Another important process affecting nitrogen in wetlands is nitrification, which refers to the aerobic oxidation of NH_3/NH_4^+ first to relatively short-lived NO_2^- ions primarily via the actions of bacteria in the genus *Nitrosomonas,* and then to the more stable NO_3^- form via the actions of microbes in the genus *Nitrobacter*. Nitrification may happen partly within an oxidized sediment layer typically less than 1 cm thick at the surface of wetland soils, and may also occur within epiphytic biofilms that coat submerged plant and litter surfaces in FWS wetlands (Bastkiven et al., 2003), or submerged substrate media in SSF wetlands (Bigambo and Mayo, 2005). Beneath the oxidized sediment layer, wetland sediments tend to be anaerobic. Because it is an anion, NO_3^- is highly mobile in soils, and in addition to diffusive transfer, is readily transported into the subsurface along with water advected into the sediments as a result of groundwater recharge and the transpiration demands of macrophytes (Martin et al., 2003). Although not the preferred nitrogen form for plants, NO_3^- can be taken up via the roots as a nutrient, in a process called "assimilatory nitrate reduction". More importantly, NO_3^- is subject to "dissimilatory reduction", primarily through a process known as "denitrification", which occurs under (at least locally) anaerobic conditions (e.g. within non-surficial wetland sediments). In denitrification, the NO_3^- ion serves as an alternate electron acceptor

for heterotrophic microorganisms typically oxidizing labile organic matter where molecular oxygen is lacking. Denitrification converts NO_3^- into gaseous forms (N_2O and N_2), thus returning nitrogen to the atmosphere. A less-well understood process called "anaerobic ammonia oxidation" or "anamox", which involves the oxidation of NH_4^+ coupled to reduction of NO_2^-, provides another potential dissimilatory mechanism for nitrogen. Like denitrification, anamox generates gaseous N_2 from inorganic nitrogen forms, but with decreased labile carbon and O_2 consumption requirements (Kadlec and Wallace, 2009). While anamox microorganisms have been found in natural environments and wastewater treatment systems, the importance of anamox to nitrogen removal in treatment wetlands is as yet unknown (Vymazal, 2007).

Ammonification (the partial oxidation of organic matter, and concurrent release of NH_3/NH_4^+) proceeds more rapidly than nitrification (Kadlec and Knight, 1996), potentially resulting in accumulation of NH_3/NH_4^+ within a wetland. The ultimate loss of this material to the atmosphere via denitrification in the subsurface can be envisioned as occurring through the following general sequence of steps (Mitsch and Gosselink, 2000): NH_3/NH_4^+ diffuses from the water column to the sediments (most importantly the aerobic surface layer and oxidized rhizosphere zones), where it is oxidized to NO_3^- ; NO_3^- then diffuses from the aerobic zones into anaerobic portions of the sediment matrix, where it is denitrified to N_2, which in turn diffuses into the water column and escapes to the atmosphere through volatilization. As is the case in any diffusive process, the movements of various nitrogen species between compartments are driven by the associated concentration gradients. Because

of its higher mobility, the mass transfer of NO_3^- between sediments and water occurs at a higher rate (i.e. with a larger effective diffusion coefficient) than the mass transfer of NH_3/NH_4^+. Thus NH_3/NH_4^+ diffusion and nitrification tend to be the rate-limiting processes governing total nitrogen loss within wetlands. Shallow water depths enhance the transfer of NO_3^- into the sediments, and therefore tend to increase denitrification rates (Mitsch and Gosselink, 2000). A similar phenomenon has been observed in stream environments (Alexander et al., 2008; Sjodin et al., 1997). For denitrification and other reactions occurring in epiphytic biofilms, plant surface density may have an analogous effect on reaction rates. Smith et al. (2000) found denitrification rates to be proportional to the number of macrophyte shoots present in wastewater treatment wetland sediments, demonstrating an important role for vegetation in denitrification, even when it takes place in the subsurface.

The ultimate loss of mineralized nitrogen to the atmosphere via denitrification occurs through a series of steps involving diffusive movement of various nitrogen species between areas that are at different redox potentials. Because diffusion is a function of temperature, the rate coefficient for removal (k_{T1}) may be adjusted for temperature using the Arrhenius relationship

$$k_{T_1} = k_{T_2}\Theta^{(T_1-T_2)} \tag{1.1}$$

where T_1 is the current wetland temperature, and T_2 is a reference temperature (typically 20°C), k_{T2} is the rate constant at T_2, and Θ is a temperature coefficient (Tchobanoglous and Schroeder, 1985). Ammonia removal rates in particular have been found to be highly temperature sensitive, varying on a seasonal basis (Kadlec and Wallace, 2009).

Besides temperature, denitrification is sensitive to pH: optimal values are between 6.5 and 7.5, and denitrification is particularly inhibited under acidic conditions (e.g. pH ≤4), such as occur in northern peat bogs (Mitsch and Gosselink, 2000). In wastewater treatment wetlands pHs are typically in the slightly acidic to circumneutral range, so that this is not usually a concern (Kadlec and Knight, 1996). Alkalinity is consumed during nitrification, and released during denitrification in the form of bicarbonate (HCO_3^-). The balance between nitrification and denitrification rates thus itself has some impact on wetland pH.

To enable denitrification, sufficient labile organic matter must be present in order to drive NO_3^- reduction. Over time, death and senescence of plant materials will contribute sufficient organic matter to create such conditions in the sediments (Bastkiven et al., 2007; Rotkin-Ellman et al., 2004). For denitrification occurring in epiphytic biofilms, phytoplankton exudates may serve as a labile carbon source (Toet et al., 2003). To avoid the need for a waiting period when starting up a new treatment wetland, organic matter, for example in the form of compost or peat, is sometimes added to the sediments. One potential concern with this approach is that it may result in a lowering of pH, as decay of these materials may result in the formation of organic acids. To mitigate this possibility, limestone may be added to wetland soils to help buffer acidity.

1.2.6 Processing of Phosphorus

By contrast with nitrogen, wetland removal of phosphorus involves different kinds of processes, none of which represents a one-way loss from the system. In runoff-treatment wetlands, a substantial fraction of total phosphorus (TP) in the

influent is typically found in the particulate form, i.e. sorbed to suspended sediments (Carleton et al., 2000; Dierberg and DeBusk 2008; Maynard et al., 2009). Sedimentation of particulates in these situations can represent an important phosphorus removal pathway, at least for a time. By contrast, wastewater typically contains little inorganic sediment, and a higher fraction of TP is found in more labile forms, especially orthophosphate ion (PO_4^-) (Bitton, 2005). A fraction of dissolved phosphorus may be removed by sorption to wetland sediments (especially those high in Fe and Al), however the capacity of wetland sediments to remove phosphorus this way is eventually exhausted as binding sites are saturated. Phosphorus may also form precipitates with cationic metals such as Fe, Al, Ca, and Mg, or may form co-precipitates with other minerals such as $CaCO_3$ (Gu and Dreschel, 2008; Siong et al., 2006). However such precipitates may re-dissolve later when conditions (e.g. pH, temperature, redox potential) change (Vymazal, 2007).

Because phosphorus is usually the limiting nutrient for primary production in freshwater wetlands, algae and plants are efficient at taking up the element into their tissues. Most of this phosphorus is eventually returned to the water column, e.g. when senescence occurs, however a portion may be incorporated into new sediments in the form of incompletely decomposed plant litter. This process and sedimentation represent the only long-term storage mechanisms for phosphorus in wetlands (Kadlec and Knight, 1996). For wetlands to continue to function as phosphorus sinks into the future, phosphorus removal capacity must eventually be regenerated, e.g. by plant harvesting or sediment removal. Food chain transfer and/or predation by non-resident organisms (e.g. wading birds), followed by excretion elsewhere may accomplish this

task automatically to some degree. The conversion of labile phosphorus into less biologically reactive organic forms (e.g. plant litter) may continue to benefit downstream ecosystems that receive this material, even when long-term equilibrium between phosphorus inputs and outputs has been reached.

1.2.7 Hydrodynamics and Flow Patterns in Wetlands

Flow patterns in wetlands and related vegetated environments may be quite complex, with various phenomena influencing water movement at different spatial and temporal scales. Open water zones may be susceptible to wind-driven surface currents coupled to deeper-water return flows (Kadlec and Knight, 1996). Under a longitudinal head gradient, mean velocities vary directly with depth and inversely with vegetation density (Kadlec and Knight, 1996; Leonard and Croft, 2006; Leonard and Luther, 1995). Bed drag causes vertical variations in velocity, and the shapes of the velocity profiles are influenced by the presence of plant stems, which tend to decrease turbulence intensity and the thickness of the benthic boundary (near-zero velocity) layer in proportion to their density (Nepf et al., 1997a). Vertical gradients in longitudinal velocity produce pressure gradients that induce vertical secondary flows on the downstream sides of emergent stems, presumably leading to increased advective exchange between sediments and the water column (Nepf, 1999). Also on the downstream sides of plant stems, laterally-recirculating “primary wakes” (vortices) of approximately stem diameter size, and larger “secondary wakes” (zones of decreased velocity) form when stem-based Reynold’s numbers (Re) exceed a magnitude of about 10. At Re values greater than about 100, the primary wakes become unstable and begin to periodically shed vortices, which increases their rate of

time-averaged exchange with the free stream (Nepf et al., 1997a). Velocity deviations in the secondary wake scale with the square root of Re, and decay exponentially in the downstream direction, such that the secondary wake extends over an effective "attenuation length" that may be substantially larger than the stem diameter scale (White and Nepf, 2003) (Figure 1.2). At sufficient stem densities, wakes overlap and superimpose, creating a degree of randomness in the velocity field.

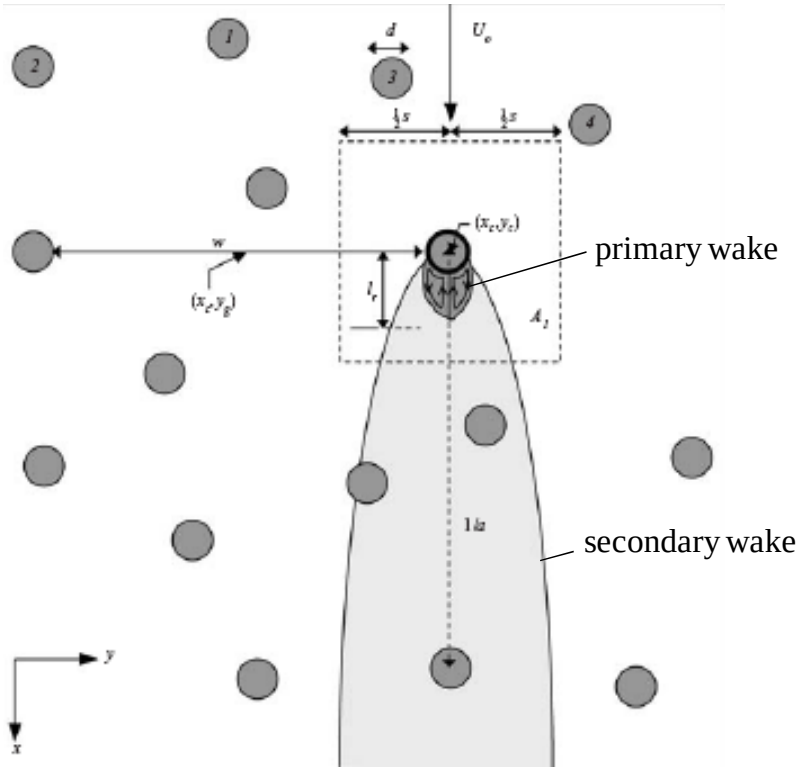

Figure 1.2 Primary and secondary wakes downstream of emergent vegetation, adapted from White and Nepf (2003).

Submerged plants tend to exert a greater influence than emergent plants on vertical profiles of longitudinal velocity. Drag induced by submerged plant beds effectively separates the flow field into a lower (slow) and an upper (fast) zone (Nepf

and Vivoni, 2000). An inflection in the velocity profile at the interface between these two zones may cause the formation of "large, coherent vortices", which serve to enhance vertical inter-zonal mixing of fluid elements (Ghisalberti and Nepf, 2002, 2005; Shi and Hughes, 2002). Analogous effects may also occur in the horizontal plane, when boundaries occur between zones of open water and zones of relatively high emergent plant density, e.g. "fringing vegetation" (White and Nepf, 2008). Regardless of spatial orientation, variations in local drag caused by variations in plant density and water column depth induce variations in velocity, which include a degree of redirection of flow that serves to maintain continuity (Fonseca et al., 1982; Sand-Jensen and Mebus, 1996).

At the whole-system scale longitudinal transport in wetlands is often dominated by "short-circuiting", or strong heterogeneity in velocity fields (Dierberg et al., 2005; Kjellin et al., 2007; Martinez and Wise, 2003; Werner and Kadlec, 2000), which may be observed with the use of visible dye tracers (Figure 1.3). Preferential flow pathways may occur as a result of decreased hydraulic resistance in deeper areas and/or where vegetation is less dense (Kadlec and Knight, 1996). Lightbody et al. (2008, 2009) have pointed out that channelized flow paths may form essentially automatically even in marshes with flat bathymetry, as a result of random minor non-uniformities that become self-reinforcing as faster flows inhibit both sedimentation and vegetation regrowth or colonization. In this sense, fast flow paths in freshwater marshes may be analogous to tidal channels in salt marshes and flow channels in sea grass beds, which form spontaneously apparently as a result of similar feedback mechanisms (D'Alpaos et al., 2006; Luhar et al., 2008; Mitsch and Jorgensen, 2004;

Moore, 2004). If this is the case, then the presence of a degree of short-circuiting in FWS treatment wetlands may be all but inevitable. Results of modeling and field experiments suggest however that short-circuiting may be actively countered by design through structural engineering approaches such as construction of alternating deeper and shallower zones oriented perpendicular to flow (Lightbody et al., 2009; Thullen et al., 2005).

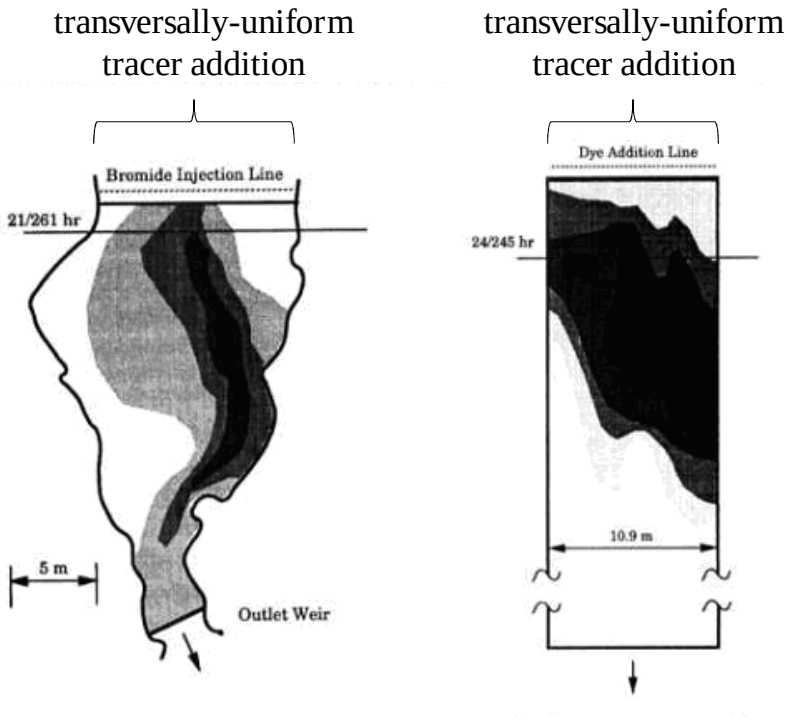

Figure 1.3 Tracer isopleths in natural (left) and constructed (right) wetlands (adapted from Kadlec and Knight, 1996).

1.2.8 Evolving Longitudinal Dispersion

Classical shear-flow dispersion (Taylor, 1954) involves an interaction between spatially non-uniform advection and solute diffusion in the transverse direction. After sufficient time or travel distance, net longitudinal flux may be

separated into a mean advective flux and a “Fickian” dispersive flux, so-named because it is characterized as if it were a diffusive process, i.e. one which follows Fick’s first law. For dispersion to be treated as Fickian implies the presence of a constant dispersion coefficient, so that the overall transport process is adequately represented using an advection dispersion equation (ADE). The dispersion coefficient has been defined as half the rate of increase of spatial concentration variance (σ_x^2) of an inert tracer following a pulse injection (Gelhar, 1993) (Figure 1.4):

$$D = \frac{1}{2}\frac{d\sigma_x^2}{dt} \tag{1.2}$$

where

$$\sigma_x^2 = \frac{\int_0^\infty (x - \bar{x})^2 \, C dx}{\int_0^\infty C dx} \tag{1.3}$$

and

$$\bar{x} = \frac{\int_0^\infty x C dx}{\int_0^\infty C dx} \tag{1.4}$$

Thus, for a transport system to be characterized as Fickian implies that the spatial variance of an inert tracer cloud increases linearly with time.

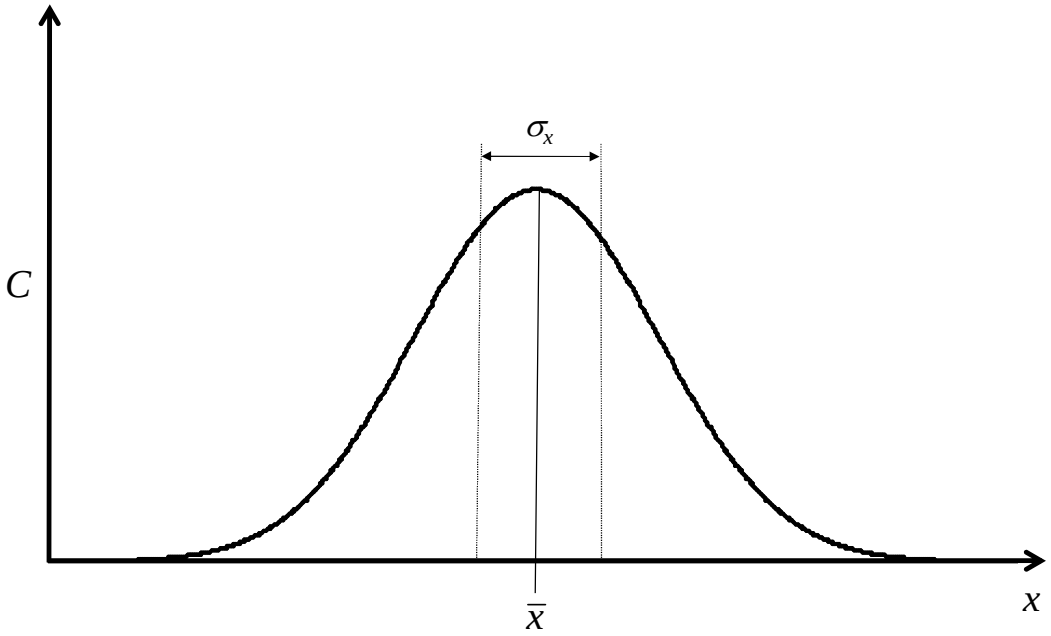

Figure 1.4 Longitudinal spatial distribution of tracer, with mean and standard deviation indicated, following pulse injection at x=0.

However, data from studies on FWS treatment wetlands and a surprisingly wide array of other transport media have documented solute spreading that is not adequately characterized by the ADE because longitudinal mixing only approaches Fickian behavior asymptotically if at all (e.g. Day, 1977; Gelhar, 1993; Werner and Kadlec, 2000). Longitudinal dispersion in these systems is described as "pre-asymptotic", "non-Fickian", or "scale-dependent" because the behavior manifests as an increase in the apparent dispersion coefficient with the scale of transport. In the near-field limit of shear flow dispersion (the "stochastic-convective" case) *D* goes to zero, and longitudinal spreading occurs solely as a function of velocity heterogeneities; i.e. transverse mixing is nil. If a PFR or an ADE model is incorrectly used to characterize a reactive transport environment that is stochastic-convective, the

result may be reaction rate coefficients (k) that appear to increase with HLR, as suggested by the analysis of Carleton (2002).

It must be noted that two fundamentally different kinds of solute concentration in fluid are of relevance to work involving heterogeneous transport systems including wetlands. As first suggested by Kreft and Zuber (1978) for fluid-bed reactors, these may be referred to as "resident" and "flux" concentrations. The first of these (resident), sometimes also referred to as "through the wall" concentration, is simply the spatially-weighted mean concentration within the reactor, in the dimension(s) perpendicular to flow. The second (flux), sometimes referred to as the "mixing cup" concentration, is the flow-weighted mean concentration in the reactor, measured also in the dimension(s) perpendicular to flow. The resident concentration is therefore a measure of mean concentration within the reactor at a particular distance from the inlet, while the flux concentration is a measure of the mean concentration of the total effluent hypothetically exiting the reactor at that same distance from the inlet.

1.2.9 Residence Time Distributions

The distribution of durations spent by water and tracer particles in a wetland under steady flow conditions can be characterized with a probability density function referred to as a residence time distribution, or "RTD". A wetland's RTD, which is analogous to a breakthrough curve in a soil column or fluid-bed reactor study, is measured by injecting a pulse of inert tracer at the inlet of a wetland, and monitoring flux concentrations at the outlet as the tracer subsequently elutes. RTDs are widely used in wetland studies, and are important because they provide quantitative

information that cannot be readily obtained in any other way, on transport and mixing processes within wetlands. RTDs may also be used in performance models, as will be discussed. The RTD function itself is obtained by normalizing the flux concentration vs. time curve so that the area under the curve equals unity. In examining RTDs from a number of treatment wetlands with different geometries, Kadlec and Knight (1996) noted that a tanks-in-series (TIS) pulse injection model appeared to fit many of them well (Figure 1.5):

$$E(t) = \frac{N}{\tau(N-1)!}\left(\frac{Nt}{\tau}\right)^{N-1} \exp\left(-\frac{Nt}{\tau}\right) \qquad (1.5)$$

where $E(t)$ is the RTD function, N refers to the number of (hypothetical) completely-stirred tanks in the model, τ is the system mean residence time, and t is time elapsed since tracer injection. Carleton (2002) noted that eq. 1.5 is mathematically equivalent to a gamma probability density function (pdf), and suggested the use of the gamma pdf as a more general model formula for wetland RTDs:

$$E(t) = \frac{\beta^{-\alpha} t^{\alpha-1}}{\Gamma(\alpha)} \exp\left(-\frac{t}{\beta}\right) \qquad (1.6)$$

where α is known as a shape parameter, β is a scale parameter, and Γ refers to the gamma function. Parameter α in eq. 1.6 is the same as parameter N in eq. 1.5, and mean residence time for a gamma RTD equals α times β, thus $\beta = \tau/\alpha = \tau/N$. Equation 1.6 offers the advantage over eq. 1.5 that non-integer values of N or α are accommodated. Given that most wetlands are not actually composed of linked well-mixed "tanks", this parameter really amounts to a simple empirical descriptor of the degree of tracer spreading, thus there is no obvious physical reason to limit its magnitude to integer values.

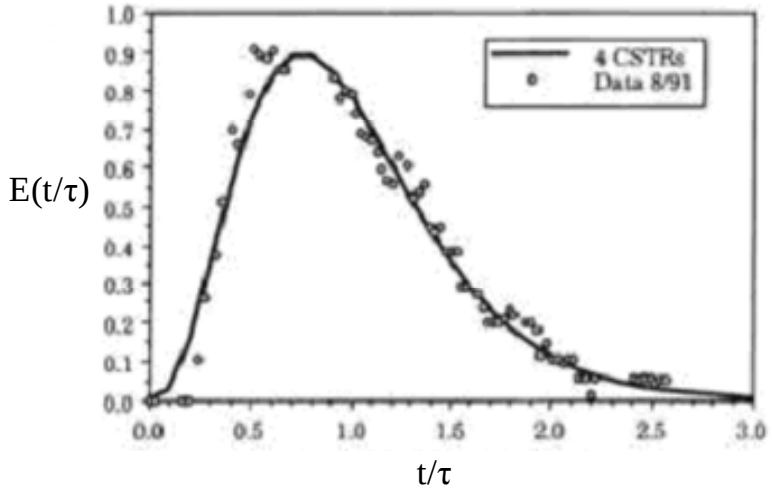

Figure 1.5 RTD plotted as a function of normalized residence time, for wetland EW3 at Des Plains, IL, with four-tank (i.e. gamma pdf with α=4) model fit to data (adapted from Kadlec and Knight, 1996).

In a related vein, Persson et al. (1999) proposed the use of a measure they called "hydraulic efficiency" (λ) to simultaneously quantify the degree of utilization of available treatment volume, and the degree of flow uniformity in stormwater treatment wetlands and ponds:

$$\lambda = \left(\frac{\tau}{t_n}\right)\left(1-\frac{1}{\alpha}\right) = \frac{t_p}{t_n} \qquad (1.7)$$

In eq. 1.7, τ is the mean residence time as determined by an RTD, t_n is the nominal detention time (volume divided by flow), α is the number of (hypothetical) CSTRs in series, and t_p is the residence time of the peak tracer concentration, i.e. the mode of the RTD. Although eq. 1.7 includes a parameter from the gamma-pdf RTD model, use of the equation does not necessarily require a wetland RTD to be well-described by this model: the term $1/\alpha$ may be interpreted as equivalent to an RTD's

dimensionless variance (σ_t^2/τ^2). The first bracketed term in eq. 1.7 quantifies the fraction of wetland volume that is hydrodynamically-active, and the second term quantifies the degree to which water movement resembles plug flow. Kadlec (2005) examined data from a number of ponds and wetlands, and concluded that wetlands have slightly higher hydraulic efficiencies than ponds, which he speculated was due to shallower water column depths in wetlands.

1.2.10 Continuous Injection Performance Models

Until recently a recommended approach to analyzing or predicting the performance of treatment wetlands was to treat these systems as plug flow reactors (PFRs) (Figure 1.6) (Kadlec and Knight, 1996). The RTD of a plug flow system is simply a Dirac delta pulse at the mean residence time. This approach, while convenient due to its simplicity, ignores factors that cause flow to be non-steady, including varying influent, precipitation, evapotranspiration, and exchanges with subsurface water. Perhaps more importantly it ignores spatial flow non-uniformity, which as previously mentioned can be substantial. The "*k-C**" version of the PFR model partially addresses this by employing a second parameter (*C**) besides the reaction rate coefficient, to empirically account for non-zero plateaus in concentration:

$$\frac{C(y) - C^*}{C_i - C^*} = \exp[-k\tau y] \qquad (1.8)$$

In eq. 1.8 C_i is the inlet concentration, $C(y)$ is concentration at dimensionless longitudinal distance y, C^* is background concentration (a fitting parameter), and k is a volumetric (units of inverse time) reaction rate coefficient. Kadlec and Knight (1996) and Kadlec and Wallace (2009) note that in FWS systems, and especially for

constituents such as NO_3^- whose removal involves diffusion into the subsurface, k values often display an inverse correlation with mean water depth (h). In these cases use of an alternative "areal" version of the reaction rate coefficient (k_a) with units of length over time is advocated, in which depth is considered separately from the coefficient. The two kinds of reaction coefficient are related to each other as follows:

$$k_a = kh \text{ , or } k_a = khe_v \tag{1.9}$$

where

$$e_v = \frac{\tau}{t_n} \tag{1.10}$$

is essentially effective porosity (see eq. 1.7), which is usually close to unity in FWS wetlands. A version of the relation in eq. 1.8 employing an areal reaction rate coefficient is

$$\frac{C(y) - C^*}{C_i - C^*} = \exp[-\frac{k_a}{q} y] \tag{1.11}$$

where q is hydraulic loading rate (flow divided by wetland surface area). For simplicity's sake the remainder of the discussion and derivations in this study are limited to consideration and use of volumetric reaction rate coefficients.

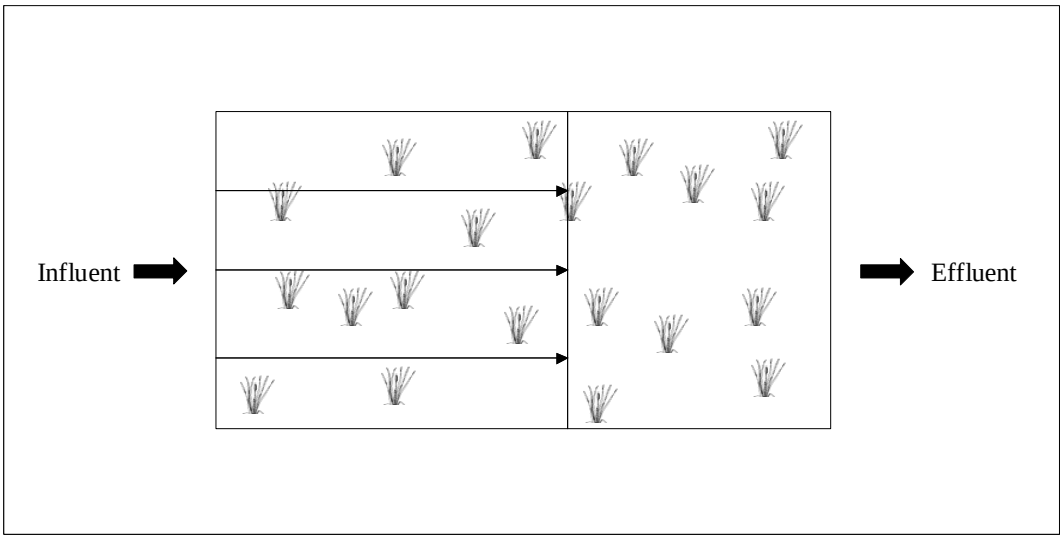

Figure 1.6 Plug-flow representation of flow through wetlands: velocity and residence time are uniform (mathematical representation is one-dimensional).

As previously mentioned, the PFR model assumes an RTD with a single residence time. An expression akin to eq. 1.8 for a reactor with a gamma distribution of residence times is the following (Carleton, 2002):

$$\frac{C(y)-C^*}{C_i-C^*}=\left(1+\frac{k\tau}{\alpha}y\right)^{-\alpha}=\left(1+k\beta y\right)^{-\alpha} \tag{1.12}$$

Equation 1.12 offers greater flexibility than eq. 1.8 in terms of shapes that the $C(y)$ vs. y curve can assume, even when parameter C^* is set to zero to produce a two parameter (k and α) model, which will be referred to as the "TIS model" in this study.

According to Kadlec and Wallace (2009), C^* is effectively zero for some constituents – notably NH_3/NH_4^+, NO_3^-, and xenobiotics – and non-zero for others, including TP, TN and organics (BOD, COD, and TOC). Non-zero C^* may result from a variety of causes including release of dissolved and particulate plant biomass to the water column, association of constituent with non-settling (fine) suspended inorganic particulates, or release from distributed external source inputs, e.g.

groundwater. An apparent non-zero C^* may also occur as a result of short-circuiting that mixes treated water with relatively untreated water at some distance from the inlet. The phenomenon has been perhaps most dramatically suggested by studies on pathogen removal, where very rapid removal results in a sharp concentration decline near the inlet, followed by a leveling-off to a low but non-zero plateau for the remainder of the wetland (Chendorain, 1998; Kadlec and Wallace, 2009).

Although the PFR model has been widely used to quantify treatment wetland performance, critical flaws with the approach have recently become apparent. Using monitoring data and simulations, Kadlec (2000) demonstrated that calibrated k values tend to increase as hydraulic loading rate (HLR) increases (or as mean residence time decreases), an observation that has since been confirmed by other researchers (Black and Wise, 2003; Coveney et al., 2002; Jamieson et al. 2007; Ran et al., 2004). Kadlec's analysis also demonstrated that this effect is not eliminated by inclusion of a longitudinal dispersion term, i.e. use of the one-dimensional ADE in place of the PFR model. Expanding upon a conceptual model presented by Kadlec (2000), Carleton (2002) suggested that wetlands could be simulated as collections of parallel, non-interacting flow paths (a "stochastic-convective" representation – see Figure 1.7). The flux concentration of a transported constituent exiting such a wetland is a flow-weighted average over a collection of stream tubes with different velocities. Carleton demonstrated that eq. 1.12 is equivalent to a model of a reactor with uniform k and a stochastic-convective transport environment characterized by a gamma RTD.

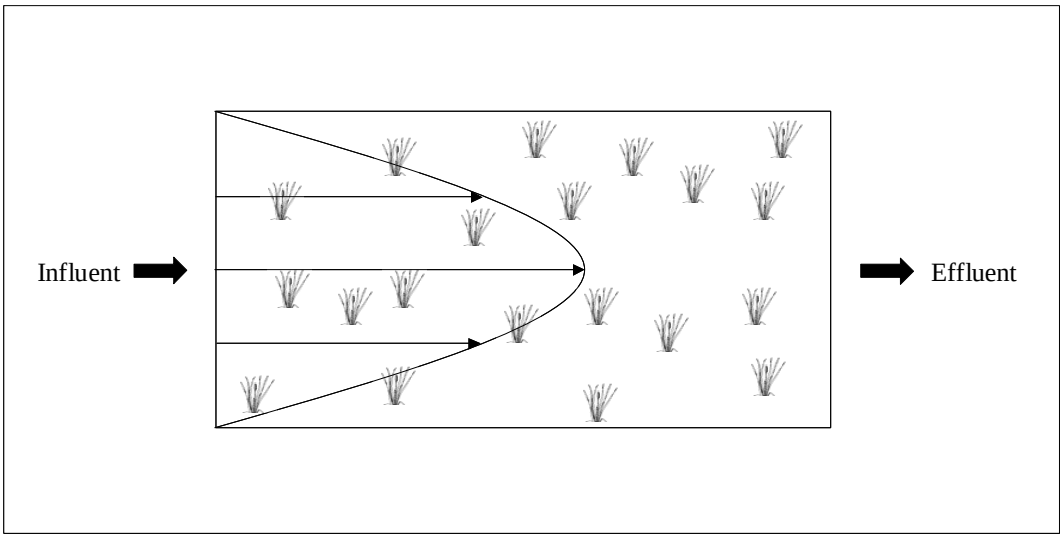

Figure 1.7 A stochastic-convective representation of flow in wetlands: velocity is non-uniform, and transverse diffusion is ignored.

In contrast with the conceptual simplicity of uniform *k* as represented by the TIS model (eq. 1.12), Carleton (2002) proposed an approach based on a wetland's Damköhler number (*Da*) distribution or "DND", which incorporates a presumption that *k* is not spatially uniform; rather, stream-tube scale velocities and *k* values vary spatially in such a fashion that they are inversely related to each other via functional dependencies of each on vegetation surface area density and/or inverse depth, *X*. Specifically, Carleton presumed velocity *u* and reaction rate coefficient *k* to be related to *X* in the following manner

$$u = \frac{\gamma}{X^{1/2}} \tag{1.13}$$

and

$$k = \zeta X \tag{1.14}$$

respectively, where γ and ζ are constants. Assuming a uniform flow path length L, Damköhler number for stream tube "i" is estimated to be a power function of residence time τ_i by combining equations and eliminating X:

$$Da = k_i \tau_i = k_i \frac{L}{u_i} = \zeta (\frac{\gamma}{L})^2 \tau_i^{\ 3} = A \tau_i^{\ 3} \qquad (1.15)$$

The Damköhler number represents the ratio of the rate of consumption by reaction to the rate of transport by advection in the wetland. Use of this relationship in an integration over the RTD (e.g. eq. 1.6) produces an expression for $C(y)$ whose parameters are unaffected by changes in HLR. The assumed underlying mechanism (eqs. 1.13 and 1.14) therefore implies an explanation for the HLR dependence of k in PFR models. The apparent dependence of k on HLR can also arise from fitting a zero-C^* PFR model to a data set that exhibits a non-zero background, as Kadlec's (2000) analysis showed.

Another potential explanation for the dependence was provided by Kadlec (2003), who suggested that water quality constituents that lump multiple constituents together (e.g. BOD, TSS, TP, and TN) are characterized by distributions of reaction rate coefficients, or "kVD"s. As transport through a wetland proceeds, such a mixture becomes "weathered", with the more reactive components disappearing more quickly, and the mean reaction rate coefficient for the remaining mixture continually decreasing. Kadlec noted that both non-uniform residence times and distributions of k values in constituent mixtures could contribute to concentration declines that do not follow the sort of behavior expected from the PFR model. In place of the PFR model, Kadlec proposed the use of a "relaxed TIS" model, identical in form to eq. 1.12, but in which the parameters (e.g. α and k) are treated solely as fitting parameters, and

which “offers the ability to embody both (RTD) and kVD effects”. Carleton’s analysis (2002) demonstrated that a relaxed TIS model can embody DND effects (meaning spatially heterogeneous reaction rates inversely related to local velocities) as well (Figure 1.8), thus for lumped parameters the effects of constituent weathering may be impossible to separate from the effects of heterogeneous Damköhler numbers.

Wong et al. (2006) noted that in addition to wetlands, various stormwater treatment practices display dependence of PFR k and C^* on HLR, and proposed use of the k-C^* TIS model as a “unified stormwater treatment model” for swales, detention ponds, biofilters, and stormwater treatment wetlands, in which the value of α can be back-calculated from t_p and τ measurements using eq. 1.7. Carleton (2002) and Kadlec (2003) both noted that α values derived from fitting data sets with eq. 1.12 would be expected to be different from those associated with RTDs measured in the same systems, because of the impacts that distributions (spatial and temporal, respectively) of k values have on net reaction dynamics. The DND model accounts for the effects of HLR mechanistically, but the issue of possible dependence of parameters of the relaxed TIS model on HLR has not yet been addressed in the literature.

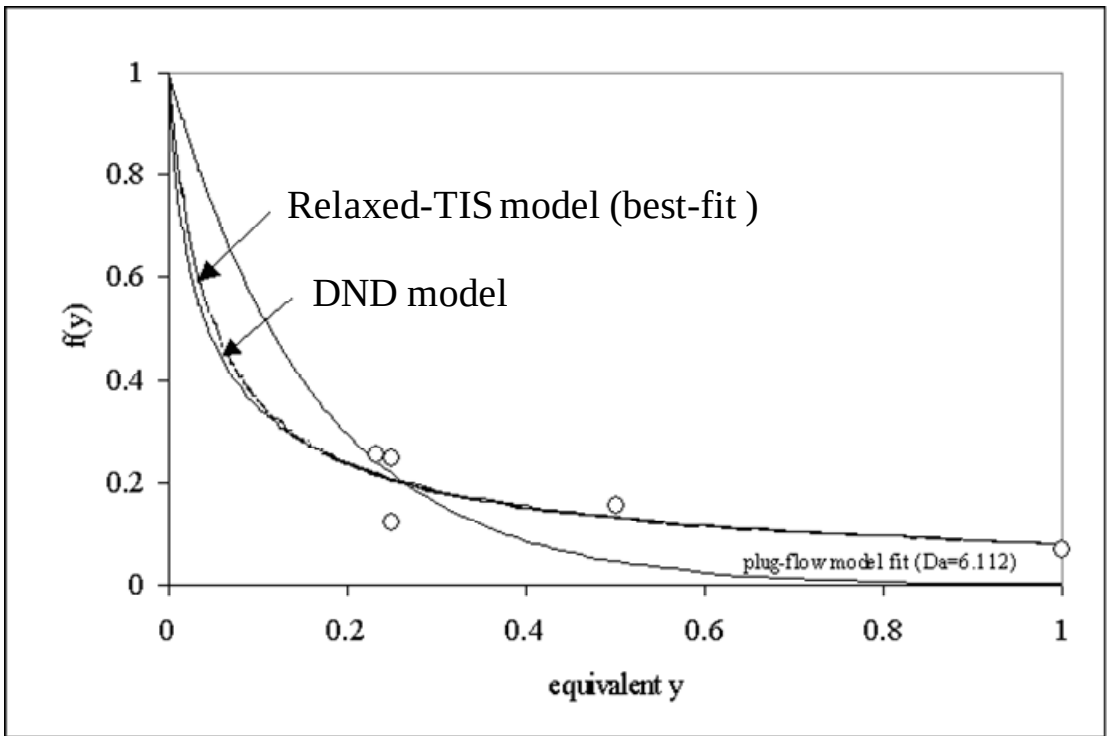

Figure 1.8 Gustine wetland cell BOD5 data and various best-fit model approximations, adapted from Carleton (2002).

1.3 Summary

Wetlands have been shown to be effective at treating a variety of water pollution problems. Plug-flow models, which presume uniform velocity, have been widely used to characterize treatment wetland performance. However, evidence suggests that far from being uniform, velocities within wetlands are highly heterogeneous as a result of spatial variations in vegetation density and water depth. Longitudinal solute dispersion within wetlands appears to be dominated by advective velocity gradients, with the consequence that flow regimes may be best described as pre-asymptotic (non-Fickian). One implication of this is that advection-dispersion models cannot necessarily be assumed to adequately describe constituent transport within wetlands.

Neither PFR nor advection-dispersion-reaction models are able to "explain" dependencies of wetland *k* values on hydraulic loading. The DND approach, which treats flow as stochastic-convective, is able to account for the phenomenon by treating *k* and velocities as both spatially heterogeneous, and inversely interrelated to each other (the TIS model of eq. 1.12 is equivalent to a DND model with uniform *k*). However, the DND approach is hampered by other potential limitations, most notably the steady-state flow and stochastic-convective transport assumptions.

For water quality parameters that lump multiple constituents together (e.g. TP, TN, BOD, etc.), Kadlec (2003) has shown that "weathering" of constituent mixtures with corresponding enrichment in less reactive components can also account for the HLR dependency of PFR *k* values. Observation of HLR-dependent *k* values in wetlands for constituents that do not fall into this category would imply the presence of DND effects, since the chemical properties of such constituents presumably do not change with time. For constituents composed of mixtures, the phenomenon may reflect a combination of DND and kVD effects that are impossible to disentangle from each other. For either category of water quality constituent (lumped or simple) the relaxed-TIS model of eq. 1.12 (and therefore potentially the DND model also, since it is able to produce essentially identical results), may provide a decent empirical fit to data, though the resulting back-calculated parameters are not necessarily physically interpretable. Specifically, the α value (apparent number of tanks or inverse dimensionless variance) for a reactive constituent's decay profile in such a wetland will not be the same as the α value estimated for the same system by measurement of an inert tracer's breakthrough curve (RTD).

The DND approach of Carleton (2002) and the related relaxed-TIS approach of Kadlec (2003) provide modeling methods that embody plausible mechanistic explanations for documented inadequacies in more established wetland modeling approaches. However both approaches presume steady-state flow conditions and constant influent concentrations, neither of which typically characterize real treatment wetlands for long periods of time. Wetland effluent at any given moment represents an average of constituent elements that entered at different times and potentially at different concentrations, and that followed different paths in getting from the inlet to the outlet. To fully account for these effects, an approach is needed that considers both DND (and/or kVD) effects and time-varying flows and influent concentrations.

An important deficit in current knowledge about wetland transport, and therefore about appropriate choice of modeling methodologies, is the degree to which longitudinal dispersion in wetlands is appropriately characterized as stochastic-convective in nature, or alternatively as Fickian, or else is intermediate between these two extremes. In the face of uncertainty on this question, approaches are needed which, like the DND approach, account for spatial heterogeneity in velocity and reaction rate coefficients, but which unlike the DND approach, also take into account transverse diffusive/dispersive flux, so that evolving longitudinal dispersion may be properly accounted for. To this end there is a need for new general purpose ("simple") reactor transport models that can account for key processes determining performance while employing a minimal number of parameters or unknowns. Because diffusive processes are to be included and then averaged over Representative Elementary Volumes (REVs), the development of such models will involve

mathematical approximations of higher order terms (closures), thus these models will constitute approximate solutions to governing transport equations. In order to evaluate the accuracy of such models, particularly with respect to the influence of evolving dispersion, exact analytical solutions to governing equations are needed as well, at least for some specific sets of conditions and/or parameters. Comparison of simple model results against these exact solutions over a range of conditions/parameters can be used to evaluate the applicability of the simple model to specific flow regimes.

1.4 Objectives

The primary objectives of this study are to develop new modeling approaches for wetlands that accomplish three specific aims:

1. Develop and evaluate a version of the DND model capable of accounting for temporally-varying flow and influent concentrations.
2. Develop and evaluate an analytical model of reactive transport in a system with spatially variable flow velocity and reaction to serve as a benchmark for evaluating simplified models.
3. Develop and evaluate a wetland performance model that contains a minimal number of parameters, but which uses stochastic principles to account for the influence of spatial heterogeneity on advection and reaction, and which (unlike the DND model) accounts for transverse diffusion and the development of shear flow dispersion.

The new models will be evaluated by examining their ability to reproduce wetland field data sets, and through comparisons of their results against those of other, more

established treatment wetland models. Results are expected to advance our understanding of the key processes that determine wetland transport behavior and enhance our ability to both quantitatively analyze wetland function and design FWS wetland systems.

Chapter 2: A Modeling Approach for Mixing and Reaction in Wetlands with Continuously Varying Flow

2.1 Abstract

Prior investigations have examined steady-state flow in surface flow treatment wetlands, with mixing modeled as advection-dominated, and reaction calculated using flow-weighted averages over collections of stream tubes with different velocities. This work extends these concepts to non-steady flow conditions and temporally varying inlet concentrations. The essential construct that makes the approach feasible is definition of a set of reference (steady) state conditions under which the residence time distribution (RTD) and stream-tube specific rate constants are defined. Residence time in any stream tube under non-steady flow is treated as a linear function of its reference-condition residence time, and the overall wetland retention time under both mean and varying flow regimes. Outlet concentration is found by convolution of the reaction term with a varying inlet concentration function. For real-world flow and concentration data collected at discrete points in time, integration for outlet concentration is approximated using linear interpolation to generate inlet concentrations and velocities at intermediate points in time. The approach is examined using data from the literature. Vegetation density and depth distributions are seen as central in determining mixing and treatment performance.

Notation

A, B	parameters of power function relating Damökhler number to residence time
A_c	vertical cross-sectional area orthogonal to direction of flow
$C_{out}(t)$	flux concentration as a function of time
C^*	background concentration
D	dispersion coefficient
Da	Damökhler number
$E(\tau)$	residence time distribution function (RTD)
h	water depth
k	volumetric reaction rate decay coefficient
L	wetland length
t	chronological time
T	residence time-upon-exit
u_i	velocity along flow path 'i', temporally varying
u_m	mean water velocity over all flow paths, temporally varying
$u_{x,z}$	horizontal velocity in x and z directions
x	dimension in the direction of flow (horizontal)
X	vegetation-litter surface area density, or reciprocal depth
y	(residence time-on-exit)/(reference condition residence time)
z	dimension in the horizontal direction orthogonal to flow
α,β	parameters relating stream tube u and k to depth (h)
γ,ζ	parameters relating stream tube u and k to vegetation density (X)
σ^2	variance of RTD

τ residence time for the reference RTD

2.2 Introduction

2.2.1 Flow Through Wetlands

Surface water movement through wetlands resembles open channel flow in some respects, and saturated porous media flow in other respects. Stands of emergent plants form a kind of porous medium in which tortuosity is forced upon flow paths by the physical obstructions created by stems and litter. Biofilms adhering to these surfaces may be largely responsible for removal of some solutes from the water column, and thus for the acknowledged tendency of wetlands to improve water quality. Unlike in flow through soils, the relatively discontinuous nature of the stationary media (plant stems and leaves) and related high "porosity" (i.e. typically 90% or higher) in wetlands allows the formation of downstream stem wakes (Nepf et al., 1997a), the properties of which depend in part on stem-based Reynold's numbers. While bulk wetland flow is typically in the laminar or transitional range, local turbulence (i.e. eddies) may therefore nevertheless occur at the scale of stem wakes (White and Nepf, 2003), resulting in dispersion that may be locally Fickian, even while bulk longitudinal mixing is non-Fickian.

Many aspects of flow and mixing in wetlands are poorly understood, including the correct form of the force-balance equation governing bulk fluid flow. According to Kadlec and Knight (1996), wetland surface flows consist of gradually varying flow on very mild slopes, so that kinetic energy changes are "usually negligible compared to potential energy changes", with the result that energy and momentum balances simplify to statements of equivalence between potential energy and resulting frictional work, i.e. gravitational forces balanced exactly by frictional

forces. Bolster and Saiers (2002) and Feng and Molz (1997) developed two-dimensional numerical models of surface wetland flow patterns, based in part upon this assumption, i.e. that the momentum balance equation simplifies to a statement of equivalence between the total energy slope *S* and the water surface gradient:

$$S = -\frac{\partial h}{\partial x} \tag{2.1}$$

where *h* is water depth and *x* is distance in the direction of flow. If precipitation, evapotranspiration, and gains or losses to groundwater seepage are ignored, for steady-flow conditions the fluid continuity (mass) equation in two dimensions becomes:

$$\frac{\partial u_x}{\partial x} + \frac{\partial u_z}{\partial y} = 0 \tag{2.2}$$

where u_x and u_z represent fluid velocity in two orthogonal horizontal directions.

For flow in one predominant direction, one-dimensional friction equations analogous to those for open channel flow may be employed to characterize advection. Manning's equation is generally not suitable, given the non-turbulent nature of wetland flow (Kadlec and Knight, 1996), therefore an alternative governing friction equation is required. Two general possibilities exist, based upon different possible relationships between velocity, water surface gradient, depth, and vegetation density.

Nepf (1999) employed the following friction-balance relation to characterize flow through emergent wetland vegetation:

$$(1 - Xd)C_B U^2 + \frac{1}{2} C_D Xd \left(\frac{h}{d}\right) U^2 = gh\frac{\partial h}{\partial x} \tag{2.3}$$

where U is bulk velocity, d is stem diameter, X is projected plant area per unit volume (i.e. vegetation surface area density), and C_B and C_D are bed and bulk vegetation drag coefficients, respectively. Nepf determined that for bulk flow, bed shear can be considered negligible compared with shear produced by vegetation. In accordance with this assumption, if the first term (bottom drag) on the left side of the equation is ignored, the result is a version of a formula also suggested by Kadlec (1990) for describing the relation between friction (i.e. water surface) slope and stem drag:

$$\frac{1}{2} C_D X d \left(\frac{h}{d} \right) U^2 = g h \frac{\partial h}{\partial x} \tag{2.4}$$

Rearranging to solve for velocity produces:

$$U = \left(\frac{2g\left(\partial h / \partial x\right)}{C_D X} \right)^{1/2} \tag{2.5}$$

or

$$U = \frac{\gamma}{X^{1/2}} \tag{2.6}$$

where

$$\gamma = \left(\frac{2g}{C_D} \frac{\partial h}{\partial x} \right)^{1/2} \tag{2.7}$$

Equations that describe the physical behavior of water at the stream-tube scale do not necessarily also describe the bulk behavior of collections of stream tubes considered in aggregate at the whole-wetland scale. Equation 2.6 describes bulk, rather than stream tube scale flow properties. However if X measurements happen to follow a lognormal distribution when sampled at a physical scale comparable to that corresponding to flow heterogeneities, the equation may also be interpreted as

describing stream tube scale properties: the mean of the distribution of U values obtained by substituting a lognormal distribution for X into equation 2.6 is the same as the U value derived with the mean value of X substituted into the equation.

It is also possible that rather than being proportional to the square root of water surface gradient as in eq. 2.5, wetland bulk fluid velocity is directly proportional to gradient. Kadlec and Knight (1996) suggested the following empirical governing equation based upon their analyses of flow data from numerous treatment wetlands:

$$U = ah^{b-1}\left(\frac{\partial h}{\partial x}\right)^{c} \tag{2.8}$$

where a, b and c are tentatively suggested to have the following values: $a = 10^7$ $m^{-1}d^{-1}$ for densely vegetated wetlands and 5×10^7 $m^{-1}d^{-1}$ for sparsely vegetated wetlands, b=3, and c=1, so that for example $U = 10^7 h^2\left(\frac{\partial h}{\partial x}\right)$ for a densely vegetated system, (h in units of meters).

2.2.2 Dispersion and Mixing in Wetlands

In transport through porous media, shear-flow dispersion, as defined by Taylor (1954), arises from an interaction between non-uniform advection and transverse diffusion of solute across stream lines. After some initial time period, the net effect of this interaction is a kind of solute spreading that is analogous to diffusion, and appears to obey Fick's first law of diffusion, in which diffusive mass flux is proportional to the concentration gradient (Chapra, 1997) via a dispersion (rather than diffusion) coefficient. For dispersion to be treated as "Fickian" implies

that the dispersion coefficient is constant. When this is the case the overall transport process can be modeled using standard advection-dispersion equation approaches.

According to Gelhar (1993), the dispersion coefficient is proportional to the rate of increase of spatial variance (σ_x^2) in concentration of an inert tracer following pulse injection:

$$D = \frac{1}{2}\frac{d\sigma_x^2}{dt} \tag{2.9}$$

Thus, for a transport system to be characterized as Fickian implies that the spatial variance of an inert tracer cloud should increase linearly with time.

By contrast, limited published tracer curves from studies on surface flow treatment wetlands (Werner and Kadlec, 2000), show dimensionless temporal variance (variance divided by the square of retention time) that appears to be invariant with distance traveled. The variance of these curves increases with the square of distance traveled (or equivalently, time elapsed), rather than in direct proportion to distance or time, as would be required for *D* to be constant. This general type of spreading, which has also been documented in situations as diverse as laminar transport through soils (Gelhar, 1993) and transport in turbulent streams (Day, 1977), has been called by various authors “pre-asymptotic”, “non-Fickian”, “anomalous”, or “stochastic-convective” (Levy and Berkowitz, 2003; Simmons et al., 1995; Zou et al., 1996). This type of mixing occurs in systems in which movement of solute transverse to the predominant flow direction is relatively negligible, so that longitudinal solute spreading is dominated by advective velocity gradients. In such systems, solutes travel as if they were being transported through collections of parallel stream tubes that do not interact with each other.

2.2.3 Explanations for Non-Fickian Mixing

Several authors have derived theoretical representations of the gradual development of longitudinal dispersion, from stochastic-convective to Fickian regimes, in steady flow through various kinds of porous media. Gelhar et al. (1979) used spectral analysis of hydraulic conductivity (*K*) fluctuations in a stationary medium to develop the relationship reproduced in Figure 2.1, where α_T is transverse dispersivity, *U* is mean velocity, and *l* is the correlation length scale for *K*, which is assumed to possess a "hole-type" autocovariance structure. In Figure 2.1 longitudinal dispersivity is expressed as a function of distance traveled multiplied by transverse dispersivity, and normalized by a characteristic length scale. The latter is a function of the sizes of heterogeneities in, and the nature of the autocorrelation structure of, the medium. Dagan (1984) derived a similar relationship for an isotropic medium with K possessing an exponential autocovariance structure. On the left side of Figure 2.1 (circled region), the quantity A/A_∞ (i.e. the relative macro-scale dispersivity) increases linearly with time; this region with a slope of 1:1 represents stochastic-convective flow. Towards the right side of this figure the asymptotic dispersivity is approached, wherein dispersion becomes Fickian. Kemblowski and Wen (1993) similarly examined the case of fractal permeability distributions, in which the variance in *K* is bounded only by the size of the system. In their example, flow remains pre-asymptotic throughout the entire range examined. These examples demonstrate theoretical bases for solute dispersion during transport through porous media manifesting non-Fickian, or asymptotically Fickian, character.

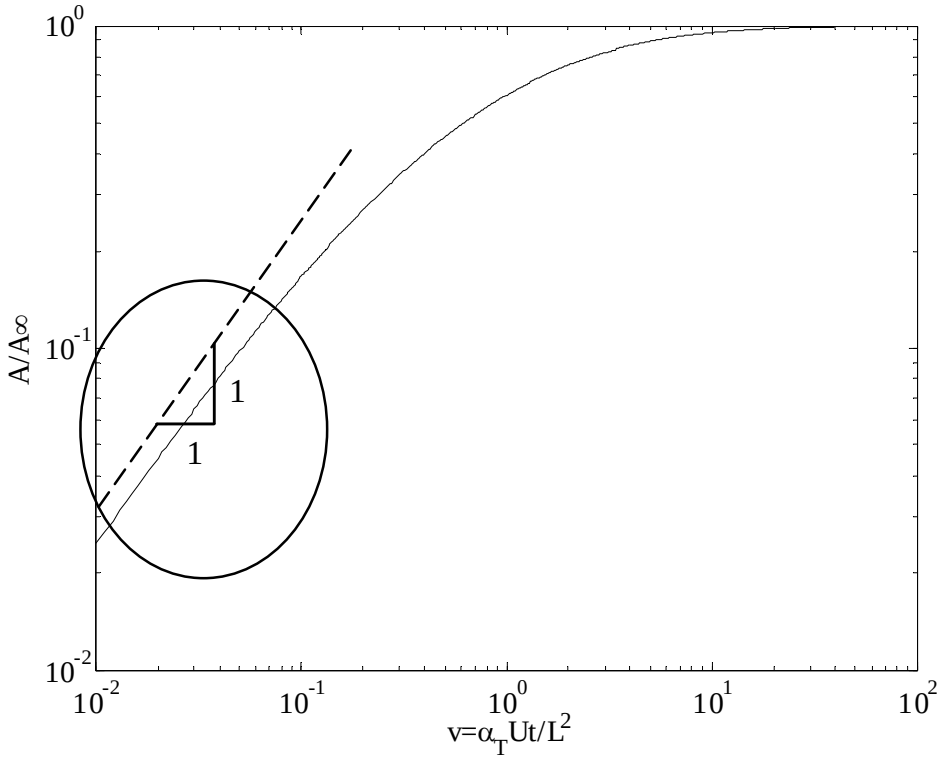

Figure 2.1 Development of longitudinal dispersion in stratified medium with hole-type conductivity covariance structure (Gelhar et al., 1979). Stochastic-convective region is circled.

Strong transverse gradients in longitudinal velocity that presumably contribute to non-Fickian mixing may also result from the effects of local depth on vertically-averaged velocity in surface flow, when depths are strongly correlated in the downstream direction, i.e. when cross-sectional shape remains relatively constant in the direction of flow. This may help explain why longitudinal mixing even in non-vegetated streams has been observed to be non-Fickian.

Employing the assumption that mixing in surface flow wetlands is stochastic-convective, Carleton (2002) proposed that the flux concentration of a solute exiting a wetland can be treated conceptually as a flow-weighted average over a collection of stream tubes with differing velocities. This "Damköhler number distribution" (DND)

approach also incorporated the presumption that local stream tube velocity (u) and volumetric constituent removal coefficient (k) are functions of vegetation surface area density ("X", for example with units of m^2/m^3). In this derivation, X was assumed to vary only in the plane perpendicular to flow, and to be invariant (or perfectly autocorrelated) in the flow direction. The primary advantage of this approach is that it provides a quantitative method, derived from a plausible mechanistic explanation, for characterizing the curious phenomena wherein reaction rate coefficients appear to be functions of hydraulic loading rate (Kadlec, 2000). Important limitations of the approach are that it is restricted to an assumption of steady flow, and that transverse and diffusive mixing are ignored.

The primary objective of this work is to extend the DND modeling approach to non-steady flow conditions, and to evaluate model adequacy by comparing predicted concentrations with monitored concentrations from field studies. A secondary objective is to compare model results with those generated using the k-C^* plug-flow model (PFR), which is commonly used to characterize wetland performance (Kadlec and Knight, 1996).

2.3 Derivation of the Model

2.3.1 The Steady-Flow Case

The DND approach employs the following assumptions. Flow is considered to be two-dimensional in the sense that vegetation density (and/or reciprocal depth) X varies only in the horizontal direction transverse to flow (dimension z in this case), and not in the direction of flow (x). Therefore k and u are functions of z but not of x. Transport in the vertical dimension is not considered: stream tube parameters (k and

u) are taken to represent depth-weighted averages. With stream-tube specific advection and reaction considered, and longitudinal dispersion ignored, the governing solute mass balance within a stream tube subject to time-varying inlet boundary conditions is:

$$\frac{\partial C}{\partial t} = -k(z)C - u(z)\frac{\partial C}{\partial x} \tag{2.10}$$

If X represents vegetation density, as discussed previously, then velocity u and reaction rate coefficient k are assumed to be related to X by (compare with eq. 2.6)

$$u = \frac{\gamma}{X^{n}} \tag{2.11}$$

and

$$k = \zeta X \tag{2.12}$$

respectively, where γ, ζ, and n are constants. With flow path length L, Damköhler number (Da) for stream tube "i" can be expressed as a power function of residence time τ_i by combining equations and eliminating X:

$$Da = k_i\tau_i = k_i\frac{L}{u_i} = \zeta(\frac{\gamma}{L})^{1/n}\tau_i^{\,1/n+1} = A\tau_i^{\,B} \tag{2.13}$$

Alternatively, if X is taken to represent the reciprocal of stream tube depth, then we may assume that vertically-averaged velocity and reaction rate coefficients are related to X by

$$u = \frac{\alpha}{X^{n}} \tag{2.14}$$

and

$$k = \beta X \tag{2.15}$$

respectively, where α, β and n are constants, with n most likely <1 (see for example velocity and depth profiles given in Bogle, 1997). The sort of inverse dependence of reaction rate on depth represented by eq. 2.15 may occur particularly for constituents that are removed via mass transfer from the water column into the benthic layer, and has been observed to occur both in wetlands (Kadlec and Knight, 1996) and in stream environments (Alexander et al., 2000, 2004). By combining equations 2.14 and 2.15 and eliminating X, a relationship results which is identical in form to equation 2.13:

$$Da = k_i \tau_i = \beta (\frac{\alpha}{L})^{1/n} \tau_i^{1/n+1} = A \tau_i^{B} \qquad (2.16)$$

Confirmation of the validity of the essential concepts inherent in this approach has recently been provided through an investigation of a wetland in Florida (Dierberg et al., 2005). In the studied wetland, locally lower k values for Total Phosphorus (TP) removal were found to characterize channels within the wetland that were both deeper (faster flowing) and less densely vegetated than other areas within the wetland.

Whether X represents vegetation density or reciprocal depth, we assume that it varies only in the plane orthogonal to flow, and is invariant in the flow direction. High degrees of long-range autocorrelation in the direction of flow may be more likely for depth than for vegetation density in some systems. It is unfortunate that the effects of vegetation and depth are indistinguishable from each other in terms of their relative contributions to coefficients A and B in equation 2.13 or 2.16. In flowing waters, vegetation density may itself also be correlated with depth (Chambers et al., 1991), further complicating interpretations of A and B, and making it unlikely that suitable values for these parameters can be derived *a priori* from quantifiable characteristics or physical principles.

With a pulse (Dirac delta) addition comprising the upstream (inlet) boundary condition in stream tube "*i*", the solute mass balance equation includes stream-tube specific advective and reactive (but no dispersive) terms:

$$\frac{\partial C_i}{\partial t} = -k_i C_i - u_i \frac{\partial C_i}{\partial x} \tag{2.17}$$

B.C.: $C_i(0,t) = \delta(t)$

This equation has the general solution

$$C_i(x,t) = e^{-k_i t} \cdot \delta(x - u_i t) \tag{2.18}$$

For more general boundary conditions $C_i(0,t) = g_i(t)$, the concentration can be found via convolution as follows

$$C_i(x,t) = \int_0^t e^{-k_i(t-\varphi)} \cdot \delta(x - u_i(t-\varphi)) g_i(\varphi) d\varphi \ , \tag{2.19}$$

where $\varphi = t - \tau$. This simplifies to

$$C_i(x,t) = e^{-k_i \tau_i} \cdot g(t - \tau_i) \tag{2.20}$$

where $\tau_i = \frac{x}{u_i}$, or $\tau_i = \frac{L}{u_i}$ at the outlet. Given a wetland's residence time distribution (RTD) function $E(\tau)$, the outlet flux concentration for the wetland as a whole can then be found by integrating over all residence times (i.e. stream tubes), as first proposed by Danckwerts (1953), and later explored by Levenspiel (1972):

$$C(t) = \int_0^\infty g(t-\tau) E(\tau) e^{-k\tau} d\tau \tag{2.21}$$

A power function relationship between Damköhler number and residence time (eq. 2.13 or 2.16) can be incorporated into this relationship either by first converting

the RTD into a distribution of Damköhler numbers and integrating over this distribution (Carleton, 2002), or by simply incorporating the power function directly into the reaction term:

$$C(t) = \int_0^\infty g(t-\tau)E(\tau)e^{-A\tau^B}d\tau \tag{2.22}$$

or

$$C_{out}(t) = \int_0^\infty C_{in}(t-\tau)E(\tau)e^{-A\tau^B}d\tau \tag{2.23}$$

where C_{in} and C_{out} refer to concentrations at the inlet and outlet of the wetland, respectively. Explicit consideration of an irreducible background concentration (C^*) can be incorporated as follows:

$$C_{out}(t) = C^* + \int_0^\infty \left(C_{in}(t-\tau) - C^*\right)E(\tau)e^{-A\tau^B}d\tau \tag{2.24}$$

Given data on percent removal of a pollutant from a wetland (or stream) under a range of hydraulic loading rates, or concentrations at different distances from the inlet under constant flow, A and/or B may be estimated using least-squares minimization of a suitably defined objective function.

2.3.2 The Non-Steady Flow Case

The approach is extended to non-steady conditions by employing the assumption that (unlike residence time) stream-tube k is not a function of velocity, and therefore does not vary over time. Wetland water volume is also assumed to be constant: velocity changes are caused by gradient changes, and do not involve changes in depth. The approach begins with consideration of flow during steady-state conditions. Figure 2.2 shows a plan view of a hypothetical velocity profile of parallel

stream tubes traversing a wetland under steady flow. Here u_{mean} refers to the mean velocity (flow divided by cross-sectional area), u_{max} to the maximum stream tube velocity, and u_i to the velocity in stream tube '*i*'. Stochastic-convective mixing implies that the ratio between the velocities in any two stream tubes is constant, even if the mean velocity changes due to an alteration in flow. If u_{mean} changes by some percentage, the velocities in all stream tubes are assumed to simultaneously change by the same percentage. Thus all stream tube velocities scale to the instantaneous mean velocity. The stream tube velocity scaling factors can be obtained from the relative velocities implied by the RTD (for uniform flow path length) under steady flow conditions. The non-steady DND approach therefore employs a wetland's RTD, which is assumed to have been measured under steady-state "reference" conditions.

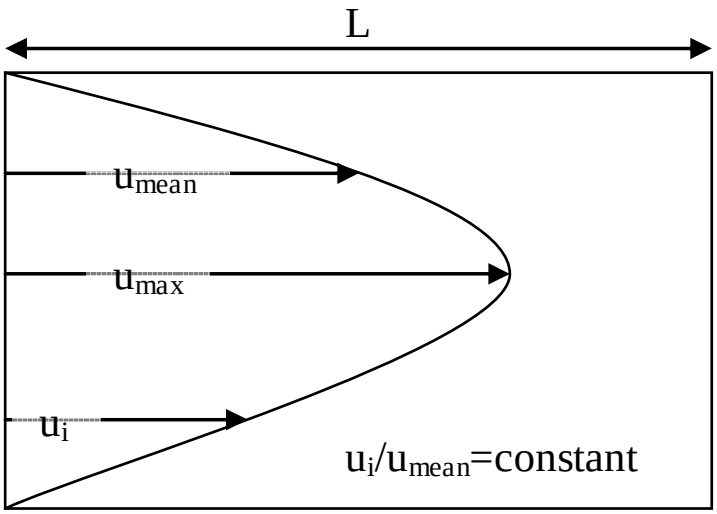

Figure 2.2 Hypothetical flow velocity profile (plan view) in a wetland or stream.

For the unsteady flow model, the calculation of outlet concentrations employs three different variables representing time: 'τ' represents residence times for the

reference RTD. Inlet and outlet concentrations are expressed as functions of '*t*', which represents true, or chronological time. The third time variable '*T*', is residence time-upon-exit; that is to say, the amount of time that water exiting the wetland at time *t* in any given stream tube has actually spent inside the wetland. Using these three interrelated time variables, the governing equation for outlet flux constituent concentration is given by the following integral, related to eq. 2.24:

$$C_{out}(t) = C^* + \int_0^\infty \left(C_{in}(t - \tau y) - C^*\right) E(\tau) e^{-k\tau y} d\tau \qquad (2.25)$$

where $y = T_i/\tau_i$, or the ratio between residence time-on-exit and reference condition residence time for flow path *i*. Under steady flow conditions this definition of *y* becomes the same as 'equivalent *y*', as defined by Carleton (2002). Under continuously varying flow conditions, *y* assumes a different value for each flow path, and for each flow path also assumes a different value at each point in time (*t*). As in the steady-state case, outlet concentration is found by integrating over the RTD, however decay is calculated as a function of residence time-upon-exit ($\tau y = T$), rather than (reference condition) residence time.

Flow and concentration data obtained from real wetlands are discrete rather than continuous in nature. The following discrete analogue to equation 2.25 is therefore used to evaluate outlet concentrations, given as input data inlet concentrations and flow rates measured at discrete points in time (e.g. daily):

$$C_{out}(t) = C^* + \sum_{i=1}^{n} \left[C_{in}(t - \tau_i y_i) - C^*\right] E(\tau_i) e^{-k\tau y_i} \qquad (2.26)$$

Interdependencies between stream tube specific k and τ that arise from their presumed simultaneous dependence on vegetation density and/or depth (eq. 2.13 or 2.16) are then easily incorporated:

$$C_{out}(t) = C^* + \sum_{i=1}^{n} \left[C_{in}(t - \tau_i y_i) - C^* \right] E(\tau_i) e^{-A\tau^B y_i} \tag{2.27}$$

To evaluate the summation in equation 2.27, it is necessary to obtain values of y for each stream tube. In other words, values of T_i are required which correspond with each value of τ_i. Under the stochastic-convective flow assumption, a relationship between T_i and τ_i may be obtained directly from the temporally varying mean velocity function (u_m), as illustrated in Figure 2.3. Given a velocity vector (e.g. daily flow values divided by mean cross-sectional area) as in Figure 2.3a, T_i is found by integrating u_m backward in time until travel distance L is reached (Figure 2.3b), making use of the assumption that for any flow path, u_i/u_{mean} is constant, irrespective of the instantaneous value of u_m. T_i is defined implicitly by the following equation:

$$\int_0^{T_i} \frac{\tau_{mean}}{\tau_i} u_m(t - \sigma) d\sigma = L \tag{2.28}$$

which may be rearranged to produce the following relationship:

$$\int_0^{T_i} u_m(t - \sigma) d\sigma = L \frac{\tau_i}{\tau_{mean}} = \tau_i u_{mean} \tag{2.29}$$

where u_{mean} is mean velocity under reference conditions, and σ is a dummy variable of integration. It should be noted that these expressions are closely related to the concept of dimensionless time (ϕ) as defined by Werner and Kadlec (1996), the primary difference being that ϕ is defined through a forward integration of velocity in time:

$$\phi(s) = \frac{V_{out}(s)}{V_{sys}} \tag{2.30}$$

Using their notation for elapsed time, $s=t-\lambda$, these quantities can be defined as follows:

$$V_{out}(s) = A_c \int_{\lambda}^{t} u_m(\sigma) d\sigma \tag{2.31}$$

and

$$V_{sys} = A_c \int_{\lambda}^{\infty} u_m(\sigma) d\sigma \tag{2.32}$$

where A_c is cross-sectional area in a plane orthogonal to the flow direction.

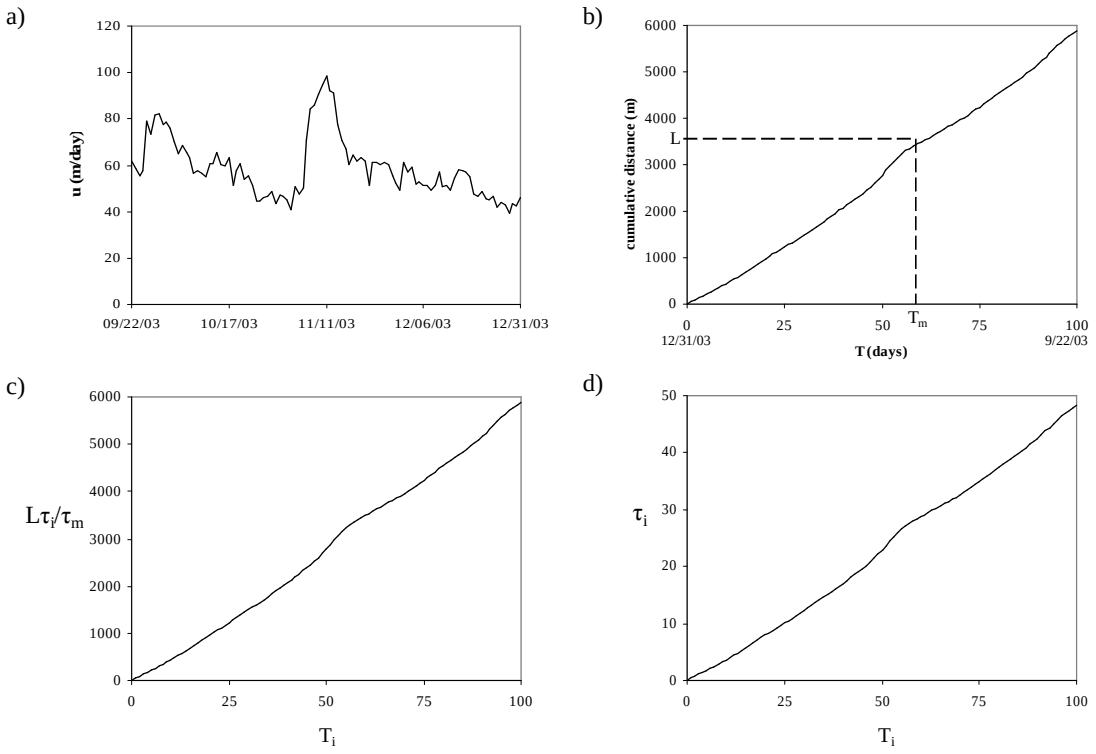

Figure 2.3 Illustration of derivation of τ vs. T curve from temporally-varying mean velocity (u_m): a) example wetland u_m for a 100 day period; b) u_m integrated backward in time over same period, with residence time-on-exit (T) for flow length L shown; c) y-axis shown scaled by ratio of flow-path residence times; d) y-axis divided by mean velocity under reference conditions to produce τ_i vs. T_i curve.

The curve in Figure 2.3b illustrates cumulative distance as a function of negative time t (relative to some fixed value of t) for an example mean wetland velocity vector (u_m), using linear interpolation to connect discrete (daily) data points. Some value on the y axis corresponds with L, the travel distance from inlet to outlet. As shown in Figure 2.3b, by reading over to the curve from L on the y-axis, and sending a line down to the x-axis, one may find the residence time-on-exit for the mean flow path, T_m. However, the curve is actually more useful than this. Given a continuous distribution of residence times, every value on the y axis corresponds with L for some flow path. The y axis can be thought of as L scaled by τ_i/τ_{mean} (Figure

2.3c). Since L and τ_{mean} are both constants whose quotient is u_{mean}, the y axis in Figure 2.3c can also be interpreted as $\tau_i u_{mean}$ (eq. 2.29). Therefore if one divides all y-axis values by u_{mean}, the resulting curve represents τ_i plotted as a function of T_i (Figure 2.3d).

The relationship embodied in this curve can thus be used to calculate y values for any i. These values can then be used in equation 2.27 to evaluate $C_{out}(t)$. This approach was implemented by the authors in a MATLAB® routine given the working designation "Wetloop". Wetloop uses a daily-discretized version of a gamma distribution (truncated on the upper end at a day representing ≥95% of the cumulative area under the theoretical curve) with user-selectable shape and scale parameters to represent the RTD (Carleton, 2002). Note that alternative functional forms for the RTD, such as would be produced by the velocity distributions explored by Grismer for subsurface flow wetlands (2005), could also be accommodated through a simple code change. Wetloop reads a text file of wetland flow velocities and inlet concentrations arranged by date, and uses linear interpolation to fill in values for any missing days. Beginning with the last date in the file and working backward one day at a time, Wetloop integrates the velocity vector backward in time from the given date, and derives a τ_i *vs.* T_i curve specific for that value of t, as in Figure 2.3d. With each day in the RTD representing a separate flow path 'i', the program uses the τ_i *vs.* T_i curve to estimate T for each value of τ in the RTD. Following equation 2.27, Wetloop computes the product of $C_{in}(t\text{-}T)$ (adjusted for C*), the RTD function, and the fraction decay, calculates the stream tube exit concentration, then repeats the process for all n 'i' values, and sums the result to give the estimated outlet

concentration for each date (t) in the input file. As with the shape and scale parameters of the RTD, flow path length L and reaction-related parameters A and B are user-selectable parameters.

In contrast with the unsteady DND model, the k-C^* PFR model, which is commonly applied to data from wetlands, employs an assumption that flow is uniform as well as steady-state. Rather than distributions, a single k and residence time (τ) are used to characterize constituent reaction and transport:

$$\frac{C_o - C^*}{C_i - C^*} = e^{-k\tau} \tag{2.33}$$

where C_i and C_o are inlet and outlet concentrations, respectively. It should be evident that this model is equivalent to a simplified version of the DND model under uniform residence time (plug-flow) conditions.

2.4 Methodology for Model Testing

To evaluate the non-steady DND approach and the Wetloop model, lengthy time series flow and concentration (inlet and outlet) data from published studies on wetlands were sought. The goal was to evaluate the performance of the model by feeding inlet velocity and concentration time series into Wetloop, then comparing the resulting predicted outlet concentrations against measured concentrations, selecting parameter values through a model error minimization process. An ideal data set for this purpose would come from a wetland possessing simple (e.g. rectangular) geometry, would include a well-characterized RTD, and would have both flow and inlet concentration that change fairly dramatically during the study, yet remain relatively constant at various levels for long enough that outlet concentrations have time to periodically stabilize. Although no data sets meeting these criteria were

found, two data sets that each met some of these criteria were obtained for model evaluation purposes. Model evaluation employing these data sets focused primarily on reasonableness of predicted outlet concentrations compared with measured ones. Regression of predicted vs. measured outlet concentrations was employed as a quantitative measure of model adequacy. For one data set, flow-related bias was also evaluated by regressing model errors against flow rates. Results were compared against the same kind of analysis conducted for a *k-C** PFR model fit to the same data.

2.4.1 Example 1: The Gustine Wetlands

The Gustine wetlands are a series of five equally sized, rectangular, vegetated cells used to provide secondary treatment of domestic wastewater in Gustine, California. Walker and Walker (1990) measured BOD_5 removal from the cells over a 13 month period, during which each cell was operated under a different mean hydraulic loading rate (3.8 to 16.2 m/year). Kadlec (2000) reported that regression of the *k-C** PFR model against inlet/outlet data results in an apparent dependence of *k* on hydraulic loading rate among these wetlands. Carleton (2002) demonstrated that this phenomenon can be understood as resulting in part from an inverse square root relationship between stream tube velocity and vegetation surface area density, i.e. $n=1/2$ and $B=3$ in equation 2.13. Using a spreadsheet method to numerically integrate the governing integral equation (eq. 21 in Carleton, 2002), an estimate for parameter *A* of 0.00029 was derived by a least-squares procedure, with *B* constrained to a value of 3. This approach essentially treats the five Gustine cells as if they were a single wetland operated under five different, constant hydraulic loading rates.

Although the mean hydraulic loading rates varied between the five cells, flow rates also fluctuated continuously within each cell during the duration of the experiments (Figure 2.4). Flow rates and inlet and outlet concentrations for each cell were measured on a weekly basis between March 1989 and March 1990.

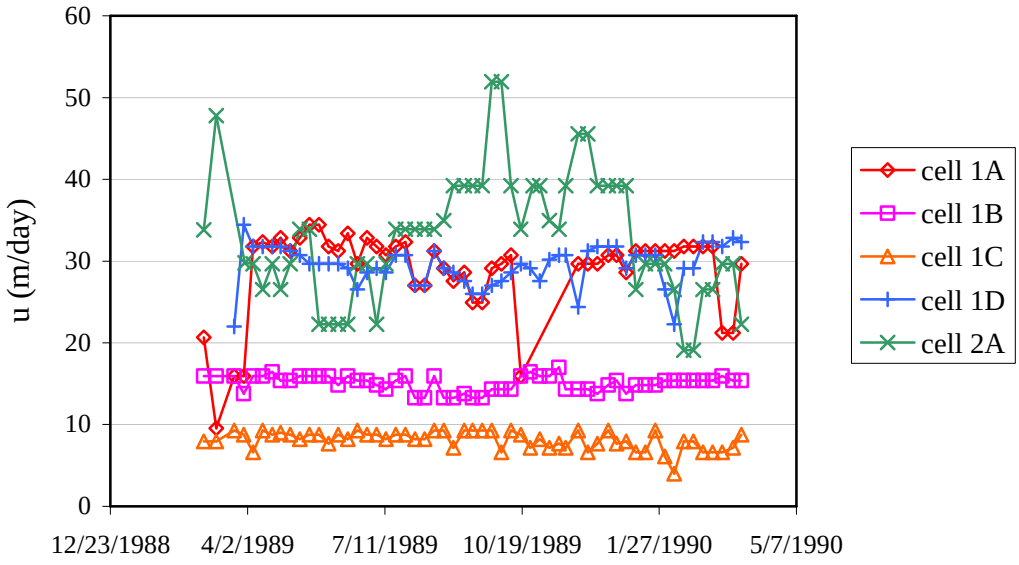

Figure 2.4 Weekly reported flow velocities in Gustine wetland cells.

2.4.2 Example 2: The Orlando Easterly Wetlands

The Orlando Easterly Wetlands (OEW) are a series of constructed wetland cells arranged in three separate treatment trains (northern, central, and southern) that have provided tertiary treatment of domestic wastewater in Orlando, Florida since 1987. Influent loadings have been approximately evenly split between the three trains except for a capacity test conducted between March 1997 and March 1998, during which time all flow was channeled through the northern train (Black and Wise, 2003). Daily measurements of flow and influent and effluent TP have been collected at OEW by the City of Orlando since 1988, providing a robust data set for model evaluation purposes. In analyzing TP input and output data over a number of years, Black and Wise (2003) documented an apparent positive relationship between monthly-averaged plug-flow *k* values (i.e. eq. 2.33) for TP, and monthly-averaged flow rates between 1992 and 1999. Martinez and Wise (2003) also studied mixing at the OEW, using pulse inputs of KBr tracer to measure RTDs in each treatment train. Their reported results include first and second temporal moments (mean and variance of residence time) for each treatment train obtained from the tracer curves. After several years of adequate performance, TP removal at OEW was observed to undergo seasonal declines each year beginning in winter of 1999, apparently due to decreased hydraulic efficiency and increased Phosphorus release from sediments (Wang et al., 2006). Because the DND approach is not designed to take such factors into account, Wetloop simulations were limited to the period from 1992 through 1999. Quantitative model evaluation was further limited to the 1992-1995 period, during

which measured concentrations appeared to provide the most reliable check on model output.

2.5 Results

2.5.1 Gustine Wetlands

With an α value of 3 again used to represent the RTD shape parameter, and the same values for *A* and *B* (0.00029 and 3) as determined in the steady-state analysis (Carleton, 2002), Wetloop was used to process the temporally-varying input data from each of the five Gustine cells, and to predict outlet concentrations. Results (Figure 2.5) show reasonable agreement between predicted and monitored outlet concentration trends over time for all five wetland cells. Correlation coefficients (r^2) between measured and simulated outlet BOD_5 concentrations were respectively 0.77, 0.59, 0.43, 0.62, and 0.70 for cells 1A, 1B, 1C, 1D, and 2A. Despite the greater than four-fold range in mean flow rates between these systems, the same set of parameter (*A* and *B*) values is able to provide representations of outlet concentration time series in all five Gustine cells that are generally consistent with observed concentration trends.

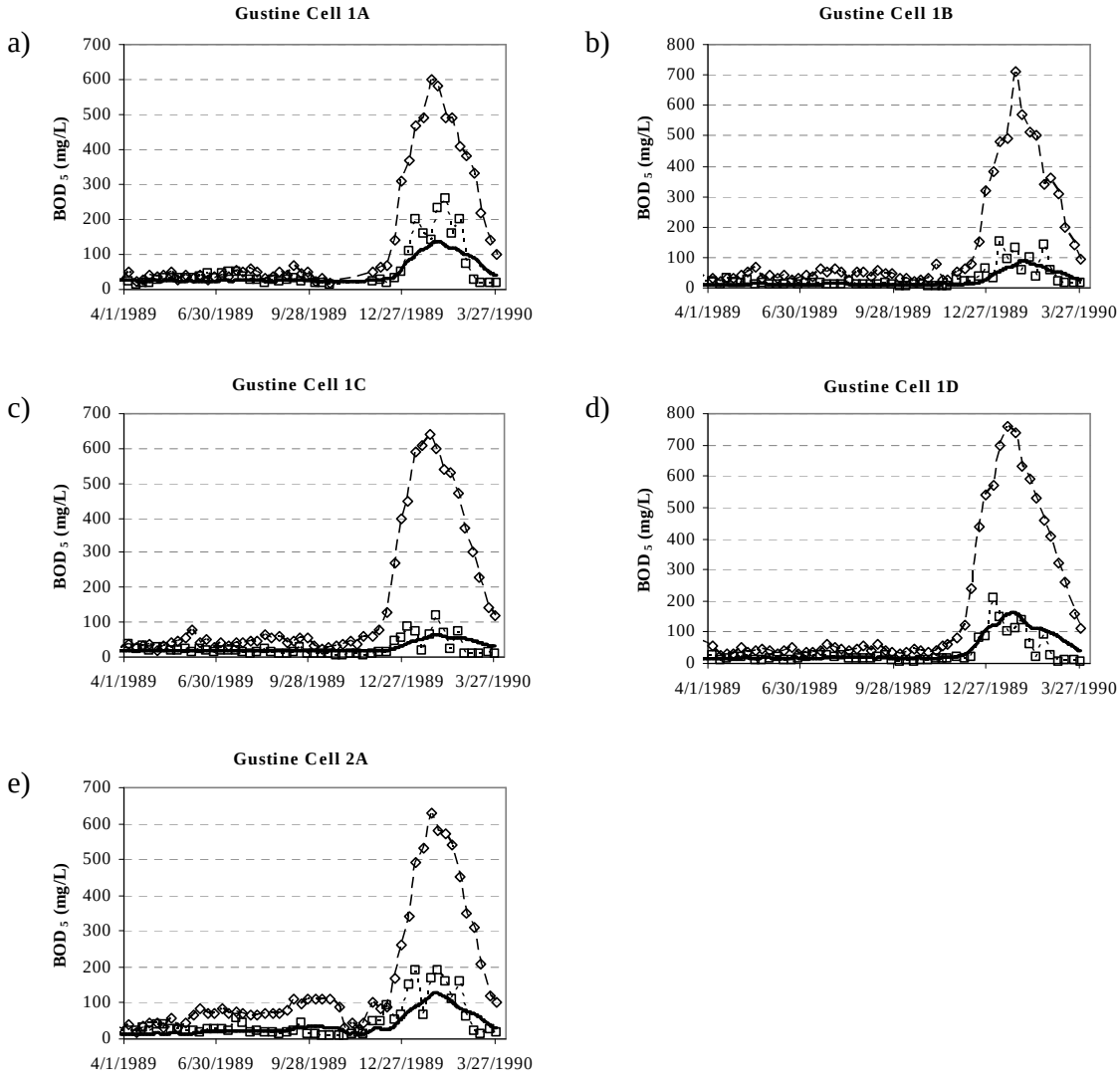

Figure 2.5 BOD_5 concentrations at the Gustine wetlands: measured inlet (diamonds), measured outlet (squares), and modeled outlet (dark line).

Variations in the apparent performance of the model in matching the data from each individual cell are likely related to inter-cell variability. For example, cells 1A and 1D were both operated at the same nominal HLR (15.15 m/yr), but outlet BOD concentrations from cell 1A were generally higher than those from cell 1D, as Figure 2.5 shows. Although the reasons for this are not entirely clear, the study report (Walker and Walker, 1990) indicates that cell 1A also had substantially

higher TSS effluent concentrations than did the other cells (e.g. a mean concentration of about 40 mg/L as compared with 21 mg/L for cell 1D), which the study authors attributed to "more open area" in cell 1A than in others thus "encouraging algae growth". The elevated BOD in the cell 1A effluent could therefore have been in part a function of increased algal biomass export. Because the same model parameter set was used to simulate all five Gustine cells, the concentrations emanating from cell 1A are slightly underestimated while the concentrations emanating from cell 1D are slightly overestimated. In a similar way, the steady-state analysis of mean data in Figure 1.8 shows the best-fit model to slightly underestimate effluent concentration from cell 1A, while it slightly overestimates effluent concentration from cell 1D (these are the two data points with identical "equivalent y" values of 0.25).

2.5.2 Orlando Easterly Wetlands

To simulate the OEW system with Wetloop, gamma probability density functions with the same moments as those found by Martinez and Wise were used to represent the RTDs of the three flow trains (Figure 2.6). Flow velocities were estimated from daily flows (mgd) by dividing by an estimated mean cross-sectional area for each train. Total influent loadings were assumed to be evenly divided between the three treatment trains, except for the March 1997 through March 1998 period, during which all influent loadings were assumed to be applied to the northern train (flow velocities for the central and southern trains during this period were set to the relatively insignificant value of 0.1 m/d in order to avoid model problems associated with zero flow). Outlet concentrations were calculated as the mean of the

effluent from the three trains, except for the March 1997 through March 1998 period, when they were set to equal the northern train effluent concentration.

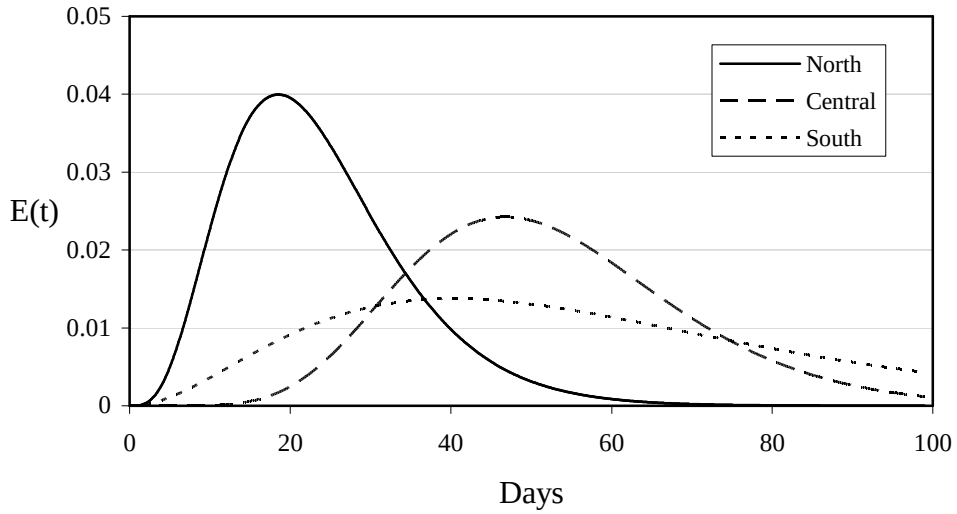

Figure 2.6 Approximations of the three OEW flow train Residence Time Distributions, E(t),(RTDs) using gamma PDFs with means and variances matching the observed. Compare with Martinez and Wise (2003), Figure 6.

Parameters *A* and *B* were assumed to be the same for all three trains: *B* was again fixed at a value of 3, corresponding to an inverse square root dependence of *U* on *X*, as in eq. 2.6 (this was primarily in order to obtain a fair comparison of results with the PFR model, so that for each model, optimization involved manipulation of a single parameter, and not because *B* is necessarily believed to optimally equal 3). An optimized value for parameter *A* of 1.57E-5 day^{-3} was found (using MATLAB® procedure 'fminsearch') by minimizing the summed squared daily differences between measured and modeled outlet concentrations. For consistency with the PFR analysis employed by Black and Wise (2004), *C** was set to zero, and parameter optimization focused on the period beginning 01/92. Unlike Black and Wise, in our analysis the optimization period only extended through 10/31/95, because the daily

record suggests a change in quantitation limit after this period, with a large number of censored values (Figure 2.7c) that might bias model fit. Results show predicted concentrations that are, for the most part, in reasonable agreement with measured ones (Figure 2.7b, 2.7c) between 1992 and 1995. Wetloop notably underpredicted performance during the capacity test (03/97-03/98) period, when all flow was routed through the northern train.

For 1992-1995, monthly averaged Wetloop results show similar agreement with measured concentrations as results obtained using a best-fit k-C^* PFR model optimized for the same time period (Figure 2.8). PFR model optimization involved selecting a value for k (in eq. 2.33) that minimized the summed squared errors between simulated and measured outlet concentrations, calculated on an average monthly basis using monthly-averaged flow (Q) to calculate residence time.

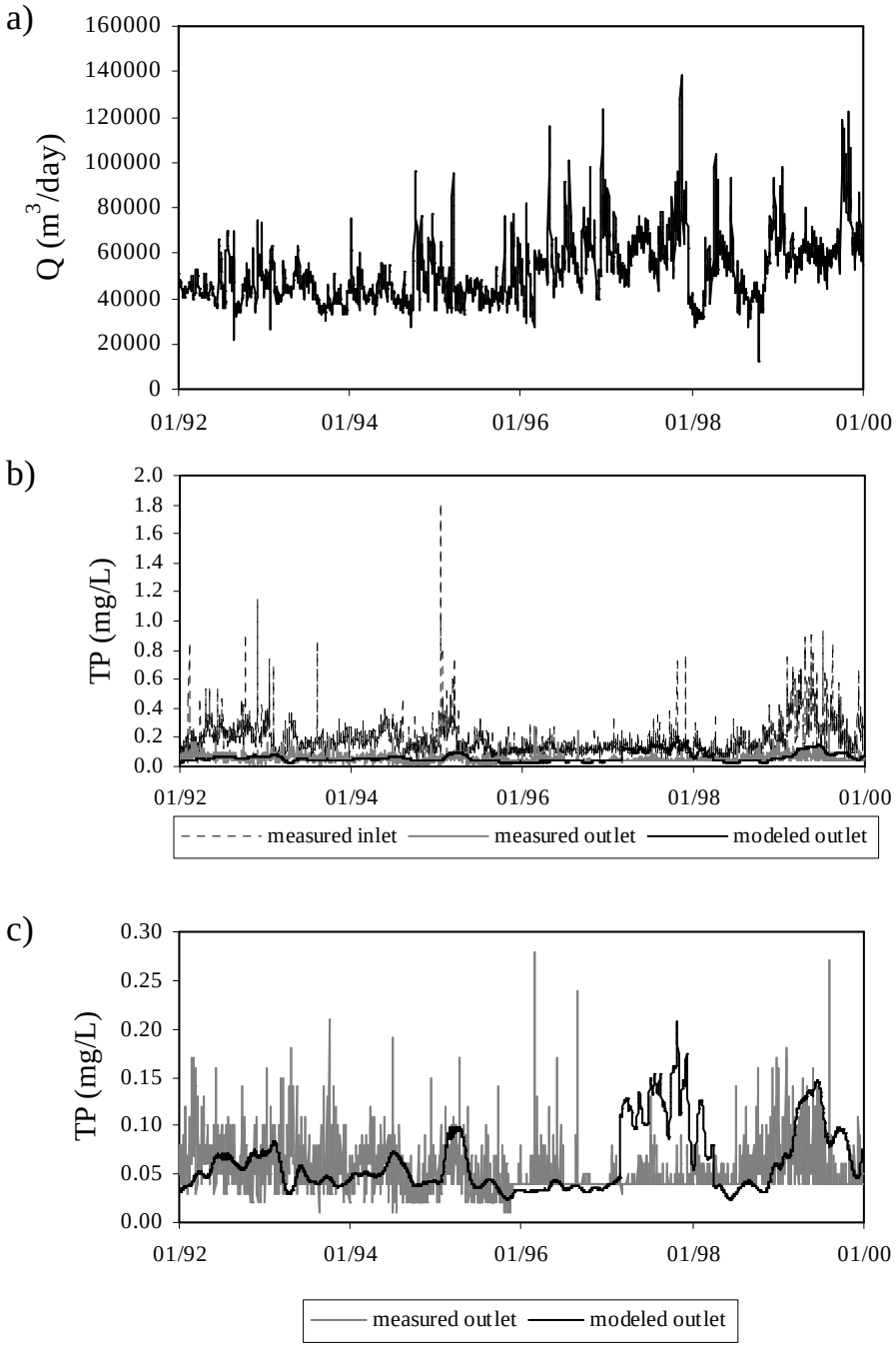

Figure 2.7 Orlando Easterly Wetlands data from 1992 through 1999; a) daily flow rate (average of inlet and outlet); b) TP concentrations measured daily at inlet and outlet, and modeled at outlet; c) expanded view of measured and modeled outlet concentration.

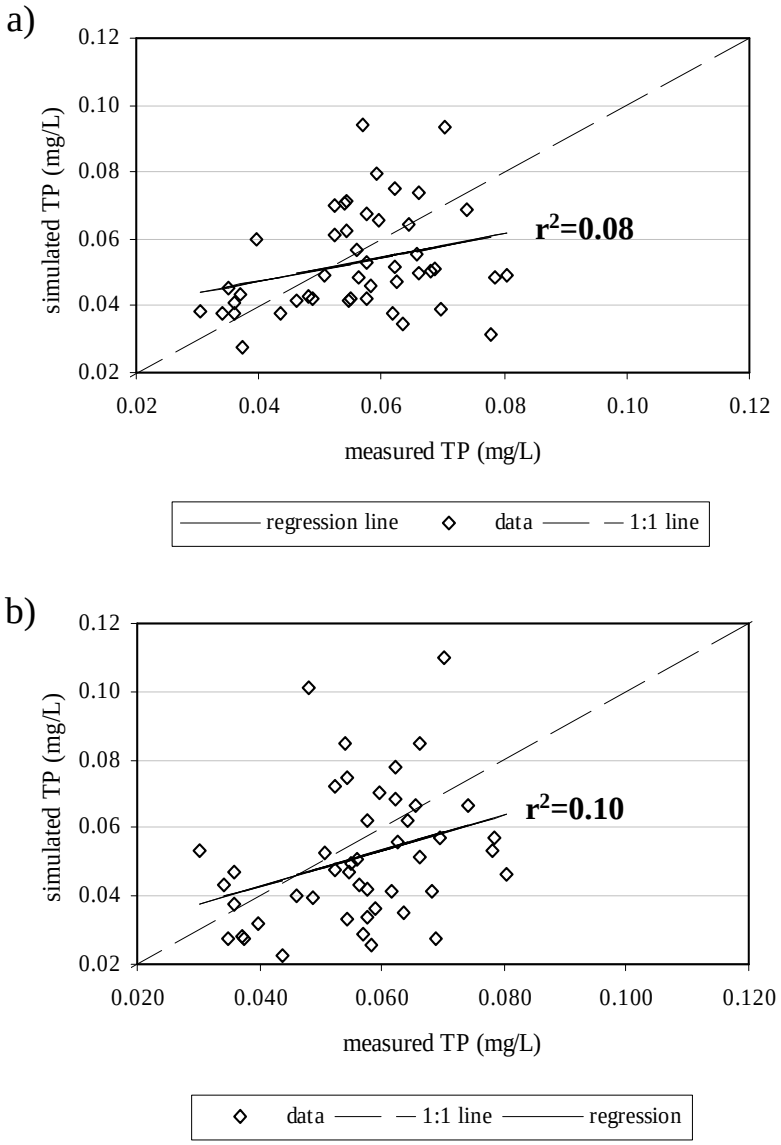

Figure 2.8 Comparisons between measured and modeled outlet TP concentrations at the Orlando Easterly Wetlands for period 01/92-10/95. Both models employed the same value for *C** (0.0 mg/L), and optimized values of just one parameter (obtained in each case by minimizing summed squared model errors): a) *A* in the case of Wetloop, and b) *k* in the case of the *k*-*C** plug-flow model.

Figure 2.9 displays model error correspondence with flow for the Wetloop and PFR models. The flow-correlated bias in *k* that was reported by Black and Wise (2004) for a PFR model of the OEW system is evident in the scatter, and reflected in the higher correlation coefficient of model error with *Q* (r^2=0.24). As expected,

because the DND approach is designed to address this effect as part of model formulation, this bias is essentially eliminated in the Wetloop results (r^2=0.01).

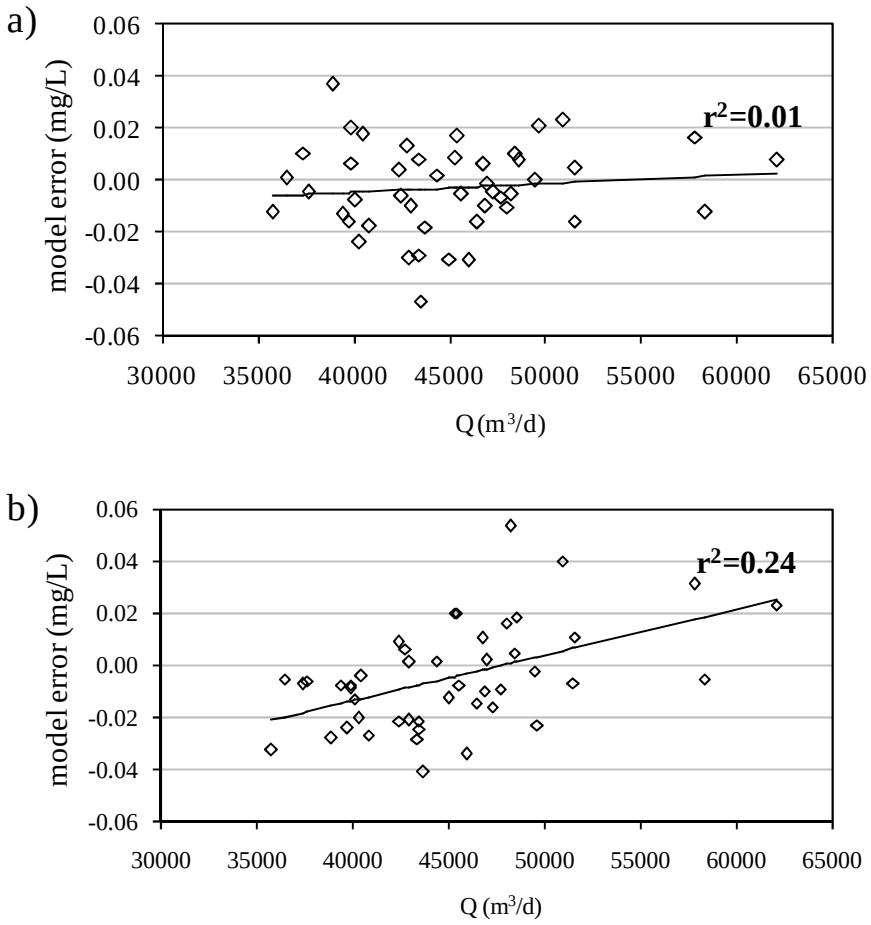

Figure 2.9 Model error regression against flow rate: a) Wetloop model; b) k-C* plug-flow model.

2.6 Discussion

The modeling approach described in this paper for non-steady flow conditions presumes that a wetland's RTD is a fixed entity that does not evolve with time, and that has the same shape (when non-dimensionalized) irrespective of flow rate or other conditions. Results of a recent investigation call into question the validity of this

assumption: in tracer studies on a stormwater treatment wetland, Holland et al. (2004) found that although flow rates by themselves had an insignificant effect, water depth had a large impact on the shapes of normalized RTDs. The approach proposed in this paper does not explicitly take water depth into consideration in outlet concentration calculations, except perhaps through variations in (spatially) mean cross-sectional area if they are used in the calculation of instantaneous bulk velocity u_m from time-varying flow rate, e.g. $u_m = Q/A_c$, where Q and A_c are the instantaneous flow and cross-sectional area, respectively. Water depths and cross-sectional areas are not typically monitored frequently enough in wetland studies to provide the kind of time-series information that would be useful in this way. For example, in the OEW and Gustine wetland examples presented in this paper, only the approximate mean water depths were available; u_m was therefore calculated from Q under an assumption of fixed cross-sectional area and fixed depth. To the extent that these quantities actually vary with time, this represents a weakness in the DND approach.

Other weaknesses in the approach derive from the presumption of stochastic-convective flow, which necessarily ignores molecular diffusion, transverse mixing, and the random impacts of wind-induced mixing as aspects of solute transport. Under very low flow conditions, the relative importance of these effects may be magnified. It should be noted that although the non-steady DND approach is designed to handle continuously-varying flows, it is not suitable for handling flow rates that fall to zero, as this results in plateaus in the τ_i *vs.* T_i curve (Figure 2.3d), and therefore indeterminacy in T_i. Use of the PFR model is of course also not strictly appropriate for systems with periodically static or wildly fluctuating flow regimes, so this

weakness in the DND approach does not represent a comparative advantage for the PFR model.

The DND modeling approach, in both the steady-state (Carleton, 2002) and non-steady state cases (this paper), derives from the presumption that treatment efficiency is a direct reflection of a wetland's distribution of vegetation density and/or depth. Many questions remain regarding the fundamental nature of the relationships between vegetation density, depth, flow rate, water surface gradient, and constituent removal kinetics in surface flow systems, including wetlands and streams.

2.7 Conclusions

The assumption of non-Fickian or pre-asymptotic longitudinal dispersion in wetlands and streams leads to convolutional solutions for flux concentrations. Stream tube velocities and constituent removal coefficients may both be dependent on local vegetation densities and/or local depths, in which case outlet concentrations can be determined through knowledge of a system's RTD in combination with two parameters that can be estimated through objective function minimization. In this paper an extension of the steady-state "Damköhler Number Distribution" modeling approach (Carleton, 2002) to cases of non-steady flow and temporally varying inlet concentration has been presented. DND-based wetland modeling addresses the dependence of apparent removal rate constants on flow, and is in this respect an improvement over the k-C^* PFR model. In two example applications of the method to existing wetland data sets, the approach provides time series estimates of outlet constituent concentrations that appear to be in reasonable agreement with measured

outlet concentration time series. Further work will focus on explicitly incorporating transverse mixing into prediction equations.

Chapter 3: Reactive Transport in Stratified Flow Fields With Idealized Heterogeneity

3.1 Abstract

A two-dimensional equation governing the steady state spatial concentration distribution of a reactive constituent within a heterogeneous advective dispersive flow field is solved analytically. The solution which is developed for the case of a single point source can be generalized to represent analogous situations with any number of separate point sources. A limiting case of special interest has a line source of constant concentration spanning the domain's upstream boundary. The work has relevance for improving understanding of reactive transport within various kinds of advection-dominated natural or engineered environments including rivers and streams, and bioreactors such as treatment wetlands. Simulations are used to examine quantitatively the impact that transverse dispersion (deviations from purely stochastic-convective flow) can have on mean concentration decline in the direction of flow. Results support the contention that transverse mixing serves to enhance the overall rate of reaction in such systems.

Notation

a, b, f	multipliers in velocity, dispersion and reaction terms, respectively
A, B, F	multipliers in velocity, dispersion and reaction terms, respectively in dimensionless equation
$C_f(x)$	flux concentration
$C_r(x)$	resident concentration
$C(x,z)$	concentration at a point
D_X	longitudinal dispersion coefficient (dimensionless coordinates)
D_z, D_Z	transverse dispersion coefficient in standard and dimensionless coordinates, respectively
$E(t)$	residence time distribution function (RTD)
$F(t)$	tracer breathrough curve function
H, L	lateral and longitudinal extents of domain, respectively
k, K	reaction term in standard and dimensionless coordinates, respectively
k_{eff}	effective plug-flow reaction rate coefficient
m, n, p	exponents in velocity, dispersion and reaction terms, respectively
x, z	coordinates in direction of and transverse to flow, respectively
X, Z	dimensionless coordinates in direction of and transverse to flow, respectively
t	time
u, U	velocity in standard and dimensionless coordinates, respectively
Ω_i	eigenvalues
λ_i	eigenvalues, modified form

3.2 Introduction

Recent decades have seen a growing recognition of limitations inherent in traditional methods of representing dispersive solute flux in the direction of motion in porous media and open channel flow. As first defined by Taylor (1954), shear-flow dispersion arises from an interaction between non-uniform advection and diffusion of solute across stream lines. Fischer et al. (1979) explain how various simplifying assumptions are used to derive from this complicated physical picture a relatively simple expression employing a bulk dispersion coefficient to represent longitudinal dispersive flux in a manner analogous to the way that molecular diffusion is described by Fick's first law. In other words, hydrodynamic dispersive flux is treated as proportional to the spatial gradient in mean concentration. Inclusion of such a flux term in a one-dimensional transport equation produces the standard one-dimensional advective-dispersive equation (ADE), for which solutions under various initial and boundary conditions are widely available (e.g. van Genuchten and Alves, 1982). However, studies on solute transport in various disparate media and environments including soils, streams, and wetlands have documented solute spreading that is not adequately characterized by the ADE because longitudinal mixing only approaches Fickian behavior asymptotically, if at all, after transport has proceeded for a certain duration or distance (e.g. Day, 1977; Gelhar, 1993; Werner and Kadlec, 2000). The behavior typically manifests as an increase in the apparent dispersion coefficient with the scale of transport. In the near-field limit (the "stochastic-convective" case), longitudinal spreading occurs solely as a function of velocity heterogeneities; i.e. transverse mixing can be ignored.

With general recognition that spatially heterogeneous velocities are at the heart of failures of the ADE to describe real transport regimes, researchers have explored various alternative approaches to transport simulation. These include stochastic methods (Dagan, 1984; Gelhar et al., 1979; Matheron and DeMarsily, 1980; Montas et al., 2000), continuous time random walk formulations (Berkowitz et al., 2006; Dentz et al., 2004), and approaches in which heterogeneity is represented explicitly (Chen and Arce, 1997; Shapiro and Brenner, 1986; Uflyand, 1988). Although some of these efforts have addressed reaction as well as transport, they have largely focused on responses to pulse addition of tracers, rather than to the continuous addition of reactive substances, such as would typify the situation in a reactor.

In one notable study, Yeh and Tsai (1976) developed an analytical solution for the spatial distribution of a conservative constituent continuously released into a steady-state two-dimensional flow field, in which both velocity and transverse dispersion coefficient are treated explicitly as power functions of the transverse dimension. The authors envisioned their transverse dimension as specifically representing the vertical, and selected power functions as approximations of more complicated boundary layer equations in order to make the governing transport equation tractable to solution. The work described in this Chapter closely follows Yeh and Tsai's approach, but incorporates a reaction term that is also governed by a power law dependence on the transverse dimension (Figure 3.1). By contrast with Yeh & Tsai, the transverse dimension in this work is envisioned as essentially representing the horizontal (lateral) rather than the vertical dimension, with heterogeneity envisioned to be a function of underlying physical attributes. The

resulting model is specifically intended to represent systems such as bioreactors that incorporate spatially heterogeneous reaction rates linked to local velocities, for example as a result of mutual dependence on underlying distributions in drag-inducing reactive surface (e.g. vegetation) density. This work represents advancement over previous modeling efforts for these kinds of reactors, in which flow was assumed to be stochastic-convective (Carleton, 2002; Carleton and Montas, 2007), because it explicitly incorporates transverse diffusive/dispersive fluxes in the governing equations. Although the functional representations of velocity, reaction and dispersion employed in this approach represent simplifications of reality, our results may be directly applicable to some particular kinds of problems, for example depth-averaged transport in U-shaped channels with fringing vegetation that increases in density toward the shallows.

Very few analytical solutions of two-dimensional reactive transport equations are known, which necessitates the use of numerical approximation techniques to simulate most cases of practical interest. Unfortunately, traditional numerical techniques for simulating heterogeneous transport domains suffer from problems such as instabilities that frequently make them difficult to solve, particularly for systems that possess hyperbolic character (Herrera and Valocchi, 2006; James and Jawitz, 2007). The solutions presented in this paper can apply to systems with strongly hyperbolic character. Despite limitations on the forms of the idealized profiles governing velocity, reaction rate and transverse dispersion, these solutions may be useful for a variety of purposes, including serving as exact answers against which the accuracy of numerical simulations can be tested.

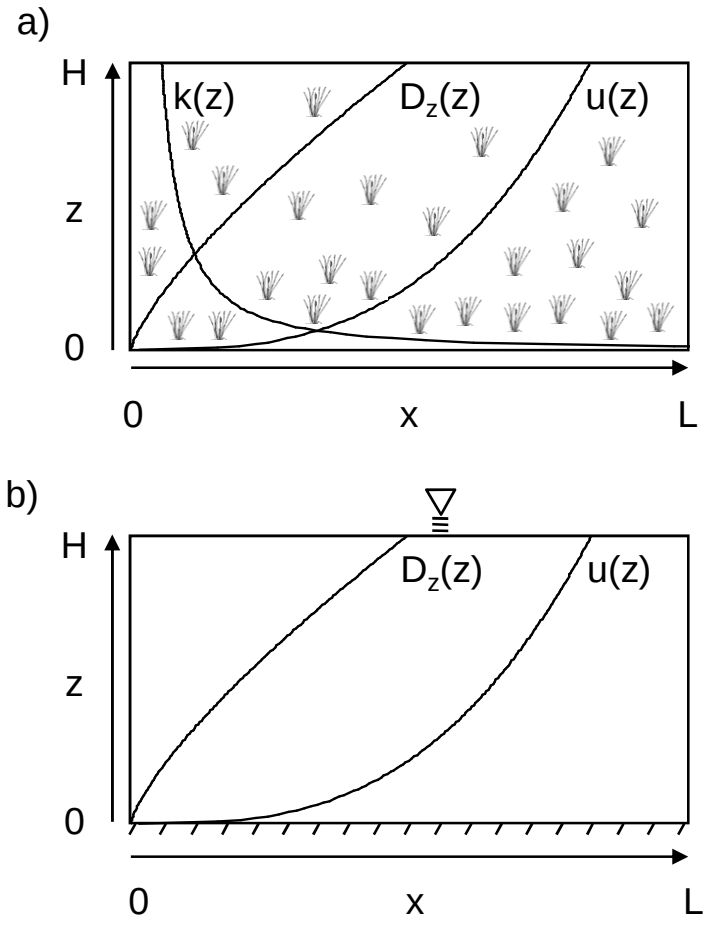

Figure 3.1 Definition sketch of 2-D heterogeneous transport environments: a) reactive regime, top view (this paper); and b) non-reactive regime (side view) considered by Yeh and Tsai (1976). Spatially heterogeneous velocities (u), transverse dispersion coefficients (D_z), and reaction rate coefficients (k) are treated as power functions of the transverse (z) dimension. Figure a indicates that heterogeneities are manifestations of the underlying spatial distribution of a controlling variate, such as vegetation surface area density in the case of a wetland.

3.3 Model Formulation

3.3.1 General Solution

The mass-balance equation for concentration (C) of a reactive constituent emanating from a source in steady unidirectional flow is

$$-k(z)C - u(z)\frac{\partial C}{\partial x} + \frac{\partial}{\partial z}\left(D_z(z)\frac{\partial C}{\partial z}\right) + S(x,z) = 0 \qquad (3.1)$$

where x and z are coordinates in the direction of and transverse to flow respectively, and S is a source function. Functions k, u, and D_z are reaction rate coefficient, velocity, and dispersion coefficient respectively. For a rectangular bounded domain of transverse and longitudinal extents H and L respectively, we define normalized coordinates in the longitudinal and transverse directions: $Z=z/H$, $X=x/L$, and define k, u, and D_z as power functions of the transverse coordinate:

$$k = fz^p = fH^pZ^p \qquad (3.2)$$

$$u = az^m = aH^mZ^m \qquad (3.3)$$

$$D_z = bz^n = bH^nZ^n \qquad (3.4)$$

Next we define constants $A = \frac{aH^m}{L}$, $B=bH^{n-2}$, and $F=fH^p$, and express eq. 3.1 in the form

$$-KC - U\frac{\partial C}{\partial X} + \frac{\partial}{\partial Z}\left(D_Z\frac{\partial C}{\partial Z}\right) + S(X,Z) = 0 \qquad (3.5)$$

where $U=aZ^m$, $D_Z=BZ^n$, and $K=FZ^p$ are velocity, transverse dispersion, and reaction rate terms respectively, expressed in terms of dimensionless coordinates. Following Yeh and Tsai (1976), a Neumann (no flux) boundary condition is imposed at the "upper" (maximum z) transverse boundary:

$$D_Z \frac{\partial C}{\partial z} = 0\,,\ Z = 1 \tag{3.6}$$

The astute reader will recognize that a Neumann boundary necessarily exists as well at the "lower" transverse boundary by virtue of the fact that D_Z equals zero there. The domain can be envisioned as potentially representing one half of a bilaterally symmetric regime, in which the "upper" transverse boundary represents the centerline. Because transverse flux is zero at $z=H$ (eq. 3.6), concentrations are continuous across this line, though the U, D_Z, and K functions all exhibit cusps (discontinuities in slope) there. This system of equations can be solved using a Green's function approach:

$$C = \int_0^1 \int_0^X G(X, Z, X_0, Z_0) S(X_0, Z_0) dX_0 dZ_0 \tag{3.7}$$

where G satisfies $G(X,Z,X_0,Z_0) = 0$, $X < X_0$, and

$$U \frac{\partial G}{\partial X_0} - KG + \frac{\partial}{\partial Z_0}\left(D \frac{\partial G}{\partial Z_0} \right) = \delta(X - X_0)\delta(Z - Z_0),\ X > X_0 \tag{3.8}$$

thus

$$U \frac{\partial G}{\partial X_0} - KG + \frac{\partial}{\partial Z_0}\left(D \frac{\partial G}{\partial Z_0} \right) = 0\,,\ X > X_0 \tag{3.9a}$$

$$\lim_{X_0 \to X} UG = \delta(Z - Z_0) \tag{3.9b}$$

Employing a separation of variables technique, we express G as

$$G = \sum_{i=0}^{\infty} \alpha_i w_i(X_0) \phi_i(Z_0) \tag{3.10}$$

which upon substitution into equation 3.9 leads to eigenfunction problems of the following form:

$$\frac{K}{U} - \frac{1}{U\phi_i}\frac{\partial}{\partial Z_0}\left(D_Z \frac{\partial \phi_i}{\partial Z_0}\right) = \Omega_i^2 \tag{3.11}$$

and

$$\frac{\partial w_i}{\partial X_0} = w_i \Omega_i^2 \tag{3.12}$$

where Ω_i are eigenvalues. Rearrangement of eq. 3.11 produces

$$\frac{\partial}{\partial Z_0}\left(D_Z \frac{\partial \phi_i}{\partial Z_0}\right) + U\phi_i\Omega_i^2 - K\phi_i = 0 \tag{3.13}$$

or

$$\frac{\partial^2 \phi_i}{\partial Z_0^2} + nZ_0^{-1}\frac{\partial \phi_i}{\partial Z_0^2} + \frac{A}{B}\Omega_i^2 Z_0^{m-n}\phi_i - \frac{F}{B}Z_0^{p-n}\phi_i = 0 \tag{3.14}$$

Parameters *A*, *B*, and *F* are all assumed to be non-negative, and for solubility's sake we require *p=n-2*. When this is the case, eq. 3.14 is in the form of Relton (1965) eq. 3.6.2, and is therefore a Bessel equation in a form for which a solution can be found (see Appendix B). If *n* is positive and smaller than two, this means that *p* is negative. For consistency with assumptions employed in previous wetland simulation work (Carleton, 2002; Carleton and Montas, 2007), we are primarily interested in situations in which *p* is negative and m is positive, so that *K* is inversely related to *U*. In the current model, *K* decreases with increasing *Z*, and approaches infinity at *Z=0*. Although an infinite reaction rate is not physically meaningful, velocity and transverse dispersion both approach zero at the boundary where this occurs, for the kinds of domains in which we are primarily interested (i.e. with m and n both positive). Thus this boundary is isolated from the rest of the domain in terms of material exchange, and its influence on concentration in the rest of the domain is

finite. Despite the idealized nature of the transport regime, the model is therefore expected to be useful for providing insights into the behavior of some real physical systems. Note that equation 3.14 is equivalent in form to eq. 9.1.53 of Abramovitz and Stegun (1965), i.e. $Z^2\phi'' + (1-2r)Z\phi' + \left(\lambda^2 q^2 Z^{2q} + r^2 - \nu^2 q^2\right)\phi = 0$, with solution $\phi = Z^r C_\nu\left(\lambda Z^q\right)$, and quantities 1 - 2*r*, $\lambda^2 q^2$, 2*q* - 2, and r^2 - $\nu^2 q^2$ are equal to *n*, $\frac{a}{b}\Omega^2$, $m - n$, and -*F*/*B* respectively, using our nomenclature.

We next define the following two quantities in terms of existing parameters:

$$\varepsilon = \frac{\left[(1-n)^2 + \frac{4F}{B}\right]^{1/2}}{(1-n)} \tag{3.15}$$

$$\nu = \frac{\varepsilon(1-n)}{2+m-n} \tag{3.16}$$

Employing these, the solution to eq. 3.14 can be expressed in terms of Z_0 as

$$\phi_i(Z_0) = Z_0^{(1-n)/2} J_\nu\left[\left(\frac{A}{B}\right)^{1/2} \frac{2\nu\Omega_i}{\varepsilon(1-n)} Z_0^{\frac{\varepsilon(1-n)}{2\nu}}\right] \tag{3.17}$$

Next, by using a modified form of the eigenvalues:

$$\lambda_i = \left(\frac{A}{B}\right)^{1/2} \frac{\Omega_i}{\varepsilon(1-n)} \tag{3.18}$$

eq. 3.17 can be expressed more compactly as

$$\phi_i(Z_0) = Z_0^{(1-n)/2} J_\nu\left[2\nu\lambda_i Z_0^{\frac{\varepsilon(1-n)}{2\nu}}\right] \tag{3.19}$$

Conditions at the "lower" transverse boundary are such that C=0 for all X, as long as F is non-zero. Thus this is a Dirichlet (zero concentration) boundary, in addition to being a Neumann (zero flux) boundary, as previously mentioned. For this

reason the orders (v) of the Bessel functions in this work are specifically defined as positive, whereas Yeh and Tsai were able to employ negative values of v in their solution for the non-reactive case: according to Abramovitz and Stegun, eq. 9.1.7 (1965), in the limit as z goes to zero the Bessel terms approach zero for positive v, but approach infinite magnitude for negative v. Because when $p < 0$ the reactive solution must be zero at Z=0, only positive order Bessel functions produce a physically sensible (i.e. non-negative concentration), bounded solution. The condition $v \geq 0$ imposes a constraint (through eq. 3.16) that $m \geq n - 2$. However, because we limit our focus to cases where m and n are both non-negative and less than 2 (in the interests of physical sensibility), this constraint does not come into play in our analysis.

Equation 3.12 has the solution

$$w_i(X_0) = w_{i,0} \exp\left[-\Omega_i^2 (X - X_0)\right] = w_{i,0} \exp\left[-\frac{B}{A}\varepsilon^2 (1-n)^2 \lambda_i^2 (X - X_0)\right] \tag{3.20}$$

where $w_{i,0}$ is the value of w_i at X_0 as X_0 approaches X. We solve for $w_{i,0}$ as follows. Combining eqs. 3.9b and 3.10, we obtain

$$\lim_{X_0 \to X} \sum_{j=1}^{\infty} U(Z_0)\alpha_j w_j(X_0)\phi_j(Z_0) = \delta(Z - Z_0) \tag{3.21}$$

Multiplying both sides by $\alpha_i \phi_i(Z_0)$ and integrating over Z_0 from 0 to 1 produces

$$\int_0^1 \sum_{j=1}^{\infty} \alpha_i \alpha_j w_{j,0} U(Z_0)\phi_j(Z_0)\phi_i(Z_0) dZ_0 = \int_0^1 \alpha_i \delta(Z - Z_0)\phi_i(Z_0) dZ_0 \tag{3.22}$$

Because of orthogonality of the eigenfunctions, the left side is zero except when $i = j$, thus eq. 3.22 simplifies to

$$w_{i,0}\alpha_i^2\int_0^1 U(Z_0)\phi_i^2(Z_0)dZ_0 = \alpha_i\phi_i(Z) \tag{3.23}$$

The Bessel series coefficients are defined as follows for the case of a Dirac delta inlet boundary condition, equivalent to imposing a normalization condition on the Sturm-Liouville problem represented by eq. 3.14 (Boyce and DiPrima, 2005):

$$\begin{aligned}\alpha_i^2 &= \frac{1}{\int_0^1 U(Z)\phi_i^2(Z)dZ} = \frac{1}{\int_0^1 aZ^{1+m-n}\left(J_\nu\left[2\nu\lambda_i Z^{\frac{\varepsilon(1-n)}{2\nu}}\right]\right)^2 dZ} \\ &= \frac{1}{\int_0^1 AZ^{1+m-n}\left(J_\nu\left[2\nu\lambda_i Z^{\frac{\varepsilon(1-n)}{2\nu}}\right]\right)^2 dZ}\end{aligned} \tag{3.24}$$

Thus eq. 3.23 simplifies to

$$w_{i,0} = \alpha_i\phi_i(Z) \tag{3.25}$$

and eq. 3.10 becomes

$$\begin{aligned}G &= \sum_{i=1}^{\infty}\alpha_i^2\phi_i(Z)\phi_i(Z_0)\exp\left[-\frac{B}{A}\varepsilon^2(1-n)^2\lambda_i^2(X-X_0)\right] \\ &= \sum_{i=1}^{\infty}\alpha_i^2 Z^{(1-n)/2}J_\nu\left[2\nu\lambda_i Z^{\varepsilon(1-n)/2\nu}\right] \\ &\quad\cdot Z_0^{(1-n)/2}J_\nu\left[2\nu\lambda_i Z_0^{\varepsilon(1-n)/2\nu}\right]\exp\left[-\frac{B}{A}\varepsilon^2(1-n)^2\lambda_i^2(X-X_0)\right]\end{aligned} \tag{3.26}$$

where the condition

$$J_\nu\left[2\nu\lambda_i\right] = \frac{2\varepsilon}{\varepsilon+1}\lambda_i J_{\nu+1}\left[2\nu\lambda_i\right] \tag{3.27}$$

applies, which derives from $\left.\frac{\partial G}{\partial Z}\right|_{Z=1} = 0$, in order to ensure that the "upper" ($Z = 1$) transverse boundary condition (eq. 3.6) is met.

For a point source of strength M, located at (X_0,Z_0), the solution for C is therefore:

$$C(X,Z,X_0,Z_0) = M\sum_{i=1}^{\infty}\alpha_i^2 Z^{(1-n)/2} J_\nu\left[2\nu\lambda_i Z^{\varepsilon(1-n)/2\nu}\right] \cdot Z_0^{(1-n)/2} J_\nu\left[2\nu\lambda_i Z_0^{\varepsilon(1-n)/2\nu}\right] \cdot \exp\left[-\frac{B}{A}\varepsilon^2(1-n)^2\lambda_i^2(X-X_0)\right], \quad X > X_0 \tag{3.28}$$

If we define the point X_0 to be zero on the X axis, eq. 3.28 becomes

$$C(X,Z,Z_0) = M\sum_{i=1}^{\infty}\alpha_i^2 Z^{(1-n)/2} J_\nu\left[2\nu\lambda_i Z^{\varepsilon(1-n)/2\nu}\right] \cdot Z_0^{(1-n)/2} J_\nu\left[2\nu\lambda_i Z_0^{\varepsilon(1-n)/2\nu}\right]\exp\left[-\frac{B}{A}\varepsilon^2(1-n)^2\lambda_i^2 X\right] \tag{3.29}$$

3.3.2 Incorporating Longitudinal Dispersion

A solution for a governing equation that includes longitudinal dispersion can be developed in an analogous fashion, subject to an additional constraint: that the longitudinal dispersion coefficient is a power function of Z with the same exponent as that of the velocity function, i.e.

$$-K(Z)C - U(Z)\frac{\partial C}{\partial X} + \frac{\partial}{\partial Z}\left(D_Z(Z)\frac{\partial C}{\partial Z}\right) + D_X(Z)\frac{\partial^2 C}{\partial X^2} + S(X,Z) = 0 \tag{3.30}$$

where

$$D_X = IZ^m \tag{3.31}$$

The solution to this equation is

$$C(X,Z,Z_0) = M\sum_{i=1}^{\infty}\left[\alpha_i^2 Z^{(1-n)/2} J_\nu\left[2\nu\lambda_i Z^{\varepsilon(1-n)/2\nu}\right]\right.$$
$$\cdot Z_0^{(1-n)/2} J_\nu\left[2\nu\lambda_i Z_0^{\varepsilon(1-n)/2\nu}\right] \qquad (3.32)$$
$$\left.\cdot \exp\left[\left[\frac{A}{2I} - \left(\left(\frac{A}{2I}\right)^2 + \frac{B}{I}\varepsilon^2(1-n)^2\lambda_i^2\right)\right]X\right]\right], \quad X > X_0$$

Details of the derivation are presented in Appendix A. As with eq. 12 in Yeh and Tsai (1976), equations 3.29 and 3.32 can be thought of as general solutions in two dimensions for situations in which a single point source exists, located at $(0,Z_0)$. Solutions for cases of multiple sources can be obtained by integrating the relevant equation (e.g. eq. 3.26) over all sources.

3.3.3 Solutions for Non-Dimensionless Domains

Equations 3.29 and 3.32 are solutions to eqs. 3.5 and 3.30 respectively, when $S(X,Z) = M\delta(X)\delta(Z - Z_0)$, i.e. the upstream boundary condition is a Dirac delta function of magnitude M, located along the upstream boundary at position $(0,Z_0)$. Note that because the governing equations are in the same form (i.e. all coefficients power functions of the transverse dimension), solutions for non-dimensionless versions of the equations are of the same form as eqs. 3.29 and 3.32, with non-dimensionless versions of the coordinates and coefficients (*A*, *B*, *X*, *Z*, etc.) substituted in appropriate places. For example, the solution to eq. 3.1 is

$$C(x,z,z_0) = M\sum_{i=1}^{\infty}\alpha_i^2 z^{(1-n)/2} J_\nu\left[2\nu\lambda_i z^{\varepsilon(1-n)/2\nu}\right]$$
$$\cdot z_0^{(1-n)/2} J_\nu\left[2\nu\lambda_i z_0^{\varepsilon(1-n)/2\nu}\right]\exp\left[-\frac{b}{a}\varepsilon^2(1-n)^2\lambda_i^2 x\right], \quad x > x_0 \qquad (3.33)$$

where in this case ε is defined by

$$\varepsilon = \frac{\left[(1-n)^2 + \frac{4f}{b}\right]^{1/2}}{(1-n)} \tag{3.34}$$

3.3.4 Reactor Model

A situation of particular interest for the purpose of this study is the case in which the "inlet" concentration is constant across the width of the domain, i.e. instead of a Dirac singularity at (x_0,z_0) we have uniform C_i at x_0 as a source function, spanning the width of what can be thought of as an upstream or inlet boundary, from $z = 0$ to $z = H$ at x_0. This arrangement is geometrically comparable to the stochastic-convective or Damköhler number distribution (DND) approaches employed previously to simulate wetland bioreactors (Carleton, 2002; Carleton and Montas, 2007). The governing equation with transverse dispersion included has the following solution for transverse-mean resident concentration normalized by C_i and expressed as a function of x:

$$C_r(x) = \frac{1}{H}\sum_{i=1}^{\infty}\left[\exp\left[-\frac{b}{a}\varepsilon^2(1-n)^2\lambda_i^2 x\right] \cdot \frac{\left(\int_0^H z^{(1-n)/2} J_\nu\left[2\nu\lambda_i z^{\varepsilon(1-n)/2\nu}\right]dz\right)\left(\int_0^H az^{\frac{1+2m-n}{2}} J_\nu\left[2\nu\lambda_i z^{\frac{\varepsilon(1-n)}{2\nu}}\right]dz\right)}{\int_0^H az^m\left(z^{\frac{1-n}{2}} J_\nu\left[2\nu\lambda_i z^{\frac{\varepsilon(1-n)}{2\nu}}\right]\right)^2 dz}\right] \tag{3.35}$$

The transverse variance of the above is then defined as

$$\sigma_r^2(x) = \frac{\int_{z_1}^{z_2}\left(C(x,z) - C_r(x)\right)^2 dz}{z_2 - z_1} \tag{3.36}$$

where

$$C(x,z) = \sum_{i=1}^{\infty}\left[\frac{\int_0^H az^{\frac{1+2m-n}{2}} J_\nu\left[2\nu\lambda_i z^{\frac{\varepsilon(1-n)}{2\nu}}\right]dz}{\int_0^H az^m\left(z^{\frac{1-n}{2}} J_\nu\left[2\nu\lambda_i z^{\frac{\varepsilon(1-n)}{2\nu}}\right]\right)^2 dz} z^{(1-n)/2} J_\nu\left[2\nu\lambda_i z^{\varepsilon(1-n)/2\nu}\right]\exp\left[-\frac{b}{a}\varepsilon^2(1-n)^2\lambda_i^2 x\right]\right] \tag{3.37}$$

is the concentration at any point (*x*,*z*).

Similarly the normalized flux concentration is

$$C_f(x) = \frac{m+1}{aH^{m+1}}\sum_{i=1}^{\infty}\left[\exp\left[-\frac{b}{a}\varepsilon^2(1-n)^2\lambda_i^2 x\right]\frac{\left(\int_0^H az^{\frac{1+2m-n}{2}} J_\nu\left[2\nu\lambda_i z^{\frac{\varepsilon(1-n)}{2\nu}}\right]dz\right)^2}{\int_0^H az^m\left(z^{\frac{1-n}{2}} J_\nu\left[2\nu\lambda_i z^{\frac{\varepsilon(1-n)}{2\nu}}\right]\right)^2 dz}\right] \tag{3.38}$$

Its transverse-mean variance can be calculated as

$$\sigma_f^2 = \frac{\int_{z_1}^{z_2}\left(C(x,z)u(z) - C_f(x)u_{mean}\right)^2 dz}{\int_{z_1}^{z_2} u(z)dz} \tag{3.39}$$

where $u_{mean} = \frac{1}{H}\int_0^H az^m dz = \frac{aH^m}{m+1}$.

The corresponding expressions for resident and flux concentrations in terms of dimensionless coordinates are

$$C_r(X) = \sum_{i=1}^{\infty} \left[\exp\left[-\frac{B}{A} \varepsilon^2 (1-n)^2 \lambda_i^2 X \right] \cdot \frac{\left(\int_0^1 Z^{(1-n)/2} J_\nu \left[2\nu\lambda_i Z^{\varepsilon(1-n)/2\nu} \right] dz \right) \left(\int_0^1 AZ^{\frac{1+2m-n}{2}} J_\nu \left[2\nu\lambda_i Z^{\frac{\varepsilon(1-n)}{2\nu}} \right] dZ \right)}{\int_0^1 AZ^m \left(Z^{\frac{1-n}{2}} J_\nu \left[2\nu\lambda_i Z^{\frac{\varepsilon(1-n)}{2\nu}} \right] \right)^2 dZ} \right] \quad (3.40)$$

and

$$C_f(X) = \frac{m+1}{A} \sum_{i=1}^{\infty} \left[\exp\left[-\frac{B}{A} \varepsilon^2 (1-n)^2 \lambda_i^2 X \right] \cdot \frac{\left(\int_0^1 aZ^{\frac{1+2m-n}{2}} J_\nu \left[2\nu\lambda_i Z^{\frac{\varepsilon(1-n)}{2\nu}} \right] dZ \right)^2}{\int_0^1 AZ^m \left(Z^{\frac{1-n}{2}} J_\nu \left[2\nu\lambda_i Z^{\frac{\varepsilon(1-n)}{2\nu}} \right] \right)^2 dZ} \right] \quad (3.41)$$

respectively, and the dimensionless-space analogue of eq. 3.37 is

$$C(X,Z) = \sum_{i=1}^{\infty} \left[\frac{\int_0^1 AZ^{\frac{1+2m-n}{2}} J_\nu \left[2\nu\lambda_i Z^{\frac{\varepsilon(1-n)}{2\nu}} \right] dZ}{\int_0^1 AZ^m \left(z^{\frac{1-n}{2}} J_\nu \left[2\nu\lambda_i Z^{\frac{\varepsilon(1-n)}{2\nu}} \right] \right)^2 dZ} \cdot Z^{(1-n)/2} J_\nu \left[2\nu\lambda_i Z^{\varepsilon(1-n)/2\nu} \right] \exp\left[-\frac{B}{A} \varepsilon^2 (1-n)^2 \lambda_i^2 X \right] \right] \quad (3.42)$$

3.4 Parameter Sensitivity Analysis

Because of the constraint $p = n - 2$, the dimensionless model (eqs. 3.29, 3.32, 3.40, 3.41, and 3.42) can be viewed as essentially governed by only five parameters: *A*, *B*, *F*, *m*, and *p*, (or *n*) (with the equations as written, exponent *n* is limited to values other than unity in order that the solutions do not produce divide-by-zero errors at $Z = 0$; however solutions can be developed for the special case of $n = 1$, as detailed in

Appendix B). Figure 3.2a presents an example normalized concentration "surface" for the dimensionless reactor model, calculated over unitary *X*-*Z* space on 20 by 20 point spacing using eq. 3.42 with the following parameters: $A = 1$, $B = 0.1$, $F = 0.2$, $m = 1/7$, and $p = -13/7$ (i.e. $n = 1/7$). Figure 3.2b displays a result generated using the same values for *A*, *B*, and *F*, but exponents $m = 4/7$ and $p = -8/7$ ($n = 6/7$). For ease in visualization, both figures are shown in the statistically equivalent bilaterally symmetrical form over an *X* domain that extends from 0 to 2, with the centerline at $X=1$, and the concentrations for *X* values greater than 1 simply plotted as a mirror image of those obtained for *X* less than 1. The mean difference over the entire *X*-*Z* domain between the two figures in terms of normalized concentration is 0.07, and the maximum difference is about 0.25. The similarity between the shapes of the response surfaces, as well as with those produced using other combinations of exponents (not shown), suggests that model results are not very sensitive to the magnitudes of the exponents within the ranges of interest (i.e. *m* and *n* positive and *p* negative, with $p = n - 2$).

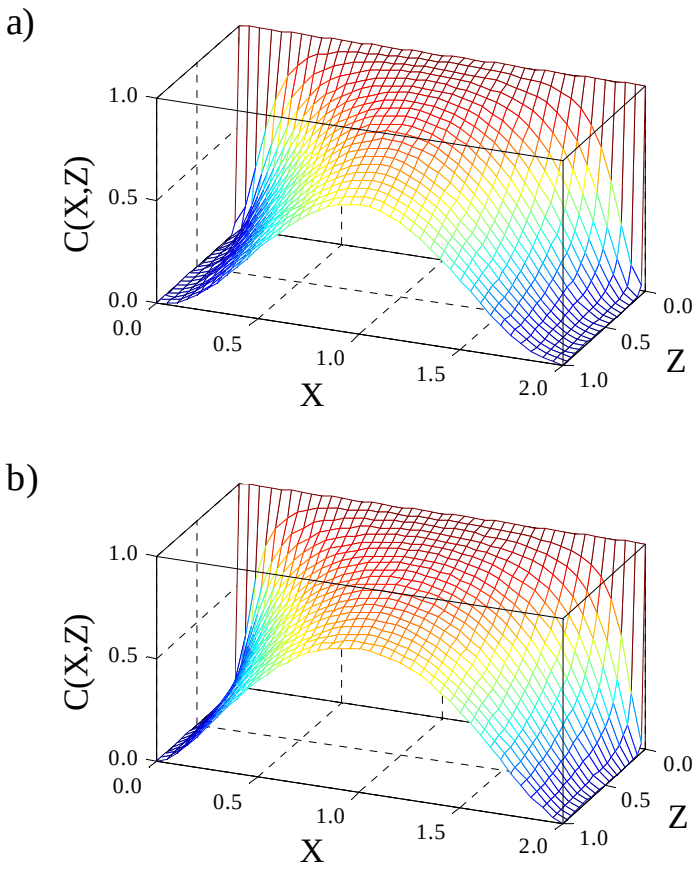

Figure 3.2 Dimensionless reactor model (eq. 3.42) results over *X*-*Z* space, with advective, dispersive, and reactive term multipliers $A = 1$, $B = 0.1$, $F = 0.2$; and exponents: a) $m = 1/7$, $n = 1/7$, $p = -13/7$; and b) $m = 4/7$, $n = 6/7$, $p = -8/7$.

By contrast, model results seem to be relatively sensitive to the magnitudes of *A*, *B*, and *F*. Sensitivity to these parameters is examined graphically in Figures 3.3a, b, and c. The figures display outlet ($X = 1$) flux concentrations calculated using eq. 3.41, for combinations of all three parameters. All simulations were conducted using $m = 4/7$, $p = -8/7$, and $n = 6/7$. Figure 3.3a demonstrates model result sensitivity to various combinations of *B* and *F*, with *A* fixed. Figure 3.3b similarly demonstrates model sensitivity to *A* and *B*, with *F* fixed, and Figure 3.3c demonstrates sensitivity to

A and *F*, with *B* fixed. As labeling of the axes indicates, and as the structures of eqs. 3.15 and 3.42 suggest, the relationships shown in these figures all scale linearly with the value of a single parameter – either *A*, *B*, or *F*. The figures also show outlet concentrations to be more sensitive to *F* than to *A* or *B*, at least for the selected values of the exponents. Model sensitivity to simultaneous variations in *A*, *B*, and *F* is examined further in Figure 3.4, which shows interpolated isocontours that represent three different values (0.2, 0.5, and 0.8) of normalized flux concentration at $X = 1$. The figure shows a roughly linear increase in *F* with *A* to be necessary in order to attain a given outlet concentration. A general but less sensitive decrease in *F* with *B* for fixed outlet concentration is also indicated by the figure.

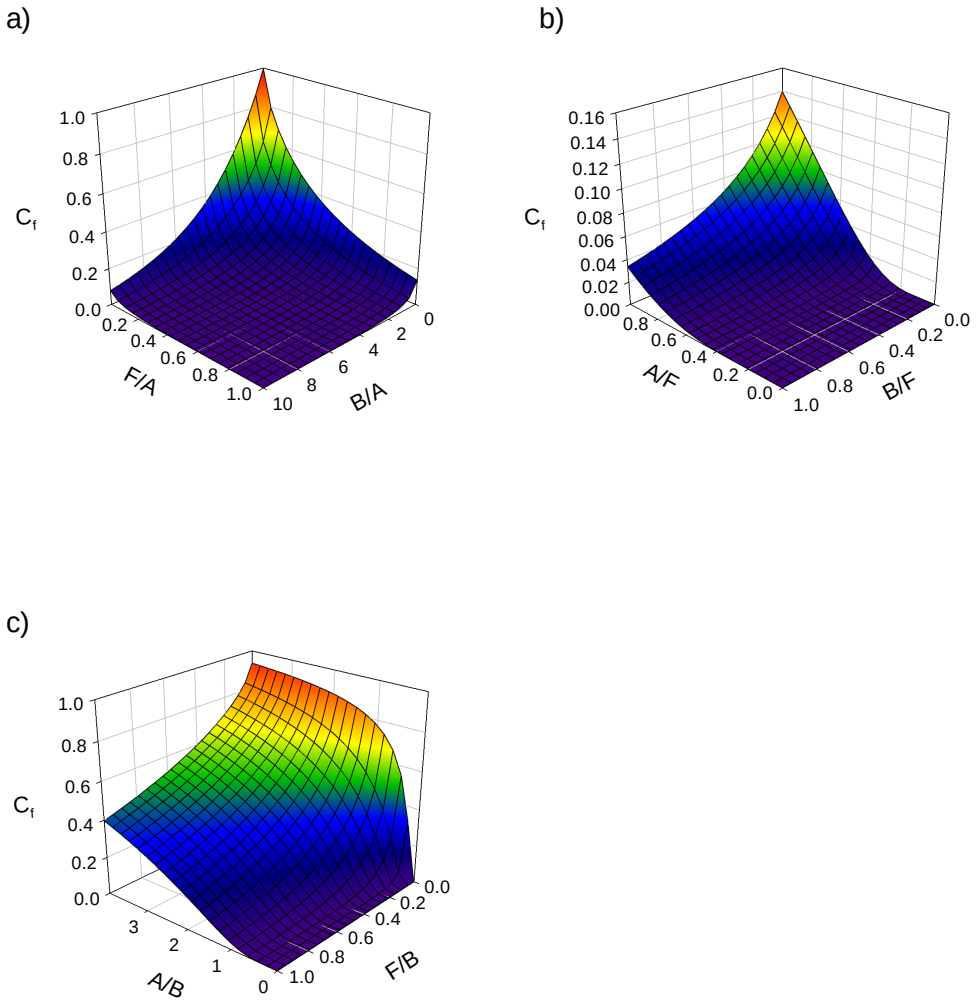

Figure 3.3 Outlet (X = 1) flux concentration reactor model (eq. 3.41) parameter sensitivity plots, with: a) A fixed, B and F variable; b) F fixed, A and B variable; c) B fixed, A and F variable.

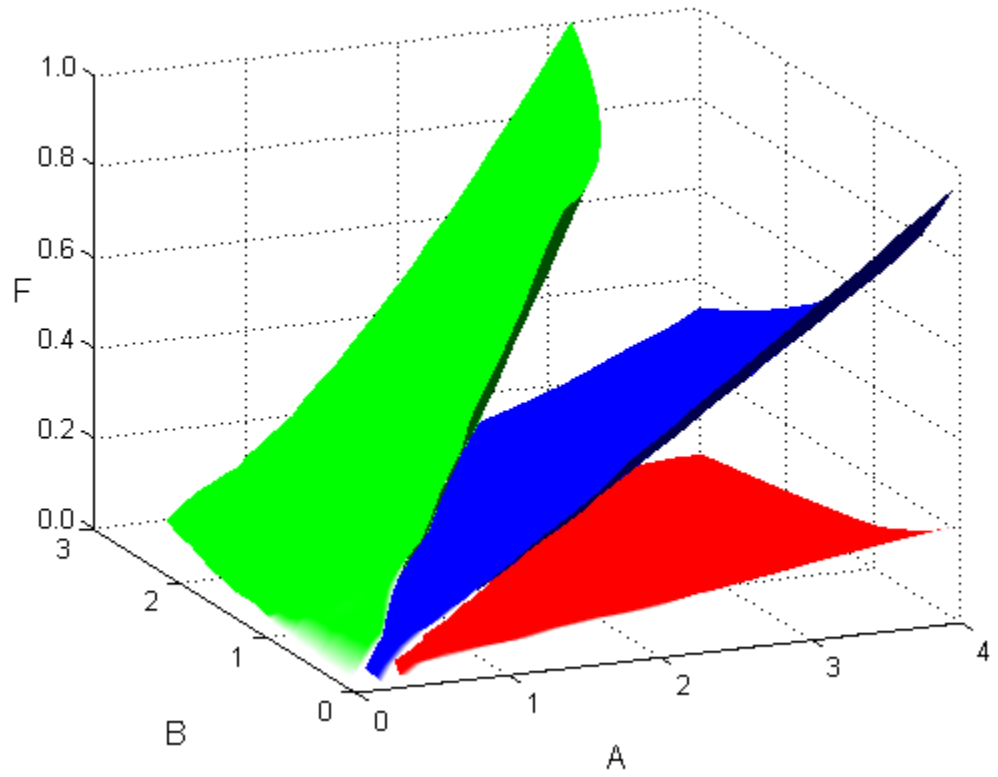

Figure 3.4 Interpolated isosurfaces in *A*-*B*-*F* space, of outlet (X = 1) normalized flux concentrations (eq. 3.41) equal to 0.2 (green), 0.5 (blue), and 0.8 (red).

3.5 Treatment Wetland Simulations

Attempting to use a value of zero for dispersion coefficient parameter *b* in order to negate the transverse dispersion term results in a divide-by-zero error in the calculation of ε (eq. 3.15), and theoretically infinite order for the Bessel functions (eq. 3.16), therefore the approaches developed in preceding paragraphs cannot be used to simulate completely hyperbolic (zero dispersion) systems. However, for the case of a "line" source (eqs. 3.35, 3.38) this kind of system can be simulated using the stochastic-convective DND model approach (Carleton, 2002). Rather than a Bessel function series, this approach calculates flux concentration by making use of the system's Residence Time Distribution (RTD), which can be directly calculated from

the power function velocity profile (eq. 3.3) as follows. The formula for a tracer breakthrough curve (BTC) following a step concentration input at the inlet boundary is:

$$\begin{cases} F(t) = 1 - \dfrac{(L/a)^{(m+1)/m}}{H^{m+1} t^{(m+1)/m}} & \dfrac{L}{aH^m} \le t \le \infty \\ F(t) = 0 & t \le \dfrac{L}{aH^m} \end{cases} \tag{3.43}$$

Differentiating $F(t)$ with respect to t we derive the RTD as:

$$\begin{cases} E(t) = \dfrac{(m+1)(L/a)^{(m+1)/m}}{mH^{m+1}} t^{-(2m+1)/m} & \dfrac{L}{aH^m} \le t \le \infty \\ E(t) = 0 & t \le \dfrac{L}{aH^m} \end{cases} \tag{3.44}$$

The DND is then derived from the RTD by employing eq. 19 from Carleton (2002) as follows, in which A and B refer in this case to parameters that relate Damköhler number (kt) to residence time t (rather than parameters relating advective and dispersive terms to dimensionless coordinate Z):

$$DND = E(Da) = \frac{(m+1)(L/a)^{(m+1)/m} A^{(\frac{1}{B}+\frac{1}{mB})}}{mH^{m+1} B} Da^{\frac{-(1+B+1/m)}{B}} \tag{3.45}$$

Normalized flux concentration, defined as in eq. 3.38 and expressed as a function of fractional longitudinal distance y, is then found by integrating over the DND:

$$C_f(y) = \int_{\frac{AL^B}{a^B H^{mB}}}^{\infty} \frac{(m+1)(L/a)^{(m+1)/m} A^{(\frac{1}{B}+\frac{1}{mB})}}{mH^{m+1} B} Da^{\frac{-(1+B+1/m)}{B}} e^{-Day} dDa \tag{3.46}$$

An example serves to graphically illustrate these ideas. The parameters in this example are: a = 0.005, m = 4/7 (mean u = 0.015 m/min); $f = 10^{-3}$, p = -8/7 (flow-weighted mean $k = 1.7\times10^{-4}$ min^{-1}); n = 6/7, and this time b is variable, for a variable

mean dispersion coefficient. The exponent (m) in the velocity term is set so that k is inversely proportional to the square of velocity, for consistency with assumptions used in previous work (Carleton, 2002; Carleton and Montas, 2007). The dimensions of the domain are 15 m width $\times$ 1000 m length, which corresponds conceptually with a treatment wetland of very long, thin dimensions, such as might be designed for the purpose of attempting to minimize short-circuiting and attain a situation as close to plug flow as possible. Figure 3.5 shows the RTD for this system calculated using eq. 3.44, and for comparative purposes a gamma-pdf RTD possessing the same first and second moments. Figure 3.6 shows longitudinal flux concentration profiles for the two DND models that result from these two RTDs. The striking differences between the shapes of the two curves, especially for x values greater than about 200 m, illustrates that flux mean concentration for stochastic-convective transport regimes is sensitive to higher moments of the velocity (or residence time) distribution, and is not simply a function of the first and second moments of the RTD.

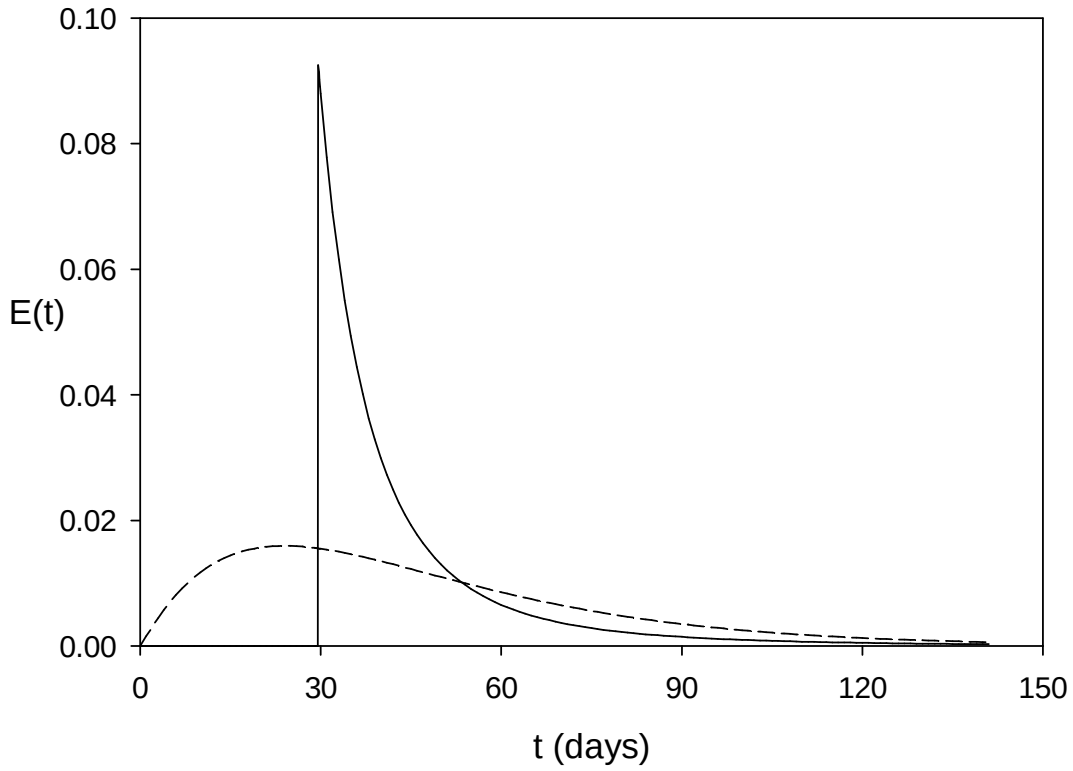

Figure 3.5 RTDs associated with stochastic-convective transport regimes (b = 0), for cases of: power function velocity profile (solid line), and traditional wetland gamma pdf RTD (dashed line). Despite the difference in shape, the two pdfs have the same first and second central moments.

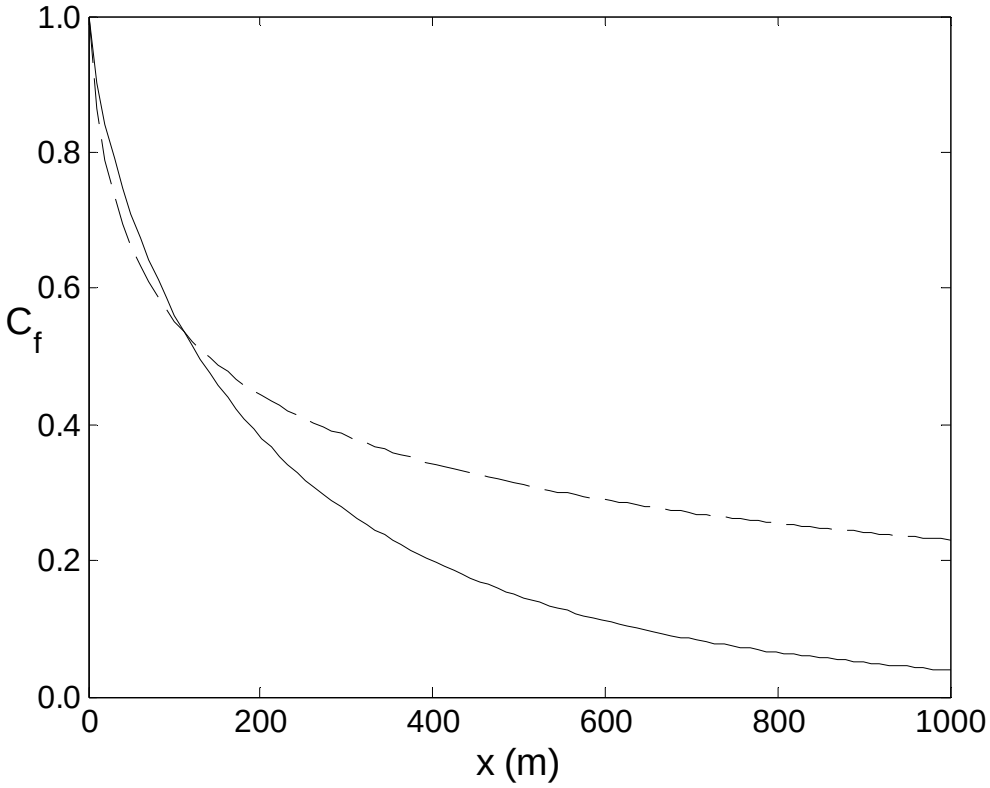

Figure 3.6 Longitudinal flux-weighted concentrations from stochastic-convective (DND) reactive transport models, derived from RTDs associated with: power function velocity profile (solid line), and gamma pdf RTD (dashed line).

The impact of transverse dispersion in the example of the system governed by a power function velocity profile is illustrated in Figure 3.7, which shows longitudinal flux concentration profiles for values of reaction term parameter *b* ranging from zero to 0.01. The figure shows that as *b* increases, the apparent efficiency of the system as a whole increases as well, with mean concentrations declining increasingly sharply with distance.

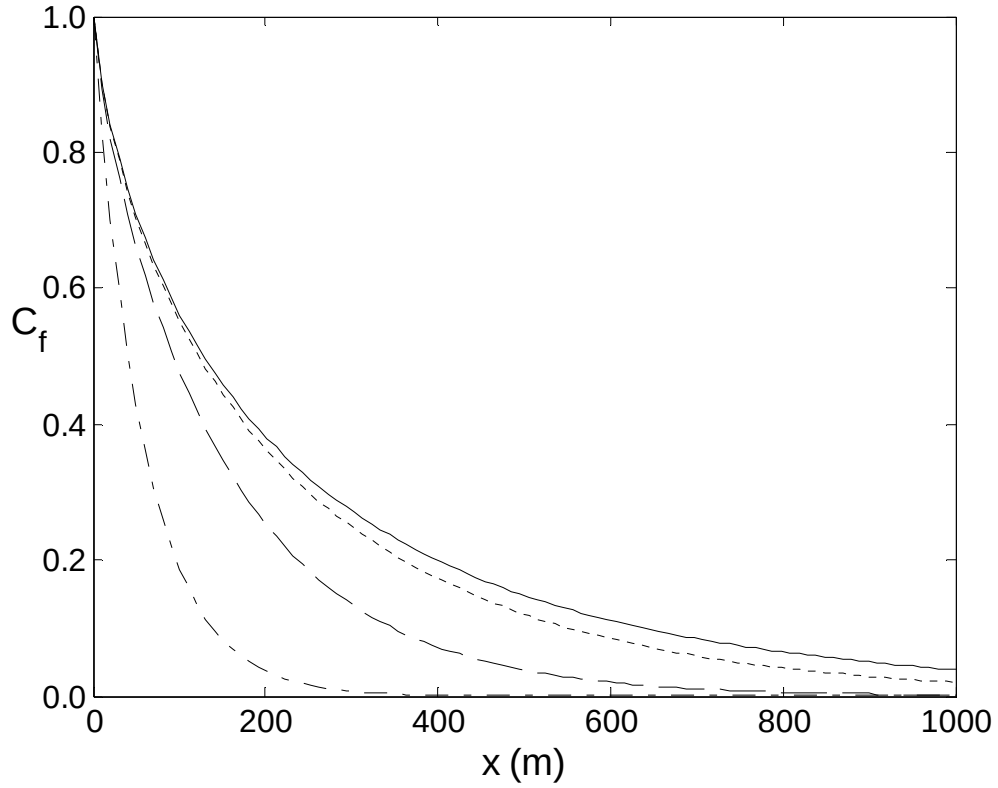

Figure 3.7 Comparison of longitudinal flux-weighted concentrations for transport domain with various degrees of transverse dispersion: b = 0 (solid line), b = 0.0001 (short dashes), b = 0.001 (long dashes), b = 0.01 (dot-dashes).

Figure 3.8 provides a view of transverse concentration profiles at various longitudinal distances, for the specific case of *b* with a value of 0.0001. The changing shape with distance of the concentration profile is a reflection of the impact of transverse dispersion tending to move constituent away from the less-reactive portion of the domain (the centerline in a bilaterally symmetric representation) and toward the more-reactive areas (the boundaries) as transport proceeds.

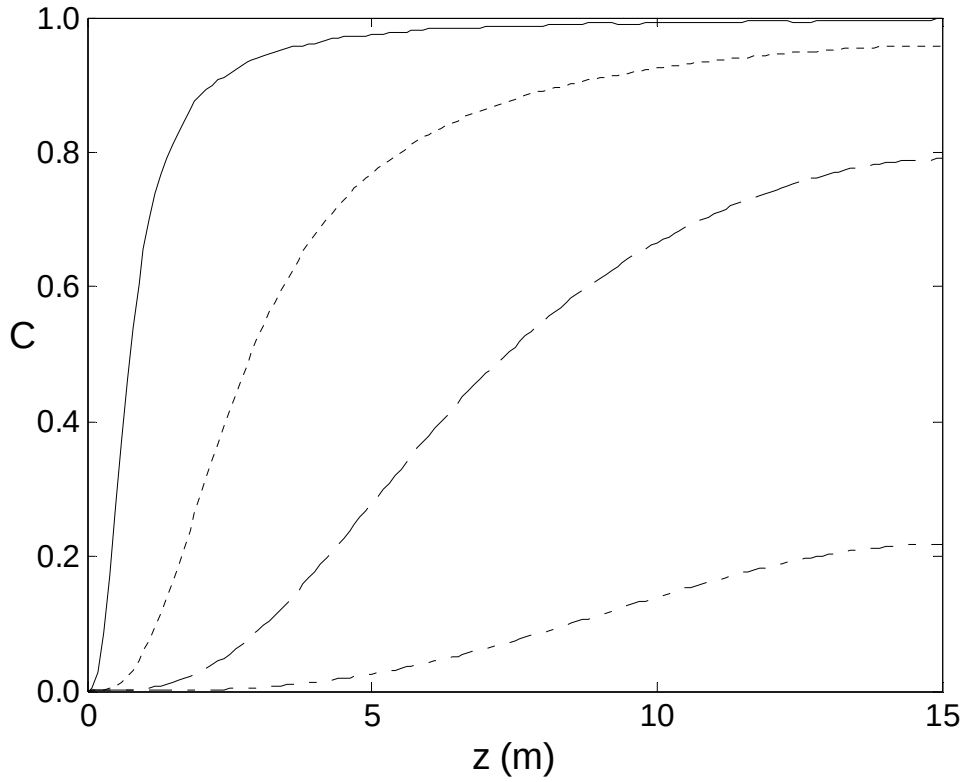

Figure 3.8 Transverse concentration profiles for simulation using b = 0.0001 at distances x = 2 m (solid line), x = 20 m (short dashes), x = 100 m (long dashes), and x = 500 m (dot-dashes).

Figure 3.9 shows equivalent plug-flow reactor (PFR) *k* values (k_{eff}) plotted as functions of longitudinal distance from the inlet ($x = 0$). These values were back-calculated from results of the simulations using the following rearrangement of the plug-flow equation

$$k_{eff} = \frac{\overline{u}}{x} \ln\left(\frac{C_i}{C_f(x)} \right) \tag{3.47}$$

where $\overline{u}$ is mean velocity, and C_i is inlet concentration (unity in this case). All of the simulations show declining k_{eff} with distance (especially near the inlet), consistent with the observation that k_{eff} in wetlands tends to increase with increasing hydraulic

loading rate (Kadlec, 2000). Most striking in the figure is the effect of *b*, which shifts the entire k_{eff} curve upward dramatically as it increases. Higher values of *b* also apparently drive k_{eff} toward (low) asymptotic values more rapidly.

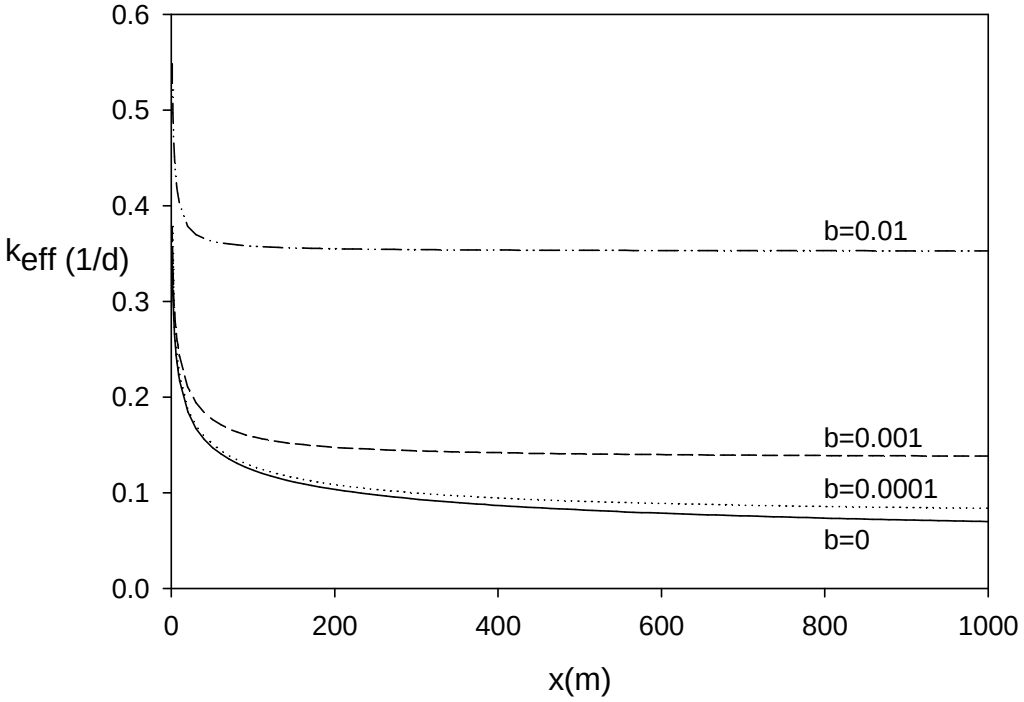

Figure 3.9 Effective plug-flow removal rate coefficients calculated as functions of longitudinal distance (eq. 3.43), for simulations with various degrees of transverse dispersion: $b = 0$ (solid line), $b = 0.0001$ (short dashes), $b = 0.001$ (long dashes), $b = 0.01$ (dot-dashes).

3.6 Discussion

The simulation results demonstrate ways that the solutions presented in this paper can be used to gain insights into interactions of idealized advective, dispersive, and reactive fluxes governing longitudinal transport of constituents. The example based on a conceptual treatment wetland illustrates that the equations provide a framework for theoretical inquiries such as quantifying the impact of transverse mixing on bulk removal rates. The outcome that transverse mixing

increases performance in a simulated wetland is qualitatively consistent with both field observations on wetlands (Kadlec, 2008) and the results of wetland simulations by other researchers (Lightbody et al., 2007). Transverse mixing essentially works to counter the effect of short-circuiting, wherein relatively untreated water passes relatively quickly through what amount to zones of preferential flow, thereby decreasing overall reactor performance.

The two-dimensional reactive transport equation solutions presented in this paper represent an improvement in realism over previous stochastic-convective modeling approaches developed to simulate heterogeneous bioenvironments (Carleton, 2002; Carleton and Montas, 2007), in the sense that they incorporate transverse dispersion as an aspect of longitudinal mixing, in addition to heterogeneous velocity. For comparison with results in this analysis, future work will investigate analogous stochastic representations of unbounded reactive transport regimes in which velocity, reaction rate coefficient, and dispersion coefficient are all treated as random, statistically stationary variables instead of simple functions of geometry.

Chapter 4: Stochastic Modeling of Reactive Transport in Wetlands

4.1 Abstract

This study describes the development of a general model of reaction and performance in spatially heterogeneous bioreactors such as treatment wetlands. The modeled domain possesses local-scale velocities, reaction rates and transverse dispersion coefficients that are functions of an underlying heterogeneity variate representing one or more controlling biophysical attributes, for example, reactive surface area (submerged plant) density. Reaction rate coefficients are treated as related to local velocities in an inverse square fashion via their mutual dependence upon the variate. The study focuses on the solution for the steady-state case with constant inlet concentration. Results compare well with exact solutions developed for laterally-bounded systems in which the heterogeneity is represented explicitly. Employing the bicontinuum analogue of the second-order model, an expression for an effective longitudinal dispersion coefficient as a function of travel distance is developed using the method of moments. The result provides insights into the behavior of concentration as transverse mixing drives the system asymptotically toward Fickian longitudinal dispersion. The model may represent an improvement over other approaches for characterizing treatment wetland performance because it accounts for evolving shear flow dispersion, and because parameters are few in number, physically based, and invariant with mean velocity.

Notation

a, b, f	multipliers in velocity, dispersion and reaction terms, respectively
A	integrated covariance parameter
c_1, c_2	characteristic concentrations
$\bar{c}$	mean (resident) concentration
c_f	mean (flux) concentration
f_1, f_2	fractions of continuum associated with each characteristic concentration
m, n, p	exponents in velocity, dispersion and reaction terms, respectively
D	transverse dispersion coefficient
D_L	effective longitudinal dispersion coefficient
$D_{L,\infty}$	asymptotic effective longitudinal dispersion coefficient
H	transverse wetland dimension or period of heterogeneity
k	reaction rate coefficient
κ_1, κ_2	velocity-independent decay coefficients in steady-state solution
L	intra-continuum mixing coefficient
r_1, r_2	decay coefficients in steady-state solution
t	time
w	heterogeneity variate ($=X^{-1/2}$)
x	coordinate in the direction of flow
$x_k^{1/2}$	distance scale for decay
$x_D^{1/2}$	distance scale for transition to Fickian dispersion
X	vegetation-litter surface area density, and/or reciprocal depth

z	coordinate transverse to direction of flow
α, β, γ	proportionality constants for D, k, and u respectively
λ	zero-mean, unit-variance version of w, or eigenvalue
Λ	longitudinal wetland dimension
$\rho_{c\lambda}$	correlation of c with λ
$\zeta_1, \zeta_2, \xi_1, \xi_2$	coefficients in steady-state solution
σ_c^2	transverse variance of concentration
σ_t^2	temporal variance of inert tracer pulse
σ_x^2	spatial (longitudinal) variance of inert tracer pulse
τ	mean residence time
θ_1, θ_2	composite coefficients in steady-state solution

4.2 Introduction

Wetlands have become popular around the world as low-cost systems for treating various kinds of wastewaters (Kadlec and Wallace, 2009). Macrophytes in wetlands may enhance pollutant removal through a variety of mechanisms, including direct uptake, physical filtration, and enhancement of microbially-mediated processes. In free water surface wetlands and natural marshes, macrophytes strongly influence water movement. Flow patterns through and around stands of rooted plants can be quite complex, and may involve recirculation-zones downstream of stems (Nepf et al., 1997a), coherent vortices at the interface between plant canopies and open water (White and Nepf, 2008), and significant heterogeneity in magnitude and direction of water velocities at various spatial scales (Nepf et al., 1997b; Nepf and Koch, 1999; Green, 2004). In general, plants are observed to increase frictional drag that slows the movement of water passing in their vicinity (Champion and Tanner, 2000; Fonseca et al., 1982; Sand-Jensen and Mebus, 1996). Studies have documented significant enhancement of sedimentation within stands of vegetation (Moore, 2004; Thornton, 1997). Epiphytic biofilms coating submerged leaves, stems and litter have been shown to play key roles in processes including nitrification (Bastkiven et al., 2003), denitrification (Eriksson, 2001; Eriksson and Weissner, 1997; Eriksson and Weissner, 1999), and phosphorus uptake (Pietro et al., 2006; Scinto and Reddy, 2003). For some chemical constituents then, plant density distributions in wetlands may be key influences on distributions of both local velocities and local reaction rates.

Because of the physical and biological complexity in wetlands, and the general lack of detailed information about the internal workings in any particular wetland, performance modeling for treatment wetlands has tended toward semi-empirical, black-box approaches that employ minimal numbers of parameters to characterize gross removal. Plug-flow reactor (PFR) models were initially popular for this purpose (Kadlec and Knight, 1996), but were found to suffer from systematic problems, including apparent parameter dependence on flow rate (Kadlec, 2000). More recently, compartmentalized models based on tanks-in-series (TIS) hydraulics have been advocated as general descriptors that account for velocity and/or reaction rate heterogeneity in wetlands, using a minimal number of parameters (Kadlec, 2003; Kadlec and Wallace, 2009). However the question of whether the parameters of such models are robust to alterations in hydraulic loading has yet to be fully addressed.

As an aspect of hydraulic complexity, researchers have noted the existence of "short-circuiting" in treatment wetlands, which allows some fraction of influent to pass through relatively untreated (Dierberg et al., 2005; Kjellin et al., 2007; Martinez and Wise, 2003), thereby adversely impacting reactor efficiency. In an extreme example, a recent study of a wetland in Georgia found a residence time distribution (RTD) that was essentially binary in nature, such that two very different velocities were judged to be "sufficient to describe water movement" in the wetland (Lightbody et al., 2008). Carleton (2002) and Carleton and Montas (2007) developed wetland models based upon the concept of broad distributions of flow paths whose velocities are precisely those implied by the transit times in a wetland's RTD. The main

limitation of this “stochastic-convective” approach is the absence of mass-transfer between stream lines.

Adequate characterization of longitudinal mixing may be crucial to developing simple yet robust models of treatment wetland performance. As defined by Taylor (1954) shear-flow dispersion arises from spatially heterogeneous advection in combination with scalar diffusion across stream lines. The early-time behavior of such a system is stochastic-convective, which corresponds to that of models described above. After sufficient transverse mixing has occurred, and with proper velocity autocorrelation systems exhibit an effective longitudinal dispersive flux that may be modeled as proportional to the mean concentration gradient (Berentsen et al., 2005; Gelhar et al., 1979; Matheron and DeMarsily, 1980). In the large-time regime dispersion is Fickian and transport can be represented by the classical one-dimensional advective dispersion equation (ADE). Like the PFR model, the ADE model is appealing because of its simplicity, which is also its weakness. Studies on transport in various media and environments, including wetlands, have documented solute spreading that cannot be properly characterized by the ADE, apparently because the observed longitudinal mixing corresponds not to the large-time asymptotic regime (ADE), but to either the early-time asymptotic regime (stochastic-convective), or to the transition between them (Day, 1977; Gelhar, 1993; Werner and Kadlec, 2000). A model which incorporates the full range of shear-flow dispersive behavior, from the stochastic-convective extreme to the advective-dispersive one, should be better able to approximate constituent dynamics, including reaction, in such systems that exhibit intermediate or evolving dispersive character.

The objective of this paper is to develop and evaluate a model of reactive solute transport applicable to treatment wetlands that overcomes the limitations of prior approaches by representing the full range of transport dynamics from early advective, through transitional, to large-time Fickian. The model is developed by volume-averaging of local transport equations where a variable related to vegetation density is taken as the primary heterogeneity variate due to its governing role in flow (obstruction and bypass) as well as reaction (e.g. biofilms and plant uptake) processes. The results of the theoretical analysis presented in this study are consistent with the general observations of Lightbody et al. (2008) but suggest that two distinctly observable velocities, or groupings of similar velocities, need not comprise the flow field in order for two flow paths to adequately represent a heterogeneous system. Rather, we will show that two characteristic velocities (and other, related key properties) derived via canonical transformation of a second-order system of governing transport equations can serve to represent the transport and reaction dynamics of a system possessing broad distributions of velocities and reaction rate coefficients.

To our knowledge mobile-mobile models have not previously been used to represent transport-reaction dynamics in wetlands or other heterogeneous ecological systems. Advantages of the approach are the flexibility it appears to offer for representing spatially complex domains using only a few, physically-based parameters, and for simulating systems that range from stochastic-convective, to evolving pre-asymptotic, to Fickian in terms of their bulk longitudinal dispersion characteristics. Although the theoretical work described in this paper is loosely

focused on free water surface wetlands, the approach is intended to be general enough to apply to other kinds of environmental systems, possibly including streams, soils, aquifers, and subsurface flow treatment wetlands.

This paper is arranged in the following fashion. We begin with development of a correlation-based second-order approximation of transport dynamics in a stochastic domain, and proceed to transformation of the resulting system of equations into bicontinuum form. The resulting mobile-mobile model is compared with mass-transfer models of biofilm-based reaction in wetlands, and then steady-state solutions for resident and flux concentrations are derived for the case of constant inlet concentration (a reactor model). For the corresponding pulse-loaded system a moment analysis based on input of a non-reacting constituent (tracer) is next used to develop an expression for the effective longitudinal dispersion coefficient as a function of travel time and distance. The model is then evaluated by comparing simulation results with the predictions of a two-dimensional transport model in which heterogeneity is specified as an explicit function of geometry. Lastly, conclusions are presented on the improvements that the proposed model offers over prior approaches.

4.3 Model Development

The transport of solutes within a treatment wetland is assumed to be correctly described at the local (stream tube) scale by a mathematically longitudinally hyperbolic (no longitudinal dispersion) and transversally parabolic (no transverse velocity), two-dimensional advective-dispersive-reactive equation of the form:

$$\frac{\partial c}{\partial t} = -k(z)c - u(z)\frac{\partial c}{\partial x} + \frac{\partial}{\partial z}\left[D(z)\frac{\partial c}{\partial z} \right] \tag{4.1}$$

where c represents solute concentration, k, u, and D are randomly varying reaction rate, longitudinal flow velocity, and transverse diffusion coefficients, respectively, t is time, x is longitudinal position from wetland inlet to outlet, and z is the transverse spatial coordinate. The transport parameters, k, u, and D are assumed to form stationary fields that result from the combined presence of wetland vegetation and of a uniform hydraulic gradient from inlet to outlet. The available reactive surface area for solutes, X, is assumed to be directly proportional to vegetation density and to form a stationary random field. This quantity is higher where plants which harbor microbiota are more abundant and smaller in the zones between such plants. It is further assumed that reaction rate coefficients, k, are locally proportional to the density of reactive surfaces and that flow velocity, u, is inversely proportional to k as flow is fastest in between plant stands. Based on the prior work of Carleton (2002) and Carleton and Montas (2007), u and k are assumed to be interrelated via functional dependencies of each on spatially variable reactive surface area density as:

$$u = \frac{\gamma}{X^{1/2}} \tag{4.2}$$

$$k = \beta X \tag{4.3}$$

Following prior studies, it is expected that flow field variability has a dominant effect on transport dynamics, and consequently we define the related primary heterogeneity variate as follows:

$$w = X^{-1/2} \tag{4.4}$$

The statistics of w (mean, variance and skewness) as well as its characteristic length (from its spatial autocorrelation function) are assumed known, from appropriate sampling of wetland vegetation density or possibly from design specifications for a

constructed wetland. For convenience, and in accordance with common statistical practice, the primary variate is normalized to zero-mean, unit-variance to produce:

$$\lambda = \frac{w - \overline{w}}{\sigma_w};\ w = \overline{w} + \lambda\sigma_w \tag{4.5}$$

where $\overline{w}$ is the mean of $X^{-1/2}$ (overbars indicate spatial averaging), and σ_w is the standard deviation. By definition then, $\overline{\lambda} = 0$ and $\overline{\lambda^2} = 1$. Substituting a change of variables into eq. 4.2, we express u in terms of λ:

$$u = \gamma w = \gamma\left(\overline{w} + \sigma_w\lambda\right) = \gamma\overline{w} + \gamma\sigma_w\lambda \tag{4.6}$$

This has the more general form

$$u = \overline{u} + \rho_{u\lambda}\lambda \tag{4.7}$$

where in this case $\overline{u} \equiv \gamma\overline{w}$, and the correlation of *u* with λ is denoted $\rho_{u\lambda} \equiv \overline{u\lambda} \equiv \gamma\sigma_w = \sigma_u$. We similarly express *k* in terms of λ as follows:

$$k = \beta\left(\overline{w} + \sigma_w\lambda\right)^{-2} \tag{4.8}$$

and expand it in a second-order Taylor series approximation

$$k = \frac{\beta}{\overline{w}^2} - \frac{2\beta\sigma_w}{\overline{w}^3}\lambda + \frac{3\beta\sigma_w^2}{\overline{w}^4}\lambda^2 + \ldots \approx \frac{\beta}{\overline{w}^2}\left[1 - 2\frac{\sigma_w}{\overline{w}}\lambda + 3\frac{\sigma_w^2}{\overline{w}^2}\lambda^2\right] \tag{4.9}$$

Truncation at second-order is accurate in this case when the coefficient of variation of *w* (i.e. $\sigma_w / \overline{w}$) is small. In similarity to eq. 4.6, this is of the general form

$$k = k_0 + \rho_{k\lambda}\lambda + \rho_{k\lambda^2}\lambda^2 \tag{4.10}$$

where k_0 and the correlation terms are defined by equating eqs. 4.9 and 4.10 term by term. Using the nomenclature of eq. 4.10, the approximate mean reaction rate is calculated as

$$\bar{k} = k_0 + \rho_{k\lambda^2} \tag{4.11}$$

since $\overline{\lambda^2} = 1$. This is an approximation of $\bar{k}$ because of the Taylor series expansion used in the derivation. To both simplify the analysis and render (in a later step) coefficient matrices diagonalizable, we next employ the assumption that skewness and kurtosis of heterogeneity are not independent, but are linked by the relation (eq. 46, Montas et al., 2000)

$$\overline{\lambda^4} = \overline{\lambda^3}^2 + 1 \tag{4.12}$$

This assumption is a necessary limitation related to the fact that in the derived model, a continuous distribution of λ values will be approximated by a binary distribution. With eq. 4.12 the following expression for the variance of *k* is derived, employing the assumption that the mean of a sum is approximately equal to the sum of the mean of individual component terms:

$$\begin{aligned}
\sigma_k^2 &= \overline{(k-\bar{k})(k-\bar{k})} = \overline{\left(\rho_{k\lambda}\lambda + \rho_{k\lambda^2}\left(\lambda^2 - 1\right)\right)^2} \\
&\approx \left(\rho_{k\lambda}\right)^2 \overline{\lambda^2} + 2\rho_{k\lambda}\rho_{k\lambda^2}\overline{\lambda^3} - 2\rho_{k\lambda}\rho_{k\lambda^2}\overline{\lambda} + \left(\rho_{k\lambda^2}\right)^2 \overline{\lambda^4} - 2\left(\rho_{k\lambda^2}\right)^2 \overline{\lambda^2} + \left(\rho_{k\lambda^2}\right)^2 \\
&= \left(\rho_{k\lambda}\right)^2 + 2\rho_{k\lambda}\rho_{k\lambda^2}\overline{\lambda^3} + \left(\rho_{k\lambda^2}\right)^2\left(\overline{\lambda^3}^2 + 1\right) - \left(\rho_{k\lambda^2}\right)^2 \\
&= \left(\rho_{k\lambda} + \rho_{k\lambda^2}\overline{\lambda^3}\right)^2
\end{aligned} \tag{4.13}$$

and a corresponding expression for the standard deviation of *k*:

$$\sigma_k \approx \rho_{k\lambda} + \rho_{k\lambda^2}\overline{\lambda^3} \tag{4.14}$$

The transverse dispersion coefficient can be expressed using the same general functional dependence upon λ and λ^2 as assumed for *k*:

$$D = D_0 + \rho_{D\lambda}\lambda + \rho_{D\lambda^2}\lambda^2 \tag{4.15}$$

where mean D is given by

$$\overline{D} = D_0 + \rho_{D\lambda^2} \tag{4.16}$$

since $\overline{\lambda^2} = 1$. Using the same approach as for k, the standard deviation of D is derived to be:

$$\sigma_D = \rho_{D\lambda} + \rho_{D\lambda^2}\overline{\lambda^3} \tag{4.17}$$

Depending upon the nature of the relationship between D and u (or k), the relationship between D and λ may correspond with a truncated Taylor series as in eq. 4.9, or an exact expression as in eq. 4.7. Either way the general form is

$$D = \alpha\left(\overline{w} + \sigma_w\lambda\right)^q \tag{4.18}$$

where q is a constant, the magnitude of which determines the functional forms of the constant, and correlation terms in eq. 4.15. For example if q=3/2, then Taylor series expansion of eq. 4.17 gives $D_0 = \alpha\overline{w}^{3/2}$, $\rho_{D\lambda} = \frac{3\alpha\overline{w}^{1/2}\sigma_w}{2}$, and $\rho_{D\lambda^2} = \frac{3\alpha\sigma_w^2}{8\overline{w}^{1/2}}$. For other values of q, other definitions of these quantities result. If we choose q=1, then D is simply proportional to u, in accordance with common practice in groundwater modeling.

4.3.1 Correlation-Based Approximation

Given the definition of λ in eq. 4.5, concentration can be decomposed into the sum of a transverse mean and a spatially-fluctuating component (c'), which is approximated in terms of its correlation with the heterogeneity variate

$$c = \overline{c} + c' \cong \overline{c} + \lambda\rho_{c\lambda} \tag{4.19}$$

where $\rho_{c\lambda}$ is the correlation between c' and λ. With this representation, transverse concentration variance can be estimated from the correlation variable as (Montas et al., 2006):

$$\sigma_c^2 = \overline{c'^2} \approx \overline{(\lambda\rho_{c\lambda})^2} = \overline{\lambda^2}(\rho_{c\lambda})^2 = (\rho_{c\lambda})^2 \tag{4.20}$$

This is only an estimate since concentrations could vary spatially with other variates, orthogonal to λ, as well but has proven to be a good first approximation in prior studies (Montas et al., 2000; Montas, 2003).

Substituting the preceding decompositions for c, k, u, and D into equation 4.1 produces the decomposed version of the transport equation

$$\begin{aligned}
&\frac{\partial\overline{c}}{\partial t} + \lambda\frac{\partial\rho_{c\lambda}}{\partial t} = \\
&-k_0\overline{c} - k_0\lambda\rho_{c\lambda} - \lambda\rho_{k\lambda}\overline{c} - \lambda^2\rho_{k\lambda}\rho_{c\lambda} - \lambda^2\rho_{k\lambda^2}\overline{c} - \lambda^3\rho_{k\lambda^2}\rho_{c\lambda} \\
&-\overline{u}\frac{\partial\overline{c}}{\partial x} - \overline{u}\lambda\frac{\partial\rho_{c\lambda}}{\partial x} - \lambda\rho_{u\lambda}\frac{\partial\overline{c}}{\partial x} - \lambda^2\rho_{u\lambda}\frac{\partial\rho_{c\lambda}}{\partial x} \\
&+D_0\frac{\partial^2\overline{c}}{\partial z^2} + D_0\frac{\partial^2(\lambda\rho_{c\lambda})}{\partial z^2} + \rho_{D\lambda}\frac{\partial}{\partial z}\left[\lambda\frac{\partial\overline{c}}{\partial z}\right] + \rho_{D\lambda}\frac{\partial}{\partial z}\left[\lambda\frac{\partial(\lambda\rho_{c\lambda})}{\partial z}\right] \\
&+\rho_{D\lambda^2}\frac{\partial}{\partial z}\left[\lambda^2\frac{\partial\overline{c}}{\partial z}\right] + \rho_{D\lambda^2}\frac{\partial}{\partial z}\left[\lambda^2\frac{\partial(\lambda\rho_{c\lambda})}{\partial z}\right]
\end{aligned} \tag{4.21}$$

Averaging eq. 4.21 then produces the mean transport equation

$$\begin{aligned}
\frac{\partial\overline{c}}{\partial t} \cong &-\left[k_0 + \rho_{k\lambda^2}\right]\overline{c} - \left[\rho_{k\lambda} + \overline{\lambda^3}\rho_{k\lambda^2}\right]\rho_{c\lambda} - \overline{u}\frac{\partial\overline{c}}{\partial x} - \rho_{u\lambda}\frac{\partial\rho_{c\lambda}}{\partial x} + D_0\frac{\partial^2\overline{c}}{\partial z^2} \\
&+\rho_{D\lambda^2}\frac{\partial^2\overline{c}}{\partial z^2} + \rho_{D\lambda}\frac{\partial^2\rho_{c\lambda}}{\partial z^2} + \overline{\lambda^3}\rho_{D\lambda^2}\frac{\partial^2\rho_{c\lambda}}{\partial z^2}
\end{aligned} \tag{4.22}$$

in which the following approximations are used

$$\overline{\frac{\partial^2(\lambda\rho_{c\lambda})}{\partial z^2}} \approx \frac{\overline{\lambda}\partial^2\overline{(\rho_{c\lambda})}}{\partial z^2} = 0 \tag{4.23a}$$

$$\overline{\frac{\partial}{\partial z}\left[\lambda\frac{\partial\overline{c}}{\partial z}\right]} \approx \frac{\overline{\lambda}\partial^2\overline{c}}{\partial z^2} = 0 \tag{4.23b}$$

$$\overline{\frac{\partial}{\partial z}\left[\lambda\frac{\partial(\lambda\rho_{c\lambda})}{\partial z}\right]}\approx\overline{\frac{\partial}{\partial z}\left[\lambda^2\frac{\partial\rho_{c\lambda}}{\partial z}\right]}\approx\overline{\lambda^2}\frac{\partial^2\rho_{c\lambda}}{\partial z^2}=\frac{\partial^2\rho_{c\lambda}}{\partial z^2} \tag{4.23c}$$

$$\overline{\frac{\partial}{\partial z}\left[\lambda^2\frac{\partial\overline{c}}{\partial z}\right]}\approx\overline{\lambda^2}\frac{\partial^2\overline{c}}{\partial z^2}=\frac{\partial^2\overline{c}}{\partial z^2} \tag{4.23d}$$

$$\overline{\frac{\partial}{\partial z}\left[\lambda^2\frac{\partial(\lambda\rho_{c\lambda})}{\partial z}\right]}\approx\overline{\frac{\partial}{\partial z}\left[\lambda^3\frac{\partial\rho_{c\lambda}}{\partial z}\right]}=\overline{\lambda^3}\frac{\partial^2\rho_{c\lambda}}{\partial z^2} \tag{4.23e}$$

Multiplying equation 4.21 by λ and averaging similarly produces the following expression for correlation of concentration with the heterogeneity variate:

$$\begin{aligned}\frac{\partial\rho_{c\lambda}}{\partial t}\cong&-\left[\rho_{k\lambda}+\overline{\lambda^3}\rho_{k\lambda^2}\right]\overline{c}-\left[k_0+\overline{\lambda^3}\rho_{k\lambda}+\overline{\lambda^4}\rho_{k\lambda^2}+\frac{D_0}{A}\rho_{c\lambda}\right]\rho_{c\lambda}\\&-\rho_{u\lambda}\frac{\partial\overline{c}}{\partial x}-\overline{u}\frac{\partial\rho_{c\lambda}}{\partial x}-\overline{\lambda^3}\rho_{u\lambda}\frac{\partial\rho_{c\lambda}}{\partial x}\\&+D_0\frac{\partial^2\rho_{c\lambda}}{\partial z^2}+\rho_{D\lambda}\frac{\partial^2\overline{c}}{\partial z^2}+\rho_{D\lambda^2}\overline{\lambda^3}\frac{\partial^2\overline{c}}{\partial z^2}+\rho_{D\lambda}\overline{\lambda^3}\frac{\partial^2\rho_{c\lambda}}{\partial z^2}+\rho_{D\lambda^2}\overline{\lambda^4}\frac{\partial^2\rho_{c\lambda}}{\partial z^2}\end{aligned} \tag{4.24}$$

in which the additional approximations are used

$$\overline{\lambda\frac{\partial}{\partial z}\left[\lambda\frac{\partial\overline{c}}{\partial z}\right]}\approx\overline{\lambda^2}\frac{\partial^2\overline{c}}{\partial z^2}=\frac{\partial^2\overline{c}}{\partial z^2} \tag{4.25a}$$

$$\overline{\lambda\frac{\partial}{\partial z}\left[\lambda\frac{\partial(\lambda\rho_{c\lambda})}{\partial z}\right]}\approx\overline{\lambda^3}\frac{\partial^2\rho_{c\lambda}}{\partial z^2} \tag{4.25b}$$

along with the following first-order closure, equivalent to eq. 9 of Montas et al. (2000):

$$D_0\overline{\lambda\frac{\partial^2(\lambda\rho_{c\lambda})}{\partial z^2}}\approx-\frac{D_0}{A}\rho_{c\lambda}+D_0\frac{\partial^2\rho_{c\lambda}}{\partial z^2} \tag{4.26}$$

The approximations in eq. 4.23 and 4.25 are justified under the assumption that λ varies mildly in the *z*-direction, and can therefore be treated as a constant within the spatial derivative terms. Equation 4.26 approximates a dispersive heterogeneity-

concentration perturbation correlation term with the sum of a mean dispersive process and a local first-order decay process for $\rho_{c\lambda}$. The parameter A (see Appendix C for derivation) represents a characteristic scale of the heterogeneity field w, and may be obtained as a function of the spatial autocorrelation function of w using eq. C11, C15, or C19.

Next, employing eq. 4.12 again, we express equations 4.22 and 4.24 together in the matrix form

$$\begin{aligned}\frac{\partial}{\partial t}\begin{bmatrix}\bar{c}\\ \rho_{c\lambda}\end{bmatrix} &= -\left\{\begin{bmatrix}k_0 & 0\\ 0 & k_0+\dfrac{D_0}{A}\end{bmatrix}+\rho_{k\lambda}\begin{bmatrix}0 & 1\\ 1 & \overline{\lambda^3}\end{bmatrix}+\rho_{k\lambda^2}\left\{I+\overline{\lambda^3}\begin{bmatrix}0 & 1\\ 1 & \overline{\lambda^3}\end{bmatrix}\right\}\right\}\begin{bmatrix}\bar{c}\\ \rho_{c\lambda}\end{bmatrix}\\ &-\left\{\bar{u}I+\rho_{u\lambda}\begin{bmatrix}0 & 1\\ 1 & \overline{\lambda^3}\end{bmatrix}\right\}\frac{\partial}{\partial x}\begin{bmatrix}\bar{c}\\ \rho_{c\lambda}\end{bmatrix}\\ &+\left\{D_0 I+\rho_{D\lambda}\begin{bmatrix}0 & 1\\ 1 & \overline{\lambda^3}\end{bmatrix}+\rho_{D\lambda^2}\left\{I+\overline{\lambda^3}\begin{bmatrix}0 & 1\\ 1 & \overline{\lambda^3}\end{bmatrix}\right\}\right\}\frac{\partial^2}{\partial z^2}\begin{bmatrix}\bar{c}\\ \rho_{c\lambda}\end{bmatrix}\end{aligned} \tag{4.27}$$

Using relations 4.11, 4.14, 4.16, and 4.17 this is expressed more compactly as

$$\begin{aligned}\frac{\partial}{\partial t}\begin{bmatrix}\bar{c}\\ \rho_{c\lambda}\end{bmatrix} &= -\left\{\begin{bmatrix}\bar{k} & 0\\ 0 & \bar{k}+\dfrac{D_0}{A}\end{bmatrix}+\sigma_k\begin{bmatrix}0 & 1\\ 1 & \overline{\lambda^3}\end{bmatrix}\right\}\begin{bmatrix}\bar{c}\\ \rho_{c\lambda}\end{bmatrix}\\ &-\left\{\bar{u}I+\sigma_u\begin{bmatrix}0 & 1\\ 1 & \overline{\lambda^3}\end{bmatrix}\right\}\frac{\partial}{\partial x}\begin{bmatrix}\bar{c}\\ \rho_{c\lambda}\end{bmatrix}+\left\{\bar{D}I+\sigma_D\begin{bmatrix}0 & 1\\ 1 & \overline{\lambda^3}\end{bmatrix}\right\}\frac{\partial^2}{\partial z^2}\begin{bmatrix}\bar{c}\\ \rho_{c\lambda}\end{bmatrix}\end{aligned} \tag{4.28}$$

Equation 4.28 indicates substantial interactions between the transport dynamics of $\bar{c}$ and $\rho_{c\lambda}$. Reactive, advective and dispersive fluxes of mean concentration are partly functions of the concentration-heterogeneity correlation. Dynamics governing the heterogeneity correlation are similarly functions of mean concentration flux terms. The magnitudes of these interactions are proportional to the standard deviations of

stochastic parameters *u*, *D* and *k*. In the case of homogeneous values of these entities the interaction terms in eq. 4.28 would disappear, leaving a simple system of two separate ADE-type transport equations.

4.3.2 Bicontinuum Form

The extensive cross-interactions between $\bar{c}$ and $\rho_{c\lambda}$ somewhat complicate analysis and solution of the system of equations in eq. 4.28. However, the appearance of the common coefficient matrix in the advective, dispersive and reactive terms offers the opportunity for a linear transformation to convert $\bar{c}$ and $\rho_{c\lambda}$ into an equivalent pair of 'canonical' concentrations whose dynamics are (except for first-order exchange) independent of each other. The transformation method is detailed in Montas et al. (2000), and produces an equivalent bicontinuum form from a second-order system of equations such as eq. 4.28. Following this approach, the eigenvalues of the coefficient matrix in the advective and dispersive terms of eq. 4.28 are first calculated to be

$$\lambda_1 = \frac{\overline{\lambda^3} + \left(\overline{\lambda^3}^2 + 4\right)^{1/2}}{2}, \text{ and } \lambda_2 = \frac{\overline{\lambda^3} - \left(\overline{\lambda^3}^2 + 4\right)^{1/2}}{2} \tag{4.29}$$

The corresponding eigenvector matrix can then be expressed as

$$P = \begin{bmatrix} \dfrac{-\lambda_2}{\lambda_1 - \lambda_2} & \dfrac{\lambda_1}{\lambda_1 - \lambda_2} \\ \dfrac{1}{\lambda_1 - \lambda_2} & \dfrac{-1}{\lambda_1 - \lambda_2} \end{bmatrix} = \begin{bmatrix} f_1 & f_2 \\ \lambda_1 f_1 & \lambda_2 f_2 \end{bmatrix} \tag{4.30}$$

where f_1 and f_2 are interpreted as fractions of the medium corresponding to each of the two canonical concentration variables in a bicontinuum approximation of the second-order system (Montas et al., 2000). The inverse eigenvector matrix is then

$$P^{-1} = \begin{bmatrix} 1 & \lambda_1 \\ 1 & \lambda_2 \end{bmatrix} \tag{4.31}$$

The canonical variables c_1 and c_2 are obtained from the original variables by multiplying from the left by the inverse eigenvector matrix

$$\begin{bmatrix} c_1 \\ c_2 \end{bmatrix} = P^{-1} \begin{bmatrix} \bar{c} \\ \rho_{c\lambda} \end{bmatrix} \tag{4.32}$$

and the original variables may be obtained from the canonical ones by the inverse process

$$\begin{bmatrix} \bar{c} \\ \rho_{c\lambda} \end{bmatrix} = P \begin{bmatrix} c_1 \\ c_2 \end{bmatrix} \tag{4.33}$$

Multiplication of eq. 4.28 from the left by P^{-1} then results in the canonical form of the transport equation matrix, with diagonalized advection, dispersion, and reaction coefficient matrices, and a full mixing matrix in the first-order terms:

$$\begin{aligned} \frac{\partial}{\partial t}\begin{bmatrix} c_1 \\ c_2 \end{bmatrix} = &-\left\{\begin{bmatrix} \bar{k} + f_2 \dfrac{D_0}{A} & -f_2 \dfrac{D_0}{A} \\ f_1 \dfrac{D_0}{A} & \bar{k} + f_1 \dfrac{D_0}{A} \end{bmatrix} + \sigma_k \begin{bmatrix} \lambda_1 & 0 \\ 0 & \lambda_2 \end{bmatrix}\right\}\begin{bmatrix} c_1 \\ c_2 \end{bmatrix} \\ &-\left\{\bar{u}I + \sigma_u \begin{bmatrix} \lambda_1 & 0 \\ 0 & \lambda_2 \end{bmatrix}\right\}\frac{\partial}{\partial x}\begin{bmatrix} c_1 \\ c_2 \end{bmatrix} + \left\{\bar{D}I + \sigma_D \begin{bmatrix} \lambda_1 & 0 \\ 0 & \lambda_2 \end{bmatrix}\right\}\frac{\partial^2}{\partial z^2}\begin{bmatrix} c_1 \\ c_2 \end{bmatrix} \end{aligned} \tag{4.34}$$

When written in the form of two equations, it becomes obvious that eq. 4.34 constitutes a bicontinuum transport model with first-order mass exchange between continua:

$$\begin{cases} \dfrac{\partial c_1}{\partial t} = -f_2 \dfrac{D_0}{A}(c_1 - c_2) - k_1 c_1 - u_1 \dfrac{\partial c_1}{\partial x} + D_1 \dfrac{\partial^2 c_1}{\partial z^2} \\ \dfrac{\partial c_2}{\partial t} = -f_1 \dfrac{D_0}{A}(c_2 - c_1) - k_2 c_2 - u_2 \dfrac{\partial c_2}{\partial x} + D_2 \dfrac{\partial^2 c_2}{\partial z^2} \end{cases} \tag{4.35}$$

In eq. 4.35 the following notation is employed:

$$k_{1,2} = \bar{k} + \sigma_k \lambda_{1,2} \tag{4.36a}$$

$$u_{1,2} = \bar{u} + \sigma_u \lambda_{1,2} \tag{4.36b}$$

$$D_{1,2} = \bar{D} + \sigma_D \lambda_{1,2} \tag{4.36c}$$

Defining the mixing coefficient (a new quantity) $L = f_1 f_2 \frac{D_0}{A}$, eq. 4.35 may be expressed as

$$\begin{cases} \dfrac{\partial c_1}{\partial t} = -\dfrac{L}{f_1}(c_1 - c_2) - k_1 c_1 - u_1 \dfrac{\partial c_1}{\partial x} + D_1 \dfrac{\partial^2 c_1}{\partial z^2} \\ \dfrac{\partial c_2}{\partial t} = -\dfrac{L}{f_2}(c_2 - c_1) - k_2 c_2 - u_2 \dfrac{\partial c_2}{\partial x} + D_2 \dfrac{\partial^2 c_2}{\partial z^2} \end{cases} \tag{4.37}$$

Equation 4.37 is the canonical version of the statistically-based second-order transport model (eq. 4.28) and is fully equivalent to it, expressing all of the same fluxes and interactions in a form that arguably lends itself more fully to intuitive comprehension. The model recasts the correlation-based system in the form of two advective-dispersive-reactive continua that interact with each other through a first-order mass-transfer exchange. The two forms are fully interchangeable: eq. 4.28 may be obtained from eq. 4.37 by multiplying from the left by eigenvector matrix *P*, just as eq. 4.37 was obtained from eq. 4.28 by multiplying from the left by P^{-1}.

4.3.3 Comparison with Boundary Layer Mass-Transfer Models

The approach described above employs a system of two linked continua, each having its own characteristic properties, to approximate the dynamics of a single stratified, multi-dimensional reactive transport domain. The terms in eq. 4.37 involving differences between c_1 and c_2 are analogous in form to expressions of

diffusive mass transfer between continua separated by a boundary layer, as will be shown.

Fick's first law for diffusion along a concentration gradient (Chapra, 1997) is

$$J = -D\frac{\partial c}{\partial x} \tag{4.38}$$

where J is mass flux and D is an effective diffusion/dispersion coefficient. This can be approximated with the following finite-difference equation

$$J = \frac{D}{\delta}(c_1 - c_2) \tag{4.39}$$

in which δ is the mixing length, c_1 is concentration in the medium of interest, and c_2 is the concentration on the other side of the boundary layer. The quantity D/δ comprises an effective velocity, which is in this case a mass-transfer coefficient. Kadlec and Knight (1996) offer the following analogous expression for removal of constituents in wetlands via mass-transfer through boundary layers surrounding biofilms adhered to stationary surfaces (e.g. plant stems and litter)

$$J = \varphi\frac{A_b}{A_w}(c_1 - c_2) \tag{4.40}$$

where c_2 in this case is concentration at the biofilm surface, A_b is total biofilm area, A_w is wetland surface area, and φ is a proportionality constant. Equating eqs. 4.39 and 40, we find

$$\varphi\frac{A_b}{A_w} = \frac{D}{\delta} \tag{4.41}$$

or

$$\varphi h\frac{A_b}{V_w} = \frac{D}{\delta} \tag{4.42}$$

where V_w is wetland volume and h is depth. Rearrangement produces

$$\varphi \frac{A_b}{V_w} = \frac{D}{h\delta} \tag{4.43}$$

If biofilms are assumed to uniformly coat all vegetation surfaces, then the quantity A_b/V_w is equivalent to X in our notation (vegetation surface area density, m^2/m^3), therefore

$$\varphi \frac{A_b}{V_w} = \varphi X = \frac{D}{h\delta} \tag{4.44}$$

In wetlands δ may be interpreted as half the inverse of vegetation density (representing the effective mean distance between bulk solution and reactive surface), which leads to

$$\varphi X = \frac{2DX}{h} \tag{4.45}$$

A simple expression for removal of constituent during advective transport in a system governed by a reaction coefficient of this nature would be a mobile-immobile model, for example of the form

$$\begin{aligned} \frac{\partial c_1}{\partial t} &= -\frac{2DX}{h}(c_1 - c_2) - u\frac{\partial c_1}{\partial x} \\ \frac{\partial c_2}{\partial t} &= -\varepsilon\frac{2DX}{h}(c_2 - c_1) - k_2 c_2 \end{aligned} \tag{4.46}$$

where subscripts 1 and 2 refer to mobile and immobile zones, respectively, and ε is defined as the ratio of the mobile zone volume to the immobile zone (biofilm) volume (i.e. f_1/f_2). If reaction inside the immobile zone is sufficiently fast (i.e. k_2 sufficiently high) that c_2 is negligible compared with c_1, then eqs. 4.46 simplify approximately to a single advection-reaction equation for the mobile zone:

$$\frac{\partial c_1}{\partial t} = -\frac{2DX}{h} c_1 - u\frac{\partial c_1}{\partial x} \tag{4.47}$$

where quantity $\frac{2DX}{h}$ comprises an effective reaction rate coefficient.

For the case of shallow flow over a biofilm-coated substrate, such as an algal turf scrubber® (Adey and Loveland, 1998), a reasonable value for δ would be half of the water column depth (i.e. the mean diffusive transport length from water column to reactive surface). This leads to an expression analogous to eq. 4.46:

$$\begin{aligned} \frac{\partial c_1}{\partial t} &= -\frac{2D}{h^2}(c_1 - c_2) - u\frac{\partial c_1}{\partial x} \\ \frac{\partial c_2}{\partial t} &= -\varepsilon\frac{2D}{h^2}(c_2 - c_1) - k_2 c_2 \end{aligned} \tag{4.48}$$

where ε is again the ratio of the mobile zone volume to the immobile zone (biofilm) volume. Again if k_2 is sufficiently high that c_2 can be considered negligible, then eqs. 4.48 simplify to a single advection-reaction equation for the mobile zone:

$$\frac{\partial c_1}{\partial t} = -\frac{2D}{h^2} c_1 - u\frac{\partial c_1}{\partial x} \tag{4.49}$$

where $\frac{2D}{h^2}$ represents an effective reaction rate coefficient.

The similarity between the forms of eqs. 4.46 and 4.35 is noteworthy. Equating the two expressions, we find that the quantity A/f_2 (see eq. C23) corresponds with the quantity $h/(2X)$. Both of these terms have units of length squared. For eq. 4.48, A/f_2 equates with $h^2/2$, and correspondence with the form of C23 is again evident. Each of these expressions describes diffusive/dispersive mass transfer between separate continua or regions. Equations 4.46 and 4.48 describe mobile phase concentration in mobile-immobile bicontinuum models, in which transport occurs

solely in the mobile phase and reaction solely in the immobile phase. By contrast, the mobile-mobile bicontinuum model of eq. 4.35 quantifies a situation in which transport and reaction both occur in each phase, though at different rates in each.

The mobile-mobile approach of this study has the advantage of providing a means to address dynamics that result from distributions of governing parameters. It has the disadvantage that one may perceive the physical interpretation of each continuum as less straightforward than in the mobile-immobile approach, where a single mobile phase representing the water column in its entirety interacts with an immobile phase that represents "transient storage", "dead zone", or a biofilm layer within which reaction occurs. However in wetlands, as in other fluid systems, it has been challenging to identify what fraction of the flow volume should be ascribed to a non-flowing "immobile" zone (e.g. within boundary layers), and the present model provides a mathematical answer to this difficult question based on the characteristics (eigenvalues) of heterogeneity statistics. More precisely, it indicates that a purely immobile zone, while conceptually appealing at first sight, results from mathematical analysis in particular cases only and is not a generally applicable concept.

4.3.4 Steady-State Analysis

The steady-state case of the transport model (eq. 4.37), with constant inlet concentration, corresponds conceptually with a bioreactor such as a treatment wetland. In this case, the system is loaded continuously and the interest is in the level of load attenuation as a function of distance from inlet for a given set of flow and reaction parameters. Additionally, for a given wetland length, effluent (flux) concentration provides an indication of the system's treatment performance and the

level to which it helps mitigate impacts to downstream aquatic environments. The results of this type of steady-state analysis can be inverted for design purposes to select the required length, flow rate, and vegetation density characteristics that meet a specified loading rate and effluent concentration. The steady-state form of eq. 4.37 is:

$$\begin{cases} 0 = -k_1 c_1 - \dfrac{L}{f_1}(c_1 - c_2) - u_1 \dfrac{\partial c_1}{\partial x} + D_1 \dfrac{\partial^2 c_1}{\partial z^2} \\ 0 = -k_2 c_2 - \dfrac{L}{f_2}(c_2 - c_1) - u_2 \dfrac{\partial c_2}{\partial x} + D_2 \dfrac{\partial^2 c_2}{\partial z^2} \end{cases} \tag{4.50}$$

Assuming transversally-uniform inlet boundary conditions, within-continuum concentrations must be laterally homogeneous; therefore the transverse spatial derivatives of canonical concentrations are zero and the corresponding terms are dropped. The influence of D_0 is (importantly) however still present within the mixing term L, which is used to approximate the sum of all transverse fluxes across the original two-dimensional domain with an inter-continuum first-order mass-transfer process

$$\begin{cases} 0 = -k_1 c_1 - \dfrac{L}{f_1}(c_1 - c_2) - u_1 \dfrac{\partial c_1}{\partial x} \\ 0 = -k_2 c_2 - \dfrac{L}{f_2}(c_2 - c_1) - u_2 \dfrac{\partial c_2}{\partial x} \end{cases} \tag{4.51}$$

This system of two equations and two unknowns ($c_1$and c_2) is readily solved using direct substitution, which produces a second-order ordinary differential equation for one of the unknowns, e.g.

$$\alpha_1 \frac{\partial^2 c_2}{\partial x^2} + \alpha_2 \frac{\partial c_2}{\partial x} + \alpha_3 c_2 = 0 \tag{4.52}$$

where

$$\alpha_1 = \frac{u_1 u_2 f_1 f_2}{f_1 L} = \frac{1}{f_1}\left[\frac{A}{D_0}(u_1 u_2)\right] \tag{4.53a}$$

$$\alpha_2 = \frac{k_1 f_2 u_2}{L} + \frac{f_2 u_2}{f_1} + u_1 + \frac{k_2 f_2 u_1}{L} = \frac{1}{f_1}\left[\bar{u} + \frac{A}{D_0}(k_1 u_2 + k_2 u_1)\right] \tag{4.53b}$$

$$\alpha_3 = k_1 + \frac{k_1 k_2 f_2}{L} + \frac{f_2 k_2}{f_1} = \frac{1}{f_1}\left[\bar{k} + \frac{A}{D_0}(k_1 k_2)\right] \tag{4.53c}$$

The roots of equation 4.52 are:

$$\begin{cases} r_1 = \dfrac{-\alpha_2 + \left(\alpha_2^2 - 4\alpha_1\alpha_3\right)^{1/2}}{2\alpha_1} \\ r_2 = \dfrac{-\alpha_2 - \left(\alpha_2^2 - 4\alpha_1\alpha_3\right)^{1/2}}{2\alpha_1} \end{cases} \tag{4.54}$$

When $\alpha_2{}^2 > 4\alpha_1\alpha_3$ both roots are real, and we have the solutions

$$\begin{cases} c_1 = \xi_1 e^{r_1 x} + \xi_2 e^{r_2 x} \\ c_2 = \zeta_1 e^{r_1 x} + \zeta_2 e^{r_2 x} \end{cases} \tag{4.55}$$

where the constants are interrelated as follows:

$$\xi_1 = \left(1 + \frac{f_2}{L}(k_2 + u_2 r_1)\right)\zeta_1 \tag{4.56a}$$

$$\xi_2 = \left(1 + \frac{f_2}{L}(k_2 + u_2 r_2)\right)\zeta_2 \tag{4.56b}$$

Applying spatially uniform constant concentration at the inlet

$$\begin{cases} \bar{c}(0) = c_0 \\ \rho_{c\lambda}(0) = 0 \end{cases} \tag{4.57}$$

allows us to solve for ζ_1 and ζ_2

$$\zeta_1 = \left[\frac{k_2 + u_2 r_2}{u_2(r_2 - r_1)}\right] c_0 \tag{4.58a}$$

$$\zeta_2 = c_0 - \zeta_1 \tag{4.58b}$$

These in turn give us values of ξ_1 and ξ_2 using eqs. 4.56.

With the values of the four constants in the bicontinuum solution determined using eqs. 4.56 and 4.58, the resident mean concentration $(\bar{c})$ and heterogeneity variate correlation ($\rho_{c\lambda}$) are calculated as weighted sums of the concentrations within the two continua, which simplify as shown assuming that c_0 equals 1 (i.e. solutions for concentrations normalized to the inlet concentration):

$$\begin{aligned}
\bar{c} &= f_1 c_1 + f_2 c_2 = (f_1\xi_1 + f_2\zeta_1)e^{r_1 x} + (f_1\xi_2 + f_2\zeta_2)e^{r_2 x} \\
&= \left(1 + \frac{A}{D_0}(k_2 + u_2 r_1)\right)\zeta_1 e^{r_1 x} + \frac{A}{D_0}(k_2 + u_2 r_2)(1 - \zeta_1)e^{r_2 x} \\
&= \left(1 + \frac{A}{D_0}(k_2 + u_2 r_1)\right)\left(\frac{k_2 + u_2 r_2}{u_2(r_2 - r_1)}\right)e^{r_1 x} + \frac{A}{D_0}(k_2 + u_2 r_2)\left(1 - \frac{k_2 + u_2 r_2}{u_2(r_2 - r_1)}\right)e^{r_2 x}
\end{aligned} \tag{4.59a}$$

$$\begin{aligned}
\rho_{c\lambda} &= \lambda_1 f_1 c_1 + \lambda_2 f_2 c_2 = (\lambda_1 f_1\xi_1 + \lambda_2 f_2\zeta_1)e^{r_1 x} + (\lambda_1 f_1\xi_2 + \lambda_2 f_2\zeta_2)e^{r_2 x} \\
&= \lambda_1 \frac{A}{D_0}(k_2 + u_2 r_1)\zeta_1 e^{r_1 x} + \lambda_1 \frac{A}{D_0}(k_2 + u_2 r_2)(1 - \zeta_1)e^{r_2 x} \\
&= \lambda_1 \frac{A}{D_0}(k_2 + u_2 r_1)\left(\frac{k_2 + u_2 r_2}{u_2(r_2 - r_1)}\right)e^{r_1 x} + \lambda_1 \frac{A}{D_0}(k_2 + u_2 r_2)\left(1 - \frac{k_2 + u_2 r_2}{u_2(r_2 - r_1)}\right)e^{r_2 x}
\end{aligned} \tag{4.59b}$$

Flux mean concentration is derived as the flow-weighted sum of concentrations in the two continua:

$$
\begin{aligned}
c_f &= \left(\frac{f_1 u_1}{\bar{u}}\right) c_1 + \left(\frac{f_2 u_2}{\bar{u}}\right) c_2 = \left(\frac{f_1 u_1}{\bar{u}}\xi_1 + \frac{f_2 u_2}{\bar{u}}\zeta_1\right) e^{r_1 x} + \left(\frac{f_1 u_1}{\bar{u}}\xi_2 + \frac{f_2 u_2}{\bar{u}}\zeta_2\right) e^{r_2 x} \\
&= \left(1 + \frac{u_1}{\bar{u}}\frac{A}{D_0}\left(k_2 + u_2 r_1\right)\right)\zeta_1 e^{r_1 x} + \left(1 + \frac{u_1}{\bar{u}}\frac{A}{D_0}\left(k_2 + u_2 r_2\right)\right)\left(1 - \zeta_1\right) e^{r_2 x} \\
&= \left(1 + \frac{u_1}{\bar{u}}\frac{A}{D_0}\left(k_2 + u_2 r_1\right)\right)\left(\frac{k_2 + u_2 r_2}{u_2\left(r_2 - r_1\right)}\right) e^{r_1 x} + \left(1 + \frac{u_1}{\bar{u}}\frac{A}{D_0}\left(k_2 + u_2 r_2\right)\right)\left(1 - \frac{k_2 + u_2 r_2}{u_2\left(r_2 - r_1\right)}\right) e^{r_2 x}
\end{aligned}
\tag{4.60}
$$

This model thus consists of a weighted sum of two exponential decline functions that represent concentration as a function of (longitudinal) travel distance. The multipliers (weights) of the two exponential terms in eq. 4.60 have the property that they sum to unity. Careful analysis of the components of eq. 4.60 reveals that r_1 and r_2 are the only terms that vary with $\bar{u}$, and that they are inversely proportional to it. The flux concentration expression (eq. 4.60) can therefore be restated in the general form

$$
c_f = \theta_1 e^{-\frac{\kappa_1}{\bar{u}}x} + \theta_2 e^{-\frac{\kappa_2}{\bar{u}}x} \tag{4.61}
$$

where $\theta_1 + \theta_2 = 1$.

Recognizing that $\bar{u} = \Lambda/\tau$, where Λ is the length of the domain, and τ is mean residence time measured at this location, eq. 4.61 can be rewritten as

$$
c_f = \theta_1 e^{-\kappa_1 \tau \frac{x}{\Lambda}} + \theta_2 e^{-\kappa_2 \tau \frac{x}{\Lambda}} = \theta_1 e^{-\kappa_1 \tau y} + \left(1 - \theta_1\right) e^{-\kappa_2 \tau y} \tag{4.62}
$$

where y is fractional distance from inlet to outlet. Equation 4.62 is a model of flux concentration for this heterogeneous system in just three parameters ($\theta_1, \kappa_1, \kappa_2$), and they are all invariant with flow velocity. A properly chosen set of these parameters should therefore produce a model that continues to characterize the decline of flux concentration with distance, even when hydraulic loading rate is changed. This

contrasts with the situation for PFR models (comprising a single exponential decline function), which exhibit a well-documented dependence of decay coefficient on hydraulic loading rate when calibrated against wetland performance data (Kadlec, 2000).

Because the formulas for mean concentration (resident and flux) that result from the preceding analysis are sums of two separate exponential decay functions, net decline curves (concentration vs. longitudinal distance) can adopt more complex shapes than result from a PFR model. Nevertheless, the distance for decay of resident concentration to half the inlet concentration (c_0) – $x_{1/2}^k$ – a pseudo characteristic distance scale for reaction, may be a useful metric for characterizing early field bulk decay within these systems. We calculate this metric using

$$\bar{c}(x_{1/2}^k) = \frac{c_0}{2} = \left(f_1\xi_1 + f_2\zeta_1\right)e^{r_1 x_{1/2}^k} + \left(f_1\xi_2 + f_2\zeta_2\right)e^{r_2 x_{1/2}^k} \tag{4.63}$$

which leads to

$$A'e^{r_1 x_{1/2}^k} + B'e^{r_2 x_{1/2}^k} = \frac{A'+B'}{2} \tag{4.64}$$

where

$$\begin{cases} A' = \left(1 + \dfrac{f_1 f_2}{L}\left(k_2 + u_2 r_1\right)\right)\zeta_1 \\ B' = \left(1 + \dfrac{f_1 f_2}{L}\left(k_2 + u_2 r_2\right)\right)\left(1-\zeta_1\right) \end{cases} \tag{4.65}$$

Employing the definition of the roots in eq. 4.54, we define

$$\begin{cases} \alpha_1' = \dfrac{\alpha_2}{2\alpha_1} \\ \alpha_2' = \dfrac{\left(\alpha_2^2 - 4\alpha_1\alpha_3\right)^{1/2}}{2\alpha_1} \end{cases} \tag{4.66}$$

and therefore

$$\frac{2}{A'+B'}\left[A'e^{\alpha_2' x_{1/2}^k} + B'e^{-\alpha_2' x_{1/2}^k}\right] = e^{\alpha_1' x_{1/2}^k} \tag{4.67}$$

Because α_2' is positive the second term on the left hand side is relatively small. Dropping it leads to

$$\frac{2}{A'+B'}\left(A'e^{\alpha_2' x_{1/2}^k}\right) \cong e^{\alpha_1' x_{1/2}^k} \tag{4.68}$$

and therefore

$$x_{1/2}^k \cong \left(\frac{1}{\alpha_2'-\alpha_1'}\right)\ln\left(\frac{A'+B'}{2A'}\right) \tag{4.69}$$

Although bulk decay is not first order in concentration, and therefore a true 'half-life' cannot be said to exist (unless θ_1 or θ_2 equals zero), equation 4.69 defines the distance for decay of flux concentration to half the inlet concentration. In the next subsection we will develop an expression for a similar metric to quantify the degree of transition toward Fickian dispersion. Comparisons between values of the two metrics provide a rough quantitative indication of the importance of longitudinal dispersion as a potential influence on decay dynamics.

4.3.5 Development of Longitudinal Dispersion

When solute is introduced as a Dirac delta pulse at the inlet of a bicontinuum system, it travels initially as two separate pulses; all solute molecules move at one of the two velocities that characterize the continua. This is an example of stochastic-convective transport. As flow proceeds however, dispersive exchange between the continua immediately begins to produce an increasing fraction of total solute that travels at velocities intermediate between the two characteristic velocities.

Asymptotically the system approaches a state in which all introduced solute has spent some time in each of the continua. At the Fickian asymptote, longitudinal solute spreading appears to occur in proportion to the mean concentration gradient.

At any point during the progression toward the Fickian asymptote, an instantaneous effective longitudinal dispersion coefficient (D_L) can be calculated from the time rate of change of the spatial variance of an inert tracer cloud (Gelhar, 1993):

$$D_L = \frac{1}{2}\frac{d\sigma_x^2}{dt} \tag{4.70}$$

where spatial variance (σ_x^2) may be defined for a semi-infinite domain as follows

$$\sigma_x^2 = \frac{\int_0^\infty \left(x - \bar{x}\right)^2 c\,dx}{\int_0^\infty c\,dx} \tag{4.71}$$

where c is transversally-averaged (resident) concentration, x is longitudinal position, and $\bar{x}$ is the spatial centroid of the tracer:

$$\bar{x} = \frac{\int_0^\infty x c\,dx}{\int_0^\infty c\,dx} \tag{4.72}$$

The solution to the one-dimensional ADE with initial condition $c(x,0) = \delta(x)$ is

$$c(x,t) = \frac{1}{2\sqrt{D_L \pi t}} e^{\frac{-(x-ut)^2}{4D_L t}} \tag{4.73}$$

while the formula for a Gaussian probability density function is

$$f(x) = \frac{1}{\sigma_x \sqrt{2\pi}} e^{\frac{-(x-\mu)^2}{2\sigma_x^2}} \tag{4.74}$$

where $\mu = \bar{x}$. Equations 4.73 and 4.74 are the same if $\sigma_x^2 = 2Dt$, or $D = \frac{1}{2}\frac{\sigma_x^2}{t}$.

According to Hunt (1999), $\sigma_t^2 = 2\frac{Dx}{u^3} + 8\frac{D^2}{u^4} \cong 2\frac{Dx}{u^3}$ when $x >> \frac{4D}{u}$

where σ_t^2 is the temporal variance of an inert tracer cloud, defined as follows:

$$\sigma_t^2 = \frac{\int_{-\infty}^{\infty} (t-\tau)^2 \, c\,dt}{\int_{-\infty}^{\infty} c\,dt} \tag{4.75}$$

where τ is the time centroid, or nominal residence time:

$$\tau = \frac{\int_{-\infty}^{\infty} t c\,dt}{\int_{-\infty}^{\infty} c\,dt} \tag{4.76}$$

This implies, at least for solutions to the one-dimensional ADE, that

$$\sigma_x^2 = u^2 \sigma_t^2 \tag{4.77}$$

Therefore an approximate expression for an effective longitudinal dispersion coefficient is

$$D_L \cong \frac{u^2}{2}\frac{d\sigma_t^2}{dt} = \frac{u^2}{2}\frac{d\sigma_t^2}{dx}\frac{dx}{dt} = \frac{u^3}{2}\frac{d\sigma_t^2}{dx} \tag{4.78}$$

where *u* corresponds with the mean velocity ($\bar{u}$) in a bicontinuum model.

The following expression for tracer temporal variance as a function of travel distance (*x*) is derived in Appendix D using the method of moments:

$$\sigma_t^2 = \frac{2(u_2 - u_1)^2 f_1 f_2}{(L\lambda_{2m})^2 \bar{u}^2 u_1 u_2}\left(e^{-L\lambda_{2m}x} + L\lambda_{2m}x - 1\right) \tag{4.79}$$

where $\lambda_{2m} = \frac{1}{f_1 u_1} + \frac{1}{f_2 u_2}$ (eq. D10). Expanding the exponential term in a Taylor series produces

$$\begin{aligned} e^{-L\lambda_{2m}x} &= 1 - L\lambda_{2m}x + \frac{(L\lambda_{2m}x)^2}{2!} - \frac{(L\lambda_{2m}x)^3}{3!} + \ldots \\ &\approx 1 - L\lambda_{2m}x + \frac{(L\lambda_{2m}x)^2}{2!} \end{aligned} \tag{4.80}$$

Substituting this approximation into eq. 4.79, we derive an expression that shows concentration variance at small values of *x* proportional to the square of *x*:

$$\sigma_t^2 \approx \frac{f_1 f_2 (u_2 - u_1)^2}{u_1 u_2} \frac{x^2}{\bar{u}^2} \tag{4.81}$$

Noting that mean residence time (τ) for distance *x* equals $\frac{x}{\bar{u}}$, we then calculate dimensionless variance (e.g. for an RTD) for the near-field transport situation as

$$\frac{\sigma_t^2}{\bar{t}^2} = \frac{f_1 f_2 (u_2 - u_1)^2}{u_1 u_2} \tag{4.82}$$

As *x* increases, the magnitude of the exponential term in eq. 4.79 declines, and the variance approaches linear dependence on *x*. The transition from stochastic-convective to Fickian spreading is thus characterized by tracer cloud variance that changes in a first-order fashion from proportionality with the square of travel distance to direct proportionality with distance. The effective "decay" coefficient governing this transition from stochastic-convective to Fickian spreading is $L\lambda_{2m}$, and a corresponding distance scale for the mid-point of the transition is therefore

$$x_{1/2}^D = \frac{\ln(2)}{L\lambda_{2m}} = \left(\frac{A}{D_0}\right)\left(\frac{u_1 u_2}{\bar{u}}\right)\ln(2) \tag{4.83}$$

Taking the derivative of eq. 4.79 and substituting it into eq. 4.78, we derive the following expression for the effective longitudinal dispersion coefficient:

$$D_L = \frac{\bar{u}(u_2 - u_1)^2 f_1 f_2}{(L\lambda_{2m})^2 u_1 u_2}\left(-L\lambda_{2m} e^{-L\lambda_{2m}x} + L\lambda_{2m}\right) \tag{4.84}$$

As x goes toward infinity, D_L approaches a constant value asymptotically:

$$D_{L,\infty} = \frac{\bar{u}^3}{2}\frac{d\sigma_t^2}{dx}\bigg|_{x=\infty} = \frac{f_1 f_2 (u_2 - u_1)^2 \bar{u}}{u_1 u_2 L\lambda_{2m}} = \frac{A u_1 u_2}{D_0}\left(\frac{\sigma_t^2}{\bar{t}^2}\right) = f_1 \alpha_1 \left(\frac{\sigma_t^2}{\bar{t}^2}\right) \tag{4.85}$$

The asymptotic dispersion coefficient is proportional to the near-field dimensionless variance, as eq. 4.85 indicates. Employing an expression for closure parameter '*A*', for periodic heterogeneity represented using a cosine Fourier series expansion (Appendix C, eq. C19), the asymptotic longitudinal dispersion coefficient can be expressed in the form

$$D_{L,\infty} = \frac{2H^2 \bar{u}(u_2 - u_1)^2}{D_0 \lambda_{2m} u_1 u_2} \sum_{n=1}^{\infty} \frac{b_n^2}{r_n^2} \tag{4.86}$$

where H is the period of the domain, b_n are Fourier coefficients, and r_n are associated wave numbers.

4.4 Model Evaluation

In related work, Carleton and Montas (2009) developed analytical solutions for a two-dimensional steady-state advective-dispersive-reactive transport equation, in which velocities, reaction rate coefficients, and transverse dispersion coefficients are all treated explicitly as power functions of the transverse (z) dimension:

$$k = fz^p \tag{4.87}$$

$$u = az^m \tag{4.88}$$

$$D = bz^n \tag{4.89}$$

Solutions, which employ a Fourier-Bessel series approach, include the following expressions for normalized resident and flux concentrations respectively, when inlet concentration is uniform across the width of the domain:

$$c_r(x) =$$

$$\frac{1}{H}\sum_{i=1}^{\infty}\exp\left[-\frac{b}{a}\varepsilon^2(1-n)^2\lambda_i^2 x\right]\frac{\left(\int_0^H z^{(1-n)/2}J_\nu\left[2\nu\lambda_i z^{\varepsilon(1-n)/2\nu}\right]dz\right)\left(\int_0^H az^{\frac{1+2m-n}{2}}J_\nu\left[2\nu\lambda_i z^{\frac{\varepsilon(1-n)}{2\nu}}\right]dz\right)}{\int_0^H az^m\left(z^{\frac{1-n}{2}}J_\nu\left[2\nu\lambda_i z^{\frac{\varepsilon(1-n)}{2\nu}}\right]\right)^2 dz} \tag{4.90}$$

and

$$c_f(x) =$$

$$\frac{m+1}{aH^{m+1}}\sum_{i=1}^{\infty}\exp\left[-\frac{b}{a}\varepsilon^2(1-n)^2\lambda_i^2 x\right]\frac{\left(\int_0^H az^{\frac{1+2m-n}{2}}J_\nu\left[2\nu\lambda_i z^{\frac{\varepsilon(1-n)}{2\nu}}\right]dz\right)^2}{\int_0^H az^m\left(z^{\frac{1-n}{2}}J_\nu\left[2\nu\lambda_i z^{\frac{\varepsilon(1-n)}{2\nu}}\right]\right)^2 dz} \tag{4.91}$$

The corresponding transverse variances of resident and flux concentration are given by

$$\sigma_r^2(x) = \frac{\int_{z_1}^{z_2}\left(c(x,z)-c_r(x)\right)^2 dz}{z_2 - z_1} \tag{4.92}$$

and

$$\sigma_{flux}^2 = \frac{\int_{z_1}^{z_2}\left(c(x,z)u(z)-c_f(x)u_{mean}\right)^2 dz}{\int_{z_1}^{z_2}u(z)dz} \tag{4.93}$$

where

$$c(x,z) = \sum_{i=1}^{\infty} \left\{ \frac{\int_0^H az^{\frac{1+2m-n}{2}} J_\nu \left[2\nu\lambda_i z^{\frac{\varepsilon(1-n)}{2\nu}} \right] dz}{\int_0^H az^m \left(z^{\frac{1-n}{2}} J_\nu \left[2\nu\lambda_i z^{\frac{\varepsilon(1-n)}{2\nu}} \right] \right)^2 dz} \right\} \cdot z^{(1-n)/2} J_\nu \left[2\nu\lambda_i z^{\frac{\varepsilon(1-n)}{2\nu}} \right] \exp\left[-\frac{b}{a} \varepsilon^2 (1-n)^2 \lambda_i^2 x \right]$$

(4.94)

Results using the bicontinuum model (eqs. 4.59 and 4.60) can be compared with results for systems such as these (eqs. 4.90 and 4.91) with identical low-order moments, but in which the heterogeneity is made explicit. Three related examples serve to illustrate comparisons between results generated using the two models (i.e. explicit and stochastic heterogeneity) for various values of the transverse dispersion coefficient D_0. For consistency with an example explored in Carleton and Montas, 2009, we employ the following parameters in the explicit heterogeneity case: a=0.005, m=4/7 ($\overline{u}$ =0.015 m/min); f=10^{-3}, p=-8/7 (flow-weighted mean k=1.7×10^{-4} min^{-1}); n=6/7, and b varies between the three examples, spanning a range of two orders of magnitude between example 1 and example 3. The domain of the 2-D simulations is 15 m in width by 1000 m in length. Velocities, reaction rate coefficients, and dispersion coefficients all vary in the z (transverse) dimension, while transport occurs in the x direction. For the stochastic/bicontinuum model, the previously stated parameters correspond to the following: $\overline{w}$ =8.954×10^{-4}; σ_w =3.495 × 10^{-4}; $\overline{\lambda^3}$ =-0.445; γ =16.7; β=8.96×10^{-11}. The value of closure parameter A is 21.72 m^2, as calculated using eq. C19, and for the first example (b=10^{-4}) we have α=19.3 and D_0 =5.17×10^{-4} m^2/min.

For this example, as Figure 4.1a illustrates, the simulated transverse-mean resident concentration from the stochastic model (eq. 4.59) is nearly identical to the corresponding result obtained using the explicit model (eq. 4.90) over the length of the domain. Flux concentration curves for this example (not shown) trace nearly identical trajectories for the two models as well. Standard deviations of transverse concentration in the two models are also very similar to each other, as shown in Figure 4.1b. Effective longitudinal dispersion during the course of the stochastic simulation within the given domain remains pre-asymptotic, as seen in the continual growth of D_L (Figure 4.1c). Values of $x_{1/2}^k$ and $x_{1/2}^D$ in this example are 56.7 and 293 m respectively, indicating that early concentration decay happens at about five times the rate of the transition from stochastic-convective to Fickian dispersion.

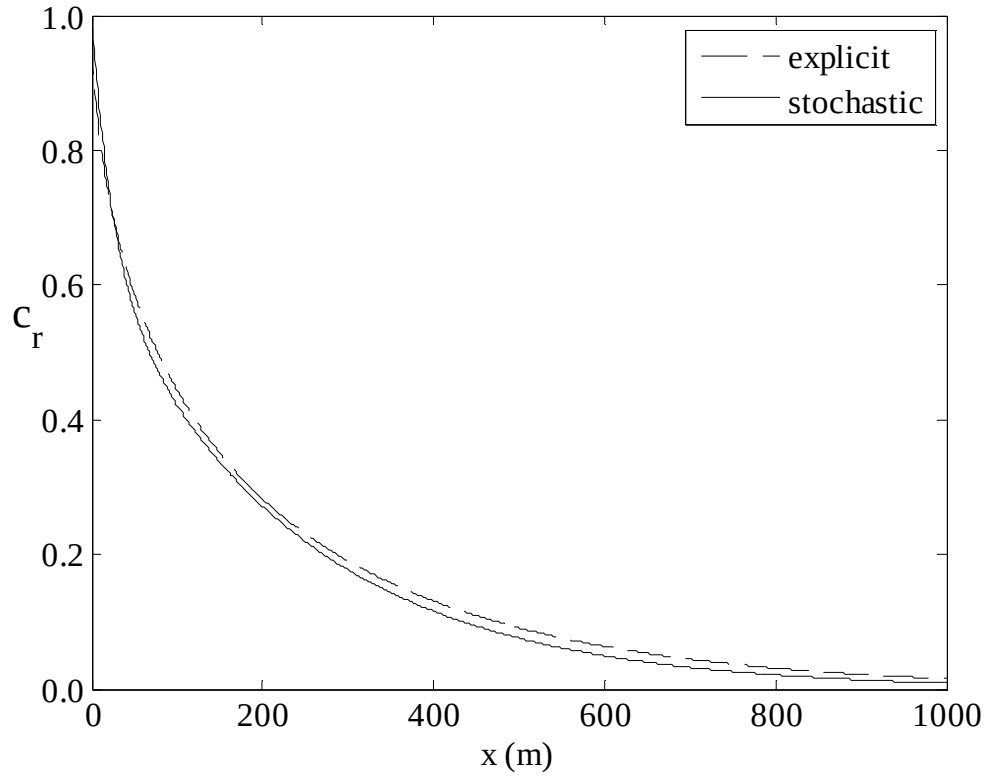

Figure 4.1a Transverse resident mean concentrations from 2-D steady-state reactive transport simulations as functions of transport dimension (x) for: model with heterogeneity explicitly specified (dashed line); and heterogeneity modeled stochastically (solid line). Governing transport parameters are $\bar{u}$ =1.50×10^{-2} m/min, $\bar{k}$ =1.63×10^{-4} min^{-1}, D_0=5.17×10^{-4} m^2/min; σ_u = 5.84×10^{-3}, σ_k =-1.10×10^{-4}, σ_D =-3.73×10^{-2}. First through third moments of heterogeneity variate λ are the same in both models.

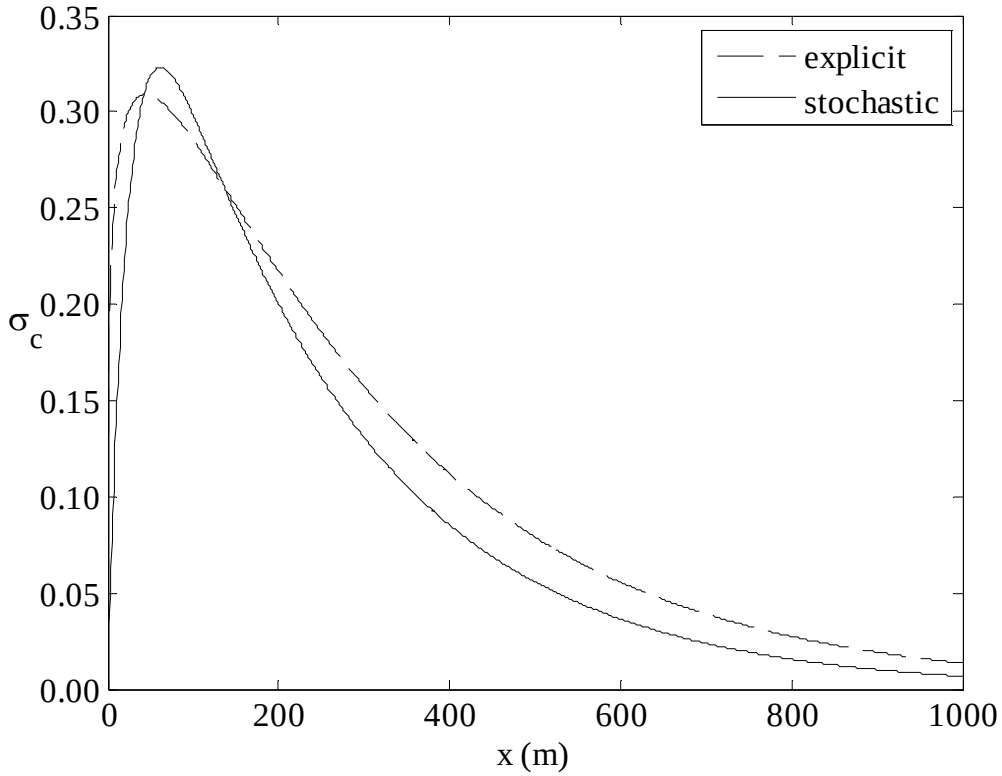

Figure 4.1b Transverse standard deviation of resident concentration as a function of transport distance (x) for the same systems as shown in Figure 4.1a: model with heterogeneity explicitly specified (dashed line); and with heterogeneity modeled stochastically (solid line). For the latter, the curve is equivalent to correlation of local concentration with the heterogeneity variate λ.

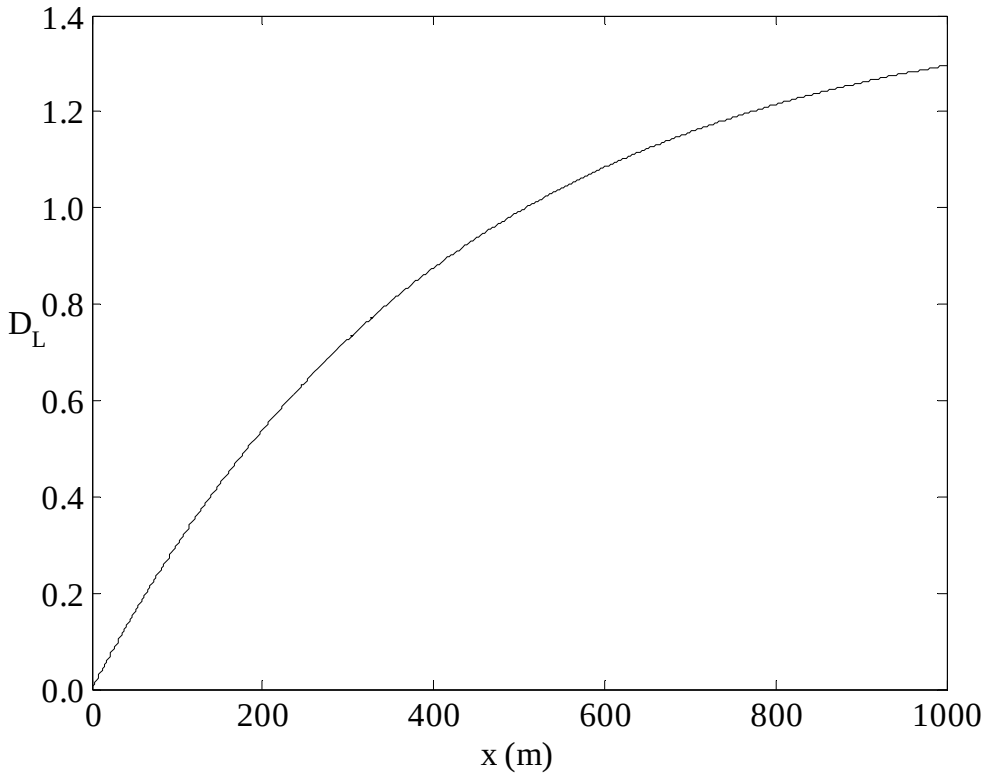

Figure 4.1c Effective longitudinal dispersion coefficient (m^2/min) for the stochastic transport system as a function of travel distance (x) when D_0=5.17×10^{-4} m^2/min, determined using eq. 4.84.

System eigenvalues λ_1 and λ_2 (which equal 0.8021 and -1.2467 respectively in this example) represent characteristic values of heterogeneity variate λ. These values of λ can be mapped directly onto values of the z-coordinate in the explicit heterogeneity model as follows, using λ_1 for illustrative purposes. Equating the expressions for velocity (u) as a function of w and as a function of z (eq. 4.6 and eq. 4.88 respectively), we express z in terms of w:

$$z = \left(\frac{\gamma}{a} w \right)^{1/m} \tag{4.95}$$

Employing eq. 4.5 expressed in terms of eigenvalue λ_1

$$w_1 = \overline{w} + \lambda_1 \sigma_w \tag{4.96}$$

equation 4.95 becomes a relation between a characteristic value of the heterogeneity variate in the stochastic model, and the corresponding transverse spatial position in the model with explicit heterogeneity:

$$z_1 = \left(\frac{\gamma}{a} \left(\overline{w} + \lambda_1 \sigma_w \right) \right)^{1/m} \tag{4.97}$$

Using eq. 4.97, the values of z_1 and z_2 corresponding with λ_1 and λ_2 in this case are found to be 10.9549 and 2.1174 respectively. Longitudinal (x dimension) concentration transects taken along these values of z in the explicit model are expected to correspond reasonably closely with characteristic concentrations c_1 and c_2, which are of course associated with λ_1 and λ_2 in the stochastic model. Figure 4.1d shows that close concordance of this kind does occur in this example. Differences that do exist between the curves can be attributed in part to the influences of transverse boundary conditions in the explicit heterogeneity model that are absent from the stochastic model, where lateral periodicity is assumed. The greater the magnitude of transverse dispersion relative to the width of the domain, the more these boundary conditions (Neumann at maximum z, and joint Dirichlet/Neumann at minimum z) are likely to influence transverse mean concentrations, and the more one might expect the two models to produce different results.

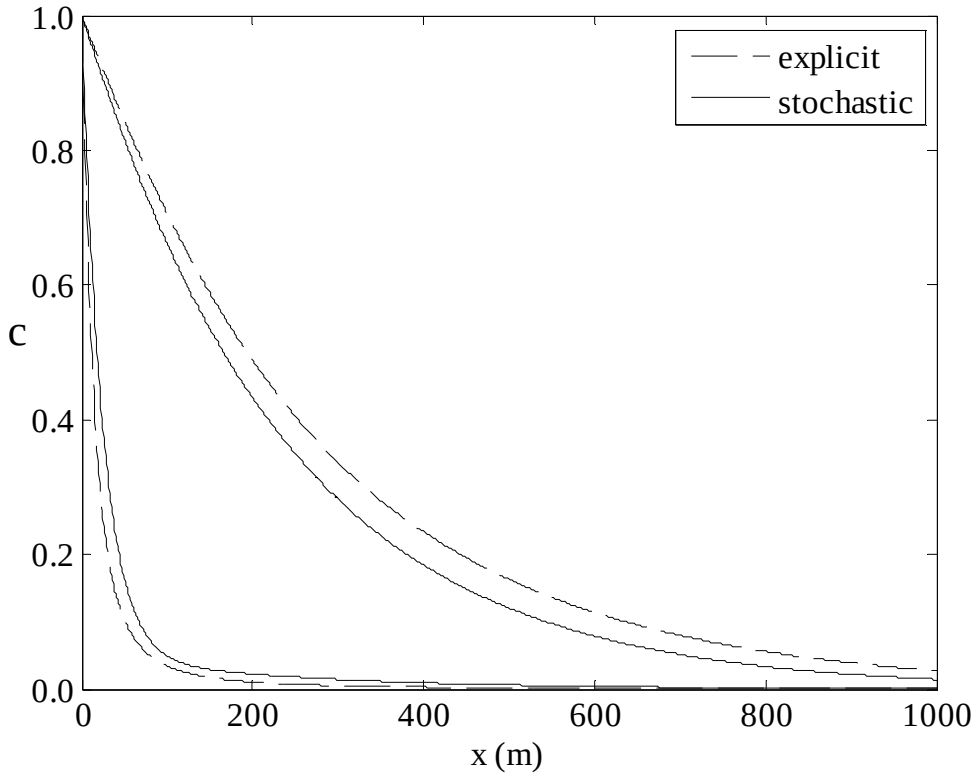

Figure 4.1d For D_0=5.17×10^{-4} m^2/min case: canonical (stochastic model) concentrations (c_1 and c_2), and corresponding longitudinal (x-dimension) transects (explicit model) for z-dimension values corresponding with eigenvalues λ_1 and λ_2, according to eq. 4.97. For each model the less rapidly-declining curve corresponds with λ_1, and the more rapidly-declining curve corresponds with λ_2.

When the strength of transverse dispersion is increased by an order of magnitude (b=10^{-3}, thus α =193 and D_0 =5.17×10^{-3} m^2/min) and advective and reactive parameters are kept the same, the result is an even better match between the two models in terms of mean concentration (Figure 4.2a), but a slightly worse match of concentration standard deviation (Figure 4.2b). Notably in this case in contrast with the previous one, as a result of the greater transverse dispersive flux, longitudinal dispersion essentially reaches the Fickian limit by about a fifth of the distance along the transport domain (Figure 4.2c). The asymptotic value of D_L is

substantially lower in this example than values attained in the first example. This is consistent with expectations based on eqs. 4.63 and 4.64, as well as with results of related analyses by other researchers (Fischer, 1979; Gelhar et al., 1979; Matheron and deMarsily, 1980), who have also found coefficients of longitudinal dispersion to be inversely related to coefficients of transverse diffusion/dispersion in shear flow. Values of $x_{1/2}^{k}$ and $x_{1/2}^{D}$ in this second example are 68.3 and 29.3 m respectively, indicating that net concentration decay happens at about half the rate of the transition to Fickian dispersion.

As in the first example, concentration transects along the *x*-dimension for *z* values that correspond with the eigenvalues closely match the bicontinuum characteristic concentration (c_1 and c_2) longitudinal decline curves (Figure 4.2d). These first and second examples illustrate how the dynamics of two-dimensional heterogeneous reactive-advective-dispersive transport fields can be closely approximated by much simpler two-path representations, by making use of the equivalence between second-order and mobile-mobile bicontinuum models (Montas et al., 2000). Examples 1 and 2 demonstrate that this correspondence between models is robust under a range of varying "Fickian-ness" in longitudinal spreading.

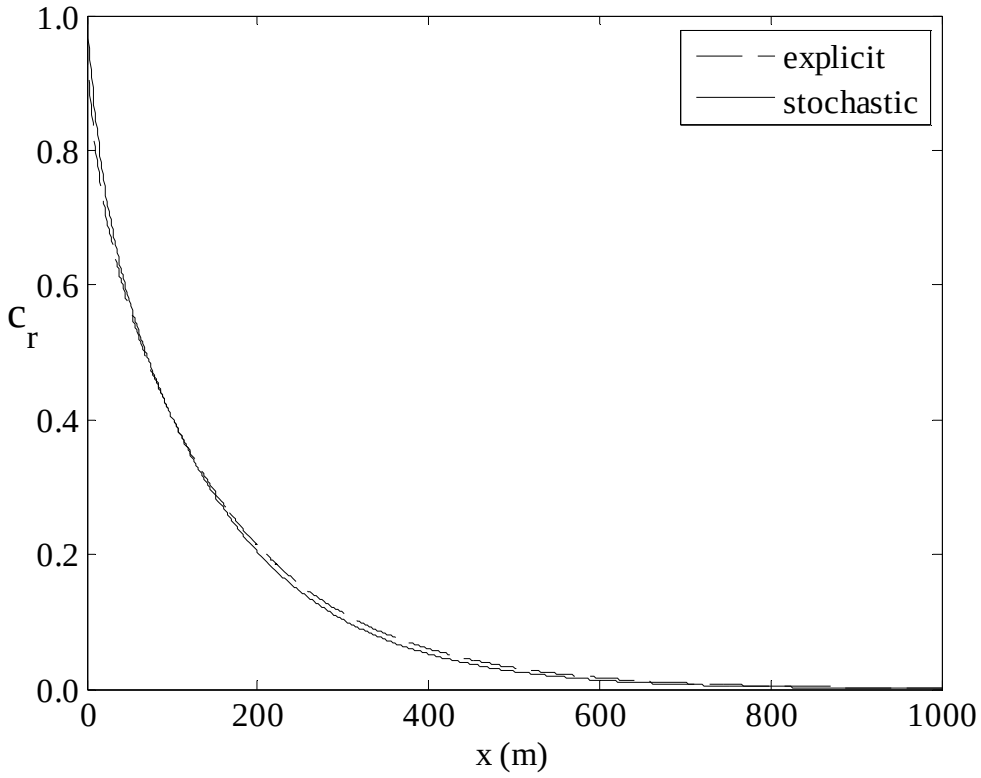

Figure 4.2a Transverse resident mean concentrations from 2-D steady-state reactive transport simulations as functions of transport dimension (x) for mean transverse D_0=5.17×10^{-3} m^2/min: model with heterogeneity explicitly specified (dashed line); and heterogeneity modeled stochastically (solid line). First through third moments of heterogeneity in the two systems match each other.

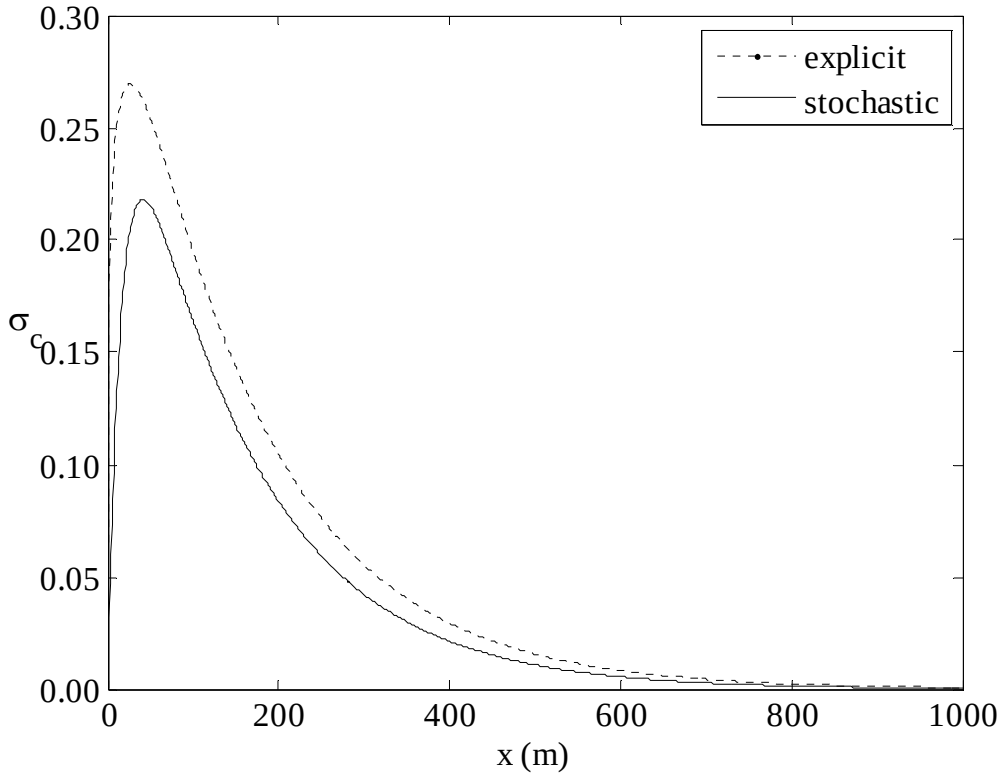

Figure 4.2b Transverse standard deviation of resident concentration as a function of transport distance (x) for the same systems as shown in Figure 4.2a: model with heterogeneity explicitly specified (dashed line); and with heterogeneity modeled stochastically (solid line).

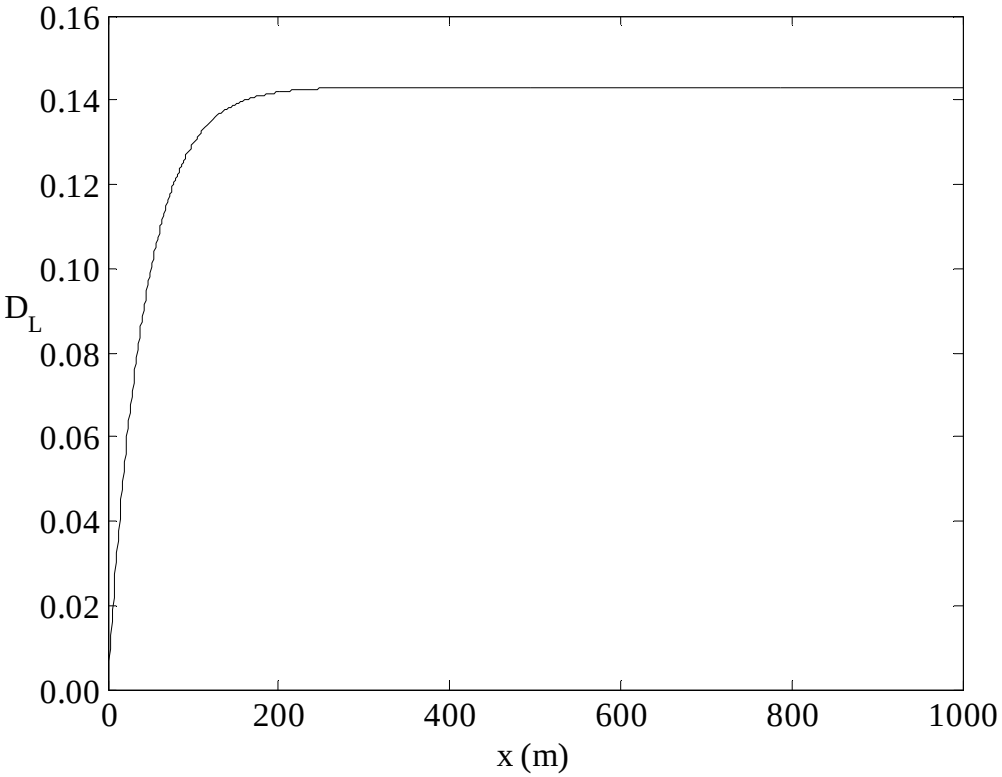

Figure 4.2c Effective longitudinal dispersion coefficient (m^2/min) for the stochastic transport system as a function of travel distance (x) when $D_0=5.17\times10^{-3}$ m^2/min, determined using eq. 4.84.

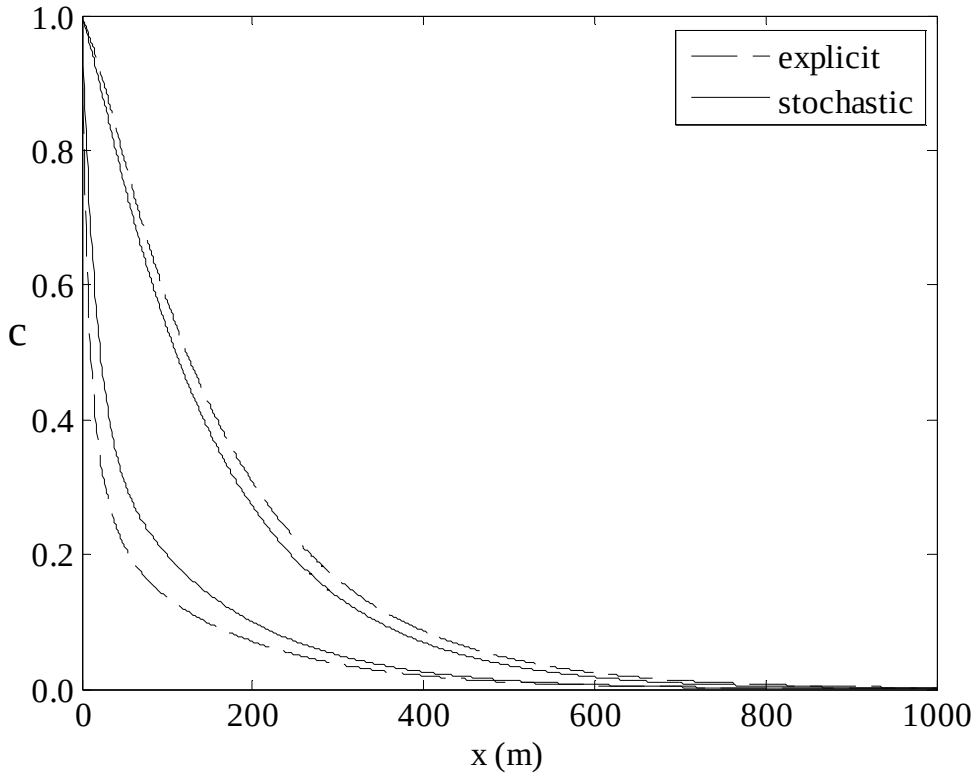

Figure 4.2d For D_0=5.17×10^{-3} m^2/min case: canonical (stochastic model) concentrations (c_1 and c_2), and corresponding longitudinal (x-dimension) transects (explicit model) for z-dimension values corresponding with eigenvalues λ_1 and λ_2, according to eq. 4.97. For each model the less rapidly-declining curve corresponds with λ_1, and the more rapidly-declining curve corresponds with λ_2.

In the third example, transverse dispersion is increased by another order of magnitude (b =10^{-2}, α =1930 and D_0 =5.17×10^{-2} m^2/min). The resulting matches between the stochastic and explicit models in terms of mean concentration (Figure 4.3a) and concentration standard deviation (Figure 4.3b) are notably poorer in this example than in the first two. This may be a result of the approximate representation of k (eq. 4.8), which as compared with the explicit heterogeneity model, tends to underestimate reaction rates at values of λ that correspond with very low velocities (i.e. the region of space where k approaches infinity in the latter case). Larger values

of transverse mixing tend to move more constituent into this zone, increasing net reaction in the explicit model more than in the stochastic one.

Matches between the characteristic concentrations c_1 and c_2, and concentration transects along z values corresponding to the eigenvalues (Figure 4.3d), are also much poorer in this example than in the previous two. However an ADE model with fixed inlet concentration boundary conditions (solution "C1" of vanGenuchten and Alves, 1982), and employing the asymptotic D_L value of 0.0143 m^2/min (eq. 4.85), matches the bicontinuum model results for resident mean concentration quite closely (Figure 4.3a). It should be noted that for the first two examples, analogous ADE model results (not shown) are not especially close to bicontinuum model results, an observation which illustrates the limitations of the ADE in pre-asymptotic situations. Values of $x_{1/2}^k$ and $x_{1/2}^D$ in example 3 are 65.6 and 2.9 m respectively, indicating that early field concentration decay happens at about one twentieth the rate of the transition to Fickian dispersion; as Figure 4.3c shows, asymptotic dispersion is attained almost instantly. Evidently the quick transition to the Fickian regime in this example allows the ADE to provide an adequate approximation of the transport/reaction dynamics that are presumably more fully represented by the bicontinuum model.

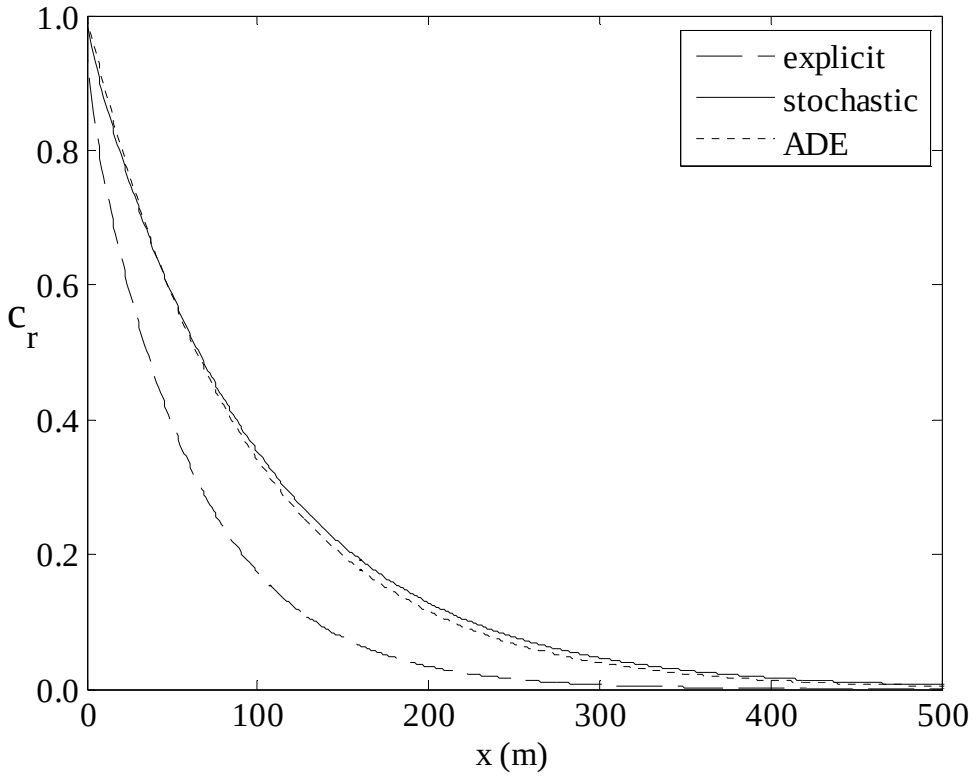

Figure 4.3a Transverse resident mean concentrations from 2-D steady-state reactive transport simulations as functions of transport dimension (x) for mean transverse D_0=5.17×10^{-2} m^2/min: model with heterogeneity explicitly specified (long dashes); heterogeneity modeled stochastically (solid line); and 1-D ADE solution (short dashes). Figure displays only the first 500 m of the transport domain for clarity.

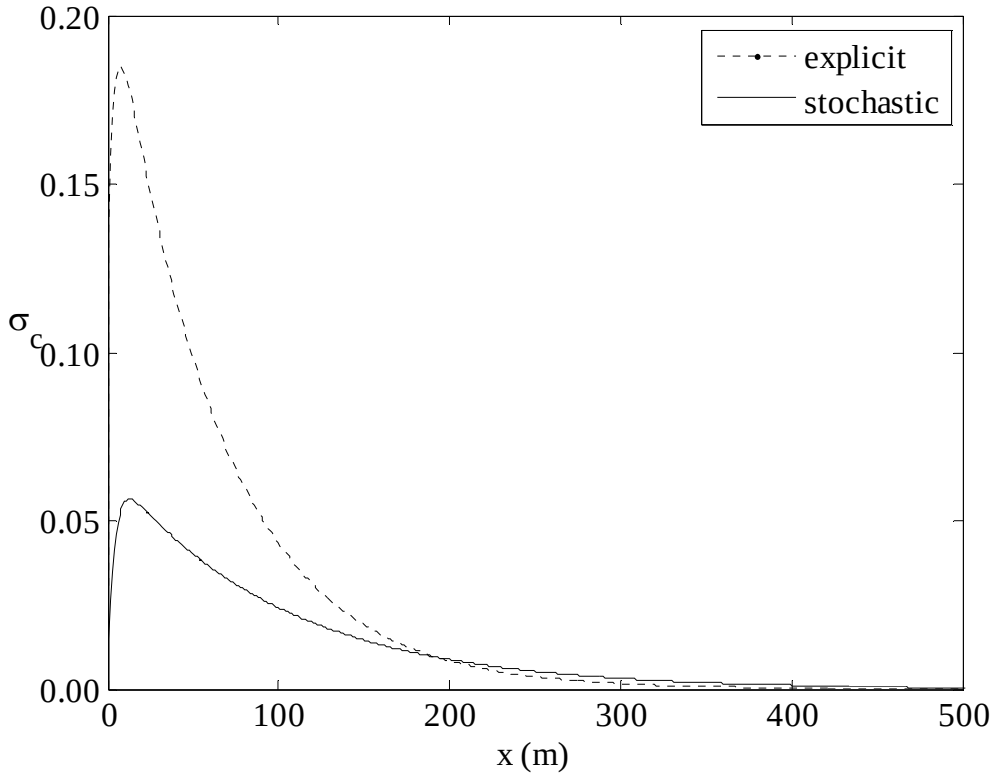

Figure 4.3b Transverse standard deviation of resident concentration as a function of transport distance (*x*) for the same systems as shown in Figure 4.3a: model with heterogeneity explicitly specified (dotted line); and with heterogeneity modeled stochastically (solid line).

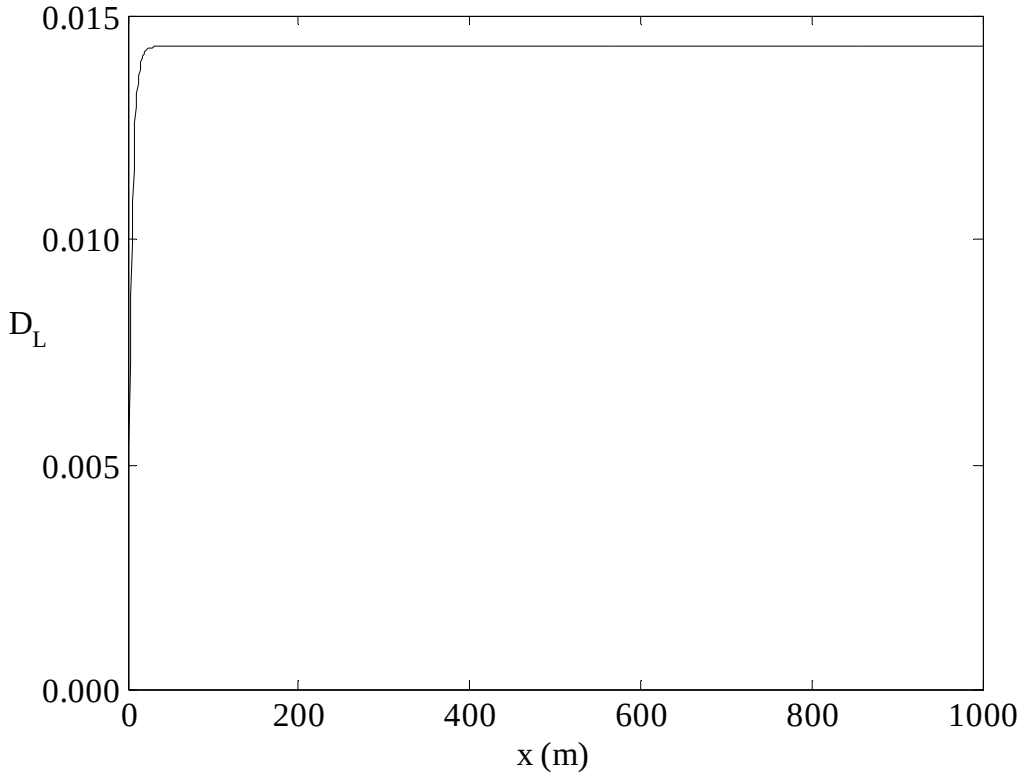

Figure 4.3c Effective longitudinal dispersion coefficient (m^2/d) for the stochastic transport system as a function of travel distance (x) when $D_0=5.17\times10^{-2}$ m^2/min, determined using eq. 4.84.

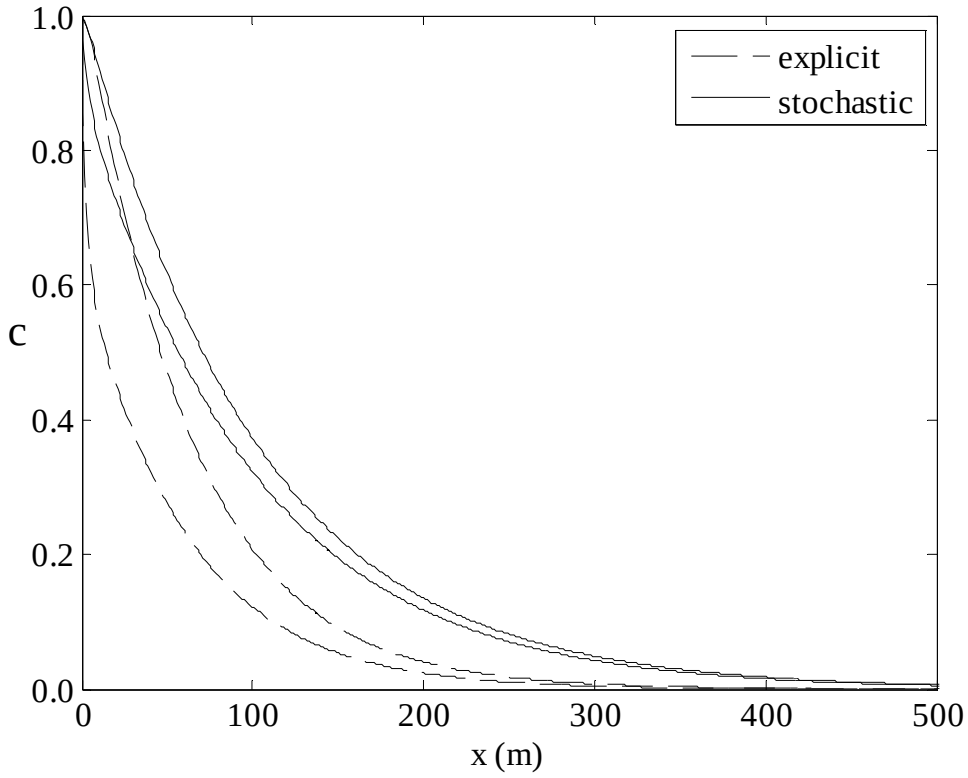

Figure 4.3d For D_0=5.17×10^{-2} m^2/min case: canonical (stochastic model) concentrations (c_1 and c_2), and corresponding longitudinal (x-dimension) transects (explicit model) for z-dimension values corresponding with eigenvalues λ_1 and λ_2, according to eq. 4.97. For each model the less rapidly-declining curve corresponds with λ_1, and the more rapidly-declining curve corresponds with λ_2.

Results from the bicontinuum model simulations using the transverse dispersion coefficients of Figures 4.1 through 4.3 (D_0 =5.17×10^{-4}, 5.17×10^{-3}, and 5.17×10^{-2} m^2/min) are displayed together for comparative purposes in Figure 4.4. Resident concentrations are shown in Figure 4.4a, in which the three simulations are seen to produce similar results for about the first half of net decay, and then to diverge from each other for the remainder of the simulations, with greater transverse dispersion resulting in more rapid decline. By contrast, flux concentrations from the three simulations and a stochastic-convective example, which are shown in Figure

4.4b, begin to diverge from each other immediately at the 'inlet' (x=0) end of the transport regime, with greater transverse dispersion also resulting in more rapid concentration decline. This result is qualitatively the same as results obtained using the explicit heterogeneity model. These examples demonstrate that the stochastic/bicontinuum model developed in this paper is capable of approximating reactive transport quite well in systems that range from essentially stochastic-convective to essentially Fickian in terms of their longitudinal dispersive characteristics. Figure 4.4b can be directly compared with Figure 3.7 in Chapter 3, which shows results from the explicit model for the same set of governing parameters.

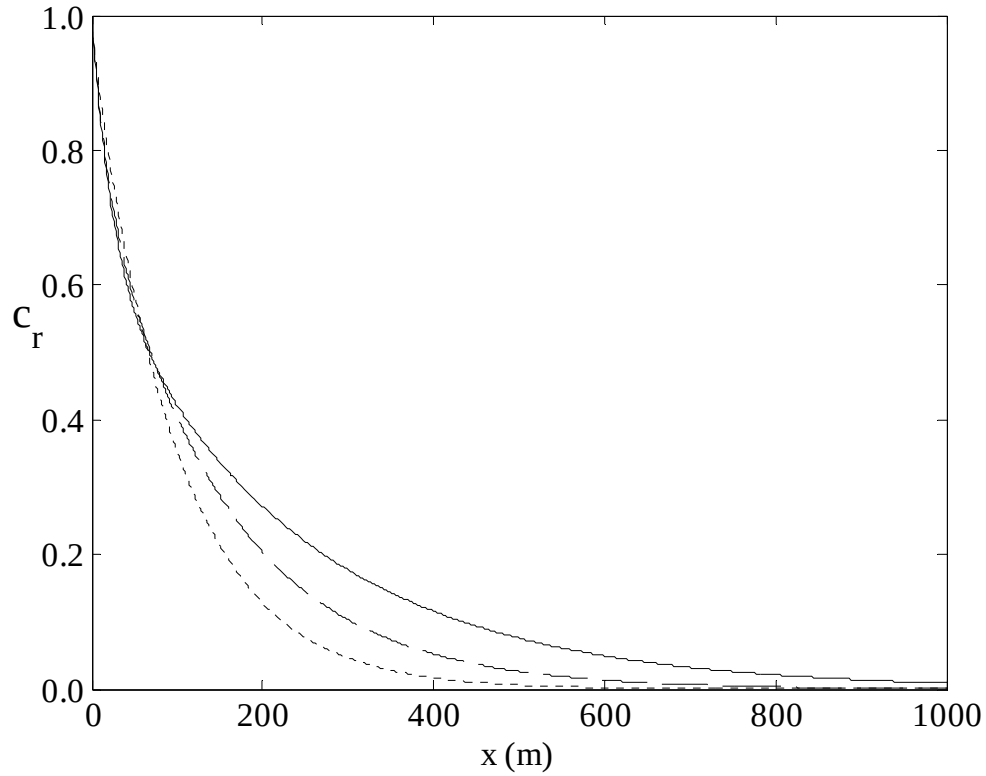

Figure 4.4a Resident concentration from stochastic/bicontinuum model with same parameters as used in Figures 4.2-4.3, and D_0=5.17×10^{-4} m^2/min (solid line), D_0=5.17×10^{-3} m^2/min (dashed line), D_0=5.17×10^{-2} m^2/min (dot-dashes).

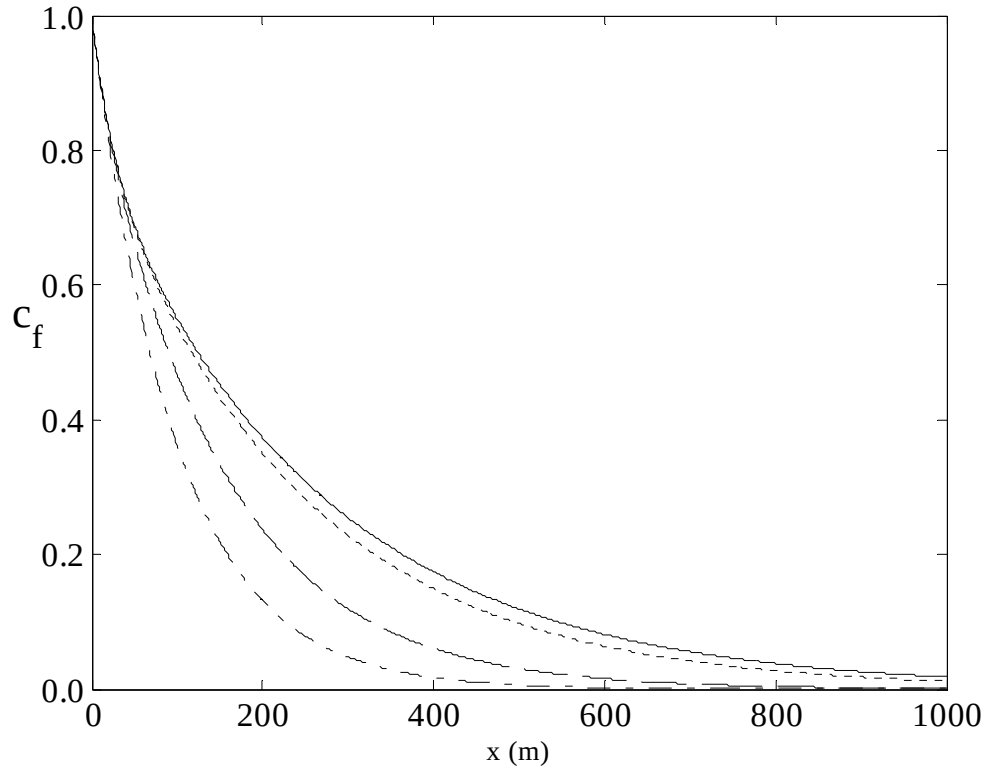

Figure 4.4b Flux concentration from stochastic/bicontinuum model with same parameters as used in Figures 4.1-4.3, and $D_0 \cong 0$ (solid line), $D_0 = 5.17 \times 10^{-4}$ m^2/min (short dashes), $D_0 = 5.17 \times 10^{-3}$ m^2/min (long dashes), $D_0 = 5.17 \times 10^{-2}$ m^2/min (dot-dashes).

4.5 Summary and Conclusions

A second-order representation of two-dimensional porous medium transport governed by correlations between flux parameters (advective, dispersive and reactive) and domain biophysical attributes, was used to develop an equivalent mobile-mobile bicontinuum model representing a spatially heterogeneous environment such as a treatment wetland. Model solutions, developed for the case of steady-state flow and constant inlet concentration, comprise a weighted sum of two exponential decay functions for describing mean concentration as a function of distance in the direction of flow. An expression was also developed to quantify the spread of an inert tracer in

the same system, allowing model results to be examined in light of evolving shear flow dispersion. When pre-asymptotic longitudinal dispersion predominated, model results compared well with solutions generated by another model in which heterogeneity (in a direction perpendicular to flow) was treated as an explicit, rather than stochastic, function of domain geometry. By contrast, when effective longitudinal dispersion approached the Fickian asymptote early, model results were similar to those obtained using a one-dimensional ADE. The model thus appears well suited for characterizing reactive transport in heterogeneous environments exhibiting a range of longitudinal dispersive characteristics.

The second-order stochastic/bicontinuum model employed in this study approximates a continuous distribution of λ values with a binary distribution (Montas et al., 2000), and constrains higher moments (eq. 4.11) to values defined in terms of the 0^{th} through 3^{rd} moments. An analogous approach employing a tricontinuum approximation to a third-order system can be envisioned, which would similarly approximate the λ (or $X^{-1/2}$) distribution with a ternary distribution, thereby increasing the accuracy of the approximation, and permitting the 4^{th} and 5^{th} moments of the distribution to also be accurately represented (Montas, 2003). In this approach a second heterogeneity field, orthonormal to λ, is defined using orthogonal polynomials, and terms representing correlations of system variables with this second field are employed. A mass-balance expression representing correlation of concentration with the second field constitutes a third governing equation, and canonical transformation produces equations for three characteristic concentrations, with mass-transfer interactions occurring between each pair of continua. Solution of

such a system of three equations would produce a more complete representation of the distribution of λ than the bicontinuum approach allows, and correspondingly better approximations of transverse mean concentration and variance as D_0 increases. The difficulties in solving such a system of equations may be daunting however, including the challenges of diagonalizing 3 x 3 matrices for unconstrained parameters, and of defining approximate dispersive flux closure terms for such a system. This task and inclusion of longitudinal heterogeneity remains areas for future investigation.

Models typically used to characterize treatment wetland performance tend to be of a fairly simple, black-box variety because chemical processes occurring in wetlands are often complex and incompletely understood, and because information on biophysical attributes that affect these processes is often lacking. A key challenge for simulating treatment wetlands would seem to be to employ models that contain the minimum number of parameters necessary to adequately embody the key processes that determine performance. Although initially popular as empirical descriptors of wetland performance, PFR models have been found to be of limited usefulness because their reaction rate coefficients often exhibit positive correlation with hydraulic loading. ADE models are also of questionable value because longitudinal spreading in wetlands appears to often be of a pre-asymptotic variety as a result of preferential flow paths or short-circuiting. Recent approaches that consider internal spatial heterogeneity (Carleton, 2002; Carleton and Montas, 2007) and temporal chemical heterogeneity (Kadlec, 2003) have shown promise in circumventing the parameter flow-dependence issue. However, these approaches are potentially limited

in their usefulness because they embody inherent assumptions of strictly stochastic-convective flow, and a retreat from mechanistic representation and toward pure empiricism, respectively. To be of maximum utility, models should employ parameters that are in theory independently measurable, whenever possible. The mobile-mobile model developed in this study may be appealing for this purpose because it is physically-based and contains a limited number of parameters. Significantly, mean velocity is a component of the composite governing parameters (i.e the exponents in eq. 4.61), making it possible to consider its effects separately, and therefore leaving as potential unknowns only parameters that should be invariant with flow. Evaluation of the adequacy of this model for the purpose of analyzing wetland performance data remains an area for future study, as does comparison of model results with those of DND and TIS-based approaches.

Chapter 5: Further Model Analyses and Comparisons

5.1 Introduction

The bicontinuum wetland reactor model developed in Chapter 4 was evaluated against analytical solutions for idealized transport regimes governed by equivalent parameters, and found to produce similar results. A remaining task is to compare the bicontinuum model against the relaxed-TIS model in terms of the ability of each model to match data measured in actual wetlands. This Chapter is organized as follows. Section 5.2 explores mathematical relationships between bicontinuum model unknowns within the context of constraints imposed by information that may be obtained from an RTD, and reduces the list of unknowns to a total of three essential underlying model parameters. Section 5.3 compares the bicontinuum and relaxed-TIS models to each other in terms of their abilities to match concentration decline curves from two FWS wetland case study examples in the literature. Section 5.4 presents a discussion of the results.

5.2 Bicontinuum Reactor Model Parameters

For wetlands in which inert tracer studies have been conducted and an RTD measured, the mean velocity ($\bar{u}$) may be readily determined as Λ/τ, where Λ is wetland length and τ is "detention time", i.e. the first moment of the RTD (eq. 4.76). A second key characteristic property which may be determined from an RTD is "dimensionless variance", obtained by dividing the variance (second central moment) of the RTD (eq. 4.75) by the square of τ. For a gamma-pdf shaped RTD, the

dimensionless variance equals $1/\alpha$ and is therefore invariant with distance, implying a longitudinal dispersive mixing process that is stochastic-convective.

By contrast, for the bicontinuum model developed in Chapter 4, dimensionless variance (σ_t^2 / τ^2) varies with distance (x) according to

$$\frac{\sigma_t^2}{\tau^2} = \frac{2(u_2 - u_1)^2 f_1 f_2}{(L\lambda_{2m})^2 u_1 u_2 x^2}\left(e^{-L\lambda_{2m}x} + L\lambda_{2m}x - 1\right) \tag{5.1}$$

In the near-field limit this becomes (eq. 4.82)

$$\frac{\sigma_t^2}{\tau^2} = \frac{f_1 f_2 (u_2 - u_1)^2}{u_1 u_2} \tag{5.2}$$

Upon substituting into eq. 5.2 the relations $u_{1,2} = \bar{u} + \rho_{u\lambda}\lambda_{1,2}$ (eq. 4.36b) and the relations (see eq. 4.30)

$$f_1 = \frac{-\lambda_2}{\lambda_1 - \lambda_2} \text{ and } f_2 = \frac{\lambda_1}{\lambda_1 - \lambda_2} \tag{5.3}$$

where (eq. 4.29)

$$\lambda_{1,2} = \frac{\overline{\lambda^3} \pm \left(\overline{\lambda^3}^2 + 4\right)^{1/2}}{2} \tag{5.4}$$

eq. 2 becomes

$$\frac{\sigma_t^2}{\tau^2} = \frac{(\rho_{u\lambda})^2}{u_1 u_2} \tag{5.5}$$

By expanding the denominator in eq. 5.5 we exploit measurement of near-field dimensionless variance to develop an expression that relates the unknowns $\rho_{u\lambda}$ and $\overline{\lambda^3}$ to each other:

$$u_1 u_2 = (\bar{u} + \rho_{u\lambda}\lambda_1)(\bar{u} + \rho_{u\lambda}\lambda_2) = \bar{u}^2 + \rho_{u\lambda}\bar{u}\,\overline{\lambda^3} - (\rho_{u\lambda})^2 \tag{5.6}$$

and therefore

$$\frac{\sigma_t^2}{\tau^2} = \frac{\left(\rho_{u\lambda}\right)^2}{\bar{u}^2 + \rho_{u\lambda}\bar{u}\overline{\lambda^3} - \left(\rho_{u\lambda}\right)^2} \tag{5.7}$$

Rearranging eq. 5.7 we derive the following quadratic expression for $\rho_{u\lambda}$:

$$\left(1 + \frac{1}{\left(\sigma_t^2/\tau^2\right)}\right)\left(\rho_{u\lambda}\right)^2 - \bar{u}\overline{\lambda^3}\rho_{u\lambda} - \bar{u}^2 = 0 \tag{5.8}$$

the roots of which are

$$\rho_{u\lambda} = \frac{\bar{u}\overline{\lambda^3} \pm \bar{u}\sqrt{\left(\overline{\lambda^3}\right)^2 + 4\left(1 + \sigma_t^2/\tau^2\right)}}{2\left(1 + \sigma_t^2/\tau^2\right)} \tag{5.9}$$

Because $\rho_{u\lambda}$ is a positive quantity, only the positive root produces a physically sensible solution, therefore we have

$$\rho_{u\lambda} = \frac{\bar{u}\overline{\lambda^3} + \bar{u}\sqrt{\left(\overline{\lambda^3}\right)^2 + 4\left(1 + \sigma_t^2/\tau^2\right)}}{2\left(1 + \sigma_t^2/\tau^2\right)} \tag{5.10}$$

All of the parameters in the derived expressions for $\bar{c}$, $\rho_{c\lambda}$, and c_f (eqs. 4.59 through 4.62) can be expressed entirely as functions of unknowns f_1, f_2, u_1, u_2, k_1, k_2 and L, and therefore ultimately of $\bar{u}$, $\rho_{u\lambda}$, $\overline{\lambda^3}$, $\bar{k}$, σ_k, and L. Of these six variables, mean velocity $\bar{u}$ is presumably known (for example determined from the RTD as described above), and $\rho_{u\lambda}$ can be expressed using eq. 5.10 as a function of $\overline{\lambda^3}$ if near-field dimensionless variance is also known, reducing the total number of unknowns to four: $\overline{\lambda^3}$, $\bar{k}$, σ_k, and L.

Another relation between variables may be exploited in the following fashion, in order to reduce the total number of unknowns to three. Equating the expressions

for $\bar{k}$ and σ_k in eqs. 4.11 and 4.14 term-by-term with the corresponding terms in the Taylor series expansion (eq. 4.9), we find

$$\bar{k} = k_0 + \rho_{k\lambda^2} = \frac{\beta}{\overline{w}^2} + \frac{3\beta\sigma_w^2}{\overline{w}^4} = \beta\left(\frac{\overline{w}^2 + 3\sigma_w^2}{\overline{w}^4}\right) \tag{5.11}$$

and

$$\sigma_k = \rho_{k\lambda} + \rho_{k\lambda^2}\overline{\lambda^3} = -\frac{2\beta\sigma_w}{\overline{w}^3} + \frac{3\beta\sigma_w^2}{\overline{w}^4}\overline{\lambda^3} = \beta\left(-\frac{2\sigma_w\overline{w} - 3\sigma_w^2\overline{\lambda^3}}{\overline{w}^4}\right) \tag{5.12}$$

Dividing eq. 5.12 by eq. 5.11 eliminates β and produces the following

$$\frac{\sigma_k}{\bar{k}} = \frac{3\sigma_w^2\overline{\lambda^3} - 2\sigma_w\overline{w}}{\overline{w}^2 + 3\sigma_w^2} \tag{5.13}$$

Making use of the relations $\bar{u} = \gamma\overline{w}$ and $\rho_{u\lambda} = \gamma\sigma_w$, eq. 5.13 becomes

$$\frac{\sigma_k}{\bar{k}} = \frac{3\left(\rho_{u\lambda}\right)^2\overline{\lambda^3} - 2\rho_{u\lambda}\bar{u}}{\bar{u}^2 + 3\left(\rho_{u\lambda}\right)^2} \tag{5.14}$$

Eq. 5.14 expresses σ_k as a function of $\bar{k}$, $\overline{\lambda^3}$, and $\bar{u}$, and thus reduces the total number of unknowns to three, e.g. $\overline{\lambda^3}$, $\bar{k}$, and *L*. This is the same as the number of unknowns in eq. 4.62, however as this analysis has shown, the latter parameters are entirely functions of the former. Further, while $\overline{\lambda^3}$, $\bar{k}$, and *L* are essentially unconstrained (except that $\bar{k}$ and *L* are non-negative), θ_1, κ_1, and κ_2 are constrained by the relations in eqs. 5.10 and 5.14. Dimensionless variance thus serves to essentially impose limits on allowable values for parameters θ_1, κ_1, and κ_2. If dimensionless variance is known, it would thus be an inappropriate use of eq. 4.62 to optimize parameters by fitting the model against a data set using an error minimization routine such as the Solver function in Excel (which uses a generalized reduced gradient

algorithm (http://support.microsoft.com/kb/214115)), or lsquonlin in MATLAB® (which uses either an interior-reflective Newton method, or a Levenberg-Marquardt method (http://dali.feld.cvut.cz/ucebna/matlab/toolbox/optim/lsqnonlin.html)). Rather, a more defensible approach constructs θ_1, κ_1, and κ_2 from unknowns $\overline{\lambda^3}$, $\bar{k}$, and L, and then minimizes model error by optimizing selections of the latter parameters.

5.3 Evaluation

5.3.1 Comparisons Between Wetland Models

The "weathering" phenomenon suggested by Kadlec (2003) to be at least partially responsible for PFR parameter dependence in water quality constituents that aggregate multiple chemical entities together, complicates attempts to develop simple but mechanistically sound models of constituent removal in wetlands. Kadlec's analysis suggested that if constituent weathering and heterogeneous velocities occur concurrently, their effects will be indistinguishable from each other, leaving empirical models as essentially the only option. For this purpose Kadlec proposed the use of a "relaxed parameter" TIS model (eq. 1.12) in which the parameters are determined solely by curve fitting. Carleton (2002) also demonstrated that even for a simple (non-aggregated) water quality constituent, a TIS model with empirically-determined parameters can generate results nearly identical to those of a stochastic-convective model derived from a gamma RTD and incorporating DND effects (*kt* proportional to t^3). The bicontinuum model of Chapter 4 also incorporates these kinds of DND effects, but within the context of a mechanistic derivation. The parameters of this model ($\overline{\lambda^3}$, $\bar{k}$, and L) may be unknown or difficult to measure, but they are physically

based and constrained, at least to some extent, by the degree of short-circuiting reflected in the measured dimensionless variance. Rather than making use of known RTD variance to constrain parameter selection in some way, the relaxed TIS model ignores such information, with the only constraint being that an α value obtained by fitting outlet concentrations against fractional distance or residence time (eq. 1.12) will be less than an α value for the same system obtained from an RTD (eq. 3.1).

Because constituent weathering confounds the results of short-circuiting and DND effects, to evaluate the performance of a bicontinuum or DND model (Carleton, 2002) compared with that of a TIS or relaxed-TIS model, preferred water quality constituents are those that are simple rather than aggregated, and therefore do not "weather". Constituents that may be suitable for this purpose include NH_3/NH_4^+, NO_3^-, OP, xenobiotics (e.g. pesticides, personal care products), and certain biological entities such as viruses. To avoid confounding affects related to simultaneous production of these entities, concentrations of potential precursors should be minimal. For example in systems treating NH_3/NH_4^+, minimal organic nitrogen should be present. When this is the case, the possible causes of non-zero background concentration C^* (see Chapter 1) are limited to hydraulic short-circuiting, assuming that external sources of the constituent are negligible. The DND and bicontinuum models are both designed to directly address short-circuiting mechanistically, thus the inclusion of C^* as a (non-zero) parameter is unnecessary as well as potentially confounding for model interpretation. Apparent concentration plateaus may arise in these models entirely through selection of suitable parameters.

The two parameters of the TIS model (eq. 1.12) are reflections of flow velocity heterogeneity (α) and net reaction (k). Similarly the three "ultimate" parameters of the bicontinuum model are measures of flow velocity heterogeneity ($\overline{\lambda^3}$) and net reaction ($\bar{k}$), along with a third parameter (L) that reflects net transverse mixing, a process not considered in the TIS model. The bicontinuum model may thus be expected to provide a better match to wetland performance data than the relaxed-TIS model, to the extent that transverse mixing influences mean concentration decline.

5.3.2 Texel Treatment Wetlands

Toet et al. (2005) studied the effect of retention time (wetland water volume divided by mean flow rate) on nutrient removal in parallel FWS wetland cells treating tertiary wastewater effluent in Holland. The wastewater was not nitrified, so roughly equivalent concentrations of NO_3^- and NH_4^+ were present in the effluent. Retention times of 0.3, 0.8, 2.3, and 9.3 days were studied in eight cells: for each retention time, one each planted with *Phragmites* and *Typha*. Biweekly grab samples collected over the course of a year at the inlets and outlets were used to calculate annual mean % removals of various conventional pollutants, including NO_3^- and NH_4^+.

Figures 5.1a and 5.1b show the removal data, for NO_3^- and NH_3 respectively, as functions of retention time (i.e. from multiple cells), along with best-fit TIS, relaxed-TIS and bicontinuum models. Because $\overline{\lambda^3}$ and L are system properties they should be the same irrespective of constituent, thus the parameter optimization routine (Excel Solver) was used to select a single value for each of these, while choosing parameter-specific values of $\bar{k}$ (one each for NO_3^- and NH_4^+) that

minimized the total model error summed for both constituents. The relaxed-TIS model parameters were optimized in the same manner, with a single α value used to represent the decline curves of both constituents, and optimization used to select k values for both constituents simultaneously. No tracer data were reported, so the bicontinuum model employed the default assumption of RTD dimensionless variance = 1/3, equivalent to $\alpha = 3$ in the TIS model. All three models provided fair representations of both data sets, however the bicontinuum model produced the smallest total summed-squared-error across both constituents: approximately 0.020, as compared with 0.021 for the relaxed-TIS model, and 0.030 for the TIS model.

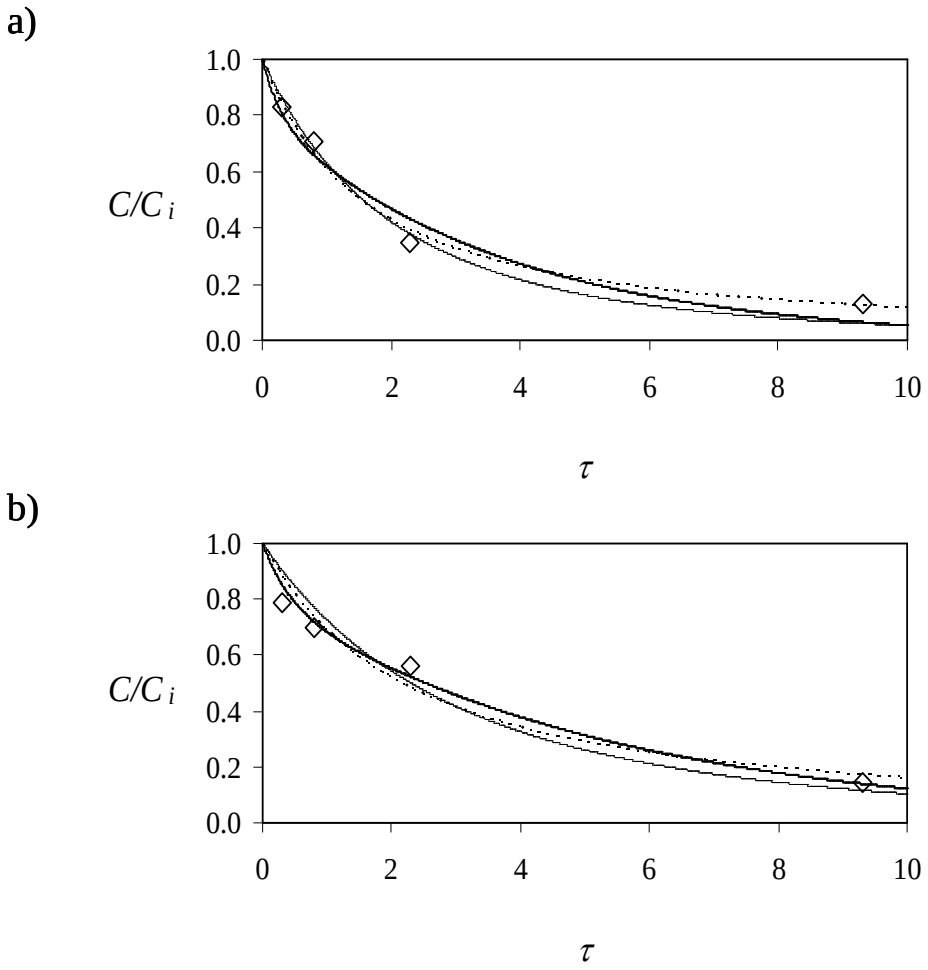

Figure 5.1 Toet et al. (2005) data plotted as a function of retention time (τ), and best-fit bicontinuum (solid line), TIS (long dashes), and relaxed-TIS (short dashes) models, for a) NH_3, and b) NO_3^-. Bicontinuum model has system parameters $\overline{\lambda^3}$ = -0.303 and $L = 1.94\times10^{-7}$, with $\bar{k}$ = 0.917 d^{-1} and 0.638 d^{-1} for NH_3 and NO_3^- respectively, while relaxed-TIS model has "shape" parameter α = 1.188, and $\bar{k}$ = 0.622 d^{-1} and 0.439 d^{-1} for NH_3 and NO_3^- respectively. TIS model has α = 3 and $\bar{k}$ = 0.501 d^{-1} and 0.339 d^{-1} for NH_3 and NO_3^- respectively.

5.3.3 The San Jacinto Wetland

Chendorain et al. (1998) studied the removal of MS2 coliphage virus in a California surface flow constructed wetland with alternating zones of vegetation and open water. Cell dimensions were 70 m in length, 15.5 m wide, and 0.46 m deep. The one-dimensional ADE was found to produce a good fit to bromide tracer RTD data using a Peclet number ($Pe = \Lambda \bar{u} / D$, where Λ is wetland length, $\bar{u}$ is mean velocity, and D is longitudinal dispersion coefficient) of 5.8. Using the following equation (Dierberg et al., 2005), we calculate from this information a value of 0.3496 for the RTD dimensionless variance:

$$\frac{\sigma_t^2}{\bar{t}^2} = \frac{2}{Pe} - \frac{2}{Pe^2}\left(1 - e^{-Pe}\right) \tag{5.15}$$

Phage concentrations were measured at six distances from the inlet along the main flow path of the wetland. These data demonstrate strongly non-first order decay, with a steep decline in concentration near the inlet, relatively gradual decline thereafter, and therefore "a large discontinuity" between apparent PFR removal rate constants for the first 3 m, and for the rest of the wetland. Presumably there are no edaphic processes capable of generating enteric viruses within the wetland, thus the concentration plateau may result solely from hydrodynamic short-circuiting within the wetland. Alternatively the steep early decline may be the result of phage inactivation or aggregation caused by chemical differences (e.g. osmotic potential or pH) between the stock solution and the wetland water, as the authors speculate.

Figure 5.2 displays this data, along with best-fit TIS, relaxed-TIS and bicontinuum models. Figure 5.2a shows the data and model results plotted as a function of travel distance x, and Figure 5.2b shows the same information for ln-

transformed data and model results. In this comparison only the relaxed-TIS model provides a decent fit to the data set beyond the first 3 m of travel, where the concentration plateau is found.

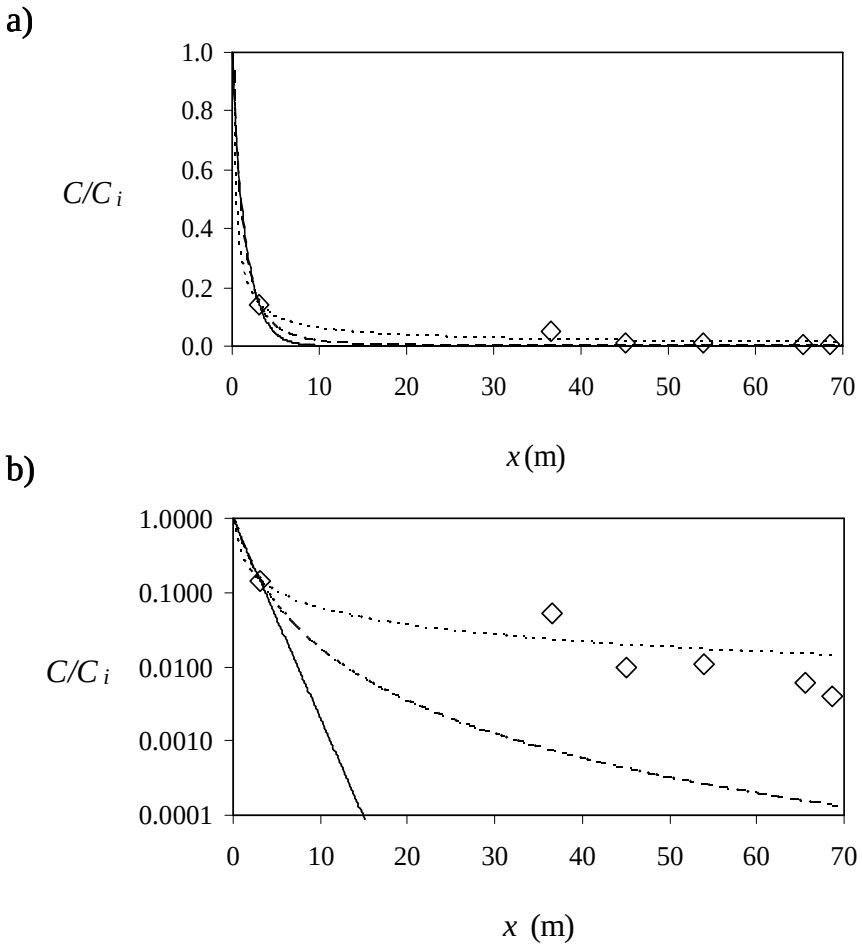

Figure 5.2 Chendorain et al. (1998) data and best-fit bicontinuum (solid line), TIS (long dashes), and relaxed-TIS (short dashes) models with a) concentrations and b) ln-transformed concentrations, plotted as functions of travel distance (x). Bicontinuum and TIS models have dimensionless variance = 0.3496, in accordance with inert tracer study results.

The preceding comparison suggests that the relaxed-TIS model provides an unambiguously better representation of the Chendorain data set than the bicontinuum

model is able to. However, the apparent linearity of the data displayed in log space in Figure 5.2b suggests another possible interpretation. The domain may be envisioned as composed of two non-interacting continua (i.e. with mixing parameter L equal to zero), one of which has zero velocity, e.g. u_2=0. If this is the case then the input concentration never "enters" the second domain, instead remaining at the inlet, and as a consequence $C(0^+)/C_i = f_1 \neq 1$. Solution of eq. 4.50 in this case reduces to a PFR equation of the following form:

$$c_1 = f_1 \exp[-k_1 \tau y] \tag{5.16}$$

Figure 5.3 displays the same results as Figure 5.2, except that in this case the "bicontinuum" model fit to the data is eq. 5.16, with optimized values of parameters f_1 and k_1. This model, with f_1=0.16 and k_1=0.043 d^{-1}, produces the lowest summed squared errors of any of the models tested, and therefore a better representation of the data than the relaxed-TIS model.

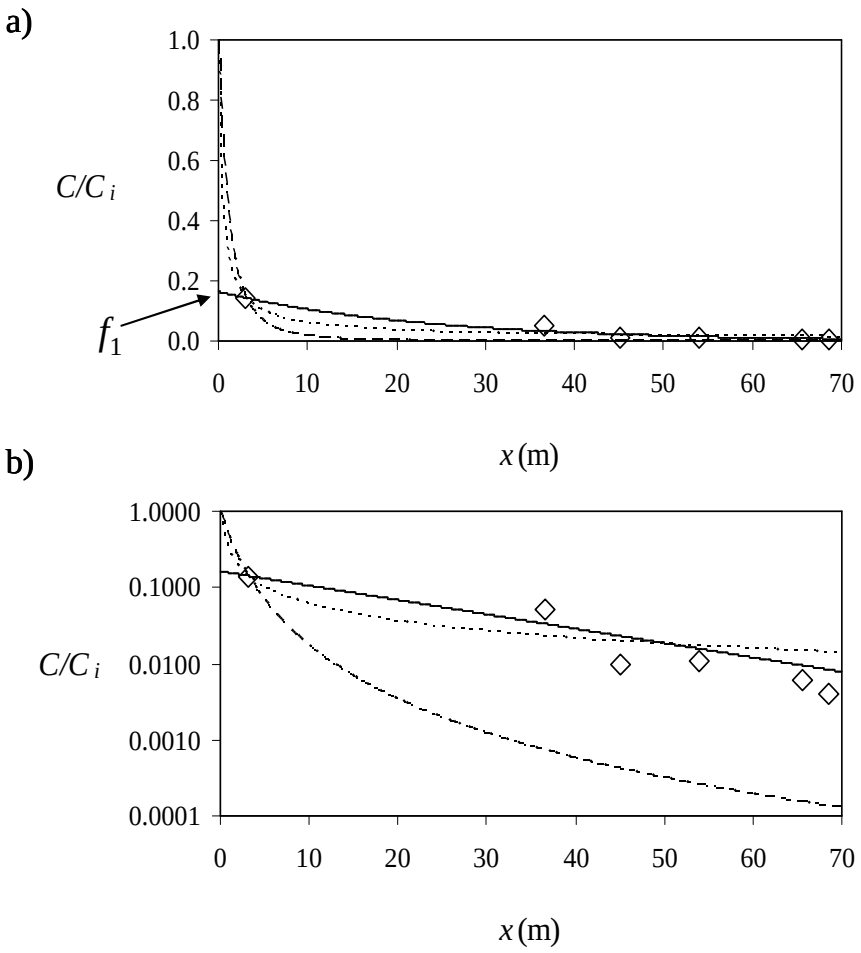

Figure 5.3 Chendorain et al. (1998) data and best-fit bicontinuum (solid line), TIS (long dashes), and relaxed-TIS (short dashes) models with a) concentrations and b) ln-transformed concentrations, plotted as functions of travel distance (x). Bicontinuum model in this case is a single PFR model of the form in eq. 5.16.

5.4 Discussion

In the Texel wetland example the bicontinuum model is seen to produce a slightly better overall representation of NH_3 and NO_3^- decline curves (as a function of retention time), than produced by either the (fixed α) TIS or relaxed-TIS models (eq. 1.12). Given that the bicontinuum model includes an additional parameter, this is perhaps not surprising. However the optimized L value of 1.94×10^{-7} reflects a negligible degree of transverse mixing: the associated $x_{1/2}^{D}$ is approximately 9×10^{6} m,

so the system is essentially stochastic-convective. Thus the inclusion of an extra parameter to quantify transverse mixing is superfluous in this example: the two-parameter relaxed-TIS model apparently incorporates sufficient information to account for the shapes of the concentration decline curves, without the need to invoke transverse mixing. The effect of transverse dispersion on the shapes of mean concentration decline curves may in fact be fairly subtle, as the results in Figure 4.4a and 4.4b suggest. Unlike in comparisons against theoretical models with exact solutions, such as the one developed in Chapter 3, real wetland monitoring data are often noisy enough to confound unambiguous parameter interpretation. Thus it may be difficult in practice to accurately "measure" values of $\overline{\lambda^3}$ and L through inverse modeling, or even to ascertain when the bicontinuum model provides a better representation of performance data than other models in such systems. One important difference between the bicontinuum and TIS models is in the shape of the tails at large time/distance, which exhibit exponential declines in the former case, and power law declines in the latter. This may enable the relaxed-TIS model to better represent concentration plateau effects arising from short-circuiting. However, alternative interpretations of the bicontinuum model may allow it to provide superior representation of wetland dynamics for some situations, as the Figure 5.3 example demonstrates. In this example, the immobile continuum may be envisioned as corresponding to a portion of the medium in which immediate phage inactivation/aggregation occurs, in concurrence with the mechanistic interpretation of their data offered by the authors of the study (Chendorain et al., 1998).

Chapter 6: Summary and Conclusions

6.1 Summary

The primary objectives of the work described in this study were to develop new modeling approaches for wetlands that accomplish three specific aims: 1) develop and evaluate a version of the DND model capable of accounting for temporally-varying flow and influent concentrations, 2) develop and evaluate an analytical model of reactive transport in a system with spatially variable flow velocity to serve as a benchmark for evaluating simplified models, and 3) develop and evaluate a wetland performance model that contains a minimal number of parameters, but which uses stochastic principles to account for the influence of spatial heterogeneity on advection and reaction, and which accounts for transverse diffusion and the development of shear flow dispersion. Chapter 2 addressed the first of these goals, Chapter 3 addressed the second, and Chapter 4 addressed the third. In Chapter 2, an RTD measured under steady conditions was made use of, and presumed to apply under varying flow conditions as well, but with spatially-local velocities scaled by the temporally-varying bulk flow rate, such that residence time-on-exit and corresponding net reaction are calculated within individual stream tubes, and then summed to produce mean exit concentration expressed as a function of time. The approach, as implemented in MATLAB® program "Wetloop" (Appendix E), successfully simulated effluent TP and BOD_5 time series from wastewater treatment wetlands in California and Florida respectively, and eliminated the flow-related bias in model errors produced by a PFR model of one of these wetlands.

The PFR model commonly used for simulating treatment wetland performance suffers from limitations related to spatial heterogeneity in controlling biophysical attributes. Wetland flow velocities are heterogeneous as a result of vegetation density and/or depth variations, and wetlands are thus characterized by a degree of hydraulic short-circuiting. For some water quality constituents, the same variables (vegetation density, water column depth) that affect flow velocities on a local scale also affect local removal rates. The combined effect of these two influences is net reaction that does not necessarily manifest as simple exponential decline of mean concentration with distance or retention time.

When heterogeneous velocities are accounted for, but not transverse diffusive/dispersive fluxes, the result is a DND model (Carleton, 2002) that can essentially explain PFR parameter dependence on flow, and non-exponential mean decline curves. However the DND model (and its more empirical analogue, the relaxed-TIS model) are potentially hampered by another limiting simplification: that flow is stochastic-convective. Like plug flow, stochastic-convective flow is a conceptual idealization that is never completely attained in reality, because diffusion is never zero when concentrations are non-uniform. In its original incarnation, the DND model was also limited to steady-state flow conditions with constant influent concentration, another idealization that does not correspond with the general situation in real wetlands.

In Chapter 3 an analytical solution to a two-dimensional time-invariant advective-dispersive-reactive transport equation was generated for a rectangular domain in which advection, dispersion, and reaction terms were all specified as

simple power functions of the transverse dimension. Solutions for transverse-mean resident and flux concentrations for domains with uniform inlet concentration (spanning the upstream boundary) were examined as idealized representations of a treatment wetland possessing something like a U-shaped depth profile with fringing vegetation whose density increases toward the shallows. Simulations were used to demonstrate the beneficial impact that transverse mixing has on reactor performance as a function of distance from the inlet. In other words, it was demonstrated that in a system with a heterogeneous flow field and reactions, the presence of transverse diffusion can improve removal efficiencies compared to systems that lack such transverse mixing.

In Chapter 4, analogous representations for laterally unbounded, periodically heterogeneous domains were developed by volume-averaging of stochastic versions of two-dimensional transport equations. Corresponding bicontinuum (mobile-mobile) representations were generated by canonical transformation of the governing system of equations. Expressions for transverse concentration variance, as well as RTD variance and effective longitudinal dispersion coefficient as a function of travel distance were also derived. The bicontinuum model was shown to closely reproduce results from the idealized heterogeneity (Chapter 3) wetland model under pre-asymptotic conditions, and of a one-dimensional ADE under nearly-asymptotic (Fickian) dispersive conditions.

In Chapter 5, bicontinuum model results were compared against TIS and relaxed-TIS (and therefore by implication, also DND) model results in matching effluent concentration data from two real world wetlands treating inorganic nitrogen

and coliphage, respectively. In the former example the bicontinuum model gave a slightly better match to the data, though optimized parameter results suggested that flow was essentially stochastic-convective. In the latter example only the relaxed-TIS model produced a reasonable match to the concentration decline curve, unless the bicontinuum model was reinterpreted as specifically a non-interacting mobile-immobile model, in which case the model produced the best fit to the data.

Despite the limitations that these two examples illustrate, the bicontinuum model may prove valuable as a simple (three parameter) model for application to wetlands or other bioreactors that are adequately characterized by neither stochastic-convective nor Fickian dispersion models. The model would be most practically applicable to long wetlands where the transition from a stochastic-convective to a transitional and possibly near-Fickian mixing regime is more likely to become important. The bicontinuum model is distinguished from the DND model by being physically based and entirely derived from first principles, with parameters that are in theory (if somewhat difficultly in practice) independently measurable rather than strictly empirical in nature. By contrast, the DND model is semi-empirical in nature, requiring either a measured or an assumed RTD which is presumed to derive entirely from a distribution of advective velocities. However, velocity distributions alone cannot account for the classical skewed bell curve shape of a wetland RTD (especially for the fastest moving tracer particles), again because some diffusion must occur, even within transport systems dominated by advective velocity gradients.

The relaxed-TIS model (eq. 1.12) appears to be capable of matching nearly perfectly the decline curves produced by a DND model, however with parameters

interpreted as empirical, which must be selected via inverse modeling. For complex constituents, Kadlec's analysis (2003) suggests that this model can account for concurrent "weathering" and DND effects. Successful application of the non-steady version of the DND model to BOD_5 simulation in the Gustine wetland example (Chapter 2) implies that the non-steady DND model can handle complex constituents, though associated parameters should be interpreted cautiously, i.e. as more empirical than mechanistic in nature, in the absence of other confirmatory information. For simple (non-weatherable) constituents, successful fitting of the relaxed-TIS model to concentration decline curves in the Chapter 5 examples, and of the non-steady DND model to effluent TP (essentially composed entirely of dissolved P) data in the Orlando Easterly Wetlands example in Chapter 2, imply that the DND construct can provide an adequate mechanistic explanation for observed concentration decline curves. However, connections between the parameters of the relaxed-TIS model (eq. 1.12 with $C^* = 0$) and the parameters of RTDs for the same wetlands have yet to be elucidated in a quantitative way, either theoretically or with data. This task remains an area for further study. Further evaluation of both the bicontinuum and DND models, by fitting each of them against data sets from additional wetlands and perhaps other kinds of reactive transport systems (e.g. streams, rivers) is also called for, to better determine the sorts of conditions under which each model might provide the most useful and/or accurate representations of reactive constituent removal. There are however at present very few published experimental studies that provide the necessary quantitative data for FWS wetlands.

6.2 Conclusions

The following specific conclusions were obtained from this work:

- In a non-steady-state version of the DND model, results compared reasonably well with measured wetland effluent time series. The model presumes flow to be entirely stochastic-convective (transverse diffusion/dispersion is assumed nil).
- Unlike a PFR model fit to monthly-averaged data, there was no correlation between non-steady-DND model error and hydraulic loading rate. However, magnitudes of errors (deviations from measured values) were about the same for both models.
- An analytical model of an idealized two-dimensional advective-dispersive reactor with space-varying coefficients was developed, representing perhaps a wetland with a roughly "U shaped" depth profile and fringing vegetation. In simulations, increasing transverse diffusion/dispersion resulted in improved reactor performance (lower mean concentrations).
- An analytical model of an advective-dispersive reactor with stochastic heterogeneity was developed by using various closures to approximate higher-order correlation terms. For steady-state conditions, in bicontinuum form the model reduces to a weighted sum of two exponential decline curves governed by a total of three parameters representing mean system attributes (essentially velocity heterogeneity, net reaction rate, and transverse mixing, respectively).
- For low and intermediate degrees of transverse mixing, wherein the effective longitudinal dispersion coefficient either continually increases, or essentially

reaches its asymptotic limit about a fifth of the way through the transport domain, bicontinuum model results (including resident concentration and transverse standard deviation), nicely matched those from the corresponding idealized heterogeneity model.

- For a high degree of transverse mixing, wherein the effective longitudinal dispersion coefficient essentially reaches its asymptotic value early in the transport domain, resident concentrations matched the results of a one-dimensional ADE employing the asymptotic longitudinal dispersion coefficient.
- Comparisons of model output against real wetland data suggested the bicontinuum model may represent wetland performance better than the relaxed-TIS model in some cases, but not in all. The relaxed-TIS model appears to be more flexible in terms of concentration curve shapes that it can assume, however the model has the disadvantage of being entirely empirical in nature. By contrast, the bicontinuum model has parameters that are physically meaningful and therefore potentially independently measurable. Unlike the relaxed-TIS model, measured dimensionless variance can be used to potentially constrain allowable values of bicontinuum model parameters.

As environmental conditions worsen in the 21st century, restoration and/or construction of wetlands grows in importance as a potential method for halting the general loss of ecosystem and hydrologic functions, while simultaneously improving water quality. This study has focused on theoretical aspects of reaction and

hydrodynamics in wetlands. The resulting developments contribute to understanding of processes that determine wetland transport behavior, and should enhance the ability to quantitatively analyze wetland function, and to design treatment wetland systems. It is hoped that these developments will lead to improved ability to construct or restore wetlands that meet multiple ecological management objectives, including treatment of polluted water.

6.3 Recommendations for Future Research

The results of this study highlight the need for further research in both experimental and theoretical fields related to wetlands. In the area of field research, more concurrent flow and concentration data collected at multiple locations within individual wetlands are needed, to better elucidate fundamental relationships between these entities. Correlations between flow and concentration and measurable variables presumed to directly affect each of them, especially vegetation surface area density, would further permit investigation of assumptions (e.g. eqs. 4.2 and 4.3) used in developing the models in this study. A related area of potentially fruitful investigation is development of methods for measuring spatial distributions of vegetation density in detail via remotely sensed image analysis. If this can be done, then it may also be possible to estimate parameters such as integrated covariance measure "*A*" (Chapter 4) through analysis of the same sorts of images. An obvious next step would then be to investigate the potential temporal dependence of such parameters.

The model-data comparisons of Chapter 5 highlight a pressing need for additional effluent concentration data collected from individual wetlands operated

under ranges of hydraulic loading rates, to allow more thorough evaluation of models such as those developed and/or discussed in this study. This sort of data would be especially useful for water quality constituents that are of a simple nature, so that constituent weathering is eliminated as a potentially confounding factor in concentration decline. In addition to FWS wetlands, application of models explored in this study to SSF wetlands (both horizontal and vertical flow) may prove to be a worthwhile endeavor. The bicontinuum model in particular may have application to naturally biphasic systems, such as wetlands characterized by significant advection in both free water and underlying porous medium phases.

In the area of theoretical research, incorporation of sorption into transport equations represents one relatively straightforward improvement. Application of the bicontinuum model to time-series inputs (as opposed to steady-state), with appropriate solution of the full time-varying equation (e.g. eq. 4.37) is also a potential next step. Another possible improvement, as suggested in Chapter 4, would be development of a tricontinuum approximation via a third-order equation system, thereby increasing the accuracy of the approximation over that of the bicontinuum, and permitting the 4^{th} and 5^{th} moments of the heterogeneity variate distribution to be accurately represented. Based upon the outcome in Chapter 4, one suspects that the results for steady-state might be a weighted sum of three exponential decline curves, though this remains to be seen. Regardless, the increase in accuracy and flexibility provided by such a model would in all likelihood be more than offset by the increased number of parameters requiring values for fitting to wetland data sets.

The derivation of stochastic models with transverse mixing whose early-time behavior is similar to that of the DND or relaxed-TIS model also remains as an area of future study. In the bicontinuum model developed in this work, transverse mixing is represented by first-order interactions between continua, which lead to the dual-exponential form of the steady-state concentration profile. Alternative inter-continua transfer formulations that may lead to a power-law form of these distributions should be investigated.

Appendix A: Incorporation of Longitudinal Dispersion

The governing mass-balance equation including a longitudinal dispersion term is obtained by employing eq. 3.31 in eq. 3.30, along with the definitions used previously for other transport parameters:

$$-FZ^{p}C - AZ^{m}\frac{\partial C}{\partial X} + \frac{\partial}{\partial Z}\left(BZ^{n}\frac{\partial C}{\partial Z}\right) + IZ^{m}\frac{\partial^{2}C}{\partial X^{2}} + S(X,Z) = 0 \qquad \text{(A1)}$$

Boundary condition (eq. 3.6) is assumed to apply, and the Green's function approach of eq. 3.7 is employed, which in this case produces

$$AZ_{0}^{m}\frac{\partial G}{\partial X_{0}} - FZ_{0}^{p}G + \frac{\partial}{\partial Z_{0}}\left(BZ_{0}^{n}\frac{\partial G}{\partial Z_{0}}\right) + IZ_{0}^{m}\frac{\partial^{2}G}{\partial X_{0}^{2}} = 0\,,\ X > X_{0} \qquad \text{(A2)}$$

in place of eq. 3.9a. The eigenfunction problem corresponding with eq. 3.12 is

$$\frac{\partial w_{i}}{\partial X_{0}} + \left(\frac{I}{A}\right)\frac{\partial^{2}w_{i}}{\partial X_{0}^{2}} = w_{i}\Omega_{i}^{2} \qquad \text{(A3)}$$

This is a second-order ordinary differential equation with roots

$$r_{1}, r_{2} = \frac{-A \pm A\sqrt{1 + 4\Omega_{i}^{2}\dfrac{I}{A}}}{2I} \qquad \text{(A4)}$$

Only the root with the positive sign produces a physically sensible result, therefore the solution for w_i corresponding with eq. 3.20 becomes

$$w_{i}(X_{0}) = w_{i,0}\exp\left\{\left[\frac{A}{2I} - \left[\left(\frac{A}{2I}\right)^{2} + \frac{A}{I}\Omega_{i}^{2}\right]^{1/2}\right](X - X_{0})\right\} \qquad \text{(A5)}$$

Expressing the eigenvalue in the form of eq. 3.18, and recognizing again that $w_{i,0}$ equals $\alpha_i \phi_i(Z)$, A5 is written as

$$w_i(X_0) = \alpha_i \phi_i(Z) \exp\left\{\left[\frac{A}{2I} - \left[\left(\frac{A}{2I}\right)^2 + \frac{A}{I}\varepsilon^2(1-n)^2\frac{B}{A}\lambda_i^2\right]^{1/2}\right](X - X_0)\right\} \tag{A6}$$

and therefore

$$\begin{aligned} G &= \sum_{i=1}^{\infty} \alpha_i^2 \phi_i(Z)\phi_i(Z_0) \exp\left\{\left[\frac{A}{2I} - \left[\left(\frac{A}{2I}\right)^2 + \frac{A}{I}\varepsilon^2(1-n)^2\frac{B}{A}\lambda_i^2\right]^{1/2}\right](X - X_0)\right\} \\ &= \sum_{i=1}^{\infty} \alpha_i^2 Z^{(1-n)/2} J_\nu\left[2\nu\lambda_i Z^{\varepsilon(1-n)/2\nu}\right] \\ &\quad \cdot Z_0^{(1-n)/2} J_\nu\left[2\nu\lambda_i Z_0^{\varepsilon(1-n)/2\nu}\right] \exp\left\{\left[\frac{A}{2I} - \left[\left(\frac{A}{2I}\right)^2 + \frac{A}{I}\varepsilon^2(1-n)^2\frac{B}{A}\lambda_i^2\right]^{1/2}\right](X - X_0)\right\} \end{aligned} \tag{A7}$$

which leads directly to equation 3.32.

Appendix B: Solution when n=1

Relton (1965) provides the following comprehensive form of the Bessel equation

$$y'' + \frac{1-2\alpha}{x} y' + \left[\left(\beta\gamma x^{\gamma-1} \right)^2 + \frac{\alpha^2 - \nu^{2\gamma^2}}{x^2} \right] y = 0 \tag{B1}$$

whose general solution in terms of the same parameters is given as

$$y = x^{\alpha} C_{\nu} \left(\beta x^{\gamma} \right) \tag{B2}$$

Comparing eq. 3.14 with (B1), we see that $\alpha = \frac{1-n}{2}$, $\gamma = \frac{2+m-n}{2}$, and

$\beta = \left(\frac{A}{B} \right)^{1/2} \frac{2\Omega_i}{2+m-n}$, which leads directly to eq. 3.17 when $n \neq 1$. When $n = 1$ we have

$\alpha = 0$, $\gamma = \frac{m+1}{2}$, and $\beta = \left(\frac{A}{B} \right)^{1/2} \frac{2\Omega_i}{m+1}$. The analogue of eq. 3.17 for this case is

$$\phi_i(Z_0) = J_{\nu} \left[\left(\frac{A}{F} \right)^{1/2} \nu\Omega_i Z_0^{\frac{m+1}{2}} \right] \tag{B3}$$

and modified eigenvalues are defined using the following alternative to eq. 3.18:

$$\lambda_i = \left(\frac{A}{F} \right)^{1/2} \Omega_i \tag{B4}$$

In place of eqs. 3.19 and 3.20 we have

$$\phi_i(Z_0) = J_{\nu} \left[\nu\lambda_i Z_0^{\frac{m+1}{2}} \right] \tag{B5}$$

and

$$w_i(X_0) = w_{i,0} \exp\left[-\frac{F}{A}\lambda_i^2\left(X - X_0\right)\right] \tag{B6}$$

The expression for concentration, analogous to eq. 3.29, is therefore

$$\begin{aligned} C\left(X, Z, Z_0\right) &= M \sum_{i=1}^{\infty} \alpha_i^2 J_\nu\left[\nu\lambda_i Z^{\frac{m+1}{2}}\right] \\ &\cdot J_\nu\left[\nu\lambda_i Z_0^{\frac{m+1}{2}}\right] \exp\left[-\frac{F}{A}\lambda_i^2\left(X - X_0\right)\right], \quad X > X_0 \end{aligned} \tag{B7}$$

with coefficients given by

$$\alpha_i^2 = \frac{1}{\int_0^1 A Z^m \left(J_\nu\left[\nu\lambda_i Z^{\frac{m+1}{2}}\right]\right)^2 dZ} \tag{B8}$$

Appendix C: Normalized dispersive flux closure calculation

We begin by considering the perturbed mean-removed equation with transverse dispersion:

$$\frac{\partial c'}{\partial t} = -\lambda \rho_{u\lambda} \delta(t) \frac{\partial \bar{c}}{\partial x} + D_0 \frac{\partial^2 c'}{\partial z^2} \tag{C1}$$

where $c' = \lambda \rho_{c\lambda}$. We define the normalized transverse coordinate $z^* = z/H$, where H is half the period of lateral heterogeneity, or the width of the domain for a bounded system. Thus $\frac{\partial c}{\partial z} = \frac{1}{H}\frac{\partial c}{\partial z^*}$ and $\frac{\partial^2 c}{\partial z^2} = \frac{1}{H^2}\frac{\partial^2 c}{\partial z^{*2}}$. Expressing C1 in terms of the normalized coordinate we obtain

$$\frac{\partial c'}{\partial t} = -\lambda \rho_{u\lambda} \delta(t) \frac{\partial \bar{c}}{\partial x} + \frac{D_0}{H^2} \frac{\partial^2 c'}{\partial z^{*2}} \tag{C2}$$

Employing Duhamel's theorem, the solution to this equation is

$$c'(z_1^*, t) = -\rho_{u\lambda} \frac{\partial \bar{c}}{\partial x} H \int_{-\infty}^{\infty} \frac{\lambda(z^*)}{\sqrt{4\pi D_0 t}} e^{-\frac{H^2 (z_1^* - z^*)^2}{4 D_0 t}} dz^* \tag{C3}$$

The dynamics of the heterogeneity correlation are described by

$$\rho_{c\lambda}(z_{1c,}^* t) = \overline{\lambda c'(z_{1c}^*, t)} = -\rho_{u\lambda} \frac{\partial \bar{c}}{\partial x} H^2 \int_0^1 \int_{-\infty}^{\infty} \frac{\lambda(z_1^*)\lambda(z^*)}{\sqrt{4\pi D_0 t}} e^{-\frac{H^2 (z_1^* - z^*)^2}{4 D_0 t}} dz^* dz_1^* \tag{C4}$$

We define the normalized lag distance $s^* = z^* - z_1^*$ and reverse the order of integration to obtain

$$\rho_{c\lambda}(z^*_{1c,}\,t) = -\rho_{u\lambda}\frac{\partial \bar{c}}{\partial x}H^2\int_{-\infty}^{\infty}\cdot\left[\int_0^1 \lambda(z^*_1)\lambda(z^*_1+s^*)dz^*_1\right]\frac{e^{-\frac{H^2 s^{*2}}{4D_0 t}}}{\sqrt{4\pi D_0 t}}ds^*$$
$$= -\rho_{u\lambda}\frac{\partial \bar{c}}{\partial x}H^2\int_{-\infty}^{\infty} Cov_\lambda(s^*)\frac{e^{-\frac{H^2 s^{*2}}{4D_0 t}}}{\sqrt{4\pi D_0 t}}ds^* \qquad \text{(C5)}$$

where $Cov_\lambda(s^*)$ is the covariance of λ in terms of normalized lag distance units.

For calculation of the closure we compare the above result to an analogous result obtained from the perturbed mean-removed equation when a first-order approximation is used in place of the transverse dispersion term:

$$\frac{\partial c'}{\partial t} = -\lambda\rho_{u\lambda}\delta(t)\frac{\partial \bar{c}}{\partial x} - \frac{D_0}{A}c' \qquad \text{(C6)}$$

The solution of this equation is

$$c'(z,t) = -\rho_{u\lambda}\frac{\partial \bar{c}}{\partial x}\lambda(z)e^{-\frac{D_0}{A}t} \qquad \text{(C7)}$$

Similar to eq. C4, the dynamics of the heterogeneity correlation are given by

$$\hat{\rho}_{c\lambda}(z^*,t) = \overline{\lambda(z^*)c'(z^*,t)} = -\rho_{u\lambda}\frac{\partial \bar{c}}{\partial x}He^{-\frac{D_0}{A}t}\int_0^1 \lambda(z^*)\lambda(z^*)dz^*$$
$$= -\rho_{u\lambda}\frac{\partial \bar{c}}{\partial x}He^{-\frac{D_0}{A}t} \qquad \text{(C8)}$$

The difference between C5 and C8 is minimized over time in an integrated sense by setting

$$\int_0^\infty\left[\rho_{c\lambda}(z^*,\tau) - \hat{\rho}_{c\lambda}(z^*,\tau)\right]d\tau = 0 \qquad \text{(C9)}$$

which leads to

$$\frac{A}{D_0} = H\int_0^\infty\int_{-\infty}^{\infty} Cov_\lambda(s^*)\frac{e^{-\frac{H^2 s^{*2}}{4D_0\tau}}}{\sqrt{4\pi D_0\tau}}ds^*d\tau \qquad \text{(C10)}$$

We next define $\tau^* = \frac{D_0}{H^2}\tau$, and therefore $d\tau^* = \frac{D_0}{H^2}d\tau$, and $d\tau = \frac{H^2}{D_0}d\tau^*$.

Substitution leads to

$$A = H^2 \int_0^{\infty}\int_{-\infty}^{\infty} Cov_\lambda(s^*)\frac{e^{-\frac{s^{*2}}{4\tau^*}}}{\sqrt{4\pi\tau^*}}ds^* d\tau^* \tag{C11}$$

We define $m_{\lambda\lambda}(r)$ as the unnormalized spectral density of λ

$$m_{\lambda\lambda}(r) = \frac{1}{2\pi}\int_{-\infty}^{\infty} e^{-irs^*} Cov_\lambda(s^*)ds^* \tag{C12}$$

thus

$$Cov_\lambda(s^*) = \int_{-\infty}^{\infty} e^{irs^*} m_{\lambda\lambda}(r)dr \tag{C13}$$

Substituting C13 into C11 and changing the order of integration, we obtain

$$A = H^2 \int_{-\infty}^{\infty} m_{\lambda\lambda}(r)\int_0^{\infty}\int_{-\infty}^{\infty} e^{irs^*}\frac{e^{-\frac{s^{*2}}{4\tau^*}}}{\sqrt{4\pi\tau^*}}ds^* d\tau^* dr \tag{C14}$$

which simplifies to

$$A = \frac{H^2}{2\pi}\int_{-\infty}^{\infty}\frac{m_{\lambda\lambda}(r)}{r^2}dr \tag{C15}$$

If λ is periodic, and can be represented by a cosine Fourier series of the form

$$\lambda(z^*) = \sum_{n=-\infty}^{\infty} b_n \cos(r_n z^*) \tag{C16}$$

in which $r_n = \frac{n\pi}{2}$, and the Fourier coefficients are obtained using

$$b_n = \int_{-1}^{1} \lambda(z^*)\cos(r_n z^*)dz^* \tag{C17}$$

as in Montas et al. (2000), then

$$Cov_{\lambda}(s^{*}) = \sum_{n=-\infty}^{\infty} b_n^2 \cos(r_n s^{*}) \tag{C18}$$

Substituting C18 into C11 and integrating over space and time, we obtain the following additional definition of *A*:

$$A = H^2 \sum_{n=-\infty}^{\infty} \frac{b_n^2}{r_n^2} = 2H^2 \sum_{n=1}^{\infty} \frac{b_n^2}{r_n^2} \tag{C19}$$

Appendix D: Temporal moment calculations

Following the procedure of Valocchi (1989), the behavior of the system following pulse introduction of a non-reactive tracer at the upstream boundary is investigated by first considering transformation of the appropriate boundary conditions to corresponding conditions for the canonical equation system, i.e.:

$$\begin{cases} \bar{c}(0) = \dfrac{a}{\bar{u}}\delta(x) \\ \rho_{c\lambda}(0) = 0 \end{cases} \tag{D1}$$

where δ is the Kronecker delta function. Substitution into eq. 4.32 produces

$$\begin{bmatrix} c_1(0) \\ c_2(0) \end{bmatrix} = \begin{bmatrix} 1 & \lambda_1 \\ 1 & \lambda_2 \end{bmatrix} \begin{bmatrix} \dfrac{a\delta(x)}{\bar{u}} \\ 0 \end{bmatrix} \tag{D2}$$

or

$$c_1(0) = c_2(0) = \frac{a\delta(x)}{\bar{u}} \tag{D3}$$

The governing transport equations for a non-reactive tracer within the canonical version of the heterogeneous system of interest are:

$$\begin{cases} \dfrac{\partial c_1}{\partial t} = -\dfrac{L}{f_1}(c_1 - c_2) - u_1 \dfrac{\partial c_1}{\partial x} \\ \dfrac{\partial c_2}{\partial t} = -\dfrac{L}{f_2}(c_2 - c_1) - u_2 \dfrac{\partial c_2}{\partial x} \end{cases} \tag{D4}$$

The temporal moment operator is $\int_0^\infty t^n [\ ] dt$. Temporal moments, of order n, of the flux mean concentration are defined as weighted averages of the corresponding

moments in the two continua. Applying the moment operator to the left hand side of one of the equations in D4 we have

$$\int_0^\infty t^n \frac{\partial c_1}{\partial t} dt = t^n c_1 \Big|_0^\infty - n\int_0^\infty t^{n-1} c_1 dt = t^n c_1 \Big|_0^\infty - n m_{n-1}^{(1)} \tag{D5}$$

which simplifies to

$$\begin{cases} for\ n = 0 : c_1 \Big|_0^\infty = -c_1(t=0) \\ for\ n > 0 : c_1 \Big|_0^\infty = -n m_{n-1}^{(1)} \end{cases} \tag{D6}$$

Applying the moment operator to the right hand side of D4 for the case of n=0 produces:

$$\begin{cases} -c_1(0) = -\dfrac{L}{f_1}\left(m_0^{(1)} - m_0^{(2)}\right) - u_1 \dfrac{\partial m_0^{(1)}}{\partial x} \\ -c_2(0) = -\dfrac{L}{f_2}\left(m_0^{(2)} - m_0^{(1)}\right) - u_2 \dfrac{\partial m_0^{(2)}}{\partial x} \end{cases} \tag{D7}$$

Rearranging and expressing D7 in matrix form we obtain the following system of linked equations governing the 'zeroth' moment:

$$\frac{\partial}{\partial x}\begin{bmatrix} m_0^{(1)} \\ m_0^{(2)} \end{bmatrix} = -L\begin{bmatrix} \dfrac{1}{f_1 u_1} & \dfrac{-1}{f_1 u_1} \\ \dfrac{-1}{f_2 u_2} & \dfrac{1}{f_2 u_2} \end{bmatrix}\begin{bmatrix} m_0^{(1)} \\ m_0^{(2)} \end{bmatrix} + \begin{bmatrix} \dfrac{c_1(0)}{u_1} \\ \dfrac{c_2(0)}{u_2} \end{bmatrix} \tag{D8}$$

or

$$\frac{\partial M}{\partial x} = -LAM + C \tag{D9}$$

The eigenvalues and eigenvectors of coefficient matrix A are:

$$\begin{cases} \lambda_{1m} = 0 \\ \lambda_{2m} = \dfrac{1}{f_1 u_1} + \dfrac{1}{f_2 u_2} \end{cases} \tag{D10}$$

and

$$S = \begin{bmatrix} 1 & -f_2 u_2 \\ 1 & f_1 u_1 \end{bmatrix} \tag{D11}$$

The inverse eigenvector matrix is:

$$S^{-1} = \frac{1}{\bar{u}} \begin{bmatrix} f_1 u_1 & f_2 u_2 \\ -1 & 1 \end{bmatrix} \tag{D12}$$

Defining transformed versions of the moments and initial conditions respectively, we have:

$$S^{-1} \begin{bmatrix} m_0^{(1)} \\ m_0^{(2)} \end{bmatrix} = \begin{bmatrix} v_1 \\ v_2 \end{bmatrix} \tag{D13}$$

or

$$S^{-1} M = V \tag{D14}$$

and

$$S^{-1} \begin{bmatrix} \dfrac{c_1(0)}{u_1} \\ \dfrac{c_2(0)}{u_2} \end{bmatrix} = \begin{bmatrix} w_1 \\ w_2 \end{bmatrix} \tag{D15}$$

or

$$S^{-1} C = W \tag{D16}$$

The diagonalized version of D8 is therefore:

$$\frac{\partial}{\partial x} \begin{bmatrix} v_1 \\ v_2 \end{bmatrix} = -L \begin{bmatrix} \lambda_{1m} & 0 \\ 0 & \lambda_{2m} \end{bmatrix} \begin{bmatrix} v_1 \\ v_2 \end{bmatrix} + \begin{bmatrix} w_1 \\ w_2 \end{bmatrix} \tag{D17}$$

or:

$$\frac{\partial V}{\partial x} = -L \Lambda V + W \tag{D18}$$

For n=0, we have initial conditions:

$$C = \begin{bmatrix} \dfrac{c_1(0)}{u_1} \\ \dfrac{c_2(0)}{u_2} \end{bmatrix} = \begin{bmatrix} \dfrac{a\delta(x)}{u_1\bar{u}} \\ \dfrac{a\delta(x)}{u_2\bar{u}} \end{bmatrix} \tag{D19}$$

therefore

$$W = \frac{1}{\bar{u}} \begin{bmatrix} f_1u_1 & f_2u_2 \\ -1 & 1 \end{bmatrix} \begin{bmatrix} \dfrac{a\delta(x)}{u_1\bar{u}} \\ \dfrac{a\delta(x)}{u_2\bar{u}} \end{bmatrix} \tag{D20}$$

and

$$\begin{cases} \dfrac{\partial v_1}{\partial x} = -L\lambda_{1m}v_1 + w_1 = \dfrac{a\delta(x)}{\bar{u}^2} \\ \dfrac{\partial v_2}{\partial x} = -L\lambda_{2m}v_2 + w_2 = -L\left(\dfrac{1}{f_1u_1} + \dfrac{1}{f_2u_2}\right)v_2 + \dfrac{a\delta(x)}{\bar{u}^2}\left(\dfrac{1}{u_2} - \dfrac{1}{u_1}\right) \end{cases} \tag{D21}$$

This has solutions

$$V = \begin{bmatrix} \dfrac{a}{\bar{u}^2} + g_1 \\ e^{-L\left(\frac{1}{f_1u_1} + \frac{1}{f_2u_2}\right)x}\left[\dfrac{a}{\bar{u}^2}\left(\dfrac{1}{u_2} - \dfrac{1}{u_1}\right) + g_2\right] \end{bmatrix} \tag{D22}$$

where g_1 and g_2 are constants. To find the values of these constants we employ the initial conditions $V(0) = S^{-1}M(0)$:

$$\begin{bmatrix} v_1(0) \\ v_2(0) \end{bmatrix} = \frac{1}{\bar{u}} \begin{bmatrix} f_1u_1 & f_2u_2 \\ -1 & 1 \end{bmatrix} \begin{bmatrix} a/\bar{u} \\ a/\bar{u} \end{bmatrix} = \begin{bmatrix} a/\bar{u} \\ 0 \end{bmatrix} \tag{D23}$$

This leads to

$$V = \begin{bmatrix} a/\bar{u} \\ 0 \end{bmatrix} \tag{D24}$$

and therefore

$$M = SV = \begin{bmatrix} 1 & -f_2 u_2 \\ 1 & f_1 u_1 \end{bmatrix} \begin{bmatrix} a/\bar{u} \\ 0 \end{bmatrix} = \begin{bmatrix} a/\bar{u} \\ a/\bar{u} \end{bmatrix} \tag{D25}$$

In other words,

$$m_0^{(1)} = m_0^{(2)} = a/\bar{u} \tag{D26}$$

and the zero-order moment of the flux concentration is

$$m_0^{(f)} = \frac{a}{\bar{u}}\left(\frac{f_1 u_1}{\bar{u}}\right) + \frac{a}{\bar{u}}\left(\frac{f_2 u_2}{\bar{u}}\right) \tag{D27}$$

With the zero-order moments given by eq. D27, first-order moments are then calculated using

$$\frac{\partial}{\partial x}\begin{bmatrix} m_1^{(1)} \\ m_1^{(2)} \end{bmatrix} = -L\begin{bmatrix} \dfrac{1}{f_1 u_1} & \dfrac{-1}{f_1 u_1} \\ \dfrac{-1}{f_2 u_2} & \dfrac{1}{f_2 u_2} \end{bmatrix}\begin{bmatrix} m_1^{(1)} \\ m_1^{(2)} \end{bmatrix} + \begin{bmatrix} \dfrac{m_0^{(1)}}{u_1} \\ \dfrac{m_0^{(2)}}{u_2} \end{bmatrix} \tag{D28}$$

therefore

$$\frac{\partial}{\partial x}\begin{bmatrix} v_1 \\ v_2 \end{bmatrix} = -L\begin{bmatrix} \lambda_{1m} & 0 \\ 0 & \lambda_{2m} \end{bmatrix}\begin{bmatrix} v_1 \\ v_2 \end{bmatrix} + \begin{bmatrix} w_1 \\ w_2 \end{bmatrix} \tag{D29}$$

where in this case $V = S^{-1}\begin{bmatrix} m_1^{(1)} \\ m_1^{(2)} \end{bmatrix}$. We also re-define $C = \begin{bmatrix} \dfrac{m_0^{(1)}}{u_1} \\ \dfrac{m_0^{(2)}}{u_2} \end{bmatrix}$, and therefore

$$\begin{cases} w_1 = \dfrac{a}{\bar{u}^2} \\ w_2 = \dfrac{a}{\bar{u}^2}\left(\dfrac{1}{u_2} - \dfrac{1}{u_1}\right) \end{cases} \tag{D30}$$

which leads to

$$V = \begin{bmatrix} \dfrac{a}{\bar{u}^2}x + g_1 \\ g_2 e^{-L\lambda_{2m}x} + \dfrac{a}{L\lambda_{2m}\bar{u}^2}\left(\dfrac{1}{u_2} - \dfrac{1}{u_1}\right) \end{bmatrix} \tag{D31}$$

where g_1 and g_2 again represent constants of integration. As in the zero-order case, we find the values of these by making use of the initial conditions

$$\begin{bmatrix} v_1(0) \\ v_2(0) \end{bmatrix} = \frac{1}{\bar{u}}\begin{bmatrix} f_1u_1 & f_2u_2 \\ -1 & 1 \end{bmatrix}\begin{bmatrix} m_1^{(1)}(0) \\ m_1^{(2)}(0) \end{bmatrix} \tag{D32}$$

where $m_1^{(1)}(0) = m_1^{(2)}(0) = 0$. Therefore

$$V = \begin{bmatrix} \dfrac{a}{\bar{u}^2}x \\ \dfrac{-a}{L\lambda_{2m}\bar{u}^2}\left(\dfrac{1}{u_2} - \dfrac{1}{u_1}\right)\left(e^{-L\lambda_{2m}x} - 1\right) \end{bmatrix} \tag{D33}$$

and the first-order moments are derived through matrix multiplication:

$$M = SV = \begin{bmatrix} 1 & -f_2u_2 \\ 1 & f_1u_1 \end{bmatrix}\begin{bmatrix} \dfrac{a}{\bar{u}^2}x \\ \dfrac{-a}{L\lambda_{2m}\bar{u}^2}\left(\dfrac{1}{u_2} - \dfrac{1}{u_1}\right)\left(e^{-L\lambda_{2m}x} - 1\right) \end{bmatrix} \tag{D34}$$

leading to

$$\begin{cases} m_1^{(1)} = \dfrac{a}{\bar{u}^2}\left[x + \dfrac{f_2 v_2}{L\lambda_{2m}}\left(\dfrac{1}{u_2} - \dfrac{1}{u_1}\right)\left(e^{-L\lambda_{2m}x} - 1\right)\right] \\ m_1^{(2)} = \dfrac{a}{\bar{u}^2}\left[x - \dfrac{f_1 v_1}{L\lambda_{2m}}\left(\dfrac{1}{u_2} - \dfrac{1}{u_1}\right)\left(e^{-L\lambda_{2m}x} - 1\right)\right] \end{cases} \tag{D35}$$

and therefore the first moment is

$$m_1^{(f)} = \frac{ax}{\bar{u}^2} \tag{D36}$$

The mean residence time (first central moment) is then calculated as

$$\tau = \mu_t = \frac{m_1^{(f)}}{m_0^{(f)}} = \frac{x}{\bar{u}} \tag{D37}$$

Second-order moments are calculated using the same approach as first-order moments, but in this case starting with

$$\frac{\partial}{\partial x}\begin{bmatrix} m_2^{(1)} \\ m_2^{(2)} \end{bmatrix} = -L\begin{bmatrix} \dfrac{1}{f_1 u_1} & \dfrac{-1}{f_1 u_1} \\ \dfrac{-1}{f_2 u_2} & \dfrac{1}{f_2 u_2} \end{bmatrix}\begin{bmatrix} m_2^{(1)} \\ m_2^{(2)} \end{bmatrix} + \begin{bmatrix} \dfrac{2m_1^{(1)}}{u_1} \\ \dfrac{2m_1^{(2)}}{u_2} \end{bmatrix} \tag{D38}$$

As before, we use the diagonalized version of the moment equation matrix

$$\frac{\partial}{\partial x}\begin{bmatrix} v_1 \\ v_2 \end{bmatrix} = -L\begin{bmatrix} \lambda_{1m} & 0 \\ 0 & \lambda_{2m} \end{bmatrix}\begin{bmatrix} v_1 \\ v_2 \end{bmatrix} + \begin{bmatrix} w_1 \\ w_2 \end{bmatrix} \tag{D39}$$

where V is again redefined, this time as $S^{-1}\begin{bmatrix} m_2^{(1)} \\ m_2^{(2)} \end{bmatrix}$, and C is redefined as $\begin{bmatrix} \dfrac{2m_1^{(1)}}{u_1} \\ \dfrac{2m_1^{(2)}}{u_2} \end{bmatrix}$.

We have in this case

$$\begin{cases} w_1 = \dfrac{2ax}{\bar{u}^3} + \dfrac{2af_1 f_2 (u_2 - u_1)}{L\lambda_{2m}\bar{u}^3}\left(\dfrac{1}{u_2} - \dfrac{1}{u_1}\right)\left(e^{-L\lambda_{2m}x} - 1\right) \\ w_2 = \dfrac{2a(u_1 - u_2)}{\bar{u}^3 u_1 u_2}x + \dfrac{2a\left(f_1 v_1^2 + f_2 v_2^2\right)}{L\lambda_{2m}\bar{u}^3 u_1 u_2}\left(\dfrac{1}{u_2} - \dfrac{1}{u_1}\right)\left(e^{-L\lambda_{2m}x} - 1\right) \end{cases} \tag{D40}$$

Skipping some tedious arithmetic, use of D40 with D39 in the same process that produced D35 from D29 and D30 produces in this case:

$$\begin{cases} m_2^{(1)} = \dfrac{a}{\bar{u}^3}x^2 - \dfrac{2af_1 f_2 (u_2 - u_1)}{L\lambda_{2m}\bar{u}^3}\left(\dfrac{1}{u_2} - \dfrac{1}{u_1}\right)x - \dfrac{2af_1 f_2 (u_2 - u_1)}{(L\lambda_{2m})^2\bar{u}^3}\left(\dfrac{1}{u_2} - \dfrac{1}{u_1}\right)\left(e^{-L\lambda_{2m}x} - 1\right) \\ \qquad - \dfrac{2af_2 u_2 (u_2 - u_1)}{L\lambda_{2m}\bar{u}^3 u_1 u_2}x + \dfrac{2af_2 v_2\left(f_1 v_1^2 + f_2 v_2^2\right)}{L\lambda_{2m}\bar{u}^3 u_1 u_2}\left(\dfrac{1}{u_2} - \dfrac{1}{u_1}\right)xe^{-L\lambda_{2m}x} \\ m_2^{(2)} = \dfrac{a}{\bar{u}^3}x^2 - \dfrac{2af_1 f_2 (u_2 - u_1)}{L\lambda_{2m}\bar{u}^3}\left(\dfrac{1}{u_2} - \dfrac{1}{u_1}\right)x - \dfrac{2af_1 f_2 (u_2 - u_1)}{(L\lambda_{2m})^2\bar{u}^3}\left(\dfrac{1}{u_2} - \dfrac{1}{u_1}\right)\left(e^{-L\lambda_{2m}x} - 1\right) \\ \qquad - \dfrac{2af_1 u_1 (u_2 - u_1)}{L\lambda_{2m}\bar{u}^3 u_1 u_2}x - \dfrac{2af_1 v_1\left(f_1 u_1^2 + f_2 u_2^2\right)}{L\lambda_{2m}\bar{u}^3 u_1 u_2}\left(\dfrac{1}{u_2} - \dfrac{1}{u_1}\right)xe^{-L\lambda_{2m}x} \end{cases} \tag{D41}$$

and therefore

$$\begin{aligned} m_2^{(f)} = {} & \frac{ax^2}{\bar{u}^3}\left(\frac{f_1 v_1 + f_2 v_2}{\bar{u}^2}\right) - \frac{2a(u_2 - u_1)}{L\lambda_{2m}\bar{u}^4}\left(f_1^2 f_2 u_1 + f_1 f_2^2 u_2\right)\left(\frac{1}{u_2} - \frac{1}{u_1}\right)x \\ & - \frac{2a(u_2 - u_1)}{L\lambda_{2m}\bar{u}^4}\left(f_1^2 f_2 u_1 + f_1 f_2^2 u_2\right)\left(\frac{1}{u_2} - \frac{1}{u_1}\right)\left(e^{-L\lambda_{2m}x} - 1\right) \end{aligned} \tag{D42}$$

The second moment is then calculated as

$$\frac{m_2^{(f)}}{m_0^{(f)}} = \left(\frac{x}{\bar{u}}\right)^2 + \frac{2(u_2 - u_1)^2 f_1 f_2}{(L\lambda_{2m})^2\bar{u}^2 u_1 u_2}\left(e^{-L\lambda_{2m}x} + L\lambda_{2m}x - 1\right) \tag{D43}$$

and the residence time variance (second central moment) is

$$\sigma_t^2 = \frac{m_2^{(f)}}{m_0^{(f)}} - \left(\frac{m_1^{(f)}}{m_0^{(f)}}\right)^2 = \frac{2(u_2 - u_1)^2 f_1 f_2}{(L\lambda_{2m})^2\bar{u}^2 u_1 u_2}\left(e^{-L\lambda_{2m}x} + L\lambda_{2m}x - 1\right) \tag{D44}$$

Appendix E: MATLAB® Wetloop code

```
function wetloop1(Cstar)
%By James N. Carleton, 2006
%Reads dates, velocities, inlet & outlet concentrations from a text
%file, interpolates to daily values and based on user-defined
%reference RTD/DND parameters, computes wetland outlet
%concentration as a function of time. RTD is assumed to be a gamma
%pdf, with parameters defined by user
%%%%%%%%%%%%%%%%%%%%%%%%%%%%%%%%%%%%%%%%%%%%%%%%%%%%%%%%%%%%%%%%%%%%%%%
%%%%%%%%%%%%%%%%%%%%%%%%%%%%%%%%%%%%%%%%%%%%%%%%%%%%%%%%%%%%%%%%%%%%%%%
%user entry section for reference RTD conditions
u_ref = input('Enter mean velocity (m/day) under reference conds>');
L = input('Enter wetland length (m)>');
tau_m= L./u_ref  %retention time (mean residence time) under ref.
(RTD) conds.
alpha = input('Enter alpha for RTD>');  %RTD parameters
beta = tau_m./alpha
%%%%%%%%%%%%%%%%%%%%%%%%%%%%%%%%%%%%%%%%%%%%%%%%%%%%%%%%%%%%%%%%%%%%%%%
%User entry section for Da relationship to res. time (Tau)
A = input('Enter A>');  %enter the relationship btwn. Da and t
B = input('Enter B>');
%%%%%%%%%%%%%%%%%%%%%%%%%%%%%%%%%%%%%%%%%%%%%%%%%%%%%%%%%%%%%%%%%%%%%%%
%Section for reading in raw data and interpolating for missing days
%read in the text file of dates and 'concentrations':
[date,v,C,Cend]= textread('Gustine2a.txt','%8c %f %f %f');
%convert dates into integer day from reference date=1/1/0000:
datex=datenum(date);
d=length(date);  %number of dates in file
%create vector of sequential integers covering span of days:
dayints=[datex(1):1:datex(d)];
dl=length(dayints)
dayindex=[1:1:dl];
u_btwn=interp1(datex,v,dayints,'linear'); %interpolate velocities
C_btwn=interp1(datex,C,dayints,'linear'); %interpolate inlet conc.
Cout_btwn=interp1(datex,Cend,dayints,'linear'); %interp outlet conc.
%concatenate integer day and interpolated value vectors:
dataint=[dayindex;dayints;u_btwn;C_btwn;Cout_btwn];
data=dataint.';  %transpose concatenated matrix
save data.txt data -ASCII
%%%%%%%%%%%%%%%%%%%%%%%%%%%%%%%%%%%%%%%%%%%%%%%%%%%%%%%%%%%%%%%%%%%%%%%
%Section for determining Ttrunc
const1 = (beta.^(-alpha))./gamma(alpha); %calculate const in pdf
%create test RTD to determine res time corresponding to 99% of
%total area under curve:
RTDtst = const1.*dayindex.^(alpha-1).*exp(-dayindex./beta);
X=0;   %dummy variable
for k=1:dl
    if X<0.95
    X=X+RTDtst(k);
    flusht=k;  %number of days covering >95% of the reference RTD
end
end
```

```
%travel distance associated with 95% flushing of wetland under ref.
%conds.:
flushl=flusht.*u_ref;
X=0;   %dummy variable
for k=1:dl
    if X<flushl
    X=X+u_btwn(k);
%number of days from start for cumulative discharge to equal
%discharge for 95% flush under ref. conds.:
    Ttrunc=k;
end
end
%%%%%%%%%%%%%%%%%%%%%%%%%%%%%%%%%%%%%%%%%%%%%%%%%%%%%%%%%%%%%%%%%%%%%%%%%%%%
%Section for calculating daily outlet concentrations
Cor=zeros(dl-Ttrunc,1);
for j=0:dl-(Ttrunc+2)
    [days,dints,u,Ci,outC]= textread('data.txt','%f%f%f%f%f',dl-j);
    %read in the flow file, one fewer day for each iteration:
    d=length(days); %the number of days in each iteration
    a=[d:-1:1];     %create reverse-time vector of flow, R
    R=u(a);
    R(1)=0;
    Rcum=cumsum(R); %create vector of cum. flow in reverse time
    Tau=Rcum./u_ref;  %convert cum. distance to equivalent tau_i
    Taumax=max(Tau);   %find maximum value in tau vector
    Taumax=fix(Taumax); %truncate at integer value
    Tauints=[1:1:Taumax];
%Create vector of T values (days) at integer values of Tau:
    Ti=interp1(Tau,(days-1),Tauints,'linear');
    RTD = const1.*(Tauints).^(alpha-1).*exp(-(Tauints)./beta);
    y_i=Ti./Tauints;   %calculate y for each integer value of Tau
%create reverse-time vector of inlet conc (Ci), Cir corrected for
%background conc.:
    Cir=Ci(a)-Cstar;
    Cirint=interp1(days-1,Cir,Ti,'linear');
%interpolate Cir (inlet conc) for (noninteger) values of Ti:
    XTD = Cirint.*RTD.*exp((-A.*(Tauints).^B).*y_i);
%the expression to be integrated (summed, actually):
    sum XTD;
%vector of outlet concentrations, in reverse time:
    Cor(j+2)=Cor(j+2)+sum(XTD)+Cstar;
end
save Cor.out Cor -ASCII -TABS;
save y_i.out y_i -ASCII -TABS;
Co=ones(dl,1); %create dummy vector to hold outlet concs. in correct
time order
for k=1:Ttrunc %backfill first entries with first real value
    Co(k)=Co(k).*Cor(dl-Ttrunc);
end

for k=Ttrunc+1:dl  %fill in rest of vector with outlet C values
    Co(k)=Co(k).*Cor(dl+1-k); %outlet concs in correct time
end

Co(dl)=Co(dl-1);  %fill in last day's value so it isn't zero
```

```
Cz=interp1(dayints,Co,datex); %get outlet values for only the
sampled days
tickint=fix((dayints(dl)-dayints(1))./4);%determine interval for
plot ticks
plot(dayints,C_btwn,'b');    %plot interpolated inlet conc.
set(gca,'XTick',dayints(1):tickint:dayints(dl));
%label x axis with dates:
set(gca,'XTickLabel',datestr(dayints(1):tickint:dayints(dl),2));
hold on;
plot(datex,C,'bo');  %plot measured inlet conc.
hold on;
plot(datex,Cend,'ro');  %plot measured outlet conc.
hold on;
plot(dayints,Co,'k');   %plot modeled outlet conc.
```

Appendix F: MATLAB® code for plotting comparisons between idealized heterogeneity and bicontinuum model results

```
function Cres
global H n f nu alpha Li Li2 a b m Cr numzer xk coef
% James N. Carleton, 2008
% Plots resident concentrations, std devs, and effective
% longitudinal dispersion coefficient for idealized heterogeneity
% model and bicontinuum model comparisons.
%%%%%%%%%%%%%%%%%%%%%%%%%%%%%%%%%%%%%%%%%%%%%%%%%%%%%%%%%%%%%%%%%%%%%%%%%%%%
% Idealized Heterogeneity Model
numzer=30; %number of eigenfunctions to sum
a = 0.005;
b = 0.0001;
f = 0.001;
m = 4/7
p = -2*m %to ensure inverse square dependence of k on u
n = p+2 %to ensure equation is expressible using a Bessel function
H = 15; %domain width
x=1000; %domain length
xpts=x+1; %longitudinal discretization of domain
xx = linspace(0,x,xpts)';
Cres = zeros(length(xx),1);
sigma = zeros(length(xx),1);
sdev = zeros(length(xx),1);
Crplus = zeros(length(xx),1);
Crminus = zeros(length(xx),1);
alpha = (sqrt(((1-n)^2)+4*f/b))/(1-n);
nu = alpha*(1-n)/(2+m-n);
aa = alpha/((alpha+1)*nu);
% multiplier of lambda inside Bessel terms:
zeromult2 = 2*nu*H^((alpha*(1-n))/(2*nu));
estzeros = besselzero(nu+1,numzer,1); % the function we need zeros
for:
g=@(y)(besselj(nu,y)-(y*aa)*besselj(nu+1,y));
root=zeros(length(estzeros),1);
for i=2:numzer;
    root(i)=fzero(g,estzeros(i-1));  %zeros to function of interest
end
eig1=root(2)-(root(3)-root(2));
root(1)=fzero(g,eig1);
% Find all the x-independent exponential term multipliers for each
% eigenfunction:
coefplus=zeros(numzer,1);
for i=1:numzer;
    Li2 = root(i)/zeromult2;
    ai = quadl(@phi_int2,0,H)/quadl(@phi_int3,0,H);
    terma2=quadl(@phi_int,0,H);
    coefplus(i)=ai *terma2;  % for determination of Cres
    coef(i)=ai; % for determination of sigma
    Li(i)=Li2;
end
%
```

```
% Calculate Cres for each point along the x-transect
for j=1:length(Cres)
    sumG2=0;
    theta2=0;
    for i=1:length(estzeros)
        Li2 = root(i)/zeromult2;
        termc2=exp(-((Li2^2)*(b/a)*(((1-n)^2)+4*f/b))*xx(j));
        sumi2=coefplus(i)*termc2;
        sumG2=sumG2+sumi2;
    end
    G2 = sumG2/H;
    Cres(j)=G2;
end
%
% Calculate std dev of C
for k=1:length(Cres)
    xk=xx(k); % xk is the x coordinate for auxiliary program sig_int
    Cr = Cres(k);
    sigma(k)=quadl(@sig_int,0,H)/H; % variance of C
    sdev(k)=sqrt(sigma(k));
end
%
%%%%%%%%%%%%%%%%%%%%%%%%%%%%%%%%%%%%%%%%%%%%%%%%%%%%%%%%%%%%%%%%%%%%%%%%%%%%%%%
% Bicontinuum Model
% Parameters of the model:
gamma=16.7;
alpha=b*(gamma/a)^(n/m);
beta=f*(gamma/a)^-2;
wbar=(a/gamma)*(H^m)/(m+1);
sigw=(a/gamma)*(H^m)*(1/(2*m+1)-1/(m+1)^2)^0.5;
A=21.7242; % the dissipative closure parameter
D=alpha*wbar^(3/2);
% %
lamb3=-0.444552; % this is mean of lambda cubed
% %
lam1=(lamb3+(lamb3^2+4)^0.5)/2; % eigenvalue 1
lam2=(lamb3-(lamb3^2+4)^0.5)/2; % eigenvalue 2
f1=-lam2/(lam1 - lam2);
f2=lam1/(lam1 - lam2);
ubar=gamma*wbar;
rho_u_lambda=gamma*sigw;
u1_star=ubar + rho_u_lambda*lam1;
u2_star=ubar + rho_u_lambda*lam2;
L=f1*f2*D/A;
kbar=beta/(wbar^2);
rho_k_lambda=-2*beta*sigw/(wbar^3);
rho_k_lambda2=3*beta*(sigw^2)/(wbar^4);
kbar_star=kbar+rho_k_lambda2;
k1_bar_star=kbar_star+(rho_k_lambda+rho_k_lambda2*lamb3)*lam1;
k2_bar_star=kbar_star+(rho_k_lambda+rho_k_lambda2*lamb3)*lam2;
alpha1=u1_star*u2_star*f2/L;
alpha2=(k1_bar_star*u2_star+k2_bar_star*u1_star)/(f1*L*(lam1-
lam2)^2)+ubar/f1;
alpha3=k1_bar_star*k2_bar_star/(f1*L*(lam1-lam2)^2) + kbar_star/f1;
r1=(-alpha2+(alpha2^2-4*alpha1*alpha3)^0.5)/(2*alpha1);
r2=(-alpha2-(alpha2^2-4*alpha1*alpha3)^0.5)/(2*alpha1);
C0=1;
```

```
zig1=((lam1*f1*L+lam1*f1*f2*k2_bar_star+lam1*f1*f2*u2_star*r2+f2*L*l
am2)/(lam1*f1*(f2^2)*u2_star*(r2-r1)))*(C0/(1-lam2/lam1));
zig2=C0/(f2*(1-lam2/lam1))-zig1;
zug1=(1+(f2/L)*(k2_bar_star+u2_star*r1))*zig1;
zug2=(1+(f2/L)*(k2_bar_star+u2_star*r2))*zig2;
c1_star=zug1*exp(r1*xx) + zug2*exp(r2*xx);
c2_star=zig1*exp(r1*xx) + zig2*exp(r2*xx);
cbar=f1*c1_star + f2*c2_star;
rho_c_lambda=f1*lam1*c1_star + f2*lam2*c2_star;
%
figure(1)
plot(xx,Cres,'--k') % plots idealized heterogeneity model
hold on
plot(xx,cbar,'k');  % plots stochastic/bicontinuum model
xlabel('x (m)','FontName','Times New Roman');
set(get(gca,'YLabel'),'Rotation',0.0)
ylabel('C_r','FontName','Times New Roman'); % the underscore makes
'r' a subscript
ylim([0 1]);
legend('explicit','stochastic')
%
lam2m=1/(f1*u1_star) + 1/(f2*u2_star);
RTDmult=((u2_star-u1_star)^2)*f1*f2/(((L*lam2m)^2)*u1_star*u2_star);
DL=ubar*RTDmult*(-L*lam2m*exp(-L*lam2m*xx) + L*lam2m); %
figure(2)
plot(xx,sdev,'--k'); % plots idealized heterogeneity model std dev
hold on
plot(xx,rho_c_lambda,'k'); % plots bicontinuum model std dev
xlabel('x (m)','FontName','Times New Roman');
set(get(gca,'YLabel'),'Rotation',0.0)
ylabel('\sigma_c','FontName','Times New Roman');
legend('explicit','stochastic')
%
figure(3)
plot(xx,DL,'k')
xlabel('x (m)','FontName','Times New Roman');
set(get(gca,'YLabel'),'Rotation',0.0)
ylabel('D_L','FontName','Times New Roman');
```

```
function Cflux
global H n f nu alpha Li Li2 a b m Cf numzer xk coef
% James N. Carleton, 2008
% Plots resident concentrations for idealized heterogeneity
% model and bicontinuum model comparisons.
%%%%%%%%%%%%%%%%%%%%%%%%%%%%%%%%%%%%%%%%%%%%%%%%%%%%%%%%%%%%%%%%%%%%%%%%%%
%%%%%%%
% Idealized Heterogeneity Model
numzer=30;
a = 0.005;
b = 0.0001;
f = 0.001;
m = 4/7;
p = -2*m; %to ensure inverse square dependence of k on u
n = p+2; %to ensure equation is expressible using a Bessel function
H = 15;
x=1000;
xpts=x+1;
xx = linspace(0,x,xpts)';
Cflux = zeros(length(xx),1);
%
alpha = (sqrt(((1-n)^2)+4*f/b))/(1-n);
nu = alpha*(1-n)/(2+m-n);
aa = alpha/((alpha+1)*nu);
% multiplier of lambda inside Bessel terms:
zeromult2 = 2*nu*H^((alpha*(1-n))/(2*nu));
% vector of zeros to besselj(v+1,z):
estzeros = besselzero(nu+1,numzer,1);
% the function we need zeros for:
g=@(y)(besselj(nu,y)-(y*aa)*besselj(nu+1,y));
root=zeros(length(estzeros),1);
for i=2:numzer;
    root(i)=fzero(g,estzeros(i-1));  %zeros to function of interest
end
eig1=root(2)-(root(3)-root(2));
root(1)=fzero(g,eig1);
% Find all the x-independent exponential term multipliers for each
% eigenfunction:
coefplus=zeros(numzer,1);
for i=1:numzer; %length(estzeros)
    Li2 = root(i)/zeromult2;
    ai = ((quadl(@phi_int2,0,H))^2)/quadl(@phi_int3,0,H);
    coefplus(i)=ai; %for determination of Cflux
    terma2=quadl(@phi_int,0,H);
    coef(i)=ai; % for determination of sigma
    Li(i)=Li2;
end
%
% Calculate Cflux for each point along the x-transect
for j=1:length(Cflux)
    sumG2=0;
    theta2=0;
    for i=1:numzer
        Li2 = root(i)/zeromult2;
        termc2=exp(-((Li2^2)*(b/a)*(((1-n)^2)+4*f/b))*xx(j));
        sumi2=coefplus(i)*termc2;
        sumG2=sumG2+sumi2;
```

```
    end
    G2 = sumG2*(m+1)/(a*H^(m+1));
    Cflux(j)=G2;
end
% %
%%%%%%%%%%%%%%%%%%%%%%%%%%%%%%%%%%%%%%%%%%%%%%%%%%%%%%%%%%%%%%%%%%%%
%%%%%%%
% Stochastic Bicontinuum Model
gamma=16.7;
alpha=b*(gamma/a)^(n/m);
beta=f*(gamma/a)^-2;
wbar=(a/gamma)*(H^m)/(m+1);
sigw=(a/gamma)*(H^m)*(1/(2*m+1)-1/(m+1)^2)^0.5;
A=21.7242; % the dissipative closure parameter
D=alpha*wbar^(3/2);
lamb3=-0.444552; % this is mean of lambda cubed
lam1=(lamb3+(lamb3^2+4)^0.5)/2; % eigenvalue 1
lam2=(lamb3-(lamb3^2+4)^0.5)/2; % eigenvalue 2
f1=-lam2/(lam1 - lam2);
f2=lam1/(lam1 - lam2);
ubar=gamma*wbar;
rho_u_lambda=gamma*sigw;
u1_star=ubar + rho_u_lambda*lam1;
u2_star=ubar + rho_u_lambda*lam2;
L=f1*f2*D/A;
kbar=beta/(wbar^2);
rho_k_lambda=-2*beta*sigw/(wbar^3);
rho_k_lambda2=3*beta*(sigw^2)/(wbar^4);
kbar_star=kbar+rho_k_lambda2;
k1_bar_star=kbar_star+(rho_k_lambda+rho_k_lambda2*lamb3)*lam1;
k2_bar_star=kbar_star+(rho_k_lambda+rho_k_lambda2*lamb3)*lam2;
alpha1=u1_star*u2_star*f2/L;
alpha2=(k1_bar_star*u2_star+k2_bar_star*u1_star)/(f1*L*(lam1-
lam2)^2)+ubar/f1;
alpha3=k1_bar_star*k2_bar_star/(f1*L*(lam1-lam2)^2) + kbar_star/f1;
r1=(-alpha2+(alpha2^2-4*alpha1*alpha3)^0.5)/(2*alpha1);
r2=(-alpha2-(alpha2^2-4*alpha1*alpha3)^0.5)/(2*alpha1);
C0=1;
zig1=((lam1*f1*L+lam1*f1*f2*k2_bar_star+lam1*f1*f2*u2_star*r2+f2*L*l
am2)/(lam1*f1*(f2^2)*u2_star*(r2-r1)))*(C0/(1-lam2/lam1));
zig2=C0/(f2*(1-lam2/lam1))-zig1;
zug1=(1+(f2/L)*(k2_bar_star+u2_star*r1))*zig1;
zug2=(1+(f2/L)*(k2_bar_star+u2_star*r2))*zig2;
c1_star=zug1*exp(r1*xx) + zug2*exp(r2*xx);
c2_star=zig1*exp(r1*xx) + zig2*exp(r2*xx);
cf=f1*(u1_star/ubar)*c1_star + f2*(u2_star/ubar)*c2_star;
%
figure(1)
plot(xx,Cflux,'--k'); % plots idealized heterogeneity model
hold on
plot(xx,cf,'k');  % plots stochastic/bicontinuum model
xlabel('x (m)','FontName','Times New Roman');
set(get(gca,'YLabel'),'Rotation',0.0)
ylabel('C_f','FontName','Times New Roman'); % the underscore makes
'r' a subscript
ylim([0 1]);
legend('explicit','stochastic')
```

```
function phi1 = phi_int(y)
global H n f nu alpha Li2
%
% % Expression of phi(z0) for integration
phi1=y.^((1-n)/2).*besselj(nu,Li2*2*nu*y.^((alpha*(1-n))/(2*nu)),1);


function phi2 = phi_int2(y)
global H n f nu alpha Li2 a m
%
% % Expression of phi(z0) for integration
% numerator
phi2=a*y.^((1-n+2*m)/2).*besselj(nu,Li2*2*nu*y.^((alpha*(1-
n))/(2*nu)),1);


function phi3 = phi_int3(y)
global H n f nu alpha Li2 a m
%
% % Expression of phi(z0) for integration
% denominator
p1 = a*y.^(1+m-n);
p2 = (besselj(nu,Li2*2*nu*y.^((alpha*(1-n))/(2*nu)),1));
p3 = p2.*p2;
phi3 = p1.*p3;


function sig1 = sig_int(y)
global a b f n nu2 alpha Li Cr numzer xk coef
%
sigsum=0;
for j=1:numzer
    sub1 = coef(j)*y.^((1-
n)/2).*besselj(nu2,Li(j)*2*nu2*y.^((alpha*(1-n))/(2*nu2)),1)*exp(-
((Li(j)^2)*(b/a)*(((1-n)^2)+4*f/b))*xk);
    sigsum=sigsum+sub1;
end
size(sigsum);
sig1=(sigsum-Cr).*(sigsum-Cr);
```

Bibliography

Abramowitz, M. and I.A. Stegun. 1965. Handbook of Mathematical Functions. Dover, New York.

Adey, W.H. and K. Loveland. 1998. Dynamic Aquaria: Building Living Ecosystems, 2nd Edition. Academic Press, San Diego.

Alexander, R.B., R.A. Smith, and G.E. Schwartz. 2000. Effect of stream channel size on the delivery of nitrogen to the Gulf of Mexico. *Nature* 403:758-761.

Alexander, R.B., R.A. Smith, and G.E. Schwartz. 2004. Estimates of diffuse phosphorus sources in surface waters of the United States using a spatially referenced watershed model. *Water Science and Technology* 49(3):1-10.

Alexander, R.B., R.A. Smith, G.E. Schwartz, E.W. Boyer, J.V. Nolan, and J.W. Brakebill. 2008. Differences in phosphorus and nitrogen delivery to the Gulf of Mexico from the Mississippi River basin. *Environmental Science and Technology* 42(3):822-830.

Bartlett, M.S., L.C. Brown, N.B. Hanes, and N.H. Nickerson. 1979. Denitrification in Freshwater Wetland Soil. *Journal of Environmental Quality*, 8(4): 460-464.

Bastkiven, S.K., P.G. Eriksson, A. Ekström, and K. Tonderski. 2007. Seasonal denitrification potential in wetland sediments with organic matter from different plant species. *Water, Air and Soil Pollution* 183:25-35.

Bastkiven, S.K., P.G. Eriksson, I. Martins, J.M. Neto, L. Leonardson, and K. Tonderski. 2003. Potential nitrification and denitrification on different surfaces in a constructed treatment wetland. *Journal of Environmental Quality* 32:2414-2420.

Berentsen CWJ, ML Verlaan, and CPJW van Kruisdijk. 2005 Upscaling and reversibility of Taylor dispersion in heterogeneous porous media. *Physical Review E* 71, 046308.

Berkowitz, B., A. Cortis, M. Dentz, and H. Scher. 2006. Modeling non-Fickian transport in geological formations as a continuous time random walk. *Reviews of Geophysics* 44:1-49.

Bigambo, T. and A.W. Mayo. 2005. Nitrogen transformation in horizontal subsurface flow constructed wetlands II: effect of biofilm. *Physics and Chemistry of the Earth* 30:668-672.

Bitton, G. 2005. Wastewater Microbiology, 3rd Edition. John Wiley & Sons, New York.

Black, A.C. and W.R. Wise. 2003. Evaluation of past and potential phosphorus uptake at the Orlando Easterly Wetland. *Ecological Engineering* 21:277-290.

Bogle, G.V. 1997. Stream velocity profiles and longitudinal dispersion. *Journal of Hydraulic Engineering* 123(9):816-820.

Bolster, C.H. and J.E. Saiers. 2002. Development and evaluation of a mathematical model for surface-water flow within the Shark River Slough of the Florida Everglades. *Journal of Hydrology* 259:221-235.

Boyce, W.E. and R.C. DiPrima. 2005. Elementary Differential Equations and Boundary Value Problems, 8th Edition. USA, Wiley and Sons, Hoboken.

Brix, H. 1997. Do macrophytes play a role in constructed treatment wetlands? *Water Science and Technology* 35(5):11-17.

Carleton, J.N. 2002. Damköhler number distributions and constituent removal in treatment wetlands. *Ecological Engineering*, 19:233-248.

Carleton, J.N., T.J. Grizzard, A.N. Godrej, and H.E. Post. 2001. Factors affecting the performance of stormwater treatment wetlands. *Water Research* 35(6):1552-1562.

Carleton, J.N., T.J. Grizzard, A.N. Godrej, H.E. Post, L. Lampe, and P. Kenel. 2000. Performance of a constructed wetland in treating urban stormwater runoff. *Water Environment Research* 72(3):295-304.

Carleton, J.N. and H.J. Montas. 2007. A modeling approach for mixing and reaction in wetlands with continuously varying flow. *Ecological Engineering*, 29:33-44.

Carleton, J.N. and H.J. Montas. 2009. Reactive transport in stratified flow fields with idealized heterogeneity. *Advances in Water Resources* 32:906-915.

Chambers, P.A., E.E. Prepas, H.R. Hamilton, and M.L. Bothewell. 1991. Current velocity and its effect on aquatic macrophytes in flowing waters. *Ecological Applications* 1(3):249-257.

Champion, P.D. and C.C. Tanner. 2000. Seasonality of macrophytes and interaction with flow in a New Zealand lowland stream. *Hydrobiologia* 441:1-12.

Chapra, S.C. 1997. Surface Water Quality Modeling. McGraw-Hill, Boston.

Chen, A. and P. Arce. 1997. An integral-spectral approach for convective-diffusive mass transfer with chemical reaction in Couette flow - mathematical formulation and numerical illustrations. *Chemical Engineering Journal* 68:11-27.

Chendorain, M., M. Yates, and F. Villegas. 1998. The fate and transport of viruses through surface water constructed wetlands. *Journal of Environmental Quality* 27:1451-1458.

Coveney, M.F., D.L. Stiles, E.F. Lowe, L.E. Battoe, and R. Conrow. 2002. Nutrient removal from eutrophic lake water by wetland filtration. *Ecological Engineering* 19:141-159.

D'Alpaos, A., S. Lanzoni, S.M. Mudd, and S. Fagherazzi. 2006. Modeling the influence of hydroperiod and vegetation on the cross-sectional formation of tidal channels. *Estuarine, Coastal, and Shelf Science* 69:311-324.

Dagan, G. 1984. Solute transport in heterogeneous porous formations. *Journal of Fluid Mechanics* 145:151-177.

Danckwerts, P.V. 1953. Continuous flow systems. Distribution of residence times. *Chemical Engineering Sciences* 2(1): 13-22.

Davis, C.B., J.L. Baker, A.G. Van der Valk, and C.E. Beer. 1981. Prairie pothole marshes as traps for nitrogen and phosphorus in agricultural runoff, pp. 153-163. In: Richardson, B. (Ed.) Selected Proceedings of the Midwest Conference on Wetland Values and Management, Minnesota Water Planning Board, St. Paul.

Day, T.J. 1977. Longitudinal dispersion of fluid particles in mountain streams: 1. Theory and field evidence. *Journal of Hydrology* 16(1):7-25.

De Blij, J. 1981. Geography: Regions and Concepts, 3rd Edition. Wiley and Sons, New York.

Dentz, M., A. Cortis, H. Scher, and B. Berkowitz. 2004. Time behavior of solute transport in heterogeneous media: transition from anomalous to normal transport. *Advances in Water Resources* 27:155-173.

Dierberg, F.E. and T.A. DeBusk. 2008. Particulate phosphorus transformations in south Florida stormwater treatment areas used for Everglades protection. *Ecological Engineering* 34:100-115.

Dierberg, F.E., J.J. Juston, T.A. DeBusk, K. Pietro and B. Gu. 2005. Relationship between hydraulic efficiency and phosphorus removal in a submerged aquatic vegetation-dominated treatment wetland. *Ecological Engineering* 25(1):9-23.

Eriksson, P.G. 2001. Interaction effects of flow velocity and oxygen metabolism on nitrification and denitrification in biofilms on submersed macrophytes. *Biogeochemistry* 55:29-44.

Eriksson, P.G. and S.E.B. Weisner. 1997. Nitrogen removal in a wastewater reservoir: the importance of denitrification by epiphytic biofilms on submersed vegetation. *Journal of Environmental Quality* 26:905-910.

Eriksson, P.G. and S.E.B. Weisner. 1999. An experimental study on effects of submersed macrophytes on nitrification and denitrification in ammonium-rich aquatic systems. *Limnology and Oceanography* 44(8):1993-1999.

Feng, K. and F.J. Molz. 1997. A 2-D, diffusion-based, wetland flow model. *Journal of Hydrology* 196:230-250.

Fetter, C.W., W.E. Sloey, and F.L. Spangler. 1978. Use of a Natural Marsh for Wastewater Polishing. *Journal of the Water Pollution Control Federation*, 50:290-307.

Fischer, H.B., E.J. List, R.C.Y. Koh, J. Imberger, and N.H. Brooks. 1979. Mixing In Inland and Coastal Waters. Academic Press, New York.

Fonseca, M.S., J.S. Fisher, J.C. Zieman, and G.W. Thayer. 1982. Influence of the seagrass, Zostera marina L., on current flow. *Estuarine, Coastal and Shelf Science* 15:351-364.

Gelhar, L.W. 1993. Stochastic Subsurface Hydrology. Prentice Hall, Englewood Cliffs.

Gelhar, L.W., A. L. Gutjahr, and R.L. Naff. 1979. Stochastic analysis of macrodispersion in a stratified aquifer. *Water Resources Research* 15(6):1387-1397.

Ghisalberti, M. and H.M. Nepf. 2006. Mass transport in vegetated shear flows. *Environmental Fluid Mechanics* 5:527-551.

Grant, R.R. and R. Patrick. 1970. Tinicum marsh as a water purifier, pp. 105-131. In: McCormick, J., R.R. Grant, and R. Patrick (Eds.) Two Studies of Tinicum Marsh, Delaware and Philadelphia Counties, Pa., The Conservation Foundation, Washington, DC.

Green, J.C. 2004. Modelling flow resistance in vegetated streams: review and development of new theory. *Hydrological Processes* DOI: 10.1002/hyp.5564.

Grismer, M.E. 2005. Simulation evaluation of the effects of non-uniform flow and degradation parameter uncertainty on subsurface-flow constructed wetland performance. *Water Environment Research* 77(7):3047-3053.

Gu, B. and T. Dreschel. 2008. Effects of plant community and phosphorus loading rate on constructed wetland performance in Florida, USA. *Wetlands* 28(1):81-91.

Herrera, P. and A. Valocchi. 2006. Positive solution of two-dimensional solute transport in heterogeneous aquifers. *Ground Water* 44(6):803-813.

Holland, J.F., J.F. Martin, T. Granata, V. Bouchard, M. Quigley, and L. Brown. 2004. Effects of wetland depth and flow rate on residence time distribution characteristics. *Ecological Engineering* 23:189-203.

Hunt, B. 1999. Dispersion model for mountain streams. *Journal of Hydraulic Engineering* 125(2): 99-105.

James, A.I. and J.W. Jawitz. 2007. Modeling two-dimensional reactive transport using a Godunov-mixed finite element method. *Journal of Hydrology* 338:28-41.

Jamieson, R., R. Gordon, N. Wheeler, E. Smith, G. Stratton, and A. Madani. 2007. Determination of first order rate constants for wetlands treating livestock wastewater in cold climates. *Journal of Environmental Engineering Science* 6:65-72.

Kadlec, R.H. 1990. Overland flow in wetlands: vegetation resistance. *Journal of Hydraulic Engineering* 116:691-707.

Kadlec, R.H. 2000. The inadequacy of first-order treatment wetland models. *Ecological Engineering* 15, 105-119.

Kadlec, R.H. 2003. Effects of pollutant speciation in treatment wetlands design. *Ecological Engineering* 20:1-16.

Kadlec, R.H. 2005. Wetland to pond treatment gradients. *Water Science and Technology* 51(9):291-298.

Kadlec, R.H. 2008. The effects of wetland vegetation and morphology on nitrogen processing. *Ecological Engineering* 33:126-141.

Kadlec, R.H. and R.L. Knight. 1996. Treatment Wetlands. CRC Lewis Press, Boca Raton.

Kadlec, R.H. and S.D. Wallace. 2009. Treatment Wetlands, 2nd Edition. CRC Press, Boca Raton.

Kemblowski, M.W. and J. Wen. 1993. Contaminant spreading in stratified soils with fractal permeability distribution. *Water Resources Research* 29(2):419-425.

Kjellin, J., A. Worman, H. Johansson, and A. Lindahl. 2007. Controlling factors for water residence time and flow patterns in Ekeby treatment wetland, Sweden. *Advances in Water Resources* 30:838-850.

Kreft A. and A. Zuber. 1978. On the physical meaning of the dispersion equation and its solutions for different initial and boundary conditions. *Chemical Engineering Science* 33:1471-1480.

Lee, G.F., E. Bentley, and R. Amundson. 1975. Effects of marshes on water quality, pp. 105-127. In: Hasler, A.D. (Ed.) Coupling of Land and Water Systems, Springer-Verlag, New York.

Leonard, L.A. and A.L. Croft. 2006. The effect of standing biomass on flow velocity and turbulence in Spartina alterniflora canopies. *Estuarine, Coastal, and Shelf Science* 69:325-336.

Leonard, L.A. and M.E. Luther. 1995. Flow hydrodynamics in tidal marsh canopies. *Limnology and Oceanography* 40:1474-1484.

Levenspiel, O. 1972. Chemical Reaction Engineering, 2nd Edition. Wiley, New York.

Levy, M. and B. Berkowitz. 2003. Measurement and analysis of non-Fickian dispersion in heterogeneous porous media. *Journal of Contaminant Hydrology* 64:203-226.

Lightbody, A.F., M.E. Avener, and H.M. Nepf. 2008. Observations of short-circuiting flow paths within a free-surface wetland in Augusta, GA, USA. *Limnology and Oceanography* 53(3):1040-1053.

Lightbody, A.F. and H.M. Nepf. 2006. Prediction of velocity profiles and longitudinal dispersion in emergent salt marsh vegetation. *Limnology and Oceanography* 51(1):218-228.

Lightbody, A.F., H.M. Nepf, and J.S. Bays. 2007. Mixing in deep zones within constructed treatment wetlands. *Ecological Engineering* 29:209-220.

Lightbody, A.F., H.M. Nepf, and J.S. Bays. 2009. Modeling the hydraulic effect of transverse deep zones on the performance of short-circuiting constructed treatment wetlands. *Ecological Engineering* 35:754-768.

Luhar, M., J. Rominger, and H. Nepf. 2008. Interaction between flow, transport, and vegetation spatial structure. *Environmental Fluid Mechanics* 8:423-439.

Martin, J., E. Hofherr, and M.F. Quigley, 2003. Effects of Typha latifolia transpiration and harvesting on nitrate concentrations in surface water of wetland mesocosms. *Wetlands* 23(4):835-844.

Martinez, C.J. and W.R. Wise. 2003. Hydraulic analysis of Orlando Easterly Wetland. *Journal of Environmental Engineering* 129(6):553-560.

Matheron, G. and D. DeMarsily. 1980. Is transport in porous media always diffusive? A counterexample. *Water Resources Research* 16(5):901-917.

Maynard, J.J., A.T. O'Green, and R.A. Dahlgren. 2009. Bioavailability and fate of phosphorus in constructed wetlands receiving agricultural runoff in the San Joaquin valley, California. *Journal of Environmental Quality* 38:360-372.

Mitsch, W.J. and J.G. Gosselink. 2000. Wetlands 3rd Edition. John Wiley and Sons, New York.

Mitsch, W.J. and S.E. Jorgensen. 2004. Ecological Engineering and Ecosystem Restoration. John Wiley and Sons, Hoboken.

Montas, H.J. 2003. An analytical solution of the three-component transport equation with application to third-order transport. *Water Resources Research* 39(2), 1036, doi:10.1029/2002WRR001288.

Montas, H.J., J. Carleton, and A. Shirmohammadi. 2006. Analysis and solution of a bicontinuum transport model. Paper number: 063066. In 2006 ASABE Annual International Meeting, Portland, Oregon.

Montas, H.J., A. Shirmohammadi, K. Haghighi, and B. Engel. 2000. Equivalence of bicontinuum and second-order transport in heterogeneous soils and aquifers. *Water Resources Research* 12:3427-3446.

Moore, K.A. 2004. Influence of seagrasses on water quality in shallow regions of the lower Chesapeake Bay. *Journal of Coastal Research* 20 (Special Issue):162-178.

Nepf, H.M. 1999. Drag, turbulence, and diffusion in flow through emergent vegetation. *Water Resources Research*, 35(2):479-489.

Nepf, H.M. and E.W. Koch. 1999. Vertical secondary flows in submersed plant-like arrays. *Limnology and Oceanography* 44(4):1072-1080.

Nepf, H.M., C.G. Mugnier, and R.A. Zavitoski. 1997a. The effects of vegetation on longitudinal dispersion. *Estuaries, Coastal and Shelf Science*, 44:675-684.

Nepf, H.M., J.A. Sullivan, and R.A. Zavistoki. 1997b. A model for diffusion within emergent vegetation. *Limnology and Oceanography* 42(8):1735-1745.

Nepf, H.M. and E.W. Koch. 1999. Vertical secondary flows in submersed plant-like arrays. *Limnology and Oceanography* 44(4):1072-1080.

Nepf, H.M. and E.R. Vivoni, 2000. Flow structure in depth-limited, vegetated flow. Journal of Geophysical Research 105(C12):28,547-28,557.

Novitsky, R.P. 1978. Hydrology of the Nevin Wetland near Madison, Wisconsin. USGS Report 78-48.

Novotny, V. 2003. Water Quality: Diffuse Pollution and Watershed Management, 2nd Edition. Wiley and Sons, New York.

Olsen, R.K. 1993. Evaluating the role of created and natural wetlands in controlling nonpoint source pollution, pp. 1-5. In: Olsen, R.K. (Ed.) Created and Natural Wetlands for Controlling Nonpoint Source Pollution, CRC Press, Boca Raton.

Persson, J., N.L.G. Somes, and T.H.F. Wong. 1999. Hydraulics efficiency of constructed wetlands and ponds. *Water Science and Technology* 40(3):291-300.

Pietro, K.C., M.J. Chimney, and A.D. Steinman. 2006. Phosphorus removal by the Ceratophyllum/periphyton complex in a south Florida (USA) freshwater marsh. *Ecological Engineering* 27:290-300.

Polprasert, C., N.R. Khatiwada, and J. Bhurtel. 1998. A model for organic matter removal in free water surface constructed wetlands. *Water Science and Technology* 38(1):369-377.

Prince, H. 1997. Wetlands of the American Midwest: A Historical Geography of Changing Attitudes. The University of Chicago Press, Chicago.

Ran, N., M. Agami, and G. Oron. 2004. A pilot study of constructed wetlands using duckweed (Lemna gibba L.) for treatment of domestic primary effluent in Israel. *Water Research* 38:2241-2248.

Relton, F.E. 1965. Applied Bessel Functions. Dover, New York.

Rotkin-Ellman, M., K. Addy, A.J. Gold, and P.M. Groffman. 2004. Tree species, root decomposition, and subsurface denitrification potential in riparian wetlands. *Plant and Soil* 263:335-344.

Saiers, J.E., J.W. Harvey, and S.E. Mylon. 2003. Surface-water transport of suspended matter through wetland vegetation of the Florida everglades. *Geophysical Research Letters* 30(19) 1987 doi:10.1029/2003GL018132.

Sand-Jensen, K. and J.R. Mebus. 1996. Fine-scale patterns of water velocity within macrophyte patches in streams. *Oikos* 76:169-180.

Scinto, L.J. and K.R. Reddy. 2003. Biotic and abiotic uptake of phosphorus by periphyton in a subtropical freshwater wetland. *Aquatic Botany* 77:203-222.

Seidel, K. 1976. Macrophytes and water purification, pp. 109-121. In: Tourbier, J. and Pierson, R.W. (Eds.) Biological Control of Water Pollution, Univ. of Pennsylvania Press.

Shapiro, M. and H. Brenner. 1986. Taylor dispersion of chemically reactive species: irreversible first-order reactions in bulk and on boundaries. *Chemical Engineering* 41(6):1417-1433.

Shi, Z. and J.M.R. Hughes. 2002. Laboratory flume studies of microflow environments of aquatic plants. *Hydrological Processes* 16:3279-3289.

Simmons, C.S., T.R. Ginn, and B.D. Wood. 1995. Stochastic-convective transport with nonlinear reaction: mathematical framework. *Water Resources Research* 31(11), 2675-2688.

Simpson, R.L., R.E. Good, R. Walker, and B.R. Frasco. 1983. The Role of Delaware River Freshwater Tidal Wetlands in the Retention of Nutrients and Heavy Metals. *Journal of Environmental Quality* 12(1):41-48.

Siong, K., T. Asaeda, T. Fujino, and A. Redden. 2006. Difference characteristics of phosphorus in Chara and two submerged angiosperm species: implications for phosphorus nutrient cycling in an aquatic ecosystem. *Wetlands Ecology and Management* 14:505-510.

Sjodin, A.L., W.M. Lewis, and J.F. Saunders. 1997. Denitrification as a component of the nitrogen budget for a large plains river. *Biogeochemistry* 39:327-342.

Tao, W.D., K.J. Hall, and S.J.B. Duff. 2006. Performance evaluation and effects of hydraulic retention time and mass loading rate on treatment of woodwaste leachate in surface-flow constructed wetlands. *Ecological Engineering* 26:252-265.

Taylor, G.I. 1954. Dispersion of solute flowing slowly through a tube. *Proceedings of the Royal Society of London* 223A: 446-468.

Tchobanoglous, G. and E.D. Schroeder. 1987. Water Quality. Addison-Wesley. Reading.

Thoren, A. 2007. Urea transformation of wetland microbial communities. *Microbial Ecology* 53:221-232.

Thornton, C.I., S.R. Abt, and W.P. Clary. 1997. Vegetation influence on small stream siltation. *Journal of the American Water Resources Association* 33(6):1279-1288.

Thullen J.S., J.J. Sartoris, and S.M. Nelson. 2005. Managing vegetation in surface-flow wastewater-treatment wetlands for optimal treatment performance. *Ecological Engineering* 25:583-593.

Toet, S., L.H.F.A. Huibers, R.S.P. Van Logtestijn, and J.T.A. Verhoeven. 2003. Denitrification in the periphyton associated with plant shoots and in the sediment of a wetland system supplied with sewage treatment plant effluent. *Hydrobiologia* 501:29-44.

Toet, S., R.S.P. Van Logtestjin, R. Kampf, M. Schreijer, and J.T.A. Verhoeven. 2005. The effect of hydraulic retention time on the removal of pollutants from sewage treatment plant effluent in a surface-flow treatment wetland system. *Wetlands* 25(2):375-391.

Uflyand, Y.S. 1988. Exact solution of a nonstationary convective heat-exchange problem in a two-dimensional channel. *Journal of Engineering Physics* 54(6):680-682.

Valocchi, A.J. 1989. Spatial moment analysis of the transport of kinetically adsorbing solutes through stratified aquifers. *Water Resources Research* 25(2):273-279.

van Genuchten, M.T. and W.J. Alves. 1982. Analytical Solutions of the One-Dimensional Convective-Dispersive Solute Transport Equation. USDA ARS Technical Bulletin Number 1661.

Vymazal, J. 2007. Removal of nutrients in various types of constructed wetlands. *Science of The Total Environment* 380:48-65.

Walker, L.P. and M.R. Walker. 1990. City of Gustine Marsh Evaluation Study. Report to City of Gustine. Larry Walker and Associates, Davis, CA.

Wang, H., J.W. Jawitz, J.R. White, C.J. Martinez, and M.D. Sees. 2006. Rejuvenating the largest municipal treatment wetland in Florida. *Ecological Engineering* 26:132-146.

Werner, T.M. and R.H. Kadlec. 1996. Application of residence time distributions to stormwater treatment systems. *Ecological Engineering* 7:213-234.

Werner, T.M. and R.H. Kadlec. 2000. Wetland residence time distribution modeling. *Ecological Engineering* 15:77-90.

White, B.L. and H.M. Nepf. 2003. Scalar transport in random cylinder arrays at moderate Reynolds number. *Journal of Fluid Mechanics* 487:43-79.

White, B.L. and H.M. Nepf. 2008. A vortex-based model of velocity and shear stress in a partially vegetated shallow channel. *Water Resources Research* 44 W01412, doi:10.1029/2006WR005651.

Wong, T.H.F., T.D. Fletcher, H.P. Duncan, and G.A. Jenkins. 2006. Modelling urban stormwater treatment – a unified approach. *Ecological Engineering* 27:58-70.

Yeh, G.T. and Y.J. Tsai. 1976. Dispersion of water pollutants in a turbulent shear flow. *Water Resources Research* 12(6):1265-1270.

Zou, S., J. Xia, and A.D. Koussis. 1996. Analytical solutions to non-Fickian subsurface dispersion in uniform groundwater flow. *Journal of Hydrology* 179: 237-258.